Investigating Therapeutic Potential of Zeb2 Inhibition and Oxidized Pullulan in Diabetic Wound Healing

A Thesis Submitted
in Partial Fulfilment of the Requirements
for the Degree of

Doctor of Philosophy

by

SOUMYAJIT ROY

Entry No. 2019BMZ0003

DEPARTMENT OF BIOMEDICAL ENGINEERING

INDIAN INSTITUTE OF TECHNOLOGY ROPAR

RUPNAGAR

January, 2025

Soumyajit Roy: *Investigating therapeutic potential of Zeb2 inhibition and oxidized pullulan in diabetic wound healing*

Dedicated

to

my parents & friends

Declaration of Originality

I hereby declare that the work which is being presented in the thesis entitled '***Investigating therapeutic potential of Zeb2 inhibition and oxidized pullulan in diabetic wound healing***' has been solely authored by me. It presents the result of my own independent investigation/research conducted during the time period from July, 2019 of joining the Ph.D. program to July, 2024 for final Ph.D. Thesis submission under the joint supervision of Dr. Durba Pal, and Dr Yashveer Singh. To the best of my knowledge, it is an original work, both in terms of research content and narrative, and has not been submitted or accepted elsewhere, in part or in full, for the award of any degree, diploma, fellowship, associateship, or similar title of any university or institution. Further, due credit has been attributed to the relevant state-of-the-art and collaborations (NIPER, SAS Nagar and DMC&H, Ludhiana) with appropriate citations and acknowledgments, in line with established ethical norms and practices. I also declare that any idea/data/fact/source stated in my thesis has not been fabricated/ falsified/ misrepresented. All the principles of academic honesty and integrity have been followed. I fully understand that if the thesis is found to be unoriginal, fabricated, or plagiarized, the Institute reserves the right to withdraw the thesis from its archive and revoke the associated Degree conferred. Additionally, the Institute also reserves the right to appraise all concerned sections of society of the matter for their information and necessary action. If accepted, I hereby consent for my thesis to be available online in the Institute's Open Access repository, inter-library loan, and the title & abstract to be made available to outside organizations.

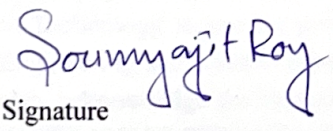

Signature

Name: Soumyajit Roy
Entry Number: 2019BMZ0003
Program: PhD
Department: Department of Biomedical Engineering
Indian Institute of Technology Ropar, Rupnagar-140001, Punjab
Date: 26/01/2025

Acknowledgments

I wish to express my profound gratitude to the individuals and organizations whose unwavering support and contributions have been pivotal throughout my Ph.D. journey. First and foremost, I owe a deep debt of appreciation to my parents for their steadfast support and encouragement at every stage of my doctoral studies. I also extend my heartfelt thanks to Dr. Durba Pal and Dr. Yashveer Singh, my esteemed Ph.D. advisors, for their invaluable academic guidance, and unwavering support. Their belief in my abilities, coupled with their expertise and commitment, has been instrumental not only in shaping my research but also in fostering my personal and professional growth.

I would like to express my gratitude to Prof. Kulbhushan Tikoo of NIPER SAS Nagar for his generous provision of laboratory facilities, which was crucial for the execution of animal studies. I also extend my sincere thanks to Mr. Shivam Sharma of NIPER for his expertise, insightful discussions, and invaluable assistance in conducting animal experiments. Additionally, I am sincerely appreciate the clinicians and team members of the Gastroenterology Unit at DMC&H, Ludhiana including Prof. Ashvind Bawa and his team, for their invaluable assistance in collecting wound patient samples.

I would like to express my deep gratitude to my doctoral committee members, Dr. Srivatsava Naidu, Dr. Narinder Singh, Dr. Rajendra Srivastava, and Dr. Anupam Bandyopadhyay, for their timely insights and academic support. My heartfelt thanks also extend to all my lab members, whose steadfast support has been integral to the success of every research endeavour. I extend my profound gratitude to Dr. Suman Dasgupta of Tezpur University. His unwavering support, meticulous approach, kindness, and intellectually stimulating discussions have continuously inspired me to push the boundaries of my research and broaden my intellectual horizons.

I wish to extend special recognition to my dear friend, Dr. Debarun Patra, whose unwavering presence has been a source of strength and inspiration throughout my academic and personal journey. His encouragement, insightful discussions, and steadfast support have been pivotal in helping me navigate the challenges and celebrate the successes of this journey, making many of my achievements possible. I would also like to express my deep appreciation to Dr. Moumita Halder for her constant support, which has strengthened me.

Lastly, I wish to express my gratitude to the Ministry of Education (MoE), Indian Institute of Technology Ropar for providing me with a fellowship and the Department of Biomedical Engineering and Central Research Facilities (CRF) for granting access to research facilities. I also acknowledge the financial assistance from the Department of Biotechnology DBT, India (BT/PR40669/MED/32/761/2020) to my supervisors.

Soumyajit Roy

January, 2025

Certificate

This is to certify that the thesis entitled '***Investigating therapeutic potential of Zeb2 inhibition and oxidized pullulan in diabetic wound healing***', submitted by Soumyajit Roy (Entry no. 2019BMZ0003) Department of Biomedical Engineering, IIT Ropar, Rupnagar for the award of the degree of Doctor of Philosophy of Indian Institute of Technology Ropar, is a record of bonafide research work carried out under my guidance and supervision. To the best of my knowledge and belief, the work presented in this thesis is original and has not been submitted, either in part or full, for the award of any other degree, diploma, fellowship, associateship or similar title of any university or institution. In my opinion, the thesis has reached the standard fulfilling the requirements of the regulations relating to the Degree.

(Supervisors)

Dr. Durba Pal
Associate Professor
Department of Biomedical Engineering
Indian Institute of Technology Ropar
Rupnagar-140001, Punjab

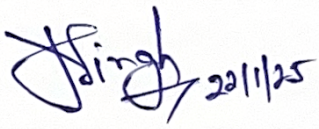

Dr. Yashveer Singh
Associate Faculty
Department of Biomedical Engineering
Indian Institute of Technology Ropar
Rupnagar-140001, Punjab

Lay Summary

Diabetes-induced chronic foot ulcers are non-healing skin injury especially in the foot, which provides a significant health problem. Zeb2, a transcription factor, has recently come to light as an essential component in this pathogenic process, which is mostly due to macrophage dysregulation. Alleviated expression of Zeb2 under hyperglycaemic situations, causes macrophages to become more pro-inflammatory. This, in turn, worsens the wound and hinders the healing process. Further, we created a multifunctional hydrogel system using chemically modified two biopolymers oxidized-pullulan and quaternized-chitosan to transport *Zeb2* ASO to silence its action and accelerate the healing process of diabetic wounds. These biopolymers feature intrinsic antibacterial and antioxidant capabilities, which are further strengthened by chemical modification—oxidized pullulan, in particular, displays greater antibacterial activity against *Staphylococcus aureus,* a predominant bacteria found in non-healing skin wound. Thus, we loaded *Zeb2* ASO in the hydrogel to target Zeb2 suppression while concurrently alleviating oxidative stress and bacterial burden, and therefore our method greatly induces wound healing in diabetic mice. In conclusion, *Zeb2*-targeted multifunctional hydrogel may provide an efficient approach to managing chronic diabetic wounds.

Abstract

Diabetic foot ulcers are a serious and challenging consequence of diabetes, characterized by chronic sores that defy healing. These ulcers occur from diabetes-induced microvascular problems that restrict blood flow, consequently reducing the supply of oxygen and vital nutrients to the wound site. The outcome is a reduced immune response and a delayed healing process. At the root of this issue is hyperglycaemia, which exacerbates inflammation by boosting levels of pro-inflammatory cytokines such as TNF-α, IL-1, and IL-6. The issue is further compounded by hypoxia inside the ulcer, which boosts NF-κB signalling pathways, resulting to an enhanced inflammatory response that hampers the healing process. The combination of hyperglycaemia and hypoxia not only disrupts the normal processes of wound healing but also creates conditions that are conducive to chronic ulceration. The continuous presence of pro-inflammatory cytokines keeps the wound in a prolonged state of inflammation, this makes diabetic foot ulcers not only difficult to treat but also prone to complications such as infections, which can further deteriorate the condition. Macrophages, are critical for shifting from an initial inflammatory phase to a reparative phase, facilitating tissue regeneration and wound healing. However, in the setting of diabetes, macrophages stay imprisoned in a pro-inflammatory state, unable to properly convert to their repairing duty. The persistent hyperglycaemic environment and the associated chronic inflammation trap macrophages in their pro-inflammatory state, rather than transitioning to their reparative role, leads to continued production of proinflammatory cytokines that adds to the chronicity of diabetic foot ulcers. Functional dysregulation at the molecular level, is the root cause of pathophysiological disturbances. This study, for the first time, uncovers transcription factor Zeb2, , as a crucial regulator of macrophage polarity in hyperglycaemic conditions. Increased glucose levels promote Zeb2 expression caused by hyperacetylation, which supports and maintains the pro-inflammatory phenotype of macrophages. Notably, downregulating Zeb2 expression leads to a decrease in wound inflammation, showing its critical engagement in chronic wound etiology.

We developed an advanced biopolymer-based hydrogel system for effective *Zeb2* ASO delivery by addressing the complexities of biomacromolecule delivery in chronic wound environments. This multifunctional hydrogel combines oxidized pullulan (OP) with quaternized chitosan (QC), leveraging their inherent antioxidant and antibacterial properties. A strategic single-step modification of the pullulan backbone demonstrated impressive antibacterial efficacy against *Staphylococcus aureus*, while ensuring biocompatibility and preventing infections. The OP@QC hydrogel not only supports controlled drug release but also

exhibits significant antibioflim activity. Diabetic mouse wound upon treated with OP@QC hydrogel loaded with *Zeb2* ASO, notably enhanced the healing rate, mitigated inflammation, and promoted tissue regeneration by shifting macrophages from a pro-inflammatory to an anti-inflammatory phenotype.

Overall, our study highlights the therapeutic potential of targeting Zeb2 to manage chronic inflammation in diabetic wounds. The OP@QC hydrogel, with its antibacterial properties and ability to deliver therapeutics, represents a significant advancement in wound care technology.

List of Publications From Thesis

Research article

1. **S. Roy,** M. Halder, P Ramprasad, S Dasgupta, Y. Singh, D Pal (2023) Oxidized pullulan exhibits potent antibacterial activity against *S. aureus* by disrupting its membrane integrity; *International Journal of Biological Macromolecules*; Jul 28;249:126049. (**IF 8.2**)

2. **S. Roy**, D. Patra, P. Ramprasad, S. Sharma, A. Bawa, K. Tikoo, S. Dasgupta, Y. Singh, D. Pal (2025). Exploring therapeutic horizons: diminishing Zeb2 eases wound-related complications. (*to be submitted soon*)

Book chapter

1. D Patra, **S Roy**, P Ramprasad, D Pal* (2023). Next-generation therapies for type 2 diabetes mellitus. Book : Functional smart nanomaterials and their theranostics approaches; *Publisher: Springer Nature Singapore*. (ISSN 3004-8273), p347-376.

List of Publications from Associated Projects

1. V. Chawla[#], **S. Roy**[#], J. Raju, D. Pal, Y. Singh (2024).Proangiogenic cyclic peptide nanotubes for diabetic wound healing. (*manuscript submitted*)

2. Patra, D., Vashisth, A., Ramprasad, P., Sharma, S., Prusty, B.M., **Roy, S**., Singh, S., Manna, D., Tikoo, K., Dasgupta, S., Pal, D. (2023) Nuclear Fetuin-A programs adipocyte senescence under chronic obesity. (*under revision*)

3. D. Patra, **S. Roy**, L. Arora, S.W. Kabeer, S. Singh, U. Dey, D. Banerjee, A. Sinha, S. Dasgupta, K. Tikoo, A. Kumar, & D. Pal (2022). miR-210-3p promotes obesity-induced adipose tissue inflammation and insulin resistance by targeting SOCS1 mediated NF-κB pathway. *Diabetes* ;72(3):375–388. (**IF:9.46**)

4. L. Arora, M. Kalia, **S. Roy**, & D. Pal (2022). Assessment of Mitochondrial Health in Cancer-Associated Fibroblasts Isolated from 3D Multicellular Lung Tumor Spheroids. *Journal of Visualized Experiments: Jove (188)*: e64315. (**IF: 1.8**).

5. L. Arora, D. Patra, **S. Roy,** S. Nanda, N. Singh, A.K. Verma, A. Chakraborti, S. Dasgupta, D. Pal*. (2024) Hypoxia-induced miR-210-3p expression in lung adenocarcinoma potentiates tumor development by regulating CCL2-mediated monocyte infiltration. *Molecular Oncology*;18(5):1278-1300. (**IF: 6.6**)

6. D. Banerjee[#], D. Patra[#], A. Sinha, **S. Roy**, R. Pant, R. Sarmah, R. Dutta, S.K. Bhagabati, K. Tikoo, D. Pal* & S. Dasgupta* (2022). Lipid-induced monokine Cyclophilin-A promotes adipose tissue dysfunction implementing insulin resistance and type 2 diabetes

in zebrafish and mice models of obesity. *Cellular and Molecular Life Sciences* ;79(5):282. (**IF:9.261**)

7. B. Kumari[#], M. Mantipally[#], **S. Roy**, L. Arora, V.N. Badavath, M. Gangireddy, S. Dasgupta, R. Gundla*, & D. Pal*. (2022). Novel imidazo [1, 2-a] pyridine derivatives induce apoptosis and cell cycle arrest in non-small cell lung cancer by activating NADPH oxidase mediated oxidative stress. *Life Sciences*; 294: 120334. (**IF:6.78**)

8. D Patra[#], D Banerjee[#], P Ramprasad, **S Roy**, D Pal* and S Dasgupta* (2023). Recent insights of obesity-induced gut and adipose tissue dysbiosis in type 2 diabetes. *Frontiers in Molecular Biosciences*; 10:1224982. (**IF 5.0**)

List of conferences

1. **S. Roy,** M. Halder, Y. Singh, D Pal. Oxidized pullulan exhibits potent antibacterial activity and used for ASO loaded wound healing matrix in chronic diabetic wounds. *International Conference on Biomaterials, Regenerative Medicine And Devices* (*BIO- Remedi 2022*) held on Dec 15- 18th 2022 organized by IIT Guwahati.

2. **S. Roy**, M. Halder, Y. Singh, D Pal. Oxidized pullulan and quaternized chitosan based hydrogel system as a wound healing matrix to deliver ASO in chronic diabetic wounds. *International Conference on Smart Materials for Sustainable Technology-II* (*SMST-II, 2022*) organized jointly by IIT Bombay and IIT BHU Varanasi, held at IIT Bombay from 13-16th October 2022.

Awards

1. ***Best Poster Award*** "Adaptive cellular reprogramming at pathophysiological condition" at the International conference on biomaterials, regenerative medicine and devices (*BIO-Remedi 2022*) held on Dec 15th -18th2022 organized by IIT Guwahati.

2. ***Best Poster Award*** "Tissue reprogramming with advanced materials: A new era in Regenerative medicine" at the International conference on smart materials for sustainable technology -II (*SMST-II, 2022*) organized jointly by IIT Bombay and IIT BHU Varanasi, held at IIT Bombay from 13-16th October 2022.

Table of Contents

Abbreviations

ADP	Adenosine diphosphate
AGE	Advanced glycation end product
ANOVA	Analysis of variance
ASO	Antisense oligonucleotide
BSA	Bovine serum albumin
CDP	Common dendritic cell progenitor
CFU	Colony forming unit
COX	Cyclooxygenase
CTAB	Cetyltrimethylammonium bromide
CTAPIII	Connective Tissue Chemokine Activating Peptide III
CXCL7	Chemokine (C-X-C motif) ligand 7
DAMP	Damage-associated molecular pattern
DAPI	4′,6-Diamidino-2-phenylindole
DC	Dendritic cell
DCFDA	2′− 7′- dichlorodihydrofluorescein diacetate
DCM	Dichloromethane
DFI	Diabetic foot infection
DFU	Diabetic foot ulcer
DIEA	N,N-Diisopropylethylamine
$DiSC_3(5)$	3,3′-Dipropylthiadicarbocyanine iodide
DMEM	Dulbecco's Modified Eagle Medium
DMF	Dimethylformamide
DMSO	Dimethyl sulfoxide
DPX	Dibutylphthalate Polystyrene Xylene
ECL	Enhanced chemiluminescence
ECM	Extracellular matrix
EGF	Epidermal growth factor
ELISA	Enzyme Linked Immunosorbent Assay
EMT	Epithelial-to-mesenchymal transition
eNOS	Endothelial nitric oxide synthase
ERK	Extracellular signal-regulated kinase
FBS	Fetal bovine serum
FDA	Food and Drug Administration
FGF	Fibroblast growth factor
FT-IR	Fourier transform infrared spectroscopy
GalNAc	N-acetylgalactosamine
GelMA	Gelatin Methacrylate
GFP	Green fluorescent protein
GLUT4	Glucose transporter type 4
GM-CSF	Granulocyte macrophage colony-stimulating factor
GM3S	Ganglioside monosialic acid 3 synthase
GMP	Granulocyte-macrophage progenitor
GPC	Gel permeation chromatography
GPCR	G protein-coupled receptor
GQD	Graphene quantum dot
GTMAC	Glycidyltrimethylammonium chloride

HAT	Histone acetyltransferases
HATU	Hexafluorophosphate Azabenzotriazole Tetramethyl Uronium
HBO	Hyperbaric oxygen therapy
HFD	High-fat diet
HG	Hyperglycaemia
HGF	Hepatocyte growth factor
HIF	Hypoxia-inducible factors
HR-TEM	High-resolution transmission electron microscopy
HSC	Hematopoietic stem cell
ICAM-1	Intercellular adhesion molecule 1
Id2	Inhibitor of DNA binding 2
IFN	Interferons
IGF	Insulin-like growth factor
IL	Interleukins
iNKT	Invariant natural killer T cell
iPSC	Induced pluripotent stem cell
IRS	Insulin receptor substrate
KGF	Keratinocyte growth factor
KLF6	Kruppel-like factor 6
kPa	kilo pascal
LDTF	Lineage-determining transcription factor
LNA	Locked nucleic acids
lncRNA	long non-coding RNA
LNP	Lipid nanoparticle
LPS	Lipopolysaccharide
MAPK	Mitogen-activated protein kinases
MBC	Minimum bactericidal concentration
MC	Mast cell
MCP-1	Monocyte chemoattractant protein-1
MHC	Major histocompatibility complex
MIC	Minimum inhibitory concentration
miRNA	microRNA
MMP	Matrix metalloproteinase
MOZ1	Monocytic leukemia zinc finger protein 1
MSC	Mesenchymal stem cells
MSN	Mesoporous silica nanoparticles
MTT	3-(4,5-Dimethylthiazolyl-2)-2,5-diphenyltetrazolium bromide
NAP2	Neutrophil-Activating Peptide 2
ncRNA	non-coding RNA
NF-κB	Nuclear factor kappa-light-chain-enhancer of activated B cells
NGF	Nerve growth factor
NPWT	Negative pressure wound therapy
OCT2	Octamer-binding protein 2
PAGE	Polyacrylamide gel electrophoresis
PAMP	Pathogen-associated molecular pattern
PAR-2	Protease-activated receptor 2
PCR	Polymerase chain reaction
PDB	Protein data bank
PDGF	Platelet-derived growth factor
PEAD	Poly-ethylene argininyl-aspartate diglyceride

PEG	Polyethylene glycol
PEI	Polyethylenimine
PGE	Prostaglandin E
PI	Propidium iodide
PI3K	Phosphatidylinositol 3-kinase
PI3K	Phosphatidylinositol 3-kinase
PIA	Polysaccharide intercellular adhesin
PLGA	Poly(lactic-co-glycolic) acid
PLIP	Protein-ligand interaction profiler
PMO	Phosphorodiamidate Morpholino Oligomer
PNA	Peptide nucleic acids
PNIPAM	Poly(N-isopropylacrylamide)
PRR	Pattern recognition receptors
PS	Phosphorothioate
PVP	Polyvinylpyrrolidone
RAGE	Receptor for advanced glycation end product
RBC	Red blood corpuscle
rhEGF	Recombinant human epidermal growth factor
RNA	Ribonucleic acid
ROS	Reactive oxygen species
RPMI	Roswell Park Memorial Institute Medium
SCF	Stem cell factor
SDF	Stromal cell-derived factor-1
SIP1	Smad-interacting protein 1
SpA	Staphylococcal protein A
STZ	Streptozotocin
SWF	Simulated wound fluid
TBS	Tris-buffered saline
TFA	Trifluoroacetic acid
TGF-β	Transforming growth factor beta
TIMP	Tissue inhibitors of metalloproteinases
TLR	Toll-like receptor
TNF	Tumor necrosis factor
VCAM-1	Vascular cell adhesion molecule-1
VEGF	Vascular endothelial growth factor
WVTR	Water vapor transmission rate
XRD	X-ray diffraction
ZEB2	Zinc finger E-box-binding homeobox 2
α-SMA	Alpha-smooth muscle actin

List of figures

List of tables

Chapter 1

Introduction

A wound denotes a rupture or break in the skin or underlying tissues, created by diverse external forces or internal processes, including accidents, burns, surgical procedures, or medical conditions like diabetes or vascular troubles. Wounds range from simple abrasions and superficial cuts that heal swiftly with minimal intervention to complex injuries like deep lacerations or surgical wounds that require attentive care (Chhabra *et al.*, 2017). The severity of a wound determines the treatment procedure and healing length. Effective wound therapy begins with a comprehensive assessment, when healthcare practitioners investigate the wound type—open (cut or abrasion), closed (bruise or contusion), or complex (tissue loss or deeper damage). The size and depth of the incision are examined to determine tissue involvement and related repercussions.

The wound-healing process is a dynamic set of mechanisms the body deploys to fix wounded tissues. Initially, the body controls bleeding and avoids infection in the inflammatory phase, highlighted by immune cell activity (Shetty and Bertolami, 2022). The proliferative phase follows, encompassing new blood vessel development, collagen production, and wound contraction by myofibroblasts (Bartold and Ivanovski, Gomes *et al.*, 2021). Finally, during the remodelling phase, the new tissue develops and strengthens, a process that can take months to years. Factors include nutrition, oxygenation, and underlying health conditions that effect the healing pace and efficacy (Rodrigues *et al.*, 2019).

Understanding wounds, particularly those connected to chronic illnesses like diabetes, is critical. Diabetes-related wounds frequently develop as a result of compromised immune and circulatory systems, necessitating specific care to promote rapid healing and prevent recurrence. Advanced wound care attempts to clean the debris, provide a moist healing environment, and control infection in delayed healing (Zheng *et al.*, 2023). Surgical techniques like debridement or suturing may be necessary for some wounds (Fitridge and Thompson, 2011). Comprehensive wound care continues after initial treatment to assist tissue regeneration and restore function, with variables such as diet, hydration, and overall health playing vital roles. Effective wound care seeks to elevate patient outcomes by easing pain, preventing complications, and restoring

tissue to its natural state through the use of evidence-backed treatments and personalized care strategies (Frykberg and Banks, 2015, Seth *et al.*, 2024).

1.1. Background: Cellular crosstalk in wound

A dermal wound is a complex interplay of immune cells, fibroblasts, and endothelial cells that drive healing by releasing a cascade of cytokines, chemokines, and growth factors. The inflammatory response removes debris and pathogens from the wound and encourages repair cell proliferation (Landén *et al.*, 2016). Growth factors like TGF-β and VEGF increase angiogenesis, enhance fibroblast and epithelial cell proliferation and engage in tissue regeneration and wound healing (Johnson and Wilgus, 2014). The wound microenvironment balances pro-inflammatory signals, propagated by M1 type macrophages, which begin the healing cascade. By converting into M2 macrophages with anti-inflammatory signals, it diminishes inflammation and helps in late phases of wound healing (Wang *et al.*, 2022, Landén *et al.*, 2016, Nirenjen *et al.*, 2023). Oxygen availability, pH, nutrition, and metabolic waste products also influence the wound, modifying cellular metabolism and enzymes involved in collagen formation, wound contraction, and bacterial defence (Guo and DiPietro, 2010, Li *et al.*, 2022, Wang *et al.*, 2024).

Cellular activation begins with chemotaxis, altering the biochemical and functional features of neutrophils, macrophages, and lymphocytes (Metzemaekers *et al.*, 2020, Wilkinson and Hardman, 2020). Macrophages and lymphocytes play critical roles in wound healing, (Leibovich and Ross, 1975) although neutrophils, needed for phagocytosis and antimicrobial defence (Simpson and Ross, 1972). Activated macrophages, caused by early platelet release and phagocytosis of debris, generate cytokines that promote wound healing procedure (**Fig. 1.1**) (Nirenjen *et al.*, 2023, Mosser *et al.*, 2021). The macrophages exhibited distinct healing responses in wound repair, influenced by their quantity and phenotypic characteristics (Beezhold and Personius, 1992). The preliminary inflammatory phase of wound healing is marked by the presence of M1 macrophages, which with proinflammatory cytokines, including IL-6, TNF-α and IL-1β, promotes inflammation and attracts other immune cells to the wound site. Activated macrophages primarily release inducible nitric oxide (iNO), which has antibacterial characteristics. iNO release is quite high in the hypoxic wound environment, which creates reactive nitrogen species like peroxynitrite ($ONOO^-$) to destroy microbial DNA, proteins, and lipids (Krzyszczyk *et al.*, 2018), to participate in phagocytosis, eliminating dead cells, debris, and pathogens; and this is crucial for establishing a clean wound bed. Inducible nitric oxide synthase (iNOS) is also overexpressed in chronic wounds due to persistent

inflammation triggered by factors like infection, hypoxia, and pro-inflammatory cytokines. This leads to excessive nitric oxide (NO) production by immune cells, which, while important for immune defense, can cause tissue damage, oxidative stress, and interfere with normal healing processes such as collagen formation and angiogenesis. The sustained iNOS expression in chronic wounds exacerbates inflammation and impairs wound healing. During the healing process, macrophages transition from M1 to the M2 phenotype happens in the latter stages, particularly during the resolution and repair phases. M2 macrophages produce anti-inflammatory cytokines including IL-10 and TGF-β to reduce inflammation and promote tissue healing. They stimulate angiogenesis, fibroblast proliferation, and collagen production, which are required for tissue regeneration, wound healing, and extracellular matrix remodelling. Cytokines generated by macrophages recruit lymphocytes, which in turn release lymphokines such as interferons (IFN) and interleukins (IL), maintaining cytokine presence in the wound and emphasizing the delicate cellular connections throughout healing process (Arango Duque and Descoteaux, 2014, Barrientos *et al.*, 2008).

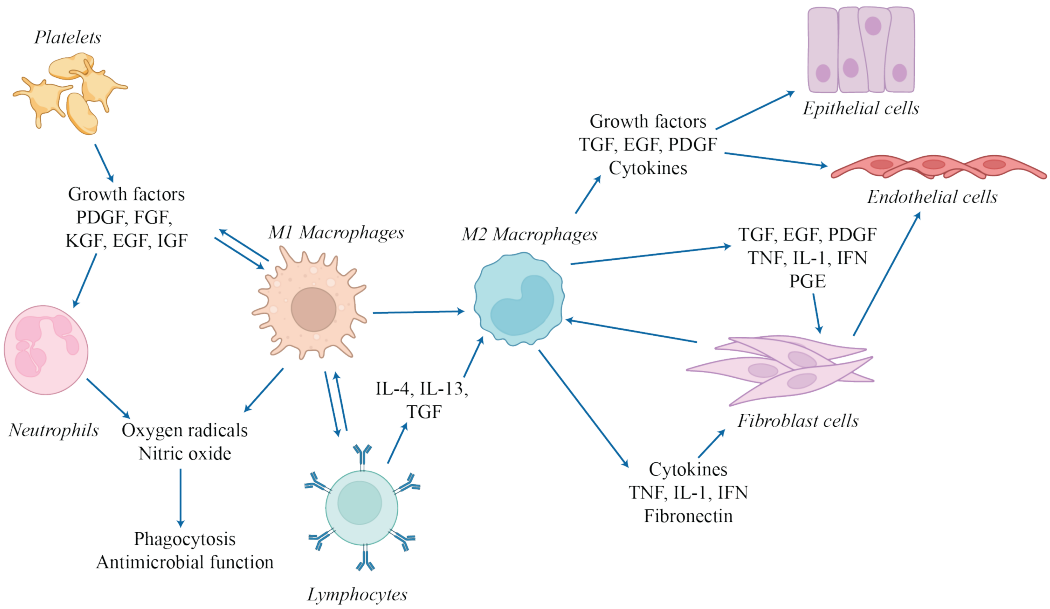

Figure 1.1. *The biological interaction between wound resident cells for the progress of healing activity.*

Fibroblasts, defined by increased collagen production and involved in contraction, entered into the wound from surrounding tissue (Gomes *et al.*, 2021). Endothelial cells also protrude from the surrounding venules, producing new capillaries by angiogenesis. Growth factors and cytokines from platelets and activated macrophages support this expansion (van Hinsbergh, 2012). Epithelial cells multiply from wound edges or undamaged islands, re-establishing a

barrier against fluid losses and infections (Rousselle *et al.*, 2019). The mechanism for completing the proliferative period and the destination of cells post-healing remain unknown, however, neutrophils undergo apoptosis and are devoured by macrophages, and drain via local lymph nodes (Ramos and Oehler, 2024).

In a complete wound healing process, macrophages perform a crucial job as a custodian of entire wound ecosystem to conclude the functions of each and every wound resident cell from the initial homeostasis imbalance and inflammation to final tissue remodelling. Therefore understanding the wound macrophage dynamics is in high demand which assists in refining wound care therapies, improving patient outcomes, and minimizing the healthcare burden of chronic wounds.

1.2. Abnormalities in diabetic chronic wound

Type 2 diabetes is a chronic metabolic disorder characterized by obesity, dyslipidaemia, insulin resistance, hyperglycaemia, and hyperinsulinemia (Rodríguez-Rodríguez *et al.*, 2022). Hyperglycaemia in diabetes promotes mitochondrial dysfunction and accelerates the generation of reactive oxygen species (ROS), creating oxidative stress in numerous tissues. This oxidative stress damages mitochondria and macromolecules like proteins, lipids, and nucleic acids, leading to vascular diseases (Bhatti *et al.*, 2022, Tangvarasittichai, 2015, Kowluru and Mishra, 2015). Additionally, non-enzymatic attachment of glucose and its toxic derivatives (such as glyoxal, methylglyoxal, and 3-deoxyglucosone) to macromolecules forms advanced glycation end products (AGEs), which promote inflammation (Berlanga-Acosta *et al.*, 2013, Kawahito *et al.*, 2009, Price *et al.*, 2010). AGEs activate receptors on immune cells, increasing pro-inflammatory cytokine production and free radical formation. Persistent high glucose levels in uncontrolled type 2 diabetes can induce glucose toxicity, leading to complications include nephropathy, neuropathy, retinopathy, and dermatopathy (Daryabor *et al.*, 2020).

A wound chronicity is defined as when the wound does not heal in a way that recovers its anatomical and functional integrity in a timely and systematic manner (Lazarus *et al.*, 1994). Inadequate development and strengthening of mature granulation tissue and repeated stalling of inflammation are prominent hallmarks of diabetic foot ulcers (DFUs), which are typical long-lasting lesions. These leads to tissue disintegration due to the excessive formation of AGEs and ROS in the wound site. This degradative environment depletes local growth factors and their receptors, hindering fibroblasts and endothelial cells from fully participating in the healing process (Berlanga-Acosta *et al.*, 2017, Edmonds *et al.*, 2021). Wound macrophages tend to shift towards an M1-like inflammatory state when exposed to high glucose levels, as seen in both lab studies and chronic diabetic patients (Torres-Castro *et al.*, 2016). Conversely, the M2

subtype is recognized for its anti-inflammatory and healing-promoting nature. Additionally, diabetic wound macrophages exhibit reduced efferocytosis, a mechanism for removing apoptotic debris in the wound bed, which amplifies the local surge of pro-inflammatory cytokines, prolonging inflammation and boosting the wound chronicity (Khanna *et al.*, 2010).

Hyperglycaemia and insulin deficiency are the primary etiological factors underlying diabetes-related immunodeficiency and heightened susceptibility to infections (Rubinstein *et al.*, 2008, Arya *et al.*, 2014). In high glucose conditions, both in vitro and *in vivo* models have revealed reduced complement receptors, adhesion capacity, phagocytosis, and antibacterial activity. Increased levels of various pro-inflammatory markers contribute to the diabetic systemic low-grade inflammatory phenotype, which can introduce chromatin alterations that promote the chronic pro-inflammatory state (Liu *et al.*, 2012). Glycoxidation products are lethal to granulation tissue, further boosting pro-inflammatory and pro-oxidative circuits via receptors of AGEs (RAGE). These glycoxidative chemicals accumulate in non-labile dermal collagen, resulting in cutaneous cell damage and early senescence (Singh *et al.*, 2014). This impairs fibroblast and endothelial cell physiology, consequently reducing granulation tissue formation and maturation.

Conclusively, within the wound, the trio of TNF-α, ROS, and AGE may drive the death of fibroblasts and vascular cells leading to inflammation, lowering growth factor availability, and opening the gate for "wound senescent cell society." Consequently, repair-committed cells in diabetics undergo proliferative arrest, senescence, and death (Lee *et al.*, 2021, Andrade *et al.*, 2022). It has been hypothesized that an incomplete program of keratinocyte activation and differentiation is the reason for the establishment of mitotically active—but not migrating—epithelial cells at the wound's leading edge. High glucose level has a deleterious effect on keratinocytes, lowering their proliferation, replicative lifetime, and migratory responses. As long as the incision is not reopened, the danger of infection and amputation remains substantial (Wang and Graves, 2020, Giri *et al.*, 2018, Li *et al.*, 2019).

About 15%–25% of diabetes patients develop foot ulcers over their lifetime, and half of these ulcers get infected. Infection can spread to soft tissues and bone, making it the leading causal factor of lower limb amputation in most nations (Boulton *et al.*, 2018, Yazdanpanah *et al.*, 2018). Diabetic foot infection (DFI) is defined as the presence of an inflammatory reaction and tissue damage that may move forward across the clinical spectrum from superficial cellulitis (mild infection) to persistent osteomyelitis (severe infection). The intensity of infection rely on interaction with host–microorganisms and being crucial in determining progression, (Casadevall and Pirofski, 2003) which suggests that infection outcomes depend on

mutual contributions of both the infectious bacteria and the host microbes (Spichler *et al.,* 2015).

It is vital to look into the variety of the microbial population and its likely interactions, as they may evolve into cooperative pathogenic loops that increase antibiotic resistance and imprint a specific signature on each unique ulcer (Sadeghpour Heravi *et al.*, 2019, Banu *et al.*, 2015). DFI is often related to existing biofilm in the formation of ulcers. Biofilm is a habitat for symbiotic microbe interactions that successfully function as a protective layer for bacterial populations, supporting survival and antibiotic resistance. This community is a combination not only of bacterial cells but also of fungi, viruses, proteins, extracellular DNA, and other biogenic components that improve virulence and degrade therapeutic efficiency (Vestby *et al.*, 2020, Decho and Gutierrez, 2017).

In conclusion, addressing hyperinflammation and restoring leukocyte function continues to be a complex challenge, resulting in infections remaining a severe consequence of DFUs. These infections prolong inflammation, decrease local immune responses, limit fibroblast and keratinocyte activity, and further upset the host's internal balance. The constant formation of biofilm in DFUs makes infection elimination a laborious effort. Despite extensive research efforts, DFUs prevalence continue to climb, and reductions in amputation rates are minor at best. However, optimism lies in developing therapy targets: regulating epigenetic drivers of chronic inflammation, decreasing wound cell-senescent drivers to restore acute wound healing, and treating the immunological deficiencies generated by hyperglycaemia and insulinopenia. These scientific initiatives must be supplemented with comprehensive diabetes self-care education and regular examinations by professionals to actually flip the trend against DFUs.

1.3. Challenges of drug delivery in diabetic chronic wound

Administering medication to diabetic wounds poses significant difficulties. Poor blood circulation, especially in the feet, makes it hard for adequate treatment to reach the wound (Spampinato *et al.*, 2020, Frykberg and Banks, 2015). Hyperglycaemia, a distinguishing characteristic of diabetes, has adverse effects on wound healing by increasing AGEs, a biochemical process that affects the structural and functional properties of therapeutic molecules, consequently lowering their efficacy and complicating their formulation. Furthermore, the wound environment is characterized by continuous inflammation, driven by high levels of pro-inflammatory cytokines and mediators, which produce circumstances unfavourable for tissue healing. Excessive protease activity exacerbates this problem, destroying therapeutic medicines before they can have their intended benefits. Additionally, the variable pH levels in chronic wounds provide a dynamic environment that further reduces the

efficiency of prescribed drugs (McCarty and Percival, 2013). This chronic inflammatory state keeps the wound in a protracted phase of immune activation, limiting the transition of cellular processes into the key stages of proliferation and remodelling necessary for tissue regeneration (Mieczkowski *et al.*, 2022).

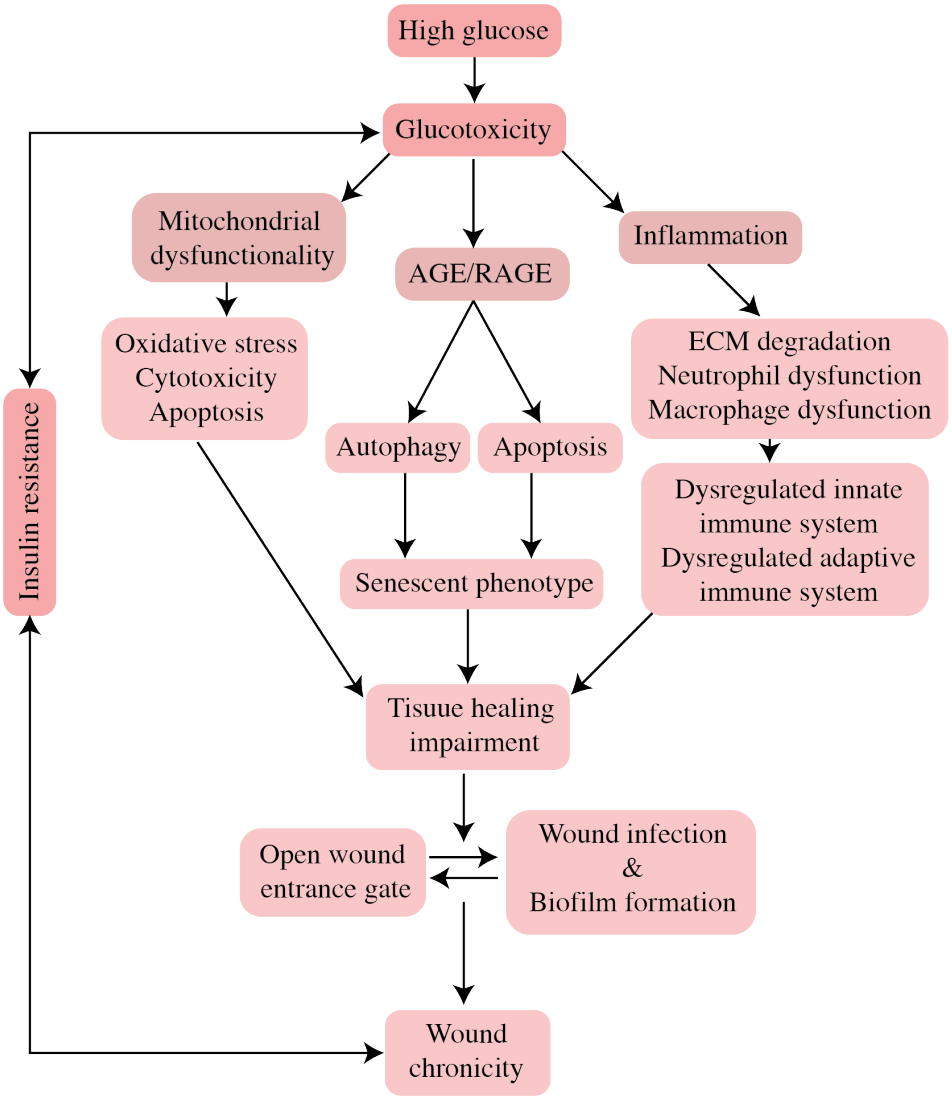

Figure 1.2. *Hyperglycaemia-associated wound healing complications.*

Within the wound environment, biofilms build a durable barrier that shields bacterial populations from both antibiotics and immune system responses. These biofilms behave as complex entities, engaged in continual communication and modification to elude even the most modern treatment methods (Vestby *et al.*, 2020). Drug resistance provides added complication to wound treatment. Repeated use of antibiotics can lead to bacteria developing and becoming more resistant, making them increasingly difficult to remove (Munita and Arias, 2016, Breijyeh *et al.*, 2020).

Despite these limitations, novel medication delivery technologies such as hydrogels, nanoparticles, and smart bandages can efficiently handle these issues. These sophisticated dressings distribute medicine gradually and consistently while promoting a healing- friendly environment and offering protection against infections. Combining multiple drugs can concurrently treat inflammation, infection, and promote recovery.

1.4. Research questions

It is well established that wounds in diabetics experience chronicity because of persistent inflammation which slows down the healing process. To effectively address inflammation in chronic diabetic wounds, a comprehensive strategy is needed that focuses on several parts of the inflammatory process and the wound environment. Effective techniques include the use of gene-targeted therapy to decrease the levels of detrimental pro-inflammatory cytokines, and modify inflammatory gene expression through epigenetic modulation, which can induce pro-healing activity. It is important to encourage the transition of macrophages from the pro-inflammatory M1 phenotype to the anti-inflammatory M2 phenotype. Advanced wound dressings, such as hydrogels and nanoparticles, provide tailored delivery of gene-specific nucleic acids and protection against low-grade bacterial infection and oxidant activity. There are several questions to address and understand healing orchestration by reducing pro-inflammatory burden, which include: (1) What is the impact of hyperglycaemia on the defensive state of macrophages in the progression of chronic wounds? (2) Who are the key players in pro-inflammatory induction under hyperglycaemic conditions? (3) Can diabetic chronic wounds with low-grade bacteria and oxidative stress be alleviated with dressings made of natural polymers? (4) How can a multifunctional hydrogel system be engineered to deliver gene-targeted nucleic acids that attenuate pro-inflammatory load and boost healing potential in the chronic wound bed? By diving into these important concerns, we may explore the impact of hyperglycaemia on wound chronicity to better control the healing process.

1.5. Relevance of the study

This thesis proposes to explore the molecular pathways involved in the development of patho-physiology in terms of inflammation, under hyperglycaemic circumstances in wound milieu. The key aim was to understand the impact of hyperglycaemia on the enrichment of pro-inflammatory macrophages in the wound environment. This endeavour will helps in identifying the molecular target of keeping the macrophage inflamed under diabetic condition and find additional factors implicated in the disease. Such insights could pave the door for discovering

possible treatment targets to address diabetic foot ulcers. Studies were planned to be done on human diabetic patient samples and *in vivo* models of Streptozotocin (STZ)-induced high-fat diet (HFD) diabetic mice model for physiological relevance. Further, this study will also examine the most efficient material which can be used for biopolymer-based dressings to decrease extracellular stressors, such as enhanced oxidant activity, low-grade bacterial infections, in chronic wounds and to study the therapeutic potential of target molecule using a multifunctional hydrogel approach in STZ-induced HFD mice models. Collectively, the unique insights on hyperglycaemia-induced molecular targets in wound macrophages and their regulation by hydrogel-based nucleic acid therapeutics promise to supply new paths for researchers and clinicians. This will pave the road for future preclinical studies targeted at developing treatments for diabetes-related wound macrophage dysfunction.

1.6. Overarching aim

This thesis aims to address the challenges in chronic diabetic wound healing by elucidating the role of key molecular regulators and managing bacteria by developing innovative therapeutic approach. The study focuses on the role of Zeb2 in macrophage polarization, the development of multifunctional biopolymers to combat bacterial infections, and the creation of an affordable, adjustable hydrogel system to effectively deliver therapeutic agents to reduce inflammation and promote wound healing.

1.7. Specific objectives

On the basis of basic understanding and research gap, this thesis work divide in three specific aims:

Objective 1: To elucidate the role of Zeb2 in macrophage phenotypic skewing associated with non-healing diabetic wound.

Objective 2: To prepare a multifunctional biopolymer to alleviate the low-grade bacterial infections in chronic wound.

Objective 3: To develop a cost-effective, tuneable biopolymer-based hydrogel for the efficient delivery of anti-sense oligonucleotides to reduce the inflammatory macrophage burden and boost the wound healing process.

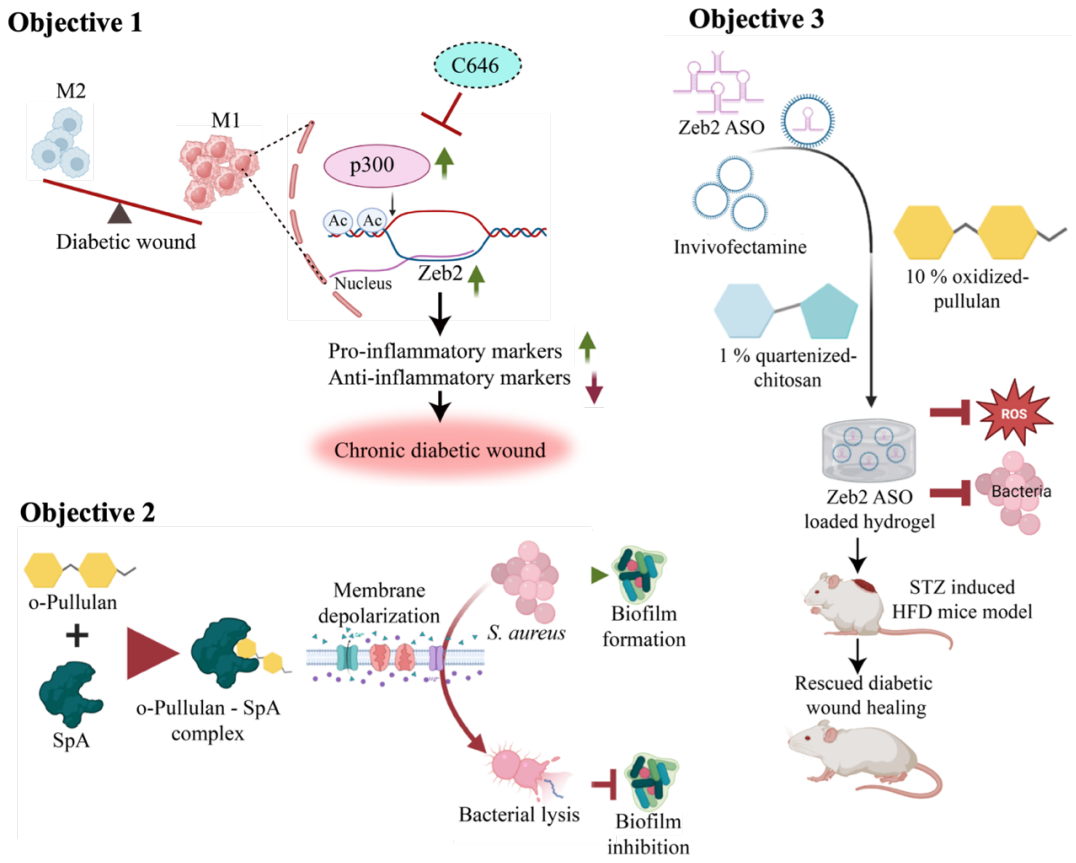

Figure 1.3. *Pictorial outline of the thesis.*

1.8. Thesis outline

This thesis is structured into **six chapters** beginning with **Chapter 1**, the *introduction*, and **Chapter 2** is the *review of the literature*, where reports of *the investigations undertaken to comprehend the wound macrophage dysfunctionality in diabetic patients and it's commercially available treatment methods* are discussed. **Chapters 3-5** *covers the study objectives*. **Chapter 6** *summarizes* the *conclusion of the thesis*.

Briefly, **Chapter 3** focused on examining the role of hyperglycaemia in sustaining the persistent proinflammatory macrophages burden in diabetic wound scenario. We observed that heightened glucose level promotes inflammation and macrophage polarization, directly correlating with increased acetyltransferase activity. Overactivation of P300 HAT functions spark a surge in proinflammatory markers while dampening anti-inflammatory ones, coupled with heightened Zeb2 expression. However, inhibiting acetyltransferase activity with C646, an acetylation inhibitor, tempers the pro-inflammatory profile and downregulates Zeb2 expression in hyperglycaemic macrophages. Interestingly, suppressing Zeb2 expression shifted macrophages from a proinflammatory to an anti-inflammatory state, correcting hyperglycaemia

(HG)-induced changes and might be aiding in the resolution of chronic wound healing issues. Moreover, trans-dermal administration of C646 to the wound edges of mice treated with STZ and fed with HFD, significantly improved the wound healing. Recognizing the potential risks of broadly inhibiting acetyltransferase activity, exploration of another specific target is needed to resolve the inflammatory state of HG-induced macrophages. Therefore, targeting Zeb2 in wound-resident macrophages might be a new strategy for tackling the complications of diabetic chronic wounds.

Chronic wounds, complicated with high ROS production and low-grade bacterial infections, pose significant challenges for drug delivery. To tackle this, in our **chapter 4**, we functionalized a biopolymer pullulan to enhance its functional activity. Oxidation of pullulan molecule formed oxidized pullulan (o-pullulan) showed strong antibacterial activity against *S. aureus,* a predominant species in non-healing wound. Molecular docking studies reveal that o-pullulan binds to the bacterial membrane protein SpA, inhibiting Ca^{2+}-Mg^{2+}-ATPase activity and triggering membrane depolarization which leads to lysis of *S. aureus* cells and diminishes biofilm formation. Due to its cytocompatibility with mammalian cells, hemocompatibility, and non-immunotoxic nature, o-pullulan can be effectively used in medical devices and implants to prevent infections in open wounds and eradicate bacterial presence in chronic wounds. This makes o-pullulan an excellent candidate for use in various dressing materials such as gauze, gels, and creams, highlighting its strong potential for drug delivery and wound healing applications.

In **chapter 5**, we fabricated a hydrogel consisting of 10 % oxidized pullulan (o-pullulan) and 1 % quaternized chitosan (q-chitosan), harnessing their powerful antibacterial and antioxidant properties to load *Zeb2* ASO. This hydrogel boasts excellent viscoelastic and self-healing properties. Release kinetics of *Zeb2* ASO incorporated invivofectamine from hydrogel sustains for up to 8 hours. However, in an *in vivo* wound study, application of *Zeb2* ASO-incorporated hydrogel showed impressive healing in STZ-induced HFD mice. This treatment reduced pro-inflammatory markers and enhanced anti-inflammatory markers throughout the healing process. Also, the percentage of wound area closure significantly increased with *Zeb2* ASO delivery. Thus, targeting Zeb2 inhibition in wound-resident macrophages emerges as a promising strategy to correct HG-induced macrophage polarity and accelerate wound healing. Yet, achieving macrophage-specific targeted delivery requires a sophisticatedly engineered hydrogel system that minimizes off-target effects, sustains delivery and ensures precise delivery tailored to the wound environment.

In conclusion, this study elucidates the molecular mechanisms underpinning the inflammatory response in macrophages under high glucose conditions. Our findings identify

Zeb2 as a compelling therapeutic target for modulating the inflammatory profile of these macrophages, presenting novel strategies for mitigating chronic wound complications. Moreover, we have discovered that oxidizing the pullulan biopolymer markedly enhances its antibacterial efficacy against *S. aureus*, suggesting its potential as an advanced wound dressing material for chronic wound management. Finally, the delivery of *Zeb2* ASO via a hydrogel system composed of o-pullulan and q-chitosan in diabetic wounds not only addresses healing challenges but also rejuvenates the healing process by precisely modulating the inflammatory status of resident macrophages.

References

ANDRADE, A. M., SUN, M., GASEK, N. S., HARGIS, G. R., SHARAFIEH, R. & XU, M. 2022. Role of Senescent Cells in Cutaneous Wound Healing. *Biology,* 11 (12)**,** 1731.

ARANGO DUQUE, G. & DESCOTEAUX, A. 2014. Macrophage cytokines: involvement in immunity and infectious diseases. *Front Immunol,* 5**,** 491.

ARYA, A. K., TRIPATHI, R., KUMAR, S. & TRIPATHI, K. 2014. Recent advances on the association of apoptosis in chronic non healing diabetic wound. *World J Diabetes,* 5**,** 756-62.

BANU, A., NOORUL HASSAN, M. M., RAJKUMAR, J. & SRINIVASA, S. 2015. Spectrum of bacteria associated with diabetic foot ulcer and biofilm formation: A prospective study. *Australas Med J,* 8**,** 280-5.

BARRIENTOS, S., STOJADINOVIC, O., GOLINKO, M. S., BREM, H. & TOMIC-CANIC, M. 2008. Growth factors and cytokines in wound healing. *Wound Repair Regen,* 16**,** 585-601.

BARTOLD, M. & IVANOVSKI, S. 2024. Biological processes and factors involved in soft and hard tissue healing. *Periodontology 2000,* 00:1–27.

BEEZHOLD, D. H. & PERSONIUS, C. 1992. Fibronectin fragments stimulate tumor necrosis factor secretion by human monocytes. *Journal of Leukocyte Biology,* 51**,** 59-64.

BERLANGA-ACOSTA, J., FERNÁNDEZ-MONTEQUÍN, J., VALDÉS-PÉREZ, C., SAVIGNE-GUTIÉRREZ, W., MENDOZA-MARÍ, Y., GARCÍA-OJALVO, A., FALCÓN-CAMA, V., GARCÍA DEL BARCO-HERRERA, D., FERNÁNDEZ-MAYOLA, M., PÉREZ-SAAD, H., PIMENTEL-VÁZQUEZ, E., URQUIZA-RODRÍGUEZ, A., KULIKOVSKY, M. & GUILLÉN-NIETO, G. 2017. Diabetic Foot Ulcers and Epidermal Growth Factor: Revisiting the Local Delivery Route for a Successful Outcome. *Biomed Res Int,* 2923759.

BERLANGA-ACOSTA, J., SCHULTZ, G. S., LÓPEZ-MOLA, E., GUILLEN-NIETO, G., GARCÍA-SIVERIO, M. & HERRERA-MARTÍNEZ, L. 2013. Glucose toxic effects on granulation tissue productive cells: the diabetics' impaired healing. *Biomed Res Int,* 256043.

BHATTI, J. S., SEHRAWAT, A., MISHRA, J., SIDHU, I. S., NAVIK, U., KHULLAR, N., KUMAR, S., BHATTI, G. K. & REDDY, P. H. 2022. Oxidative stress in the pathophysiology of type 2 diabetes and related complications: Current therapeutics strategies and future perspectives. *Free Radical Biology and Medicine,* 184**,** 114-134.

BOULTON, A. J. M., ARMSTRONG, D. G., KIRSNER, R. S., ATTINGER, C. E., LAVERY, L. A., LIPSKY, B. A., MILLS, J. L., SR. & STEINBERG, J. S. 2018. Diagnosis and Management of Diabetic Foot Complications. *Compendia,* 1-20.

BREIJYEH, Z., JUBEH, B. & KARAMAN, R. 2020. Resistance of Gram-Negative Bacteria to Current Antibacterial Agents and Approaches to Resolve It. *Molecules,* 25.

CASADEVALL, A. & PIROFSKI, L. A. 2003. The damage-response framework of microbial pathogenesis. *Nat Rev Microbiol,* 1**,** 17-24.

CHHABRA, S., CHHABRA, N., KAUR, A. & GUPTA, N. 2017. Wound Healing Concepts in Clinical Practice of OMFS. *J Maxillofac Oral Surg,* 16**,** 403-423.

DARYABOR, G., ATASHZAR, M. R., KABELITZ, D., MERI, S. & KALANTAR, K. 2020. The Effects of Type 2 Diabetes Mellitus on Organ Metabolism and the Immune System. *Frontiers in Immunology,* 11.

DECHO, A. W. & GUTIERREZ, T. 2017. Microbial Extracellular Polymeric Substances (EPSs) in Ocean Systems. *Frontiers in Microbiology,* 8.

EDMONDS, M., MANU, C. & VAS, P. 2021. The current burden of diabetic foot disease. *J Clin Orthop Trauma,* 17**,** 88-93.

FITRIDGE, R. & THOMPSON, M. 2011. *Mechanisms of Vascular Disease. A Reference Book for Vascular Specialists*, University of Adelaide Press.

FRYKBERG, R. G. & BANKS, J. 2015. Challenges in the Treatment of Chronic Wounds. *Adv Wound Care (New Rochelle),* 4**,** 560-582.

GIRI, B., DEY, S., DAS, T., SARKAR, M., BANERJEE, J. & DASH, S. K. 2018. Chronic hyperglycemia mediated physiological alteration and metabolic distortion leads to organ dysfunction, infection, cancer progression and other pathophysiological consequences: An update on glucose toxicity. *Biomedicine & Pharmacotherapy,* 107**,** 306-328.

GOMES, R. N., MANUEL, F. & NASCIMENTO, D. S. 2021. The bright side of fibroblasts: molecular signature and regenerative cues in major organs. *npj Regenerative Medicine,* 6**,** 43.

GUO, S. & DIPIETRO, L. A. 2010. Factors Affecting Wound Healing. *Journal of Dental Research,* 89**,** 219-229.

JOHNSON, K. E. & WILGUS, T. A. 2014. Vascular Endothelial Growth Factor and Angiogenesis in the Regulation of Cutaneous Wound Repair. *Adv Wound Care (New Rochelle),* 3**,** 647-661.

KAWAHITO, S., KITAHATA, H. & OSHITA, S. 2009. Problems associated with glucose toxicity: role of hyperglycemia-induced oxidative stress. *World J Gastroenterol,* 15**,** 4137-42.

KHANNA, S., BISWAS, S., SHANG, Y., COLLARD, E., AZAD, A., KAUH, C., BHASKER, V., GORDILLO, G. M., SEN, C. K. & ROY, S. 2010. Macrophage dysfunction impairs resolution of inflammation in the wounds of diabetic mice. *PLoS One,* 5**,** e9539.

KOWLURU, R. A. & MISHRA, M. 2015. Oxidative stress, mitochondrial damage and diabetic retinopathy. *Biochimica et Biophysica Acta (BBA) - Molecular Basis of Disease,* 1852**,** 2474-2483.

KRZYSZCZYK, P., SCHLOSS, R., PALMER, A. & BERTHIAUME, F. 2018. The Role of Macrophages in Acute and Chronic Wound Healing and Interventions to Promote Pro-wound Healing Phenotypes. *Front Physiol,* 9**,** 419.

LANDÉN, N. X., LI, D. & STÅHLE, M. 2016. Transition from inflammation to proliferation: a critical step during wound healing. *Cell Mol Life Sci,* 73**,** 3861-85.

LAZARUS, G. S., COOPER, D. M., KNIGHTON, D. R., MARGOLIS, D. J., PECORARO, R. E., RODEHEAVER, G. & ROBSON, M. C. 1994. Definitions and Guidelines for Assessment of Wounds and Evaluation of Healing. *Archives of Dermatology,* 130**,** 489-493.

LEE, Y. I., CHOI, S., ROH, W. S., LEE, J. H. & KIM, T. G. 2021. Cellular Senescence and Inflammaging in the Skin Microenvironment. *Int J Mol Sci,* 22(8), 3849.

LEIBOVICH, S. J. & ROSS, R. 1975. The role of the macrophage in wound repair. A study with hydrocortisone and antimacrophage serum. *Am J Pathol,* 78**,** 71-100.

LI, L., ZHANG, J., ZHANG, Q., ZHANG, D., XIANG, F., JIA, J., WEI, P., ZHANG, J., HU, J. & HUANG, Y. 2019. High Glucose Suppresses Keratinocyte Migration Through the Inhibition of p38 MAPK/Autophagy Pathway. *Frontiers in Physiology,* 10, 24.

LI, X., YANG, Y., ZHANG, B., LIN, X., FU, X., AN, Y., ZOU, Y., WANG, J.-X., WANG, Z. & YU, T. 2022. Lactate metabolism in human health and disease. *Signal Transduction and Targeted Therapy,* 7**,** 305.

LIU, H. F., ZHANG, H. J., HU, Q. X., LIU, X. Y., WANG, Z. Q., FAN, J. Y., ZHAN, M. & CHEN, F. L. 2012. Altered polarization, morphology, and impaired innate immunity germane to resident peritoneal macrophages in mice with long-term type 2 diabetes. *J Biomed Biotechnol,* 867023.

MCCARTY, S. M. & PERCIVAL, S. L. 2013. Proteases and Delayed Wound Healing. *Adv Wound Care (New Rochelle),* 2**,** 438-447.

METZEMAEKERS, M., GOUWY, M. & PROOST, P. 2020. Neutrophil chemoattractant receptors in health and disease: double-edged swords. *Cellular & Molecular Immunology,* 17**,** 433-450.

MIECZKOWSKI, M., MROZIKIEWICZ-RAKOWSKA, B., KOWARA, M., KLEIBERT, M. & CZUPRYNIAK, L. 2022. The Problem of Wound Healing in Diabetes-From Molecular Pathways to the Design of an Animal Model. *Int J Mol Sci,* 19;23(14):7930.

MOSSER, D. M., HAMIDZADEH, K. & GONCALVES, R. 2021. Macrophages and the maintenance of homeostasis. *Cellular & Molecular Immunology,* 18**,** 579-587.

MUNITA, J. M. & ARIAS, C. A. 2016. Mechanisms of Antibiotic Resistance. *Microbiol Spectr,* 4(2):10.1128.

NIRENJEN, S., NARAYANAN, J., TAMILANBAN, T., SUBRAMANIYAN, V., CHITRA, V., FULORIA, N. K., WONG, L. S., RAMACHAWOLRAN, G., SEKAR, M., GUPTA, G., FULORIA, S., CHINNI, SURESH V. & SELVARAJ, S. 2023. Exploring the contribution of pro-inflammatory cytokines to impaired wound healing in diabetes. *Frontiers in Immunology,* 14:1216321.

PRICE, C. L., HASSI, H. O., ENGLISH, N. R., BLAKEMORE, A. I., STAGG, A. J. & KNIGHT, S. C. 2010. Methylglyoxal modulates immune responses: relevance to diabetes. *J Cell Mol Med,* 14**,** 1806-15.

RAMOS, C. & OEHLER, R. 2024. Clearance of apoptotic cells by neutrophils in inflammation and cancer. *Cell Death Discovery,* 10**,** 26.

RODRIGUES, M., KOSARIC, N., BONHAM, C. A. & GURTNER, G. C. 2019. Wound Healing: A Cellular Perspective. *Physiological Reviews,* 99**,** 665-706.

RODRÍGUEZ-RODRÍGUEZ, N., MARTÍNEZ-JIMÉNEZ, I., GARCÍA-OJALVO, A., MENDOZA-MARI, Y., GUILLÉN-NIETO, G., ARMSTRONG, D. G. & BERLANGA-ACOSTA, J. 2022. Wound Chronicity, Impaired Immunity and Infection in Diabetic Patients. *MEDICC Rev,* 24**,** 44-58.

ROUSSELLE, P., BRAYE, F. & DAYAN, G. 2019. Re-epithelialization of adult skin wounds: Cellular mechanisms and therapeutic strategies. *Advanced Drug Delivery Reviews,* 146**,** 344-365.

RUBINSTEIN, R., GENARO, A. M., MOTTA, A., CREMASCHI, G. & WALD, M. R. 2008. Impaired immune responses in streptozotocin-induced type I diabetes in mice. Involvement of high glucose. *Clin Exp Immunol,* 154**,** 235-46.

SADEGHPOUR HERAVI, F., ZAKRZEWSKI, M., VICKERY, K., D, G. A. & HU, H. 2019. Bacterial Diversity of Diabetic Foot Ulcers: Current Status and Future Prospectives. *J Clin Med,* 8(11):1935.

SETH, I., LIM, B., CEVIK, J., GRACIAS, D., CHUA, M., KENNEY, P. S., ROZEN, W. M. & CUOMO, R. 2024. Impact of nutrition on skin wound healing and aesthetic outcomes: A comprehensive narrative review. *JPRAS Open,* 39**,** 291-302.

SHETTY, V. & BERTOLAMI, C. N. 2022. Wound Healing. *In:* MILORO, M., GHALI, G. E., LARSEN, P. E. & WAITE, P. *Peterson's Principles of Oral and Maxillofacial Surgery.* Cham: Springer International Publishing. ISBN : 978-3-030-91920-7.

SIMPSON, D. M. & ROSS, R. 1972. The neutrophilic leukocyte in wound repair a study with antineutrophil serum. *J Clin Invest,* 51**,** 2009-23.

SINGH, V. P., BALI, A., SINGH, N. & JAGGI, A. S. 2014. Advanced glycation end products and diabetic complications. *Korean J Physiol Pharmacol,* 18**,** 1-14.

SPAMPINATO, S. F., CARUSO, G. I., DE PASQUALE, R., SORTINO, M. A. & MERLO, S. 2020. The Treatment of Impaired Wound Healing in Diabetes: Looking among Old Drugs. *Pharmaceuticals (Basel),* 13(4):60.

SPICHLER, A., HURWITZ, B. L., ARMSTRONG, D. G. & LIPSKY, B. A. 2015. Microbiology of diabetic foot infections: from Louis Pasteur to 'crime scene investigation'. *BMC Med,* 13**,** 2.

TANGVARASITTICHAI, S. 2015. Oxidative stress, insulin resistance, dyslipidemia and type 2 diabetes mellitus. *World J Diabetes,* 6**,** 456-80.

TORRES-CASTRO, I., ARROYO-CAMARENA Ú, D., MARTÍNEZ-REYES, C. P., GÓMEZ-ARAUZ, A. Y., DUEÑAS-ANDRADE, Y., HERNÁNDEZ-RUIZ, J., BÉJAR, Y. L., ZAGA-CLAVELLINA, V., MORALES-MONTOR, J., TERRAZAS, L. I., KZHYSHKOWSKA, J. & ESCOBEDO, G. 2016. Human monocytes and macrophages undergo M1-type inflammatory polarization in response to high levels of glucose. *Immunol Lett,* 176**,** 81-9.

VAN HINSBERGH, V. W. M. 2012. Endothelium—role in regulation of coagulation and inflammation. *Seminars in Immunopathology,* 34**,** 93-106.

VESTBY, L. K., GRØNSETH, T., SIMM, R. & NESSE, L. L. 2020. Bacterial Biofilm and its Role in the Pathogenesis of Disease. *Antibiotics (Basel),* 9(2):59.

WANG, Y. & GRAVES, D. T. 2020. Keratinocyte Function in Normal and Diabetic Wounds and Modulation by FOXO1. *J Diabetes Res,* 2020:3714704.

WANG, Z., QI, F., LUO, H., XU, G. & WANG, D. 2022. Inflammatory Microenvironment of Skin Wounds. *Front Immunol,* 13**,** 789274.

WANG, Z., ZHAO, F., XU, C., ZHANG, Q., REN, H., HUANG, X., HE, C., MA, J. & WANG, Z. 2024. Metabolic reprogramming in skin wound healing. *Burns & Trauma,* 12:tkad047.

WILKINSON, H. N. & HARDMAN, M. J. 2020. Wound healing: cellular mechanisms and pathological outcomes. *Open Biology,* 10**,** 200223.

YAZDANPANAH, L., SHAHBAZIAN, H., NAZARI, I., ARTI, H. R., AHMADI, F., MOHAMMADIANINEJAD, S. E., CHERAGHIAN, B. & HESAM, S. 2018. Incidence and Risk Factors of Diabetic Foot Ulcer: A Population-Based Diabetic Foot Cohort (ADFC Study)-Two-Year Follow-Up Study. *Int J Endocrinol,* 2018**,** 7631659.

ZHENG, S. Y., WAN, X. X., KAMBEY, P. A., LUO, Y., HU, X. M., LIU, Y. F., SHAN, J. Q., CHEN, Y. W. & XIONG, K. 2023. Therapeutic role of growth factors in treating diabetic wound. *World J Diabetes,* 14**,** 364-395.

Chapter 2

Literature review

The skin, being the largest organ in the body, has essential functions like thermoregulation, excretion, vitamin D production, defense against toxins and viruses, and maintenance of physiological hydration (Borena *et al.*, 2015). The skin is a complex and layered anatomical structure, containing the epidermis, dermis, and hypodermis (**Fig. 2.1**). It has constantly renewed stratified squamous epithelial cells, mostly keratinocytes. The dermis, a powerful layer of connective tissue lying underneath the epidermis, provides both structural support, flexibility, and also offers a rich tapestry of extracellular matrix, nutrition, and immunity. Collagen and elastin fibers surround blood vessels, neurons, hair follicles, and sweat glands in the dermis. The epidermis needs this layer for thermoregulation, sensation, and nutrition. The hypodermis, largely adipose tissue, insulates, shock absorbs, and stores energy. These layers operate together to protect the body, manage temperature, and improve sensory awareness, demonstrating the skin's versatility and durability (McGrath and Uitto, 2024).

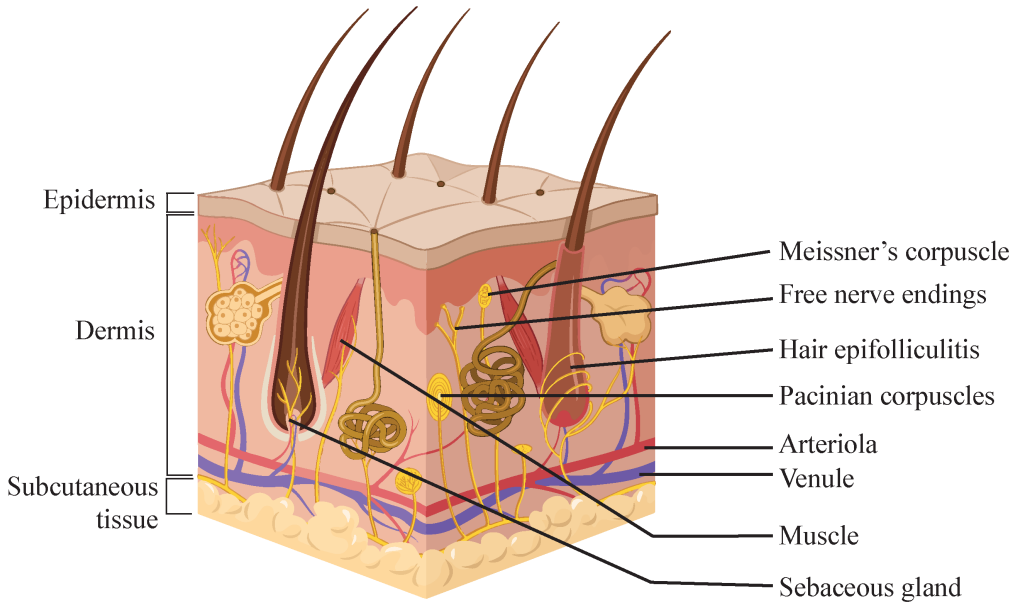

Figure 2.1. *Anatomy of mammalian skin ©Biorender.*

2.1. Overview of wound

A wound is defined as any disturbance to the integrity of the skin, mucous membrane, or organ tissue. Wounds can be classified into two primary categories depending upon the affected tissues upon the injury: *Simple wound*, characterized as a skin injury that does not affect deeper anatomical structures like muscles, bones, nerves, tendons, or major arteries and accompanied by minimal bleeding and pain, without any significant loss of tissue or involvement of critical underlying components (Lalonde *et al.*, 2019). Whereas *complex wound* characterized by exposed bones or tendons and accompanied by excessive bleeding (Ferreira *et al.*, 2006). Wounds may develop from mechanical trauma (cuts, abrasions, lacerations), thermal damage (burns, frostbite), chemical exposure, radiation, and surgery. Additionally, physiological conditions like diabetes may produce chronic ulcers, venous or arterial insufficiency may lead to leg ulcers, and immunological or dermatological diseases may result in persistent or recurring sores (Kujath and Michelsen, 2008). Injuries are characterized as acute or chronic depending on the causes and results. Acute wounds normally follow a well-coordinated healing process, where the body regulates bleeding, manages infection, repairs tissues, and returns the wound site to its former condition within a short, predictable period, maintaining maintained anatomical and functional integrity (Tottoli *et al.*, 2020).

The main goals of wound care are rapid closure and producing a functional, aesthetically acceptable scar. Quick closure lowers infection risk, pain, and speeds healing. A functional scar assures the healed area can manage daily activities efficiently, while an attractive scar improves the patient's psychological well-being. Effective wound care includes thorough cleanliness, precise dressing selection, and sometimes advanced treatments like skin transplants, negative pressure therapy, or bioengineered tissues. Pain therapy, infection control, and addressing underlying disorders are also key components (Nicks *et al.*, 2010).

The surgical wound classification (SWC) system was first created in 1964 by the National Academy of Sciences and the National Research Council to show the bacterial burden in a surgical field (Onyekwelu *et al.*, 2017). These classes include:

Class 1 wounds are classified as *clean wounds*, which are not polluted, do not present any indicators of inflammation, and are generally closed and which do not influence the respiratory, alimentary, vaginal, or urinary systems. Examples of clean wounds are an inguinal hernia repair or a thyroidectomy.

Class 2 wounds are described as *clean-contaminated*, comprising low level of contamination. These sorts of wounds entail invasion into the pulmonary, alimentary, vaginal, or urinary systems but only under regulated circumstances.

Class 3 wounds are recognized as *contaminated* and generally result from a breach in sterile procedures or bleeding from the gastrointestinal system from acute or non-purulent inflammation.

Class 4 wounds are regarded to be *filthy or dirty infected* and generally originate from poor treatment of serious wounds, substantial purulence, and obvious infections. Where tissues lose vitality, and generally caused by surgery or bacteria discovered in pierced organs.

Cutaneous wound healing is a complex biological process that involves hemostasis, inflammation, proliferation, and remodeling in order to restore skin integrity (Borena *et al.*, 2015). Following injury, blood vessels contract and platelets form a clot, closing the wound and avoiding infection while attracting immune cells. Damage signals such as DAMPs and PAMPs activate immune cells, with neutrophils clearing debris and germs before being replaced by macrophages, which flip from promoting inflammation to releasing growth factors for tissue repair. During the proliferative phase, keratinocytes, fibroblasts, and endothelial cells aid in wound healing, granulation tissue formation, and angiogenesis. ECM remodeling replaces fibrin with collagen, resulting in a scar aided by MMPs and elastin synthesis. The process culminates in cellular death, resulting in a scar with incomplete skin strength and structure (Wilkinson and Hardman, 2020).

2.2. Cellular architecture of wound

Restoring skin is the consequence of sequential steps of events where various cells enter and exists in a timely manner (**Fig. 2.2**). Gurtner and his team described skin healing as a biological marvel, showcasing nature's astounding intricacy and perfection (Gurtner *et al.*, 2008). Immediately after an injury, intracellular and intercellular pathways get activated, including the immune response, blood coagulation, and inflammation. This induces changes in gene expression and cell activity, leading to proliferation, differentiation, and migration, which orchestrate a successful healing process over the following days.

2.2.1. Platelets

Platelets play a critical function as gatekeepers of artery integrity through intricate bidirectional relationship with the endothelium. They operate as sentinels, sensing and responding to irregularities in the blood flow and the endothelium layer (Becker *et al.*, 2018). In the early stages of wound healing, platelets control bleeding by contracting vascular smooth muscle and exposing the thrombogenic matrix after injury. Through GPCR activation, they

undergo shape changes and release granules containing ADP, serotonin, calcium, cytokines, and growth factors, leading to fibrin clot formation. This clot limits bleeding, supports inflammation, and serves as a scaffold for tissue repair. Platelets also promote inflammation by producing prostaglandins, leukotrienes, and thromboxanes, attracting immune cells to aid healing (Peña and Martin, 2024). This synchronized activity of platelets not only prevents bleeding but also lays the framework for efficient mending by regulating the early inflammatory processes, crucial for commencing repair processes (Locatelli *et al.*, 2021). Platelets also contribute to sprouting angiogenesis by creating vascular endothelial growth factor (VEGF), hepatocyte growth factor (HGF), epidermal growth factor (EGF), insulin growth factor (IGF) and fibroblast growth factor (FGF) (Italiano *et al.*, 2008). Throughout the healing period, platelets release various proteins from alpha granules, contributing considerably to the repair and regeneration processes (Nurden *et al.*, 2008).

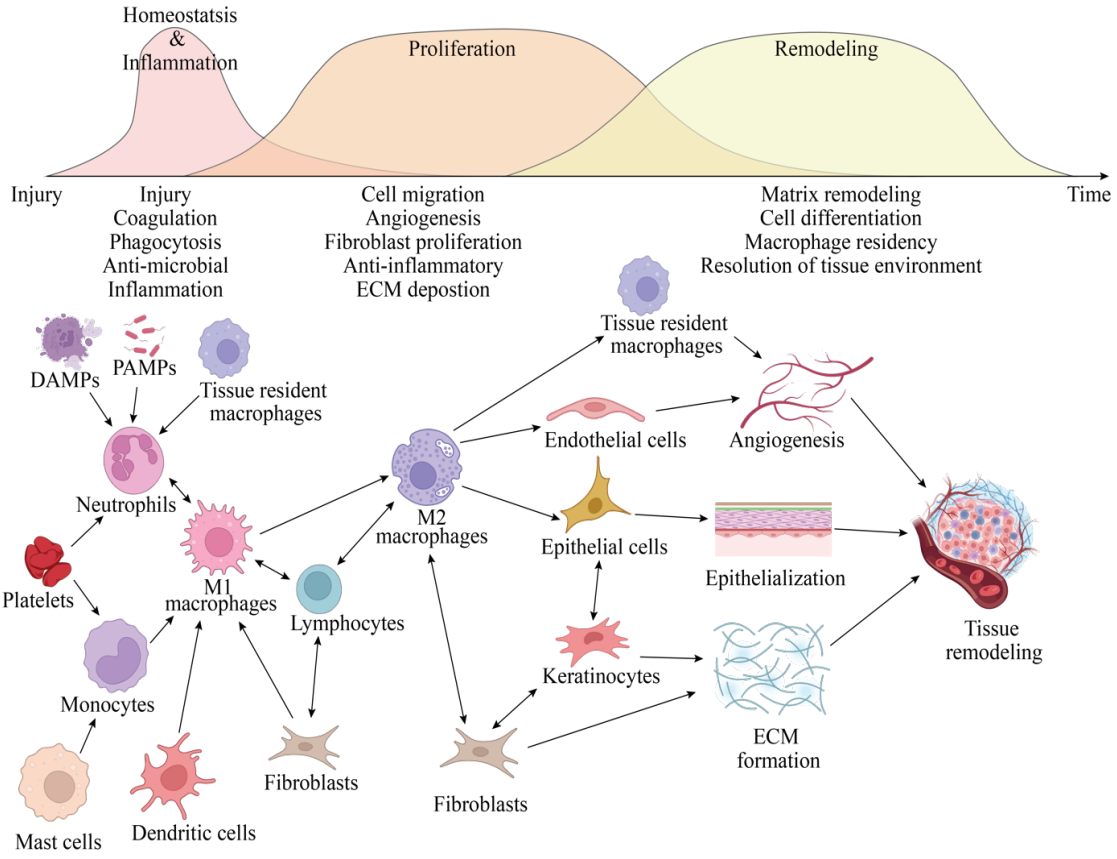

Figure 2.2. *Cellular orchestration in wound healing dynamics.*

2.2.2. Mast cells

Immediately after a wound, mast cells rush to the site, swiftly degranulating and releasing a torrent of vasoactive and proinflammatory mediators such histamine, serotonin, TNF, kinins,

and proteases. This stimulates a cascade of healing activities in the surrounding tissue (Trautmann *et al*., 2000). Histamine enhances capillary permeability and induces vasodilation, enabling neutrophils to overwhelm the injured site. Additionally, VEGF, IL-6, and IL-8 further boost the vascular response (Komi *et al.*, 2020). Increased cellular activity is induced by increased MCP-1 and TGF-β, attracting more mast cells. These cells emit TNF-α, which promotes clot stability by boosting Factor XIIIa production. Leukotrienes, proteases, and cytokines subsequently attract granulocytes, whereas tryptase and cathepsin G enhance endothelial-leukocyte interactions. (Bacci, 2022). Mast cells, equipped with cellular proteases, play a vital role in re-epithelialization, angiogenesis, and fibroplasia. Secreted tryptase induces endothelial cell migration into the ECM, laying the stage for cell proliferation. Positioned near small arteries, connective tissue mast cells ensure a steady supply of essential mediators for effective angiogenesis (Norrby, 2002). The deliberate location of connective tissue MCs near tiny arteries provides a consistent supply of critical mediators for optimum angiogenesis.

Mast cells-released tryptase promotes PAR-2, boosting fibroblast migration, proliferation, and ECM formation. Other mediators include TGF-β, SCF, NGF, GM-CSF, PDGF, VEGF, FGF-2, histamine, and proteases further aid fibroblast proliferation and differentiation, coordinating effective tissue repair and regeneration (Landolina *et al.*, 2015).

2.2.3. Neutrophils

Neutrophils, the unsung heroes of the innate immune system, burst into action in the aftermath of an injury, completing a complex ballet that is important for wound healing. Typically, scarce in healthy skin, these watchful cells are recruited in large number when tissue is harmed (Peña and Martin, 2024). Neutrophils, as first responders, defend against infection and coordinate recovery by following chemical signals to the wound site. Platelet-derived growth factor (PDGF) and connective tissue chemokine activating peptide III (CTAPIII) from platelets, induced by neutrophil-activating peptide 2 (NAP2) and CXCL7, control cellular migration (Brandt *et al.*, 2000). The invasion is activated by DAMPs and mediators such TGF-β, C3a, C5a, and hydrogen peroxide from platelets. These signals activate pattern recognition receptors (PRRs) on neutrophils, like Toll-like receptors (TLRs), guiding them to the spot where they release antimicrobial chemicals and proteases to attack infections (Serhan et al., 2008b), decreasing the threat of infection and giving the foundation for repair. Neutrophils release pro-inflammatory mediators such TNF-α, IL-1β, IL-6, and CXCL8, boosting the inflammatory response and calling more immune cells to join the fight (Wilgus *et al.*, 2013).

As task done, neutrophils die via apoptosis and eliminated with debris phagocytosed by macrophages. At the end of inflammatory phase of healing, various pro-resolving mediators

like lipoxins, resolvins, and protectins are released, which assist in eliminating apoptotic neutrophils from the wound area and leads to decreased inflammation (Serhan et al., 2008a), which moves the wound to the next phase of healing (Serhan et al., 2008b). Therefore, neutrophils not only fight infection but also control inflammation and produce mediators that activate other healing cells which restores tissue integrity with accuracy and efficiency (Nathan, 2006).

2.2.4. Macrophages

Macrophages serve a vital function as important regulators in the delicate process of wound healing, orchestrating a series of events needed for optimum tissue repair. Skin tissue-resident macrophages play a vital role in wound healing process by encouraging the inflow of diverse immune and repair cells into the wound site. Upon injury, these macrophages are activated by the detection of DAMPs (damage-associated molecular patterns) and PAMPs (pathogen-associated molecular patterns), prompting the release of pro-inflammatory cytokines like TNF-α and IL-1β, and chemokines like CXCL8 and CCL2, which recruit immune cells, including neutrophils and monocytes, to the wound site. The cytokines also excite endothelial cells in adjacent blood arteries, prompting them to produce adhesion molecules (e.g., selectins and integrins) that permit the adherence and migration (diapedesis) of immune cells from the circulation into the tissue (Krzyszczyk *et al*., 2018). Typically arriving at the site of injury within 48 to 72 hours, these adaptive cells are recruited by a broad assortment of chemotactic signals emitted by various cell types (Mosser and Edwards, 2008). In the early wound healing phase, pro-inflammatory "M1" macrophages penetrate the site to eliminate infections, debris, and dead cells. Induced by TLR4 and IFN-γ, these macrophages produce a pro-inflammatory milieu necessary for defense and debris clearance. (Ferrante and Leibovich, 2012). As the wound develops to the reparative phase, macrophages change to the anti-inflammatory "M2" phenotype. M2 macrophages enhance tissue regeneration by increasing fibroblast, keratinocyte, and endothelial cell activity. This shift, mediated by IL-4 and IL-13, promotes the production of growth factors including PDGF, FGF-α and β, and TGF-α and β, with FGF-β boosting angiogenesis and cell proliferation (Krzyszczyk *et al.*, 2018). In the proliferative phase, macrophages become important architects of angiogenesis, placing themselves around nascent blood vessels to stimulate the development and stability. They stimulate endothelial cell growth and further promotes angiogenesis. Alongside FGF-β, TNF, IL-6, and IL-1, these macrophages coordinate the creation of collagen, fibronectin, and proteoglycans, laying down the necessary foundation for wound contraction and epithelium regeneration (Qing, 2017).

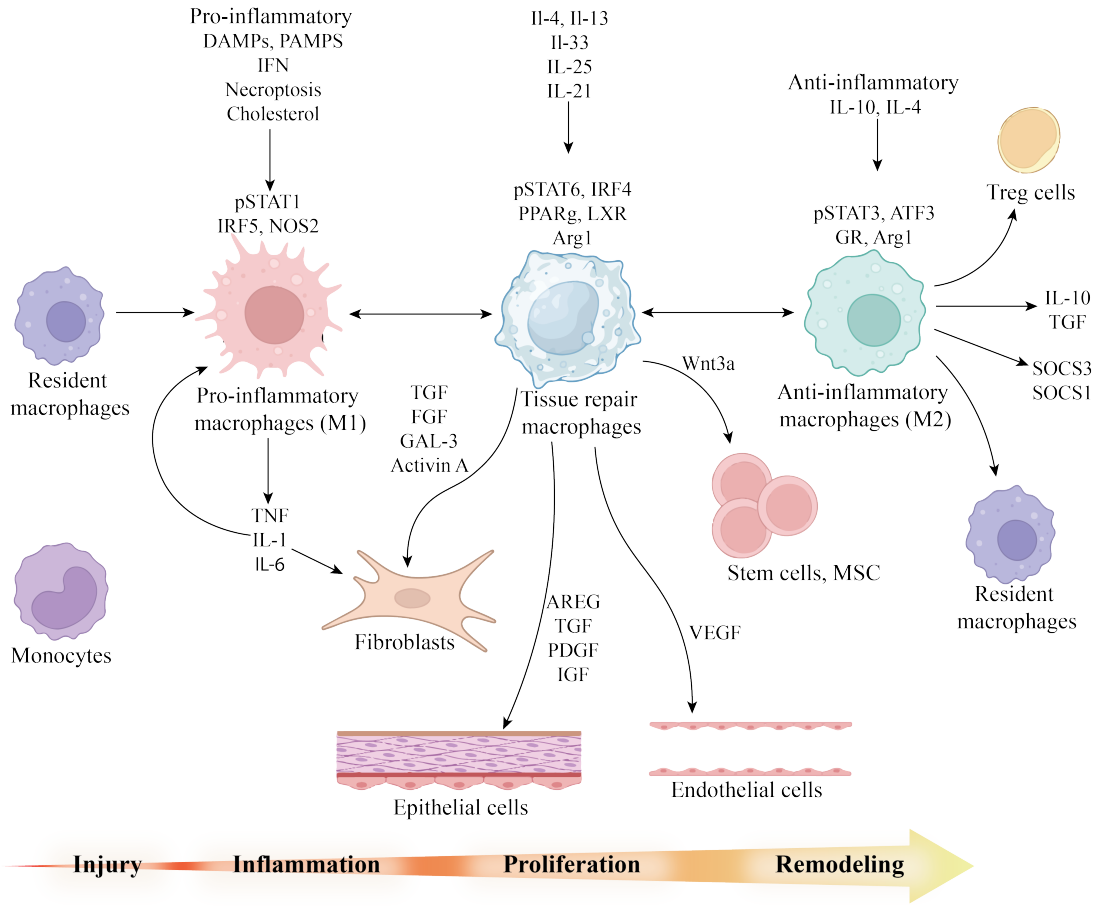

Figure 2.3. *Mechanisms governing the activation of macrophage profiles in wound healing.*

2.2.5. Dendritic cells

Dendritic cells (DCs) operate as crucial directors in the symphony of immune system reactions, orchestrating a complex concerto of immunological activities necessary for keeping balance and repelling threats. In the epidermis, these cells develop into Langerhans cells, adept sentinels vigilantly protecting against any intruders. Associating with mast cells (MCs) is vital for creating major soluble factors like transforming growth factor-beta (TGF-β) and tumor necrosis factor-alpha (TNF-α), which are necessary for the growth and functional readiness of developing DCs. By collecting and processing extracellular antigens and displaying them on major histocompatibility complex (MHC) Class I molecules (Ahrens *et al.*, 2012). These cells also detect "danger signals" like as F-actin from dying cells through receptors like Clec9A, making sure apoptotic cells are rapidly eliminated and T cell responses are correctly managed (Kissenpfennig *et al.*, 2005). Constantly monitoring the epidermis, these sentinel cells check for infections and manage hypersensitive reactions. Upon meeting an antigen, Langerhans cells undergo a radical transformation—reducing E-cadherin levels, a protein that maintains them attached to keratinocytes.

After skin injury, plasmacytoid dendritic cells (pDCs) momentarily reach the wound site, where they react to self-nucleic acids generated by damaged cells. Activated by Toll-like Receptors 7 (TLR7) and 9 (TLR9), these cells create type I interferons, including interferon-alpha (IFN-α) and interferon-beta (IFN-β) (Gregorio *et al.*, 2010). These interferons are crucial for lowering inflammation and increasing antiviral defenses, hence accelerating the healing process. In summary, dendritic cells are the master builders of immune responses, fluidly moving between activity in antigen presentation, inflammation management, and tissue repair.

2.2.6. T Lymphocytes

In the inflammatory phase of wound healing, a cascade of cytokines generated within the microenvironment orchestrates the recruitment and activation of Th1 cells, which are important to this stage of the healing process (Boothby *et al.*, 2020). The activation and recruitment of Th1 cells are further boosted by the presence of IFN-γ and TNF-α in the local environment, with interactions with antigen-presenting cells (Chodaczek *et al.*, 2012). This stimulation causes a morphological change in T cells from dendritic to a more spherical shape. Activated T cells subsequently create a range of keratinocyte growth factors (KGFs), including KGF-1 and KGF-2, as well as insulin-like growth factor-1 (IGF-1). These factors are crucial in promoting the proliferation and migration of keratinocytes, hence speeding the repair of the epidermal layer and permitting effective wound healing and regeneration (Havran and Jameson, 2010).

In the wound healing process, αβ T cells, with subgroups Th1, Th2, and regulatory T cells (Tregs) contributing distinct functions, each subgroup providing a particular flare to the performance (Heath and Carbone, 2013). Th1 cells are adept at targeting and destroying aberrant cells through cytokines like IL-2 and IFN-γ. In contrast, Th2 cells and Tregs moderate the immune response. Th2 cells release IL-4, IL-5, IL-13, and IL-10, which control inflammation and enhance collagen production by fibroblasts, aiding in skin restoration (**Fig 2.4**). Meanwhile, Tregs, often carrying the characteristics of memory, produce cytokines like IL-10 and TGF-β. These substances stimulate macrophages to adopt an M2 phenotype, hence flattening the inflammatory boundaries and promoting a more harmonious healing process (Short *et al.*, 2022).

Invariant natural killer T cells (iNKTs) are like the adaptable maestros of the immune orchestra, incorporating the properties of both T cells and natural killer (NK) cells. In wound healing, iNKTs are vital, producing interferon-gamma (IFN-γ) to regulate inflammation, remove infections, and stimulate tissue regeneration (Cruz *et al.*, 2018).

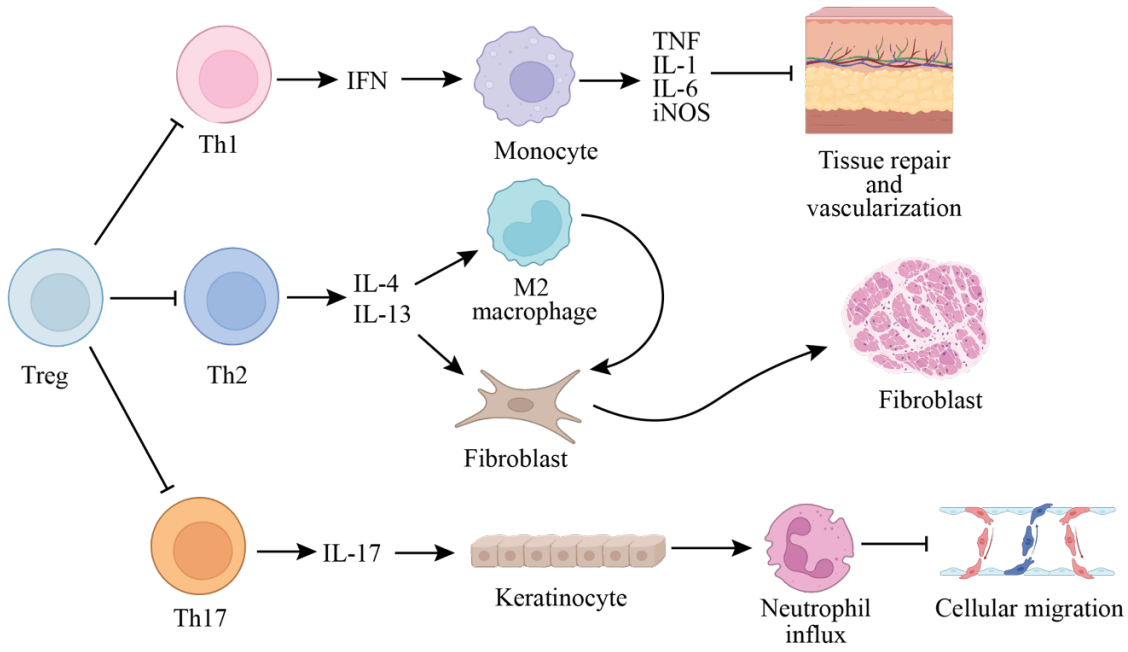

Figure 2.4. *Functional regulation of T lymphocytes in wound healing orchestration.*

2.2.7. Keratinocytes

Keratinocytes are vital for skin wound healing, functioning as alert guardians. Within 24 hours, they immediately move to the injured site. During the inflammatory phase, they create cytokines including interleukins, TNF-α, and TGF-β to attract immune cells, coordinating a robust inflammatory response that eliminates debris and fights infection. Association with immune cells promotes a successful shift from harm to recovery (Piipponen *et al.*, 2020). During the proliferation phase, keratinocytes at the wound margins multiply and travel over the wound bed in a process dubbed re-epithelialization. This stage is crucial for covering the wound with new epithelial tissue and restoring the skin's barrier function (Pastar *et al.*, 2014). Keratinocytes lay down a new basement membrane and manufacture fibronectin and collagen, generating an ECM that promotes cell movement, tissue structure, and new tissue creation during wound healing (Tanzer, 2006). During the remodeling phase, keratinocytes regulate ECM remodeling, balancing collagen production and breakdown to minimize scarring and maintain tissue strength and flexibility. They also release MMPs to fine-tune the healing process by breaking down excess ECM components (Cialdai *et al.*, 2022). Keratinocytes repair the skin barrier by forming tight junctions, producing lipids, and activating stem cells from hair follicles to aid in tissue regeneration and continuous repair. (Piipponen *et al.*, 2020).

Keratinocytes respond to hypoxia in the wound environment by raising the production of angiogenic factors like VEGF, driving new blood vessel development to supply oxygen and

nutrients to healing tissue. They also produce antimicrobial peptides to protect the wound from infection and manufacture immune-modulating chemicals to maintain a healthy immune response.

2.2.8. Endothelial cells

Endothelial cells play a critical role in wound healing by quickly triggering and controlling the inflammatory response. They upregulate adhesion molecules (E-selectin, P-selectin, ICAM-1, VCAM-1) to lead immune cells like neutrophils and macrophages to the wound site by trans-endothelial migration. In tissue healing, angiogenesis is crucial, with new blood vessels sprouting from old ones. This process is driven by growth factors including VEGF, bFGF, and angiopoietins. VEGF stimulates endothelial cells via pathways including PI3K/Akt and MAPK, boosting proliferation and migration (Liu *et al.*, 2023, Akbarian *et al.*, 2022). Endothelial cells produce MMPs to break down ECM for capillary expansion while generating collagen and fibronectin to stabilize new tissue (Gualdoni *et al.*, 2023).

In the remodeling phase of wound healing, endothelial cells become master builders, driving the formation of new blood vessels with the support of signaling molecules like PDGF and TGF-β. Meanwhile, endothelial cells take on the role as attentive builders, directing the deposition and alteration of collagen—the fundamental skeleton of the extracellular matrix. By carefully balancing MMPs and TIMPs, they minimize excessive scarring and guarantee that the newly repaired tissue reaches its optimal strength and usefulness (Witjas *et al.*, 2019).

In response to hypoxia, or low oxygen levels in the wound environment, endothelial cells stimulate hypoxia-inducible factors (HIFs), especially HIF-1α. HIF-1α translocate to the nucleus and increases the transcription of genes associated in angiogenesis, like VEGF and angiopoietin-2 (Krock *et al.*, 2011). This chemical reaction accelerates the formation of new blood vessels, enhancing oxygen supply to the healed tissue. Hypoxia-driven angiogenesis is critical for the survival and function of the newly generated tissues, as it ensures they get sufficient oxygen and nutrients.

2.2.9. Fibroblast cells

Fibroblasts serve a critical role in wound healing, stimulated by cytokines and growth factors such PDGF, TGF-β, and FGF from platelets, macrophages, and endothelial cells (Demidova-Rice *et al.*, 2012b, Barrientos *et al.*, 2008). These factors drive signaling pathways like MAPK/ERK and PI3K/Akt, encouraging fibroblast proliferation and migration to the wound site (Liu *et al.*, 2023). Once there, fibroblasts construct the new tissue by secreting ECM

components such type I and III collagen, fibronectin, and proteoglycans, needed for tissue strength and structure.

In the drama of wound contraction, fibroblasts change into myofibroblasts under the influence of TGF-β and mechanical stress. These specialist cells don the uniform of alpha-smooth muscle actin (α-SMA), which forms stress fibers that flex and draw the wound borders closer, speeding up closure (Putra *et al.*, 2020). During the remodeling phase, fibroblasts become master sculptors of the extracellular matrix (ECM). They manufacture matrix metalloproteinases (MMPs) including MMP-1, MMP-2, and MMP-9 to break down damaged ECM components, clearing the stage for the rearrangement of collagen fibers (Page-McCaw *et al.*, 2007). To maintain balance, fibroblasts also produce tissue inhibitors of metalloproteinases (TIMPs), ensuring ECM turnover is precise and avoids excessive scarring while supporting effective tissue remodeling.

Fibroblasts interact with many cell types during healing by secreting cytokines and growth factors. They create substances that encourage keratinocyte proliferation and migration for re-epithelialization and release chemokines to recruit immune cells for wound cleaning. They also detect mechanical stress and environmental changes by mechano-transduction, with integrins sticking to ECM components to relay signals that modulate gene expression, fibroblast movement, ECM creation, and myofibroblast differentiation.

2.2.10. Epithelial cells

Epithelial cells are crucial for wound healing, stimulated by signalling molecules including EGF, TGF-α, and HGF. These signals drive pathways like MAPK/ERK and PI3K/Akt, causing cell proliferation, migration, and survival (Yao *et al.*, 2024). As epithelial cells migrate, they restore the skin's barrier by forming tight and adherents' junctions. These junctions maintain the epithelial layer's integrity, preventing leaks and protecting against pathogens (Jafari and Rohn, 2022). Epithelial cells also create lipid layers with ceramides and cholesterol to enhance barrier function and prevent dehydration (Choudhary *et al.*, 2024). Additionally, they secrete growth factors like EGF to boost cell proliferation and migration, cytokines like IL-1β to modulate inflammation, and antimicrobial peptides like defensins and cathelicidins to protect the wound from infection (Agier *et al.*, 2015).

Epithelial cells communicate with fibroblasts and endothelial cells to coordinate recovery. They generate fibroblast growth factor (FGF), which energizes fibroblast proliferation and stimulates ECM formation. At the same time, they make VEG), spurring angiogenesis to transport a enough quantity of oxygen and nutrients to the mending tissue. This teamwork precisely connects the new epithelial layer with the underlying connective tissue and blood

vessels (Hong *et al.*, 2014). This sophisticated adaptation boosts oxygen transmission, crucial for the survival and function of the newly forming cells and ensuring that the mending process continues on track. In the remodelling phase, epithelial cells change the ECM and control MMPs to arrange collagen and tissue structure. They cooperate with fibroblasts and, as healing advances, undergo apoptosis, directed by TGF-β, to avoid excessive development and fibrosis, restoring tissue homeostasis. (Theocharis *et al.*, 2019).

In summary, wound healing starts with blood vessel constriction and platelet activation to form a fibrin clot, stopping bleeding and supporting inflammatory cells. Neutrophils first tackle bacteria, followed by monocytes that turn into macrophages within 48-96 hours. The adaptive immune system, including Langerhans cells, dendritic cells, and T cells, manages antigens. As inflammation decreases, angiogenesis begins with endothelial cells forming new blood vessels, aided by pericytes and progenitor cells. Fibroblasts then proliferate, creating granulation tissue and myofibroblasts to contract the wound. They also lay down ECM, transitioning the environment from inflammatory to growth. Re-epithelialization involves epidermal stem cells and differentiated cells repairing the skin, with tissue-resident stem cells from glands and follicles supporting localized healing and releasing growth factors for neovascularization (Rodrigues *et al.*, 2019).

2.3. Chronic wounds

On the contrary chronic wounds frequently find themselves locked in a tenacious standoff with the healing process, failing to move through its stages as they should. This disturbance can be produced by a multitude of circumstances. Underlying problems including diabetes, venous insufficiency, and arterial insufficiency can transform the healing road into a lengthy, painful fight. Diabetes, for instance, alters the delicate balance of blood glucose, compromising immune function and collagen formation, which can put the brakes on recovery. Venous insufficiency inhibits the return of blood from the extremities, creating unrelenting inflammation and a paucity of nutrients at the wound site. Meanwhile, arterial insufficiency throttles blood flow, robbing the tissue of the oxygen and nutrients required for healing, leaving the wound in a condition of protracted limbo. Chronic inflammation can impair recovery by prolonging the inflammatory phase beyond its regular length. In chronic wounds, continuous inflammation leads to continued production of cytokines and proteases, which destroy the ECM and inhibit fibroblast and keratinocyte activity, further delaying the healing process (Martin and Nunan, 2015).

Infections in chronic wounds are a severe concern, potentially hindering the healing process. Persistent infections may lead to inflammation, tissue damage, and poor healing.

Biofilms, thick clumps of bacteria, are exceedingly difficult to eradicate, hiding infections from the immune system and medicines. This prolongs inflammation, hinders healing, and delays wound closure. (Maheswary *et al.*, 2021).

Inadequate blood flow is a key stumbling block in the healing approach. Blood delivers the necessary oxygen and nutrients needed for every phase of wound healing—from inflammation to proliferation to remodeling. When blood flow falters, the wound is deprived of vital resources, leaving cells warring and tissue repair behind. This shortfall can result in longer inflammation and diminished cellular responses, bringing the healing process to a standstill and turning a typical recovery into a drawn-out war (Landén *et al.*, 2016).

The protracted presence of chronic wounds additionally presents significant medical dangers but also dramatically damages the patient's quality of life. Patients with chronic wounds frequently experience continuing pain, discomfort, and restricted mobility. The constant wound care tasks may lead to emotional anguish, loneliness, and poor general state of life. Therefore, treating the underlying causes and implementing suitable treatment is critical to manage persistent wounds efficiently and optimize patient outcomes.

2.4. Chronic Diabetic Wounds

Type 2 diabetes is a complex metabolic disorder distinguished by insulin resistance and reduced insulin production (Petersen and Shulman, 2018). In this condition, cells become less responsive to insulin, which inhibits glucose uptake and metabolism. Prolonged hyperglycemia and elevated fatty acids produce stress on pancreatic β-cells, resulting to lower insulin production. Inflammatory cytokines including TNF-α and IL-6 further impair insulin signaling (Wang *et al.*, 2010, Dludla *et al.*, 2023). Genetic and epigenetic factors also contribute to the disease's development. Chronic hyperglycemia results in repercussions including cardiovascular disease, neuropathy, and nephropathy, while disrupting cellular processes essential for wound healing, increasing the chance of chronic wounds (**Fig. 2.5**) (Suárez *et al.*, 2023, Khullar *et al.*, 2017).

2.4.1. Impaired immune response

In diabetic wounds, high blood glucose levels create advanced glycation end-products (AGEs), which attach to the receptor, RAGE, on immune cells. This stimulates pathways like NF-κB and MAPK. NF-κB leads to pro-inflammatory cytokines like TNF-α and IL-6, whereas MAPK pathways aggravate inflammation and disturb normal cell function (Pradhan *et al.*, 2009, Giri *et al.,* 2018). In diabetes, high oxidative stress from ROS—caused by the polyol

pathway and mitochondrial dysfunction—exacerbates inflammation. ROS damage proteins, lipids, and DNA, disrupting immune cell activities and critical receptors, which affects phagocytosis and chemotaxis, resulting to extended inflammation and increased infection risk (Masenga *et al.*, 2023, Newsholme *et al.*, 2016).

In diabetic wounds, macrophages stay in an inflammatory M1 state due to persistent inflammation. High amounts of cytokines and ROS disturb the signaling essential for switching to a healing M2 state, producing persistent inflammation and delayed resolution. Altered insulin signaling via the IRS-PI3K-Akt pathway further compromises immune cell function, lowering proliferation, migration, and survival, and limiting wound healing (Wu *et al.*, 2022b, Wolf *et al.*, 2021). Reduced antimicrobial peptides such defensins and cathelicidins diminish the innate immune response, increasing infection risk. This combination of factors—AGEs, oxidative stress, decreased immune cell function, and diminished antimicrobial peptides—creates a chronic inflammatory milieu that inhibits normal healing and slows recovery in diabetes patients. Addressing these factors is critical for promoting wound healing in diabetes (Roby and Nardo, 2013, Alford *et al.*, 2020).

2.4.2. Reduced angiogenesis

Diabetes generally decreases levels of vascular endothelial growth factor (VEGF), necessary for developing new blood vessels. Chronic high blood sugar and inflammation reduce VEGF synthesis and receptor activation, reducing endothelial cell function (Kolluru *et al.*, 2012). This leads in diminished blood vessel growth. In diabetic wounds, the balance between pro- and anti-angiogenic factors is altered, with elevated levels of anti-angiogenic factors including endostatin and thrombospondin-1 further limiting vessel development (Okonkwo and DiPietro, 2017).

Chronic inflammation exacerbates the situation, with high levels of pro-inflammatory cytokines like TNF-α and IL-6 exacerbating endothelial dysfunction and hindering new vessel creation (Nirenjen *et al.*, 2023). Additionally, excessive MMPs tear down extracellular matrix (ECM) components, while inadequate TIMPs fail to moderate them, resulting to poor ECM stability and reduced endothelial cell adhesion (Cabral-Pacheco *et al.*, 2020).

Together, these molecular disruptions—troubled endothelial cell function, reduced VEGF signaling, heightened anti-angiogenic hormones, oxidative stress, and chaotic ECM remodeling—culminate in inadequate blood vessel expansion. This lack of angiogenesis hinders the healing of diabetic wounds, leading to longer recovery durations, a heightened risk of infection, and overall worse wound regeneration. Tackling these underlying difficulties is critical for boosting angiogenesis and speeding up wound healing in diabetes patients.

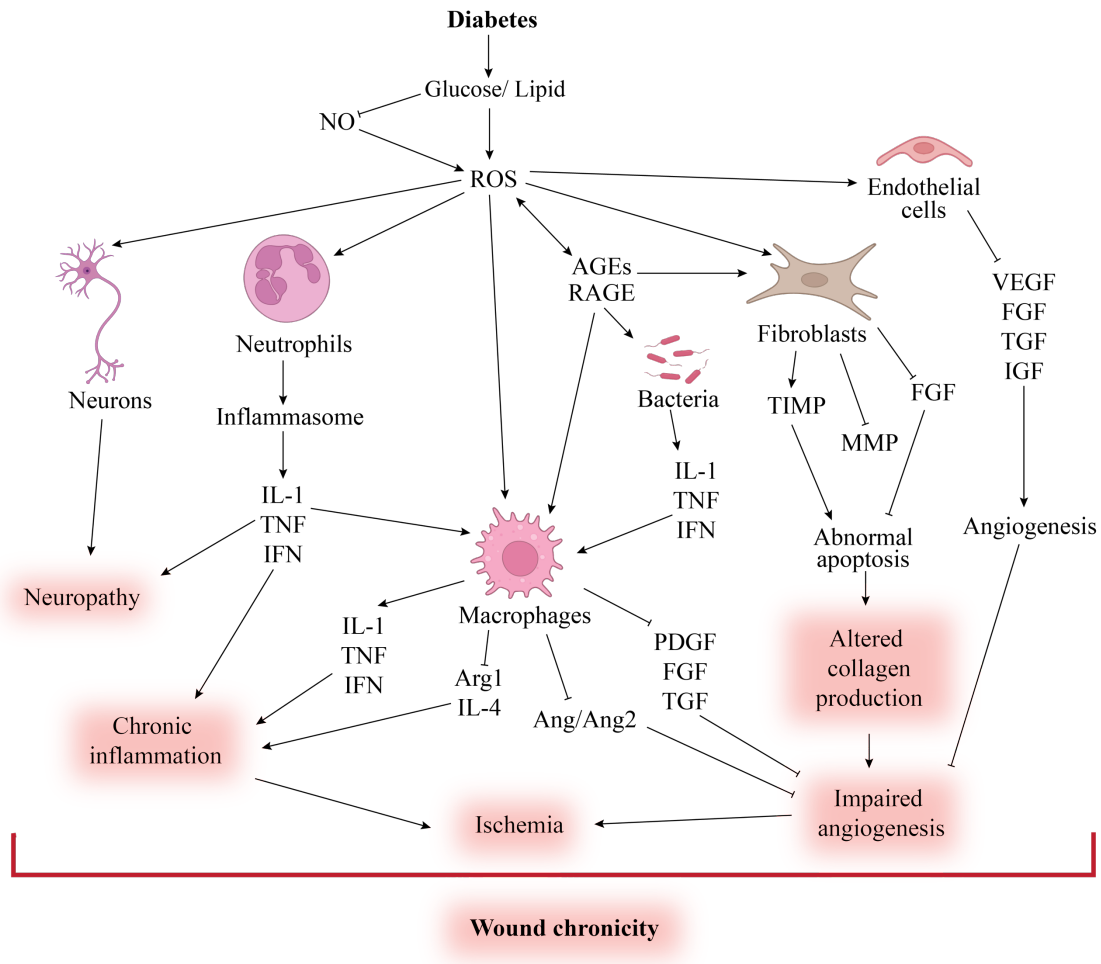

Figure 2.5. *Molecular mechanism of diabetic wound chronicity.*

2.4.3. Dysregulation in MMPs

In chronic diabetic ulcers, the dysregulation of matrix metalloproteinases (MMPs) plays a significant role in delaying the healing process. MMPs are enzymes that degrade extracellular matrix (ECM) components including collagen, elastin, and proteoglycans, which are necessary for tissue remodelling and repair (Fu *et al.*, 2022). In diabetic ulcers, hyperglycaemia exacerbates this dysregulation by encouraging the production of advanced glycation end products (AGEs), which further upregulate MMP activity and there is commonly an overexpression of MMPs, notably MMP-1, MMP-2, and MMP-9, leading to excessive degradation of ECM components. This results in weaker, unstable tissue that cannot properly regenerate, delaying wound healing (Ayuk *et al.*, 2016). Additionally, the persistent inflammation typically found in diabetic lesions upregulates MMP production, further increasing ECM degradation and extending the inflammatory phase. Moreover, in these lesions, there is commonly an imbalance between MMPs and tissue inhibitors of metalloproteinases

(TIMPs), with reduced TIMP levels or malfunction, permitting unregulated MMP activity. This imbalance effects normal ECM remodelling, limiting the deposition of new collagen and other matrix components essential for tissue healing.

Furthermore, the excessive ECM disintegration raises the risk of infection, notably by encouraging bacterial invasion and biofilm formation, which complicates the healing process (Sharma *et al.*, 2023b). In summary, the dysregulation of MMPs in chronic diabetic wounds leads to decreased ECM remodelling, protracted inflammation, poor tissue regeneration, and increased infection risk, making wound healing a complicated and difficult process in these patients.

2.4.4. Altered collagen production and remodeling

In diabetic wounds, healing is impeded by high blood glucose levels, which contribute to the development of AGEs. These AGEs attach to RAGE receptors on fibroblasts, eliciting inflammatory signals like NF-κB and affecting collagen production. Additionally, ROS act as corrosive agents, destroying fibroblasts and enzymes required for collagen modification (Tóbon-Velasco *et al.*, 2014, Chuah *et al.*, 2013). These enzymes are the crafters of collagen production and maturation, and depletion leads to greater disruption.

Growth factor signaling, which normally drives the healing process, falters. Growth factor signaling, necessary for healing, is disrupted. TGF-β, needed for fibroblast activation and collagen formation, is inadequate, and reduced growth hormones like VEGF further impede recovery (Xie and Percipalle, 2018, Massagué and Sheppard, 2023). Additionally, MMPs, which break down collagen, are hyperactive, while TIMPs, which control them, are missing. This imbalance leads to a damaged ECM and improperly oriented collagen fibers (Cabral-Pacheco *et al.*, 2020).

Myofibroblasts, which are necessary for wound contraction, are dysregulated in diabetic wounds, leading to poor wound closure and longer healing durations. The prolonged inflammatory milieu, defined by high levels of pro-inflammatory cytokines like TNF-α and IL-6, exacerbates collagen breakdown and hampers the healing process. As a result, wounds become structurally weakened and encounter severe obstacles in recuperation. This adds to the delayed nature of chronic wound healing in diabetes, demonstrating the complexity and difficulty of the healing process under these conditions (Nirenjen *et al.*, 2023).

2.4.5. Neuropathy and ischemia

In diabetic wounds, neuropathy occurs from a complex array of molecular changes that significantly impede nerve activity and wound healing. Chronic hyperglycaemia, a characteristic of diabetes, induces the production of AGEs by non-enzymatic glycation of proteins, which accumulates in nerve tissues, attaching to the receptor, RAGE, and starting intracellular signaling cascades, including NF-κB and MAPK pathways. This activation leads in prolonged inflammation and oxidative stress inside nerve cells (Lushchak *et al.*, 2021, Li *et al.*, 2023). Hyperglycaemia induced ROS aggravate this damage by lipid peroxidation, protein oxidation, and DNA damage, leading to neuronal death. As a result, nerve cells struggle to retain function and repair, extending pain and slowing the wound healing process (Su *et al.*, 2019, Juan *et al.*, 2021).

A crucial component to diabetic neuropathy is the reduction of nerve growth factor (NGF), a necessary protein for neuronal survival, axonal development, and nerve regeneration (Aloe *et al.,* 2015). In diabetes, NGF synthesis diminishes, and its receptor, TrkA, undergoes altered signaling, affecting neuronal repair and regeneration (Capsoni *et al.*, 2010). This diminished NGF function produces an environment conducive to neuropathy, where nerve function deteriorates, and the healing process is further hampered. Consequently, the significance of NGF in aiding nerve cell regeneration is greatly weakened, complicating the obstacles experienced in diabetic wound healing (Mardy *et al.*, 1999).

Chronic inflammation also exacerbates neuropathy in diabetic wounds. Pro-inflammatory cytokines like TNF-α and IL-1β accelerate nerve damage by triggering neuronal death and affecting Schwann cells, which are required for myelination and nerve regeneration. Disruption of Schwann cell function leads to exposed and injured nerves, resulting in sensory and motor impairments, including numbness, discomfort, and impaired coordination. The lack of feeling adds to delayed detection of injuries, allowing tiny wounds to grow into chronic, non-healing ulcers. This combination of neuropathy, reduced nerve function, and sensory loss forms a feedback loop that greatly hinders the wound healing process (Ivanov *et al.*, 2023).

2.4.6. Bacterial burden and biofilm formation

Diabetes increases chronic inflammation and immunological dysfunction, decreasing the body's capacity to battle infections. Neutrophils, essential infection-fighting cells, demonstrate impaired function in diabetes circumstances (Thimmappa et al., 2023, Darwitz et al.). Elevated blood glucose and oxidative stress limit neutrophil chemotaxis and ability for phagocytosis, resulting to a reduced immunological response and allowing germs to survive and multiply (Huang *et al.*, 2024). Macrophage function is also reduced in diabetic wounds. Chronic hyperglycemia and AGEs modify macrophage activation, triggering pro-inflammatory

pathways that impair the capacity to remove infections and generate essential cytokines (Darwitz *et al.*). This leads in poor infection clearance and decreased wound healing.

Biofilm production is another significant element in increasing bacterial load in chronic diabetic wounds (Pouget *et al.*, 2020). Bacteria in these wounds generally develop biofilms (**Fig. 2.6**), dense colonies protected by an extracellular matrix. This matrix, mostly consisting of polysaccharides like alginate and polysaccharide intercellular adhesin (PIA), protects bacteria from both immune responses and antimicrobial therapies (Singh *et al.*, 2021). The biofilm environment traps medications and immune cells, hindering efficient bacterial elimination and leading to recurrent infections that further hamper recovery.

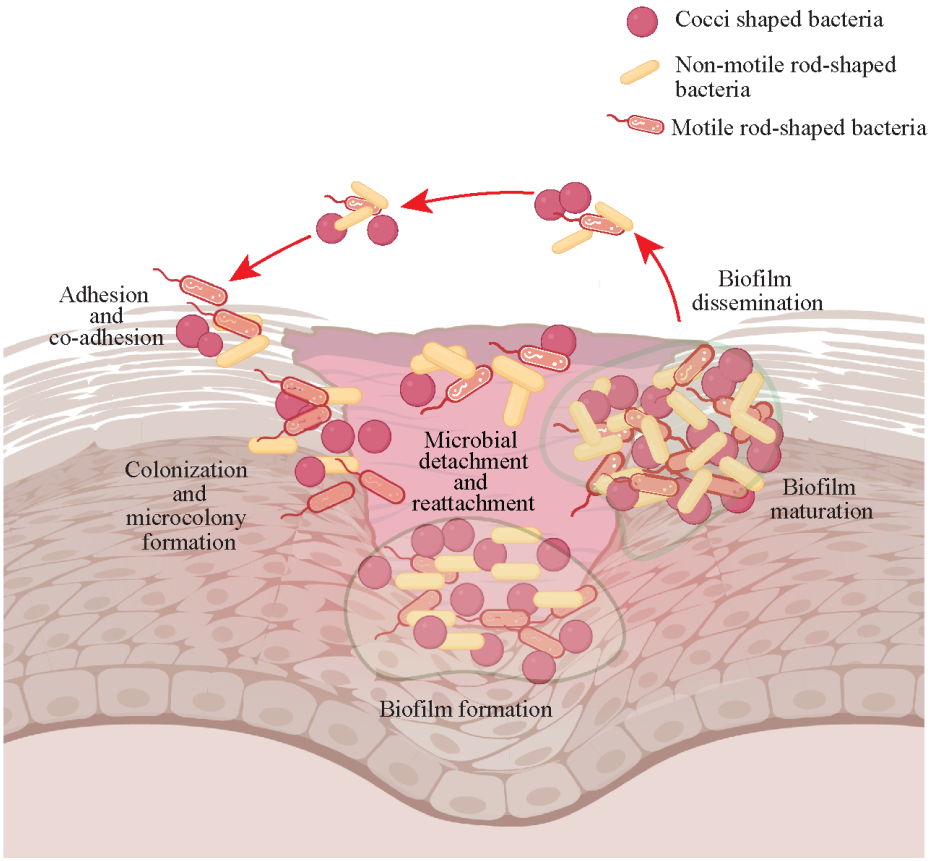

Figure 2.6. *Development and maturation of biofilm in wound bed. © Biorender.*

The altered wound microenvironment in diabetes patients, marked by elevated glucose levels, stimulates bacterial growth and biofilm formation, increasing the problems of tissue healing (Waldrop *et al.*, 2014). As bacteria generate harmful metabolic by-products, they damage surrounding tissues and create a hostile environment for regeneration. This vicious cycle of infection and inflammation significantly impairs wound healing. These characteristics also raise the risk of systemic problems. Chronic infections in diabetic wounds can develop to

bacteremia and proceed to sepsis, offering considerable health concerns and complicating wound treatment

2.5. Macrophage dysfunctionality in diabetic chronic wound

In the intricate process of wound healing, macrophages play a dual role: first removing cellular waste and pathogens, and subsequently guiding cellular differentiation and tissue remodeling with precision; acting as regulators of the wound microenvironment, they steer diverse resident cells toward respective tasks (Luo *et al.*, 2022). The functional change during wound healing might be related to the Yin-Yang theory from Chinese philosophy, which emphasizes the dynamic interaction of opposing yet complementary forces. This theory is governed by three principles: (a) Duality and complementarity, where opposing forces coexist in all aspects of the universe; (b) Dynamic equilibrium, an ever-changing balance achieved through continuous adjustment; and (c) Interdependence and transformation, where these forces not only complement but also convert into each other (Fang, 2012). The M1 phenotype, comparable to Yang, begins the inflammatory response, battling infections and cleaning debris, whereas the M2 phenotype, akin to Yin, supports resolution of inflammation, tissue healing, and immunological regulation. Just as Yin and Yang must balance for harmony, the equilibrium between M1 and M2 macrophages is crucial for appropriate immune activity and tissue homeostasis. In this situation, macrophages dynamically move between both activities, establishing a precise balance between inflammation and healing, destruction and repair (Martin and García, 2021, Ross *et al.*, 2021).

In chronic diabetic wounds, macrophages lose the balance due to the high accumulation of AGEs, ROS, inflammatory signals, and persistent low-grade infections. This disruption at the molecular level profoundly alters macrophage function, resulting in relentless inflammation and compromised healing.

2.5.1. Altered macrophage activation

Macrophages, the flexible guardians of wound healing, generally dance through a transformation process as wounds grows. In a healthy condition, they transform effortlessly from the M1 pro-inflammatory persona to the healing M2 phenotype, guiding the wound from inflammation to repair. Yet, in the arena of chronic diabetic wounds, this flawless dance falters. Persistent high blood glucose levels and oxidative stress keep these cells trapped in a perpetual state of unrest. Elevated hyperglycemia stimulates the development of ROS, which activate the inflammatory transcription factor NF-kB. This, in turn, stokes the fires of inflammation by

raising the production of pro-inflammatory cytokines including TNF- α and IL-1β. Instead of smoothly moving towards the M2 reparative function, macrophages stay entangled in the M1 state, imprisoned in a perpetual cycle of inflammation. The wound, however, languishes in a position of unrelenting irritation and unresolved conflict, unable to advance towards healing (Krzyszczyk *et al.*, 2018).

2.5.2. Impaired phagocytosis and clearance

In diabetic wounds, macrophages demonstrate severe impairments in phagocytosis due to the effect of AGEs and oxidative stress. AGEs, which result from the non-enzymatic glycation of proteins, lipids, and nucleic acids under elevated glucose conditions, connect to the receptor, RAGE, on macrophages. This link enhances inflammatory signaling pathways via MAPK and NF-κB. The subsequent signaling cascade induces the generation of inflammatory cytokines and ROS, further restricting the macrophages' ability to effectively engulf and kill pathogens, necrotic cells, and cellular debris. The subsequent reduction in phagocytic activity improves the survival of germs and debris, extending a cycle of chronic inflammation and slowing the resolution of tissue repair (Singh *et al.*, 2014).

2.5.3. Reduced synthesis of growth factors

Macrophages, the diligent architects of wound healing, are charged with manufacturing important growth factors like VEGF and TGF-β. VEGF orchestrates the symphony of angiogenesis, the delicate process of generating new blood vessels that supply critical oxygen and nutrients to the healing tissue. In the challenging context of diabetic wounds, this orchestration is interrupted. Elevated glucose levels and oxidative stress change the signaling pathways, notably the critical activation of HIF-1α. This transcription factor is necessary for VEGF synthesis, and its faulty activation resulted in a shortage of VEGF, delaying the development of new blood vessels. Similarly, TGF-β, which drives the remodeling of the extracellular matrix (ECM) and collagen deposition, suffers under diabetic situations. The reduced TGF-β signaling affects ECM formation, compromising tissue integrity and dragging out the healing process. In this situation, the generally harmonious healing process is thrown off balance, leaving the wound straining to mend (Koh and DiPietro, 2011, Krzyszczyk *et al.*, 2018).

2.5.4. Increased generation of inflammatory mediators

In diabetic wounds, macrophages become chronic producers of inflammatory mediators, including prostaglandins and MMPs. Prostaglandins are churned out by the activity of COX (cyclooxygenase) enzymes, with COX-2 being extremely active during protracted inflammation. These growing prostaglandins kindle the flames of inflammation, enhancing pain and edema. Meanwhile, MMPs like MMP-2 and MMP-9 start on a destructive binge, dismantling crucial ECM components like collagen and fibronectin. This MMP-driven degradation, spurred by inflammatory cytokines and oxidative stress, tears away the ECM's structural scaffolding. The consequence is a chaotic environment where cell migration falters and tissue regeneration are stopped, leaving the wound imprisoned in a cycle of chronic damage and delayed healing (Wolf *et al.*, 2021).

2.5.5. Impaired inflammation

The resolution of inflammation is the last act in the theatrical performance of wound healing, with macrophages as the major characters. These cells not only sweep up apoptotic debris but also release anti-inflammatory cytokines to calm the storm. In the realm of diabetic wounds, however, this determination is hindered. The setting is created with persistent inflammatory stimulation and a shortage of essential peacekeepers like IL-10, which is crucial for reducing the inflammatory upheaval and guiding macrophages from the aggressive M1 state to a more healing M2 state. Without appropriate IL-10 and other resolution factors, the inflammatory process carries on, culminating to a never-ending conflict. This unrelenting inflammation further hinders tissue repair, providing an environment where chronic wounds continue to struggle and endure (Luo *et al.*, 2024).

2.6. Role of Zeb2 in macrophages' inflammatory profile

Zeb2 (Zinc finger E-box-binding homeobox 2), also known as Smad-interacting protein 1 (SIP1), is a transcription factor that occupies a crucial role in various biological processes, including cell differentiation, migration, and tissue formation (Bar Yaacov *et al.*, 2019). Zeb2 is located on chromosome 2q22.3 in humans spanning from 144384081-144520118 nucleotide and encode 133.5 kDa protein, whereas in mice, it's located on chromosome 2 B; 2 27.3, spanning from 44873523-45007407 nucleotide and encode 133.6 kDa protein. Characterized by its zinc finger patterns, Zeb2 may bind to certain E-box sequences in the promoters of target genes, therefore influencing its' transcription. Zeb2 is highly stimulated by the TGF-β signaling pathway via the Smad2/3-Smad4 complex, which induces its transcription (Nakao *et al.*, 1997). Additionally, Zeb2 works with the Wnt/β-catenin pathway, synergistically inhibiting epithelial

gene expression to increase cellular plasticity and migration (Sun *et al.*, 2024). Crosstalk with the Notch signaling pathway further modifies Zeb2 expression, influencing EMT and stemness, especially in oncogenesis (Lindsey and Langhans, 2014). Depending on the cellular environment and target genes, Zeb2 operates either as a transcriptional repressor or activator. It performs this dual purpose by binding co-repressors to suppress gene expression or engaging with transcriptional activators to increase gene expression (Xu *et al.*, 2019). Zeb2's varied regulatory capacities are crucial for embryonic development and cell differentiation, underlining its vital significance in developmental biology. It affects processes like epithelial-to-mesenchymal transition (EMT), which is crucial for embryogenesis, tissue remodeling, and organ development. Zeb2 is important for the development of the nervous system. It regulates neuronal growth and the creation of neural networks. Mutations or dysregulation of Zeb2 may lead to neurological disorders and developmental abnormalities (Hegarty *et al.*, 2015).

Zeb2 may potentially influence epigenetic modifications by interacting with chromatin-remodeling complexes. These interactions may affect chromatin structure and accessibility, thereby controlling gene expression. Mutations in the Zeb2 gene may lead to hereditary disorders like Mowat-Wilson syndrome, which is distinguished by developmental delays, intellectual impairments, and various physical abnormalities. Understanding Zeb2's role in these illnesses can provide insights into prospective therapy options (Birkhoff *et al.*, 2020).

In the immune system, it has recently been shown that ZEB2 functions to influence maturation of NK cells (Van Helden *et al.*, 2015), CD8+ effector T cells' terminal differentiation (Dominguez *et al.*, 2015), and the diversification and growth of dendritic cells (Scott *et al.*, 2018). Germline deletion of Zeb2 in mice boosts embryonic mortality, and also acts in development of the brain system and melanocytes (Higashi *et al.*, 2002). Conditional deletion of Zeb2 in hematological lineages induces a deficit in HSC mobilization and leading in neonatal mortality (Goossens *et al.*, 2011). Additionally, Zeb2 has been discovered to play a function in selecting the fate of the granulocyte-macrophage progenitor (GMP) (Wu *et al.,* 2016b). Another group showed that Zeb2 is significantly expressed in macrophages throughout tissues, which indicated that Zeb2 was important to preserve the cellular identity of macrophages with its absence leading to the elimination from all tissues. A loss of function study of Zeb2 leads to loss of Nr1h3 (Scott *et al.*, 2018), showing that one mode of action of Zeb2 is to maintain the levels of transcription factors driving the tissue-specific characteristics of the different tissue specific macrophage populations.

But the significance of Zeb2 in macrophages' inflammatory phenotype in the context of diabetes is not yet clarified. Multiple investigations have suggested that the transcription factor T-bet may influence Zeb2 transcription in T cells and NK cells (Van Helden *et al.*, 2015,

Dominguez *et al.*, 2015). Furthermore, work has found c-MyC as a crucial component for Zeb2 expression in $CD8^+$ T cells (Gautam *et al.*, 2019). A particularly noteworthy work established a transcriptional circuit of reciprocal suppression between Inhibitor of DNA binding 2 (Id2) and Zeb2, which acts in the common dendritic cell progenitor (CDP) (Huang *et al.*, 2021, Durai *et al.*, 2019). This regulatory system is critical for resolving the destiny choice among plasmacytoid dendritic cells and type 1 conventional dendritic cells. Since ID2 may function by limiting the activity of E-proteins, speculated E proteins could favorably control Zeb2 expression in the CDP but couldn't identify the regulatory factors that might facilitate this regulation.

Therefore, it is indispensable to unravel the influence of deviations in Zeb2 expression levels on the phenotypic activities of macrophages. Particularly in the setting of diabetes circumstances, the contribution of Zeb2 in the deregulation of macrophage-mediated persistent inflammation remains poorly unknown. Understanding this link might give vital insights into the processes driving prolonged inflammatory responses and delayed wound healing in diabetes.

2.7. Diabetic wound care management and its limitations

Treatment of diabetic chronic wounds, especially DFUs, can be challenging due to factors like decreased blood flow, poor nerve function, weakened immune system, and elevated blood sugar levels. DFUs harm 19–34% of people with diabetes during their lifetimes, with the International Diabetes Federation expecting 9.1–26.1 million new DFU cases yearly. A population-based cohort research found that DFUs are connected with a 5% death risk within the first year and a 42% mortality rate within five years. Despite known treatment regimens, managing DFUs remains problematic, stimulating research into novel therapies to improve wound healing (Stancu *et al.*, 2022). When a wound fails to react to routine care within four weeks, advanced treatments including negative pressure wound therapy (NPWT), hyperbaric oxygen therapy (HBO), bioengineered skin replacements, and cell-based therapies come into play, giving complex options for obstinate wounds (Kim *et al.*, 2019). Amputation of a leg is more likely, infection is more likely, and the healing process is slowed down by these variables (Akkus and Sert, 2022). Strict glycaemic control, better wound care, infection prevention, and patient education must be the tenets of an interdisciplinary approach for treatment to be successful (Wang *et al.*, 2020). Continuous observation and prompt delivery of antibiotics are critical for infection prevention. Patient education is critical for proactive wound care and early issue detection. Combining advanced medical therapy with patient-centered care in a coordinated, evidence-based strategy is critical to accelerating healing, decreasing

complications, and enhancing the quality of life for patients with diabetic chronic wounds (Dhole *et al.*, 2023, Muteeb *et al.*, 2023).

To manage diabetic chronic wounds, today's core treatment pillars include meticulous local wound management with surgical debridement, advanced dressings that preserve a moist wound environment, operational wound off-loading, meticulous vascular assessment, chronic infection treatment, and strict glycaemic control (Everett and Mathioudakis, 2018). In addition to basic procedures, numerous medications are available or being studied as sophisticated wound care approaches (**Table 2.1**). The relevance of managing wound exudate and its molecular components has spurred the creation of various dressings. These novel dressings seek to restore natural epithelium, maintain moisture levels, and minimize liquid and bacterial penetration. They also supply critical pressure for haemostasis, facilitate air exchange, preserve peri-wound skin, and encourage re-epithelialization during the healing process (Demidova-Rice *et al.*, 2012a, Frykberg and Banks, 2015).

Table 2.1. Commercially available hydrogel dressing for chronic wound management *(Firlar et al.*, 2022).

Commercial name	Manufacturer	Contents	Secondary wound dressing requirement
ActivHeal®	Advanced Medical Solutions Ltd.	Primary wound dressing with 85% water	No
AquaDerm™	DermaRite Industries	2-Acrylamido-2 methyl-1 propanesulfonic acid sodium Propylene Glycol Polyethylene glycol dimethacrylate 2-Hydroxy-2 methylpropiophenone 38–55% water	No
DermaGauze™	DermaRite Industries	Impregnated gauze with acrylate polymer	Yes
DermaSyn®	DermaRite Industries	Vitamin E Primary wound dressing	No
INTRASITE Gel	Smith and Nephew	Carboxymethyl cellulose Propylene glycol	No
MEDIHONEY® (adhesive hydroge sheet)	Integra LifeSciences Cbrp.	Adhesive hydrogel sheet Glucose oxidase and Leptospermum compounds	No
Neoheal® Hydrogel	Kikgel	Polyethylene glycol Polyvinyl pyrrolidone	No

		Agar Electron beams for crosslinking 90% water	
NU-GEL™	Systagenix	Sodium alginate Primary wound dressing	No
Purilon®	Coloplast	Calcium alginate Sodium carboxymethyl cellulose N/A% purified water	No
Restore Hydrogel	Hollister Incorporated	Gauze pad Hyaluronic acid	No
Simpurity™ Hydrogel	Safe n'Simple	Absorbent sheets Acrylate Polyvinyl alcohol Polyethylene oxide Polyurethane Purified water	No
SOLOSITE Gel	Smith and Nephew	Carboxymethyl cellulose Glycerol Sodium salt At least 60% water	No
Suprasorb® G	Lohmann & Rauscher Global	Acrylic polymers Polyethylene Phenoxyethanol 70% water	Yes
Woun' Dres®	Coloplast	Carbomer Collogen Other polymers Linkage molecules (N/A)	No

While various wound care medicines are under research, only a handful complete the arduous clinical clearance procedure. The FDA underscores the importance for a deep understanding of harm mechanisms to create viable medicines. Success hinges on collaboration across disciplines, early participation of clinicians, and preclinical models that appropriately replicate human tissue reactions (Sharma et al., 2023a). The current boom in wound care breakthroughs since 2017 is driven by the convergence of biotechnology, nanotechnology, and digital wellness, propelling advances like smart dressings and bioactive materials. Next-generation wound therapies aim to promote healing through regeneration rather than mere repair, enabling the functional recovery of wounded skin and the restoration of its appendages in a precise, site-specific, and time-specific manner.

2.8. Innovative design and properties, crucial for clinical excellence

Effective wound care demands the conscious invention of materials and technologies specifically suited for the intricacy of clinical applications (**Table 2.2**), although standard values

represent typical performance benchmarks for advanced wound dressings. Specific ranges may vary depending on material composition and clinical applications. Designing biomaterials for wound healing includes a rigorous approach to maintaining the physiological environment while enhancing therapeutic efficacy (Wang *et al.*, 2022) (Yuk *et al.*, 2022, Brown *et al.*, 2018).

Table 2.2: The key physical characteristics of advanced wound dressings

Characteristics	**Importance in wound healing**	**Standard value/ Range**
Moisture Retention (Thomas, 2010)	Promotes faster healing by preventing desiccation and aiding cell migration	Optimal Relative Humidity: ~85–90%
Oxygen Permeability (Queen et al., 2004)	Supports cell proliferation and angiogenesis while reducing infection risk	Oxygen Transmission Rate (OTR): 8,000–10,000 cc/m²/day at 23°C, 50% RH
Exudate absorption Capacity (Vowden et al., 2009)	Reduces maceration and keeps the wound environment clean and conducive to healing	Absorption of 5–20 g of fluid per gram of dressing
Thermal Insulation (Winter, 1995)	Enhances healing by preventing hypothermia-induced delays in cellular activity	Thermal Conductivity: ~0.04–0.06 W/m·K
Biocompatibility	Prevents inflammation or allergic responses, ensuring safety for prolonged use	Cytotoxicity: Cell viability ≥70% (ISO 10993-5)
Antimicrobial Properties (Donelli and Vuotto, 2014)	Minimizes infection risk and supports a healthier wound environment	Reduction in microbial load: ≥99% (log reduction ≥3)
Ease of Application/Removal (Queen et al., 2004)	Improves patient comfort and adherence to treatment protocols	Force required: ≤1 N/cm² for gentle removal

2.8.1. Mechanical properties: The mechanical characteristics of wound care materials are crucial for reducing injury and encouraging healing. Given that human skin may expand up to 15%, materials must be elastic to ensure excellent adherence and protection. These properties strongly impact tissue regeneration, inflammation, and scar formation. For example, a substrate stiffness of 10 kPa and a dressing length of 7–9 cm are effective for encouraging fibroblast growth by imitating skin's natural environment. Materials with programmable mechanical

characteristics offer personalized support, promoting wound healing by providing controlled contraction on moist surfaces (Liu *et al.*, 2017, McElvain *et al.*, 2022).

2.8.2. Porosity, breathability and transparency: The porous aspect of a scaffold is vital for encouraging cell invasion and fostering vascular expansion, since its network of linked pores assists in the efficient transfer of nutrients, oxygen, and waste products. Equally critical is the breathability of wound dressings, which facilitates oxygen flow while guarding against bacterial invasion. Transparency in dressings enables for easier monitoring of the healing process. When adopting transparent fabrics, it's crucial to include UV-protective layers to avoid changes in skin pigmentation and keep the integrity and performance of the garment (Griffin *et al.*, 2015, Jiang *et al.*, 2023).

2.8.3. Wettability: Wettability in wound dressings is crucial to managing biofluids properly. Self-pumping dressings efficiently transport surplus fluid from hydrophobic to hydrophilic sides, decreasing the dangers of over-moisturization that can cause infections and impede healing. Water vapor transmission rate (WVTR) is vital for creating the proper moisture balance: whereas normal skin has a WVTR of 204–278 g/m² per day, more fluid-prone lesions, like burns, demonstrate substantially higher rates. Optimal dressings maintain a WVTR below 840 g/m² per day, ensuring they neither dry out the wound too soon nor retain excess moisture (Langer *et al.*, 2015, Negut *et al.*, 2020).

2.8.4. Adhesion: Adhesive dressings are increasingly proposed in wound care owing to its' easy application, which obviates the need for more surgical tape. By adhering firmly to the wound, these dressings enhance the healing environment and limit the risk of infection. However, caution is essential to avoid any downsides. Excessive adhesive strength may lead to the unintentional loss of delicate layers of the stratum corneum, whether from recently created epithelium or the surrounding healthy skin. Thus, although adhesive dressings offer a major advance in wound treatment, therefore administration must be painstakingly controlled to balance effective adherence with preservation of skin integrity (Wu *et al.*, 2022a).

2.8.5. Haemostasis: Retaining haemostatic components in dressings is vital for effective wound therapy. These components—clotting proteins, cells, and growth factors—control bleeding and support healing by providing a scaffold for cell migration, proliferation, and extracellular matrix deposition. Incorporating laponites, a synthetic nano clay with haemostatic properties, enhances this retention. Laponites' shear-thinning behaviour, which makes the material fluid under

pressure and solid when still, is ideal for 3D-printed dressings, improving both immediate hemostatic response and long-term tissue healing (Guo *et al.*, 2021, Gaharwar *et al.*, 2014).

2.8.6. Biochemical properties: The effectiveness of wound biomaterials relies on the biochemical properties, including biocompatibility, interaction with the wound environment, degradation patterns, and drug release. These materials attract a protein layer upon application, which influences immune response and foreign body reaction. Managing inflammation is crucial for optimal performance. The degradation rate is affected by the wound environment; for example, chronic wounds with high protease levels accelerate the breakdown of peptide-based matrices. Tailoring wound care to individual needs is essential, considering factors like wound type, underlying conditions (e.g., diabetes or venous insufficiency), pain levels, and cost. A comprehensive, patient-specific approach is vital for effective healing and overall well-being. *(Briquez et al., 2016, Preman et al., 2020, Falanga et al.*, 2022).

2.9. Advanced chronic wound care

Traditional procedures of wound evaluation, which have based mostly on visual inspection and subjective judgment, are presently being revolutionized by cutting-edge technology. These innovations are ushering in a new era of wound care (**Fig. 2.7**) that is not only more precise and data-driven but also customized and efficient. The combination of wearable gadgets and advanced imaging technologies allows a seamless blend of engineering and clinical practice, offering a degree of monitoring that was once unthinkable. This adjustment reduces issues, speeds up recuperation, and dramatically increases therapy outcomes. With improved monitoring systems that cater to varied wound morphologies and intricate biomarkers, the future of wound therapy is emerging into a realm of smart, responsive solutions.

2.9.1. Nanoparticle based

Nanoparticulate drug delivery systems improve therapy by offering controlled or sustained release of medications, lengthening the half-life, increasing bioavailability, optimizing pharmacokinetics, removing the need for frequent administration, and offering the potential for minimized inflammatory responses compared to conventional delivery methods. Through size optimization, surface modifications, and biocompatible materials, nanoparticles can decrease immune system activation, prevent wasteful inflammation, and improve focused therapeutic advantages. By bypassing immune identification and administering drugs in a controlled and sustained way, these systems serve to boost the effectiveness and safety of

treatments (Zolnik *et al.*, 2010). Various nanocarriers—including polymeric, peptide, lipid-based, and inorganic nanoparticles—are being explored for wound healing. Polymeric nanocarriers are highly sought for the compatibility with the body, ability to break down naturally, simplicity of injection, and capability to deliver drugs straight into cells.

PLGA-based nanoparticles are valued incorporating recombinant human epidermal growth factor (rhEGF) into these nanoparticles greatly speeds the healing of full-thickness wounds in diabetic rats (Chu *et al.*, 2010). Cationic polymers excel in transporting anionic medicines, including nucleic acids, by interactions. Liu et al. produced cationic nanofibers that enhanced the antibacterial activity of piperacillin-tazobactam (PT) and greatly expedited re-epithelization in wounds infected with *P. aeruginosa* in a mouse model (Liu *et al.,* 2014, Fukushima *et al.*, 2013). Using siRNA with poly(sorbitol-co-PEI) (PSPEI) to decrease CTGF expression greatly diminished wound contraction in mice (Georgiou *et al.*, 2004). Fumakia *et al.* created a solid lipid-based nanoparticle (SLN) formulation capable of co-delivering antibacterial LL37 and Serpin A1 against *S. aureus* and *E. coli* to chronic wounds (Fumakia and Ho, 2016). Xu et al. created liposomes with a silk fibroin (SF) hydrogel core (SF-LIP), encapsulating bFGF for increased therapeutic effectiveness (Xu *et al.*, 2017). Das et al. increased liposomes by integrating the co-receptor protein syndecan-4, which binds to FGF-2, to raise the efficiency of FGF-2 administration in diabetic wound healing (Das *et al.*, 2016).

Inorganic nanoparticles like gold, silica, iron oxide, and quantum dots are promising drug carriers due to its' enormous surface area, variable size, facile functionalization, and multifunctionality. Topical treatment of ganglioside monosialic acid 3 synthase (GM3S) siRNA-immobilized gold nanoparticles (siGM3SAuNPs) enhances keratinocyte migration and proliferation (Choi *et al*., 2011). Gold nanodots coated with the antimicrobial peptide surfactin (SFT) displayed better antibacterial efficacy and facilitated fast wound healing, increased epithelialization, and elevated collagen synthesis (Chen *et al.*, 2015b).

Porous silicon microparticles loaded with the therapeutic antibody Infliximab successfully sequestered TNF-α inside human chronic wound beds (McInnes *et al.*, 2015). Porous silicon nanoparticles loaded with Flightless I (Flii) siRNA or Flii neutralizing antibodies (FnAbs) dramatically decreased Flii activity in human chronic wounds (Turner *et al.*, 2017). Silane hydrogel nanoparticles, a silicon-based nanoparticle, are often utilized to deliver nitric oxide and curcumin by adding PEG and chitosan, to improve wound healing efficiency (Martinez *et al.*, 2009). Wu et al. cleverly coupled ceria with mesoporous silica nanoparticles (MSN), to accomplish quick closure of deep wounds by bridging particles with the tissue matrix for better healing (Wu *et al.*, 2018). Graphene quantum dots (GQDs) demonstrate higher peroxidase-like

activity, and considerably improving antibacterial efficiency against *E. coli* and *S. aureus* (Sun *et al.*, 2014).

Peptide-based nanoparticles are nanomaterials made of short chains of amino acids. Its' natural biocompatibility, biodegradability, and structural variety make them useful for drug delivery and therapeutic purposes (Li *et al.*, 2022, Tarvirdipour *et al.*, 2020). These nanoparticles may self-assemble into various shapes, including micelles, vesicles, and fibrils, applying non-covalent interactions like hydrogen bonding and hydrophobic forces (Lombardo *et al.*, 2020, Yadav *et al.*, 2020). Notable examples are RGD-functionalized peptides (arginine-glycine-aspartate motifs) for tailored cancer treatment and doxorubicin-conjugated peptide nanoparticles, which have shown promise in oncological uses (Castillo-Ecija *et al.*, 2020). A hierarchical assembly of peptide-based nanofibers with alginate to make microparticles (Hartgerink *et al.*, 2002), whereas poly(amidoamine) (PAMAM) dendrimers linked with cell-penetrating peptides (CPPs) have a branching topology that is favourable to successful drug administration (Abedi-Gaballu *et al.*, 2018). In the world of antimicrobial uses, gold nanoparticles functionalized with peptides like melittin have been studied for their antibacterial properties (Daniel and Astruc, 2004). Tumour-specific methods include matrix metalloproteinase (MMP)-responsive peptide nanoparticles that target MMP-overexpressing tumours (Vadevoo *et al.*, 2023). Furthermore, enzyme-instructed peptide self-assembly inside biological contexts repeats the production of biomolecular condensates, with sources frequently including short peptides and small molecules like naproxen (Howard and Delafontaine, 2004). PLGA nanoparticles linked with peptides were applied for brain-targeted medicine delivery, showing the versatility of peptide-based systems (Kamaly *et al.*, 2016). Polypeptides are naturally occurring proteins with excellent biocompatibility and have proved successful as nucleic acid carriers, confirming their place as key components in biomedical innovation (Crombez *et al.*, 2009).

2.9.2. Microcarrier based

When intracellular delivery isn't a prerequisite, microspheres give enormous advantages thanks to the ability to precisely modify drug release properties. Unlike other delivery systems, microspheres may be adjusted to produce a controlled, continuous release of therapeutic medications, removing the hazard of an early burst release that might otherwise lead to quick drug degradation or unwanted outcomes. Lin et al. established an emulsion technique to manufacture microparticles employing hydrophobic phase-change materials, 1-tetradecanol and paraffin wax, encapsulating sodium hydrosulfide (NaHS) to speeds up the healing of full-thickness wounds in diabetic mice by promoting cell proliferation, migration, and angiogenesis

(Lin *et al.*, 2017). Poly(ethylene glycol) (PEG) microspheres, loaded with VEGF-binding peptides (VBPs), provide precise regulation of VEGF-mediated angiogenesis (Belair *et al.*, 2016). The synthetic polycation (poly-ethylene argininyl-aspartate diglyceride) (PEAD) greatly increases angiogenesis, enhancing endothelial cell proliferation and promoting tube formation by co-delivering VEGF and HGF (hepatocyte growth factor) within this matrix (Awada *et al.*, 2014). The precise release of FGF-2 from the coacervate substantially sped up skin wound healing in mice, boosting granulation tissue formation and fostering strong angiogenesis (Wu *et al.*, 2016a).

2.9.3. Scaffold based

An ideal wound dressing combines biocompatibility, biodegradability, efficient moisture retention, antibacterial properties, and low cytotoxicity, allowing infection prevention, gas exchange, and ease of removal while successfully regulating exudates to promote healing. Conventional dressings, while cost-effective and user-friendly, are limited by issues such as ischemia, the need for frequent changes, and wound adhesion. Non-adhesive gauze-cotton composites, for example, aim to alleviate discomfort while still protecting newly healed tissue during removal. (Kamoun *et al.*, 2017).

Artificial dressings come in semi-occlusive or occlusive varieties and are crafted from materials like film, foam, hydrogel, or hydrocolloid, each offering unique benefits for wound care (Strecker-McGraw *et al.,* 2007). Dressings are crucial in wound therapy due to significant biological benefits. The large surface area of these nanofibrous scaffolds not only promotes excellent cell attachment but also allows for extensive integration of medicinal medicines (Kim *et al.*, 2012, Xu *et al.*, 2015). Gelatin-hydroxyphenyl propionic acid (GH) gels containing interleukin-8 and macrophage inflammatory protein-3α, dramatically increased cellular infiltration, expedited wound healing, and promoted robust re-epithelialization, neovascularization, and collagen accumulation (Yoon *et al.*, 2016). A dopamine-modified ε-poly-L-lysine-polyethylene glycol-based hydrogel (PPD hydrogel) could also form in situ via HRP induced crosslinking of catechol moieties of the dopamine, displayed excellent anti-infection activity due to the inherent antibacterial ability of ε-poly-L-lysine (Wang *et al.*, 2017a). Zhao et al. created injectable conductive hydrogels with quaternized chitosan-g-polyaniline (QCSP), dramatically increases the hydrogel's free radical scavenging capabilities (Zhao *et al.*, 2017b). Recent improvements in wound care include combining growth hormones, enzymes, and antibacterial agents into dressings. Notable products include Cutisorb™, Iodosorb, Actisorb Silver 220, and Acticoat, which contains silver-coating to inhibit adhesion and bacterial development. Xiao *et al.* established a slow-release technique for copper ions by

putting copper benzene tricarboxylate ($Cu_3(BTC)_2$, or HKUST-1) nanoparticles into an antioxidant-rich citrate-based hydrogel (Xiao *et al.*, 2017). Another component poly(polyethylene glycol citrate-co-N-isopropylacrylamide) (PPCN), a smart-biodegradable material that responds to temperature changes, was exploited to permit a controlled release of stromal cell-derived factor-1 (SDF-1) to the wound site (Zhu *et al.*, 2016). PEG-based ointment embedding NO-releasing polymer (FBN) composed of Pluronic F127, PEI and N-diazeniumdiolates not only facilitated NO release in a slow manner, but also served as a moisturizer to enhance the wound healing (Kang *et al.*, 2015).

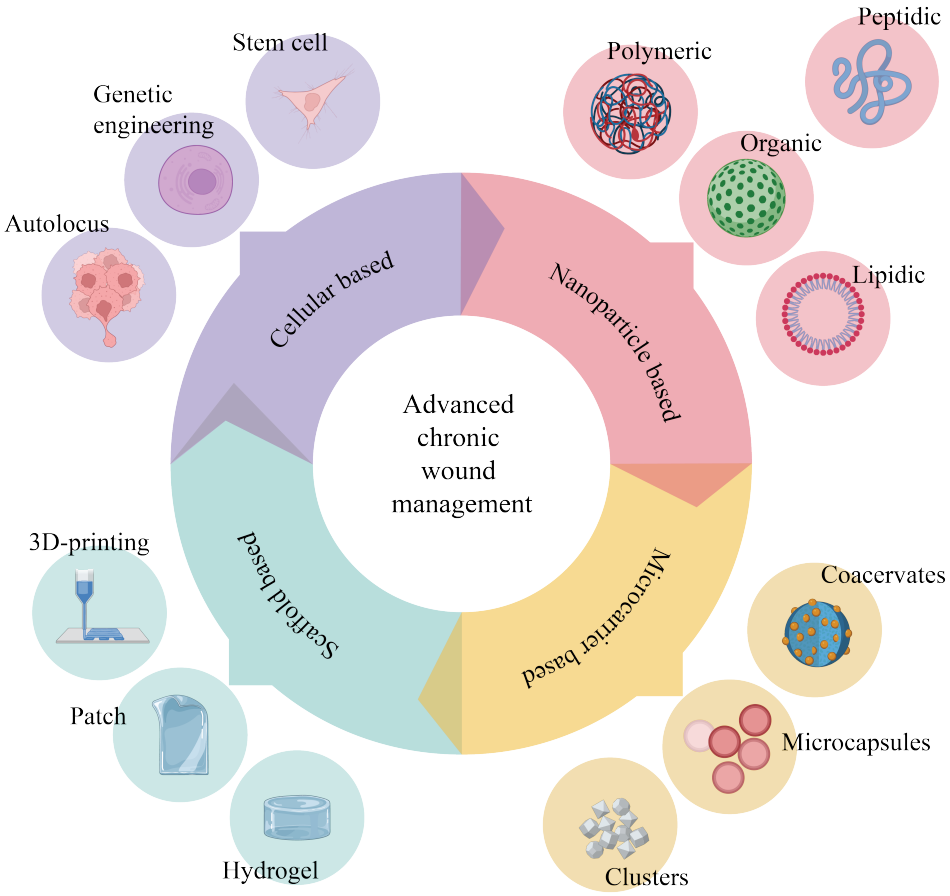

Figure 2.7. *Advanced drug delivery system for chronic wound management.*

Choi *et al.* devised a dual-release system by encapsulating bFGF in the core (Choi *et al.*, 2011). Hammond's team employed a layer-by-layer (LbL) approach to coat dressings, permitting regulated and sustained release of several medicines, including a hydrolytically degradable siRNA depot on a nylon bandage (Castleberry *et al.*, 2016). Advanced therapeutic dressings were created using a multilayer structure comprising hydrolytically degradable poly(β-amino ester), poly(acrylic acid) (PAA), VEGF and/or PDGF-BB, and heparin sulfate

(HS). ROS-degradable poly(thioketal urethane) (PTK-UR) scaffolds showed improved tissue regeneration in diabetic rat wounds (Martin *et al.*, 2016). Biodegradable scaffolds constructed from polysaccharides and peptides with bioactive sequences may imitate ECM proteins to assist wound healing (Capila and Linhardt, 2002). Wang's team created EUP3, a polysaccharide that binds PDGF-BB, boosting its effects and speeding wound healing in mice, enabling neovascularization and neo tissue development without additional growth factors (Li *et al.*, 2017). Zhu's team created injectable hydrogels sensitive to pH and glucose using phenylboronic-modified chitosan, poly(vinyl alcohol), and benzaldehyde-capped PEG, promoted wound healing in diabetes animals (Zhao *et al.*, 2017a). Kim et al. established LPEI-modified nanofibrous meshes MMP-responsive gene delivery systems to deliver EGF and MMP-2 siRNAs, increasing wound healing. They also produced StarPEG-heparin hydrogels that, following MMP cleavage, enhanced fibroblast infiltration and the release of heparin and growth hormones at the wound site (Kim and Yoo, 2010). Similarly, hyaluronic acid hydrogels, crosslinked with MMP-degradable peptides, leading to a rapid release of VEGF-encoding plasmids and boosting angiogenesis in diabetic ulcers (Tokatlian *et al.*, 2015).

2.9.4. Cellular based

Cell-based treatments accelerate wound healing by employing adaptable human skin cells keratinocytes. Bilayered constructions containing both cell types have been produced for large wounds. Commercial solutions include EpiCel (keratinocytes), Dermagraft (fibroblasts), and Apligraft (both cell types). Mesenchymal stem cells (MSCs) provide a potent answer for chronic wound healing, due to the ability to multiply and change into numerous skin cell types (Sasaki *et al.*, 2008). By genetically modifying MSCs to generate therapeutic factors such stromal cell-derived factor-1 (SDF), its' survival and efficiency at wound sites are considerably improved (Nakamura *et al.*, 2013). VEGF-boosted adipose-derived stromal cells promoted wound healing, promoting blood vessel formation and collagen production (Nauta *et al.*, 2013). Similarly, dox-inducible HGF-secreting MSCs promoted sustained angiogenesis in a rat hindlimb ischemia paradigm (Chang *et al.*, 2016).

Adult cells can be converted into iPSCs with characteristics comparable to embryonic stem cells (Takahashi *et al.*, 2007). Bilousova et al. employed iPSCs to repair skin tissues in mice, (Bilousova *et al.*, 2011), whereas Ohta *et al.* created autologous melanocytes (Ohta *et al.*, 2011). Zhang et al. found that exosomes from iPSC-MSCs accelerated wound healing and enhanced collagen structure in mice (Zhang *et al.*, 2015). However, issues like the low efficiency of reprogramming, imperfect differentiation, and potential teratoma formation underscore the need for advanced techniques in iPSC-based therapies.

2.9.5. Skin equivalent

Current skin substitutes often fall short in vascularization, leading to longer healing times and less ideal cosmetic results (Dias *et al.*, 2016). By using cell sheet technology, growth-arrested allogenic newborn keratinocytes and fibroblasts have been produced as restorative additives (HP802–247), presently entering Phase III clinical trials (Kirsner *et al.*, 2016). The application of temperature-responsive polymers like poly(N-isopropylacrylamide) (PNIPAM) has hastened the development of cell sheet technology, refining the process and boosting its effectiveness (Silva *et al.*, 2015).

Scaffold-free cell sheets encounter difficulties such extended culture durations, restricted volume, and poor vascularization. To combat this, biomaterials like hydrogels and nanofibers are utilized as substrates, boosting physical strength and vascularization (Fukuda *et al.*, 2006, Ng *et al.*, 2005). Hydrogels, which securely load cells and factors, adapt to wound locations and dissolve as required (Nicholas *et al.*, 2016). MSCs in hydrogels produce growth factors and develop into keratinocytes, fibroblasts, and endothelial cells, expediting wound healing by boosting vascularization, minimizing granulation tissue, and promoting re-epithelialization (Burdick *et al.*, 2016). In vivo transplantation of fibroblast-encapsulated hydrogels into mouse skin wounds enhanced collagen deposition, neovascularization, and wound closure (Chen *et al.*, 2015a). Kim *et al.* engineered a hybrid comprising human hair keratin/chitosan nanofibers and GelMA hydrogel (Kim *et al.*, 2017). Pan et al. developed a composite of electrospun PLCL/Poloxamer nanofibers and dextran/gelatin hydrogel, demonstrating significant potential for skin regeneration (Pan *et al.*, 2014). 3D bioprinting has emerged as a vital technique for tissue engineering, including skin regeneration (DuRaine *et al.*, 2015). Among the different methods, thermal inkjet-based 3D printing stands out for its superior cytocompatibility and operational simplicity, surpassing piezoelectric and electromagnetic techniques (Cui *et al.*, 2012). Extrusion-based 3D printing has developed as a flexible technology for generating skin replacements, utilizing a variety of bioinks like collagen (Long *et al.*, 2018), fibrin-collagen (Skardal *et al.*, 2012), GelMA/collagen (Shi *et al.*, 2018), and self-healing hydrogels made of chitosan, poly(acrylic acid), and ferric ions (Darabi *et al.*, 2017).

2.10. Hydrogel: a promising candidate for chronic wound management

Hydrogels are versatile hydrophilic polymers characterized by a three dimensional network structure that can absorb significant quantities of water, rendering them highly effective for wound care (Habib *et al.*, 2015). Their crosslinked polymer chains, produced by chemical or physical means, exhibit swelling behaviour influenced by water diffusion (Aswathy

et al., 2020). Hydrogels offer mechanical support, biocompatibility, antibacterial and anti-inflammatory properties, and are biodegradable, rendering them suitable for temporary wound care. Their porous architecture replicates the extracellular matrix, allowing for fluid absorption, oxygen exchange, and nutrient delivery while keeping the wound wet and protected. Advanced formulations incorporating therapeutic ingredients facilitate extended drug release, hence enhancing healing and establishing hydrogels as a feasible alternative for chronic wound care. (Xiong *et al.*, 2021).

Hydrogel dressings provide a diverse and sophisticated option for chronic wound treatment, adeptly meeting the special needs of such wounds. These dressings assist healing by improving autolytic debridement and maintaining adequate moisture levels in the wound bed, hence encouraging granulation and re-epithelialization. The design enables for simple removal without damaging freshly created keratinocytes, and its biodegradable nature may remove the need for physical removal. Moreover, hydrogel features may be carefully tailored to improve adhesiveness, antibacterial activity, vascularization, anti-inflammatory responses, and antioxidant capacities. To guarantee maximum function, hydrogel dressings should display minimum toxicity, good biocompatibility, and support for cellular growth. Synthetic hydrogels should furthermore have substantial mechanical strength, excellent moisture retention, and appropriate air permeability (Shiekh *et al.*, 2020). A plethora of commercially available hydrogel-based wound dressing solutions are presently on the market, including amorphous gels, hydrogel sheets, films, and gauze impregnated with hydrogel. All these products seek to stimulate moist wound healing, especially by improving autolytic debridement. Researchers have generated hydrogels with variable characteristics using various physical and chemical cross-linking processes to satisfy the wide-ranging demands of different wound types (**Table 2.3**). Both natural and synthetic polymers demonstrate remarkable biological activity and various uses, and combination typically accentuates unique advantages, expediting wound healing (**Table 2.4**). The intrinsic stability of hydrogel components gives intriguing prospects to build new hydrogels with better physical and chemical characteristics, greater biocompatibility, controlled biodegradability, and minimum toxicity. This development is accomplished by combining natural and synthetic polymers or changing native biopolymers via novel cross-linking processes.

Table 2.3. Hydrogels as promising chronic wound dressing.

Base component	Secondary component	Function	Outcome
Chitosan (Hu *et al.*, 2021)	Dextran-dopamine	pH-responsive controlled drug release Antibacterial activity Angiogenic activity Adhesive property	In acidic environments, controlled release of silver nanoparticles (AgNPs) provides rapid antibacterial action, while deferoxamine boosts angiogenesis by increasing HIF-1α and VEGF expression
Chitosan (Lee *et al.*, 2021)	Poly(vinyl alcohol) (PVA)	Antimicrobial effect Sustained release of Ag+ and epidermal growth factor (EGF)	Boosted skin renewal and robust collagen buildup
Chitosan (Zheng *et al.*, 2020)	Poly(d,l-lactide)-poly(ethylene glycol)-poly(d,l-lactide) (PLEL)	Thermo-sensitive Antibacterial activity Adhesive properties	Catechol-modified quaternized chitosan (QCS-C) boosts tissue adhesion, has strong antibacterial properties, and promotes angiogenesis through VEGF and b-FGF upregulation, enhancing wound healing
Chitosan (Puertas-Bartolomé *et al.*, 2019)	Hyaluronic acid (HA)	Adhesive properties Anti-inflammatory activity Antioxidant effect	Catechol-containing hydrogels offer strong adhesion to wet surfaces, support mesenchymal stem cell growth and migration, protect against oxidative stress with controlled catechol release, and reduce IL-1β inflammation
Chitosan (Jing *et al.*, 2021)	Alginate and Polydeoxyribonucleotide (PDRN)-loaded $CaCO_3$ nanoparticle (PCNP)	Controlled gene delivery Anti-inflammatory Pro-angiogenic	PCNP enhanced PDRN delivery, boosted fibroblast proliferation, increased collagen, blood vessels, and cell attachments, and accelerated wound healing
Chitosan (Carvalho and Mansur, 2017)	Gelatin	Biodegradable Biocompatible	Uniform 3D porous structures with adjustable swelling and degradation via increased photo-crosslinking and gelatin concentration

Chitosan (Qu *et al.*, 2019)	Oxidized HA-graft-aniline tetramer (OHA-AT)	Biodegradable Antibacterial activity Electroactive Antioxidant effect Neovascularization	Accelerated wound healing with increased granulation tissue, collagen, and angiogenesis; amoxicillin loading enhanced antibacterial activity
Chitosan (Yin *et al.*, 2021)	Arginine-based poly(ester urea urethane) (Arg-PEUU)	Anti-inflammatory activity Antibacterial activity Biodegradable	Methacrylate-modified chitosan (CS-GMA) and Arg-PEUU hybrid hydrogels demonstrated excellent antibacterial activity, high water content, a 3D microporous structure, cytocompatibility, and enzymatic biodegradability
Chitosan (Xu *et al.*, 2021)	Decellularized extracellular matrix (dECM) and Gelatin	Antibacterial Biocompatible	The interconnected pore structure and high porosity fostered cell growth, with a degradation rate aligning with new tissue formation. It also exhibited antibacterial activity and maintained moisture and nutrition balance
Chitosan (Sun *et al.*, 2022)	Gallic acid (GA)	Adhesive property Antibacterial activity Homeostasis properties	Showed excellent antioxidant, biocompatibility, and hemocompatibility; supported homeostasis and wound healing
Chitosan (Zhao *et al.*, 2017a)	PVA and PEG	pH/glucose-triggered drug release Anti-inflammatory Neovascularization	pH and glucose-responsive drug delivery; improved wound closure, inflammation, neovascularization, and collagen deposition with insulin/L929 in diabetic wounds
Gelatin (Yan *et al.*, 2021)	Lipopeptide-surfactin (SF)	Angiogenic activity Anti-inflammatory	GelMA-SF hydrogels enhanced diabetic wound healing by regulating macrophage polarization and promoting angiogenesis
Dextran (Sun *et al.*, 2011)	Poly(ethylene glycol) diacrylate (PEGDA)	Biodegradable Neovascularization Pro-angiogenic	The dextran hydrogel, with high PEGDA content and cross-linking, degrades slowly and promotes rapid

			neovascularization without extra growth factors. Neutrophil infiltration accelerates hydrogel degradation and vascular cell infiltration, leading to complete skin regeneration
Dextran (Johnson *et al.*, 2020)	PEG	Controlled release of immune stimulatory cargo proteins Anti-inflammatory	Controlled cargo protein release improved retention and effectiveness of immune-stimulatory proteins in the wound
Methyl-cellulose (Lan *et al.*, 2021)	Pluronic F-127	Thermosensitive controlled release of MMP-9 siRNA Gene delivery	Reduced MMP-9 expression and improved diabetic wound healing

Research on hydrogel dressings is advancing towards more cost-effective and multifunctional solutions. While current hydrogel options are diverse and continually improving, there's still a gap, particularly for chronic wound care. Future developments should focus on enhancing antibacterial, antioxidant, or controlled-release properties and refining the structure of natural polymers. Optimizing hydrogel performance involves addressing challenges related to material stability, processability, and solubility. Researchers should explore new technologies and materials while considering these factors to advance hydrogel dressing efficacy.

Table 2.4. Polymers used for hydrogel preparation.

Nature	**Polymer**	**Properties**
Synthetic polymer	Polyvinylpyrrolidone (Kurakula and Rao, 2020)	Water solubility Heat resistance Wettability Film-forming properties Adhesion
	Poly(*N*-isopropyl acrylamide) (Santhamoorthy *et al.*, 2022)	Temperature sensitive Non-toxic
	Polyurethane	Blood compatibility Chemical stability Mechanical properties

	Polyethylene glycol (Zhou and Yi, 1999)	Low cost Water soluble Lubricity Moisture retention Dispersibility
	Poly (vinyl alcohol) (Gaaz *et al.*, 2015)	Water soluble Non-carcinogenic Good mechanical properties
	Acrylamide (Sennakesavan *et al.*, 2020)	Non-carcinogenic Non-toxic Mechanically adjustable Elastic properties Swelling ability
Natural polymer	Sodium alginate (Lee and Mooney, 2012)	Haemostasis Water soluble Enhance cell migration Enhance type 1 collagen production
	Pullulan (Teixeira *et al.*, 2023)	Anti-oxidant Water retention Haemocompatible Non-immunogenic
	Collagen (Mathew-Steiner *et al.*, 2021)	Mild immunogenic Promote cell growth and proliferation Avoid scar formation
	Starch (Ojogbo *et al.*, 2020)	Low cost Wide source Renewable
	Cellulose (Ojogbo *et al.*, 2020)	Low cost Wide source
	Chitosan (Dai *et al.*, 2011)	Non-toxic Antimicrobial Antifungal Haemostatic Anti-inflammatory
	Hyaluronic acid (Pérez *et al.*, 2021)	Hydrophobic Mechanically adjustable Swelling ability

2.11. Hydrogels used for oligonucleotide delivery

The basic principle of molecular biology says that DNA is transcribed into RNA, which is subsequently translated into proteins. Recent findings into RNA biology have shown its

expanded roles beyond its traditional function. Initially, mRNA was seen largely as a messenger between DNA and ribosomes for protein production. However, the finding of different non-coding RNAs (ncRNAs) has emphasized the critical regulatory activities. These include microRNAs (miRNAs), transfer RNA-derived small RNAs, pseudogenes, PIWI-interacting RNAs, long non-coding RNAs (lncRNAs), and circular RNAs, which regulate gene expression and are vital in regulating biological processes (Dhuri *et al.*, 2020).

Unlike small molecule medications that target proteins, antisense oligonucleotides (ASOs) attach directly to nucleic acid sequences through Watson–Crick base pairing. This accuracy helps the development of nucleic acid-targeted medicines, making them effective for tackling uncommon and hereditary disorders. Recently, mRNA-targeting medicines have garnered emphasis for lowering inflammatory and neoplastic illnesses by suppressing protein synthesis. Key approaches include ASOs, which block mRNA translation, and RNA interference (RNAi) oligonucleotides, both allowing targeted gene expression regulation (Chery, 2016, Chan *et al.*, 2006).

Antisense oligonucleotides (ASOs) are single-stranded DNA molecules that bind directly to target mRNA, decreasing gene expression by RNase H activity, splicing failure, or ribosomal interference. Advances in sequencing and design have boosted their medicinal and scientific value. Effective ASOs, generally ~20 nucleotides long, target translation start or splice sites. Validation entails measuring protein-level knockdown and assuring accuracy by avoiding polymorphism regions or tetraplex formation (Di Fusco *et al.*, 2019).

Advances in oligonucleotide chemistry and delivery have propelled antisense research, with FDA-approved nucleic acid therapeutics spurring clinical trials. Traditional ASOs faced challenges like nuclease degradation and low uptake, prompting the development of chemically modified ASOs for improved stability, efficacy, and reduced side effects; like:

Phosphorothioate (PS): Phosphorothioate (PS) ASOs, a first-generation antisense technology, the non-bridging oxygen in the phosphate group is substituted with a sulphur atom, creating a PS bond that resists nuclease-mediated degradation (Furdon *et al.*, 1989, Eckstein, 2000).

Phosphorodiamidate Morpholino Oligomer (PMO): In PMOs, the five-membered sugar component is swapped with a six-membered morpholine ring, and each morpholine ring is joined by phosphorodiamidate bonds. PMOs are charge-neutral and exert its actions through steric hindrance or modification of splicing. The absence of a carbonyl group in PMOs promotes the resistance to proteases and esterases, whereas the morpholine ring increases the solubility in water (Summerton and Weller, 1997).

Peptide Nucleic Acids (PNA): PNAs are synthetic nucleic acid analogs with neutral N-2-aminoethyl glycine units and nucleobases connected by a flexible methyl carbonyl linker. The unique neutral backbone makes PNAs resistant to enzymatic degradation and enhances the binding affinity to RNA sequences compared to unmodified ASOs (Pellestor and Paulasova, 2004).

Locked Nucleic Acids (LNA): LNAs include a methylene bridge linking the 2′ oxygen and 4′ carbon of the ribose ring, which improves the binding affinity to DNA or RNA due to its preorganized structure. Each LNA change enhances the melting temperature of the duplex by 2–8 °C. LNAs function through steric hindrance to execute the antisense effects. Various LNA designs, including gapmers and mixmers, have been investigated for the antisense activity in contrast to unmodified ASOs. Gapmers consist of a continuous DNA sequence bordered by LNAs and cause RNase H1-mediated cleavage. Mixmers, which intersperse DNA and LNA nucleotides, control mRNA expression by steric hindrance without causing RNase H1 cleavage (Braasch and Corey, 2001).

Ribose Modification: Modifications in the 2′ position of ribose sugars, like 2′-fluoro, 2′-O-methyl, and 2′-O-methoxyethyl, improve binding affinity and resistance to degradation in ASOs. These adjustments raise the duplex melting temperature by roughly 2 °C and diminish nonspecific protein binding. In gapmer designs, 2′-modified nucleotides border a core area of unmodified nucleotides, improving binding and protection while encouraging RNase H1-mediated RNA cleavage (Juliano, 2016, Hebb and Robertson, 1997).

Nucleobase Modification: Nucleobase alterations increase the characteristics of antisense oligonucleotides (ASOs), with cytosine analogs being particularly frequent. To address immunological stimulation produced by CpG dinucleotides in PS-ASOs, 5-methylcytosine analogs have been utilized. Additionally, G-clamp analogs, which have phenoxazine residues establishing five hydrogen bonds with complementary guanine through Watson–Crick and Hoogsteen base pairing, boost ASO potency (Ortega *et al.*, 2007).

Although nucleic acids efficiently influence protein regulation *in vivo*, the therapeutic use of ASOs has met significant difficulties. ASOs based therapeutics may stimulate immunological responses, and, because to its enormous size and negative charge, cannot passively penetrate the cell membrane. Therefore, ASOs must be provided with particular delivery techniques to enable cellular entrance and endosomal escape, which is crucial for its transport into the cytoplasm. The area of nucleic acid delivery focuses on methods and materials for transferring RNA therapeutics. Non-viral techniques are key, with nanoparticles being frequently employed because to the capacity to preserve ASOs and promote cellular absorption. Cationic polymers like poly-L-lysine and polyethyleneimine assist compress RNA and allow endosomal egress.

Lipid-based nanoparticles, especially those with ionizable lipids, increase distribution efficiency and minimize toxicity. Direct conjugation of bioactive ligands, like N-acetyl-galactosamine (GalNAc), to RNA targets particular cells and has proven therapeutic success (Kaczmarek *et al.*, 2017).

ASOs based therapeutics encounter obstacles like escaping off-target clearance, accessing particular tissues, and avoiding immune reactions. Researchers have devised different approaches, including polymers and lipid nanoparticles (LNPs), to increase ASOs delivery and potency (Cheng *et al.*, 2015). Hydrogels, with the particular physicochemical features, are revolutionizing ASOs delivery strategies. Its adeptly preserve ASOs' biological activity while enabling localized and sustained release employing complicated stimuli-responsive mechanisms. By carefully regulating the release of high ASOs concentrations, hydrogels reduce systemic loss, minimize off-target toxicity, and obviate the need for repeated injections (Zhong *et al.*, 2023). This innovative technique enhances ASOs stability and delivers a more controlled and efficient treatment plan (**Fig. 2.8**).

ASOs can be added to hydrogels either direct embedding or encapsulation in nanocarriers. Direct loading is based on interactions such as ionic, hydrogen, covalent, or hydrophobic linkages between ASOs and the hydrogel. Using nanocarriers enhances ASO stability and controlled release, but they must be compatible with the hydrogel. For naked ASOs, balancing hydrophobic and hydrophilic components is crucial for water absorption, with hydrophobic interactions mostly governed by ASO modifications (Lv *et al.*, 2006). Incorporating ASOs into hydrogels using nanocarriers, such as liposomes, lipid nanoparticles, or inorganic materials, offers an advanced alternative to direct inclusion. This method enhances loading efficiency, stability, and transfection efficacy without requiring chemical modifications of ASOs or hydrogel polymers. Nanocarriers can be made from cationic lipids, polymers like polyethylenimine (PEI) and chitosan, or inorganic nanoparticles such as gold, iron oxide, silica, and quantum dots (Mendes *et al.*, 2022).

At last the release profile of ASOs from designed hydrogel networks—encompassing both the length of availability and the release pattern (continuous or pulsatile depending upon stimuli)—is precisely tuned to the exact needs of the application (Zhong *et al.*, 2023). To accomplish this, a variety of hydrogel architectures has been created to permit regulated ASOs release using either passive or active methods. Passive methods provide both continuous short- and long-term release, while active systems enable more nuanced, pulsatile release patterns, harmonizing with exact therapeutic demands. Continuous passive release from hydrogels is handled by a mix of diffusion, matrix breakdown, and swelling properties (Wang *et al.*, 2017b). Engineering features like as molecular weight, matrix concentration, crosslinking density,

hydrophilicity, and pore size may be carefully changed to correctly manage the release kinetics and increase therapeutic benefits.

In conclusion, our study highlights the key role of macrophages in maintaining tissue homeostasis after injury. Diabetes disrupts macrophage function by impairing activation pathways, reducing phagocytosis, and increasing pro-inflammatory mediators, which in turn affect wound healing processes like immune response, angiogenesis, collagen formation, and neuropathy management. The dysregulation of macrophage activity in diabetic wounds calls for further exploration of therapies targeting macrophage dysfunction. Additionally, diabetes-induced oxidative stress and AGEs promote bacterial growth, complicating wound care. We propose designing a multifunctional, cost-effective hydrogel system to reduce oxidative stress and bacterial load while delivering ASOs to alleviate the inflammatory burden and create an optimal healing environment.

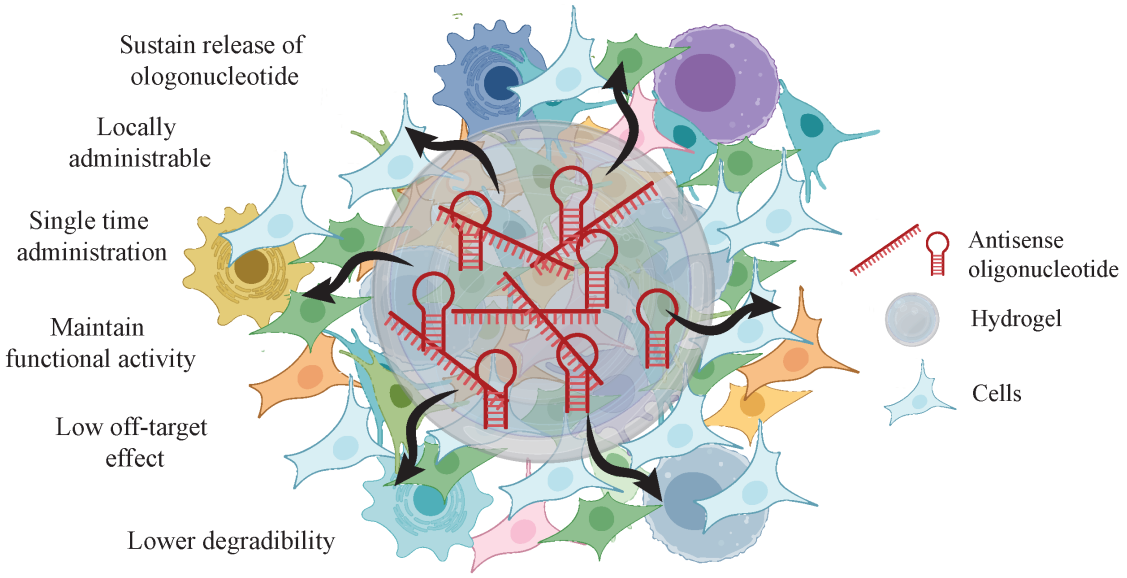

Figure 2.8. *Properties of hydrogel for ASOs delivery.*

References

ABEDI-GABALLU, F., DEHGHAN, G., GHAFFARI, M., YEKTA, R., ABBASPOUR-RAVASJANI, S., BARADARAN, B., EZZATI NAZHAD DOLATABADI, J. & HAMBLIN, M. R. 2018. PAMAM dendrimers as efficient drug and gene delivery nanosystems for cancer therapy. *Applied Materials Today,* 12**,** 177-190.

AGIER, J., EFENBERGER, M. & BRZEZIŃSKA-BŁASZCZYK, E. 2015. Cathelicidin impact on inflammatory cells. *Cent Eur J Immunol,* 40**,** 225-35.

AHRENS, S., ZELENAY, S., SANCHO, D., HANČ, P., KJÆR, S., FEEST, C., FLETCHER, G., DURKIN, C., POSTIGO, A., SKEHEL, M., BATISTA, F., THOMPSON, B., WAY, M., REIS E SOUSA, C. & SCHULZ, O. 2012. F-Actin Is an Evolutionarily Conserved Damage-Associated Molecular Pattern Recognized by DNGR-1, a Receptor for Dead Cells. *Immunity,* 36**,** 635-645.

AKBARIAN, M., BERTASSONI, L. E. & TAYEBI, L. 2022. Biological aspects in controlling angiogenesis: current progress. *Cellular and Molecular Life Sciences,* 79**,** 349.

AKKUS, G. & SERT, M. 2022. Diabetic foot ulcers: A devastating complication of diabetes mellitus continues non-stop in spite of new medical treatment modalities. *World J Diabetes,* 13**,** 1106-1121.

ALFORD, M. A., BAQUIR, B., SANTANA, F. L., HANEY, E. F. & HANCOCK, R. E. W. 2020. Cathelicidin Host Defense Peptides and Inflammatory Signaling: Striking a Balance. *Front Microbiol,* 11**,** 1902.

ASWATHY, S., NARENDRAKUMAR, U. & MANJUBALA, I. 2020. Commercial hydrogels for biomedical applications. *Heliyon,* 6.

AWADA, H. K., JOHNSON, N. R. & WANG, Y. 2014. Dual delivery of vascular endothelial growth factor and hepatocyte growth factor coacervate displays strong angiogenic effects. *Macromol Biosci,* 14**,** 679-86.

AYUK, S. M., ABRAHAMSE, H. & HOURELD, N. N. 2016. The Role of Matrix Metalloproteinases in Diabetic Wound Healing in relation to Photobiomodulation. *J Diabetes Res,* 2016**,** 2897656.

BACCI, S. 2022. Fine Regulation during Wound Healing by Mast Cells, a Physiological Role Not Yet Clarified. *International Journal of Molecular Sciences,* 23**,** 1820.

BAR YAACOV, R., ESHEL, R., FARHI, E., SHEMULUVICH, F., KAPLAN, T. & BIRNBAUM, R. Y. 2019. Functional characterization of the ZEB2 regulatory landscape. *Hum Mol Genet,* 28**,** 1487-1497.

BARRIENTOS, S., STOJADINOVIC, O., GOLINKO, M. S., BREM, H. & TOMIC-CANIC, M. 2008. PERSPECTIVE ARTICLE: Growth factors and cytokines in wound healing. *Wound Repair and Regeneration,* 16**,** 585-601.

BECKER, R. C., SEXTON, T. & SMYTH, S. S. 2018. Translational Implications of Platelets as Vascular First Responders. *Circ Res,* 122**,** 506-522.

BELAIR, D. G., MILLER, M. J., WANG, S., DARJATMOKO, S. R., BINDER, B. Y. K., SHEIBANI, N. & MURPHY, W. L. 2016. Differential regulation of angiogenesis using degradable VEGF-binding microspheres. *Biomaterials,* 93**,** 27-37.

BILOUSOVA, G., CHEN, J. & ROOP, D. R. 2011. Differentiation of mouse induced pluripotent stem cells into a multipotent keratinocyte lineage. *J Invest Dermatol,* 131**,** 857-64.

BIRKHOFF, J. C., BROUWER, R. W. W., KOLOVOS, P., KORPORAAL, A. L., BERMEJO-SANTOS, A., BOLTSIS, I., NOWOSAD, K., VAN DEN HOUT, M., GROSVELD, F. G., VAN, I. W. F. J., HUYLEBROECK, D. & CONIDI, A. 2020. Targeted chromatin conformation analysis identifies novel distal neural enhancers of ZEB2 in pluripotent stem cell differentiation. *Hum Mol Genet,* 29**,** 2535-2550.

BOOTHBY, I. C., COHEN, J. N. & ROSENBLUM, M. D. 2020. Regulatory T cells in skin injury: At the crossroads of tolerance and tissue repair. *Sci Immunol,* 5.

BORENA, B. M., MARTENS, A., BROECKX, S. Y., MEYER, E., CHIERS, K., DUCHATEAU, L. & SPAAS, J. H. 2015. Regenerative Skin Wound Healing in Mammals: State-of-the-Art on Growth Factor and Stem Cell Based Treatments. *Cell Physiol Biochem,* 36**,** 1-23.

BRAASCH, D. A. & COREY, D. R. 2001. Locked nucleic acid (LNA): fine-tuning the recognition of DNA and RNA. *Chem Biol,* 8**,** 1-7.

BRANDT, E., PETERSEN, F., LUDWIG, A., EHLERT, J. E., BOCK, L. & FLAD, H. D. 2000. The beta-thromboglobulins and platelet factor 4: blood platelet-derived CXC chemokines with divergent roles in early neutrophil regulation. *J Leukoc Biol,* 67**,** 471-8.

BRIQUEZ, P. S., CLEGG, L. E., MARTINO, M. M., GABHANN, F. M. & HUBBELL, J. A. 2016. Design principles for therapeutic angiogenic materials. *Nature Reviews Materials,* 1**,** 15006.

BROWN, M. S., ASHLEY, B. & KOH, A. 2018. Wearable Technology for Chronic Wound Monitoring: Current Dressings, Advancements, and Future Prospects. *Front Bioeng Biotechnol,* 6**,** 47.

BURDICK, JASON A., MAUCK, ROBERT L. & GERECHT, S. 2016. To Serve and Protect: Hydrogels to Improve Stem Cell-Based Therapies. *Cell Stem Cell,* 18**,** 13-15.

CABRAL-PACHECO, G. A., GARZA-VELOZ, I., CASTRUITA-DE LA ROSA, C., RAMIREZ-ACUÑA, J. M., PEREZ-ROMERO, B. A., GUERRERO-RODRIGUEZ, J. F., MARTINEZ-AVILA, N. & MARTINEZ-FIERRO, M. L. 2020. The Roles of Matrix Metalloproteinases and Their Inhibitors in Human Diseases. *Int J Mol Sci,* 21.

CAPILA, I. & LINHARDT, R. J. 2002. Heparin–protein interactions. *Angewandte Chemie International Edition,* 41**,** 390-412.

CAPSONI, S., TIVERON, C., VIGNONE, D., AMATO, G. & CATTANEO, A. 2010. Dissecting the involvement of tropomyosin-related kinase A and p75 neurotrophin receptor signaling in NGF deficit-induced neurodegeneration. *Proceedings of the National Academy of Sciences,* 107**,** 12299-12304.

CARVALHO, I. C. & MANSUR, H. S. 2017. Engineered 3D-scaffolds of photocrosslinked chitosan-gelatin hydrogel hybrids for chronic wound dressings and regeneration. *Mater Sci Eng C Mater Biol Appl,* 78**,** 690-705.

CASTILLO-ECIJA, H., MONTERRUBIO, C., PASCUAL-PASTO, G., GOMEZ-GONZALEZ, S., GARCIA-DOMINGUEZ, D. J., HONTECILLAS-PRIETO, L., RESA-PARES, C., BURGUEÑO, V., PACO, S., OLACIREGUI, N. G., VILA-UBACH, M., RESTREPO-PERDOMO, C., CUADRADO-VILANOVA, M., BALAGUER-LLUNA, L., PEREZ-JAUME, S., CASTAÑEDA, A., SANTA-MARIA, V., ROLDAN, M., SUÑOL, M., DE ALAVA, E., MORA, J., LAVARINO, C. & CARCABOSO, A. M. 2020. Treatment-driven selection of chemoresistant Ewing sarcoma tumors with limited drug distribution. *J Control Release,* 324**,** 440-449.

CASTLEBERRY, S. A., ALMQUIST, B. D., LI, W., REIS, T., CHOW, J., MAYNER, S. & HAMMOND, P. T. 2016. Self-Assembled Wound Dressings Silence MMP-9 and Improve Diabetic Wound Healing In Vivo. *Advanced Materials,* 28**,** 1809-1817.

CHAN, J. H., LIM, S. & WONG, W. F. 2006. Antisense oligonucleotides: from design to therapeutic application. *Clinical and experimental pharmacology and physiology,* 33**,** 533-540.

CHANG, H.-K., KIM, P.-H., CHO, H.-M., YUM, S.-Y., CHOI, Y.-J., SON, Y., LEE, D., KANG, I., KANG, K.-S., JANG, G. & CHO, J.-Y. 2016. Inducible HGF-secreting Human Umbilical Cord Blood-derived MSCs Produced via TALEN-mediated Genome Editing Promoted Angiogenesis. *Molecular Therapy,* 24**,** 1644-1654.

CHEN, S., SHI, J., ZHANG, M., CHEN, Y., WANG, X., ZHANG, L., TIAN, Z., YAN, Y., LI, Q., ZHONG, W., XING, M., ZHANG, L. & ZHANG, L. 2015a. Mesenchymal stem cell-laden anti-inflammatory hydrogel enhances diabetic wound healing. *Sci Rep,* 5**,** 18104.

CHEN, W.-Y., CHANG, H.-Y., LU, J.-K., HUANG, Y.-C., HARROUN, S. G., TSENG, Y.-T., LI, Y.-J., HUANG, C.-C. & CHANG, H.-T. 2015b. Self-Assembly of Antimicrobial Peptides on Gold Nanodots: Against Multidrug-Resistant Bacteria and Wound-Healing Application. *Advanced Functional Materials,* 25**,** 7189-7199.

CHENG, C. J., TIETJEN, G. T., SAUCIER-SAWYER, J. K. & SALTZMAN, W. M. 2015. A holistic approach to targeting disease with polymeric nanoparticles. *Nat Rev Drug Discov,* 14**,** 239-47.

CHERY, J. 2016. RNA therapeutics: RNAi and antisense mechanisms and clinical applications. *Postdoc journal: a journal of postdoctoral research and postdoctoral affairs,* 4**,** 35.

CHODACZEK, G., PAPANNA, V., ZAL, M. A. & ZAL, T. 2012. Body-barrier surveillance by epidermal γδ TCRs. *Nature Immunology,* 13**,** 272-282.

CHOI, J. S., CHOI, S. H. & YOO, H. S. 2011. Coaxial electrospun nanofibers for treatment of diabetic ulcers with binary release of multiple growth factors. *Journal of Materials Chemistry,* 21**,** 5258-5267.

CHOUDHARY, V., CHOUDHARY, M. & BOLLAG, W. B. 2024. Exploring Skin Wound Healing Models and the Impact of Natural Lipids on the Healing Process. *Int J Mol Sci,* 25.

CHU, Y., YU, D., WANG, P., XU, J., LI, D. & DING, M. 2010. Nanotechnology promotes the full-thickness diabetic wound healing effect of recombinant human epidermal growth factor in diabetic rats. *Wound Repair Regen,* 18**,** 499-505.

CHUAH, Y. K., BASIR, R., TALIB, H., TIE, T. H. & NORDIN, N. 2013. Receptor for advanced glycation end products and its involvement in inflammatory diseases. *Int J Inflam,* 2013**,** 403460.

CIALDAI, F., RISALITI, C. & MONICI, M. 2022. Role of fibroblasts in wound healing and tissue remodeling on Earth and in space. *Front Bioeng Biotechnol,* 10**,** 958381.

CROMBEZ, L., ALDRIAN-HERRADA, G., KONATE, K., NGUYEN, Q. N., MCMASTER, G. K., BRASSEUR, R., HEITZ, F. & DIVITA, G. 2009. A new potent secondary amphipathic cell-penetrating peptide for siRNA delivery into mammalian cells. *Mol Ther,* 17**,** 95-103.

CRUZ, M. S., DIAMOND, A., RUSSELL, A. & JAMESON, J. M. 2018. Human αβ and γδ T Cells in Skin Immunity and Disease. *Front Immunol,* 9**,** 1304.

CUI, X., BOLAND, T., D.D, APOS, LIMA, D. & MARTIN, K. L. 2012. Thermal Inkjet Printing in Tissue Engineering and Regenerative Medicine. *Recent Patents on Drug Delivery & Formulation,* 6**,** 149-155.

DAI, T., TANAKA, M., HUANG, Y. Y. & HAMBLIN, M. R. 2011. Chitosan preparations for wounds and burns: antimicrobial and wound-healing effects. *Expert Rev Anti Infect Ther,* 9**,** 857-79.

DANIEL, M.-C. & ASTRUC, D. 2004. Gold Nanoparticles: Assembly, Supramolecular Chemistry, Quantum-Size-Related Properties, and Applications toward Biology, Catalysis, and Nanotechnology. *Chemical Reviews,* 104**,** 293-346.

DARABI, M. A., KHOSROZADEH, A., MBELECK, R., LIU, Y., CHANG, Q., JIANG, J., CAI, J., WANG, Q., LUO, G. & XING, M. 2017. Skin-Inspired Multifunctional Autonomic-Intrinsic Conductive Self-Healing Hydrogels with Pressure Sensitivity, Stretchability, and 3D Printability. *Adv Mater,* 29.

DARWITZ, B. P., GENITO, C. J. & THURLOW, L. R. Triple threat: how diabetes results in worsened bacterial infections. *Infection and Immunity,* 0**,** e00509-23.

DAS, S., SINGH, G., MAJID, M., SHERMAN, M. B., MUKHOPADHYAY, S., WRIGHT, C. S., MARTIN, P. E., DUNN, A. K. & BAKER, A. B. 2016. Syndesome Therapeutics for Enhancing Diabetic Wound Healing. *Adv Healthc Mater,* 5**,** 2248-60.

DEMIDOVA-RICE, T. N., HAMBLIN, M. R. & HERMAN, I. M. 2012a. Acute and impaired wound healing: pathophysiology and current methods for drug delivery, part 1: normal and chronic wounds: biology, causes, and approaches to care. *Adv Skin Wound Care,* 25**,** 304-14.

DEMIDOVA-RICE, T. N., HAMBLIN, M. R. & HERMAN, I. M. 2012b. Acute and impaired wound healing: pathophysiology and current methods for drug delivery, part 2: role of growth factors in normal and pathological wound healing: therapeutic potential and methods of delivery. *Adv Skin Wound Care,* 25**,** 349-70.

DHOLE, S., MAHAKALKAR, C., KSHIRSAGAR, S. & BHARGAVA, A. 2023. Antibiotic Prophylaxis in Surgery: Current Insights and Future Directions for Surgical Site Infection Prevention. *Cureus,* 15**,** e47858.

DHURI, K., BECHTOLD, C., QUIJANO, E., PHAM, H., GUPTA, A., VIKRAM, A. & BAHAL, R. 2020. Antisense Oligonucleotides: An Emerging Area in Drug Discovery and Development. *J Clin Med,* 9.

DI FUSCO, D., DINALLO, V., MARAFINI, I., FIGLIUZZI, M. M., ROMANO, B. & MONTELEONE, G. 2019. Antisense Oligonucleotide: Basic Concepts and Therapeutic Application in Inflammatory Bowel Disease. *Frontiers in Pharmacology,* 10.

DIAS, J. R., GRANJA, P. L. & BÁRTOLO, P. J. 2016. Advances in electrospun skin substitutes. *Progress in Materials Science,* 84**,** 314-334.

DLUDLA, P. V., MABHIDA, S. E., ZIQUBU, K., NKAMBULE, B. B., MAZIBUKO-MBEJE, S. E., HANSER, S., BASSON, A. K., PHEIFFER, C. & KENGNE, A. P. 2023. Pancreatic β-cell dysfunction in type 2 diabetes: Implications of inflammation and oxidative stress. *World J Diabetes,* 14**,** 130-146.

DOMINGUEZ, C. X., AMEZQUITA, R. A., GUAN, T., MARSHALL, H. D., JOSHI, N. S., KLEINSTEIN, S. H. & KAECH, S. M. 2015. The transcription factors ZEB2 and T-bet cooperate to program cytotoxic T cell terminal differentiation in response to LCMV viral infection. *Journal of Experimental Medicine,* 212**,** 2041-2056.

DONELLI, G. & VUOTTO, C. 2014. Biofilm-based infections in long-term care facilities. *Future Microbiol,* 9**,** 175-88.

DURAI, V., BAGADIA, P., GRANJA, J. M., SATPATHY, A. T., KULKARNI, D. H., DAVIDSON IV, J. T., WU, R., PATEL, S. J., IWATA, A. & LIU, T.-T. 2019. Cryptic activation of an Irf8 enhancer governs cDC1 fate specification. *Nature immunology,* 20**,** 1161-1173.

DURAINE, G. D., BROWN, W. E., HU, J. C. & ATHANASIOU, K. A. 2015. Emergence of Scaffold-Free Approaches for Tissue Engineering Musculoskeletal Cartilages. *Annals of Biomedical Engineering,* 43**,** 543-554.

ECKSTEIN, F. 2000. Phosphorothioate oligodeoxynucleotides: what is their origin and what is unique about them? *Antisense Nucleic Acid Drug Dev,* 10**,** 117-21.

EVERETT, E. & MATHIOUDAKIS, N. 2018. Update on management of diabetic foot ulcers. *Ann N Y Acad Sci,* 1411**,** 153-165.

FALANGA, V., ISSEROFF, R. R., SOULIKA, A. M., ROMANELLI, M., MARGOLIS, D., KAPP, S., GRANICK, M. & HARDING, K. 2022. Chronic wounds. *Nature Reviews Disease Primers,* 8**,** 50.

FANG, T. 2012. Yin Yang: A New Perspective on Culture. *Management and Organization Review,* 8**,** 25-50.

FERRANTE, C. J. & LEIBOVICH, S. J. 2012. Regulation of Macrophage Polarization and Wound Healing. *Adv Wound Care (New Rochelle),* 1**,** 10-16.

FERREIRA, M. C., TUMA, P., JR., CARVALHO, V. F. & KAMAMOTO, F. 2006. Complex wounds. *Clinics (Sao Paulo),* 61**,** 571-8.

FIRLAR, I., ALTUNBEK, M., MCCARTHY, C., RAMALINGAM, M. & CAMCI-UNAL, G. 2022. Functional Hydrogels for Treatment of Chronic Wounds. *Gels,* 8**,** 127.

FRYKBERG, R. G. & BANKS, J. 2015. Challenges in the Treatment of Chronic Wounds. *Adv Wound Care (New Rochelle),* 4**,** 560-582.

FU, K., ZHENG, X., CHEN, Y., WU, L., YANG, Z., CHEN, X. & SONG, W. 2022. Role of matrix metalloproteinases in diabetic foot ulcers: Potential therapeutic targets. *Frontiers in Pharmacology,* 13.

FUKUDA, J., KHADEMHOSSEINI, A., YEH, J., ENG, G., CHENG, J., FAROKHZAD, O. C. & LANGER, R. 2006. Micropatterned cell co-cultures using layer-by-layer deposition of extracellular matrix components. *Biomaterials,* 27**,** 1479-1486.

FUKUSHIMA, K., LIU, S., WU, H., ENGLER, A. C., COADY, D. J., MAUNE, H., PITERA, J., NELSON, A., WIRADHARMA, N., VENKATARAMAN, S., HUANG, Y., FAN, W., YING, J. Y., YANG, Y. Y. & HEDRICK, J. L. 2013. Supramolecular high-aspect ratio assemblies with strong antifungal activity. *Nat Commun,* 4**,** 2861.

FUMAKIA, M. & HO, E. A. 2016. Nanoparticles Encapsulated with LL37 and Serpin A1 Promotes Wound Healing and Synergistically Enhances Antibacterial Activity. *Mol Pharm,* 13**,** 2318-31.

FURDON, P. J., DOMINSKI, Z. & KOLE, R. 1989. RNase H cleavage of RNA hybridized to oligonucleotides containing methylphosphonate, phosphorothioate and phosphodiester bonds. *Nucleic Acids Res,* 17**,** 9193-204.

GAAZ, T. S., SULONG, A. B., AKHTAR, M. N., KADHUM, A. A., MOHAMAD, A. B. & AL-AMIERY, A. A. 2015. Properties and Applications of Polyvinyl Alcohol, Halloysite Nanotubes and Their Nanocomposites. *Molecules,* 20**,** 22833-47.

GAHARWAR, A. K., AVERY, R. K., ASSMANN, A., PAUL, A., MCKINLEY, G. H., KHADEMHOSSEINI, A. & OLSEN, B. D. 2014. Shear-Thinning Nanocomposite Hydrogels for the Treatment of Hemorrhage. *ACS Nano,* 8**,** 9833-9842.

GAUTAM, S., FIORAVANTI, J., ZHU, W., LE GALL, J. B., BROHAWN, P., LACEY, N. E., HU, J., HOCKER, J. D., HAWK, N. V. & KAPOOR, V. 2019. The transcription factor c-Myb regulates CD8+ T cell stemness and antitumor immunity. *Nature immunology,* 20**,** 337-349.

GEORGIOU, T. K., VAMVAKAKI, M., PATRICKIOS, C. S., YAMASAKI, E. N. & PHYLACTOU, L. A. 2004. Nanoscopic cationic methacrylate star homopolymers: synthesis by group transfer polymerization, characterization and evaluation as transfection reagents. *Biomacromolecules,* 5**,** 2221-9.

GIRI, B., DEY, S., DAS, T., SARKAR, M., BANERJEE, J. & DASH, S. K. 2018. Chronic hyperglycemia mediated physiological alteration and metabolic distortion leads to organ dysfunction, infection, cancer progression and other pathophysiological consequences: An update on glucose toxicity. *Biomedicine & Pharmacotherapy,* 107**,** 306-328.

GOOSSENS, S., JANZEN, V., BARTUNKOVA, S., YOKOMIZO, T., DROGAT, B., CRISAN, M., HAIGH, K., SEUNTJENS, E., UMANS, L. & RIEDT, T. 2011. The EMT regulator Zeb2/Sip1 is essential for murine embryonic hematopoietic stem/progenitor cell differentiation and mobilization. *Blood, The Journal of the American Society of Hematology,* 117**,** 5620-5630.

GREGORIO, J., MELLER, S., CONRAD, C., DI NARDO, A., HOMEY, B., LAUERMA, A., ARAI, N., GALLO, R. L., DIGIOVANNI, J. & GILLIET, M. 2010. Plasmacytoid dendritic cells sense skin injury and promote wound healing through type I interferons. *J Exp Med,* 207**,** 2921-30.

GRIFFIN, D. R., WEAVER, W. M., SCUMPIA, P. O., DI CARLO, D. & SEGURA, T. 2015. Accelerated wound healing by injectable microporous gel scaffolds assembled from annealed building blocks. *Nat Mater,* 14**,** 737-44.

GUALDONI, G. S., BARRIL, C., JACOBO, P. V., PACHECO RODRÍGUEZ, L. N. & CEBRAL, E. 2023. Involvement of metalloproteinase and nitric oxide synthase/nitric oxide mechanisms in early decidual angiogenesis–vascularization of normal and experimental pathological mouse placenta related to maternal alcohol exposure. *Frontiers in Cell and Developmental Biology,* 11.

GUO, B., DONG, R., LIANG, Y. & LI, M. 2021. Haemostatic materials for wound healing applications. *Nat Rev Chem,* 5**,** 773-791.

GURTNER, G. C., WERNER, S., BARRANDON, Y. & LONGAKER, M. T. 2008. Wound repair and regeneration. *Nature,* 453**,** 314-321.

HABIB, M., AKTER, M., ALAM, M., KARIM, Z. & JOARDER, M. 2015. Hydrogel: a noble approach to healthcare. *Int. J. Innovat. Pharmaceut. Sci. Res,* 3**,** 1372-1388.

HARTGERINK, J. D., BENIASH, E. & STUPP, S. I. 2002. Peptide-amphiphile nanofibers: A versatile scaffold for the preparation of self-assembling materials. *Proceedings of the National Academy of Sciences,* 99**,** 5133-5138.

HAVRAN, W. L. & JAMESON, J. M. 2010. Epidermal T cells and wound healing. *J Immunol,* 184**,** 5423-8.

HEATH, W. R. & CARBONE, F. R. 2013. The skin-resident and migratory immune system in steady state and memory: innate lymphocytes, dendritic cells and T cells. *Nature Immunology,* 14**,** 978-985.

HEBB, M. O. & ROBERTSON, H. A. 1997. End-capped antisense oligodeoxynucleotides effectively inhibit gene expression in vivo and offer a low-toxicity alternative to fully modified phosphorothioate oligodeoxynucleotides. *Brain Res Mol Brain Res,* 47**,** 223-8.

HEGARTY, S. V., SULLIVAN, A. M. & O'KEEFFE, G. W. 2015. Zeb2: A multifunctional regulator of nervous system development. *Prog Neurobiol,* 132**,** 81-95.

HIGASHI, Y., MARUHASHI, M., NELLES, L., VAN DE PUTTE, T., VERSCHUEREN, K., MIYOSHI, T., YOSHIMOTO, A., KONDOH, H. & HUYLEBROECK, D. 2002. Generation of the floxed allele of the SIP1 (Smad-interacting protein 1) gene for Cre-mediated conditional knockout in the mouse. *genesis,* 32**,** 82-84.

HONG, W. X., HU, M. S., ESQUIVEL, M., LIANG, G. Y., RENNERT, R. C., MCARDLE, A., PAIK, K. J., DUSCHER, D., GURTNER, G. C., LORENZ, H. P. & LONGAKER, M. T. 2014. The Role of Hypoxia-Inducible Factor in Wound Healing. *Adv Wound Care (New Rochelle),* 3**,** 390-399.

HOWARD, P. A. & DELAFONTAINE, P. 2004. Nonsteroidal anti-Inflammatory drugs and cardiovascular risk. *J Am Coll Cardiol,* 43**,** 519-25.

HU, C., LONG, L., CAO, J., ZHANG, S. & WANG, Y. 2021. Dual-crosslinked mussel-inspired smart hydrogels with enhanced antibacterial and angiogenic properties for chronic infected diabetic wound treatment via pH-responsive quick cargo release. *Chemical Engineering Journal,* 411**,** 128564.

HUANG, X., FERRIS, S. T., KIM, S., CHOUDHARY, M. N. K., BELK, J. A., FAN, C., QI, Y., SUDAN, R., XIA, Y., DESAI, P., CHEN, J., LY, N., SHI, Q., BAGADIA, P., LIU, T., GUILLIAMS, M., EGAWA, T., COLONNA, M., DIAMOND, M. S., MURPHY, T. L., SATPATHY, A. T., WANG, T. & MURPHY, K. M. 2021. Differential usage of transcriptional repressor Zeb2 enhancers distinguishes adult and embryonic hematopoiesis. *Immunity,* 54**,** 1417-1432.e7.

HUANG, Y., GUO, X., WU, Y., CHEN, X., FENG, L., XIE, N. & SHEN, G. 2024. Nanotechnology's frontier in combatting infectious and inflammatory diseases: prevention and treatment. *Signal Transduction and Targeted Therapy,* 9**,** 34.

ITALIANO, J. E., JR, RICHARDSON, J. L., PATEL-HETT, S., BATTINELLI, E., ZASLAVSKY, A., SHORT, S., RYEOM, S., FOLKMAN, J. & KLEMENT, G. L. 2008. Angiogenesis is regulated by a novel mechanism: pro- and antiangiogenic proteins are organized into separate platelet α granules and differentially released. *Blood,* 111**,** 1227-1233.

IVANOV, E., AKHMETSHINA, M., ERDIAKOV, A. & GAVRILOVA, S. 2023. Sympathetic System in Wound Healing: Multistage Control in Normal and Diabetic Skin. *International Journal of Molecular Sciences,* 24**,** 2045.

JAFARI, N. V. & ROHN, J. L. 2022. The urothelium: a multi-faceted barrier against a harsh environment. *Mucosal Immunol,* 15**,** 1127-1142.

JIANG, S., DENG, J., JIN, Y., QIAN, B., LV, W., ZHOU, Q., MEI, E., NEISIANY, R. E., LIU, Y., YOU, Z. & PAN, J. 2023. Breathable, antifreezing, mechanically skin-like hydrogel textile wound dressings with dual antibacterial mechanisms. *Bioact Mater,* 21**,** 313-323.

JING, X., SUN, Y., LIU, Y., MA, X. & HU, H. 2021. Alginate/chitosan-based hydrogel loaded with gene vectors to deliver polydeoxyribonucleotide for effective wound healing. *Biomater Sci,* 9**,** 5533-5541.

JOHNSON, M., LLOYD, J., TEKKAM, S., CROOKE, S. N., WITHERDEN, D. A., HAVRAN, W. L. & FINN, M. G. 2020. Degradable Hydrogels for the Delivery of Immune-modulatory Proteins in the Wound Environment. *ACS Appl Bio Mater,* 3**,** 4779-4788.

JUAN, C. A., PÉREZ DE LA LASTRA, J. M., PLOU, F. J. & PÉREZ-LEBEÑA, E. 2021. The Chemistry of Reactive Oxygen Species (ROS) Revisited: Outlining Their Role in Biological Macromolecules (DNA, Lipids and Proteins) and Induced Pathologies. *International Journal of Molecular Sciences,* 22**,** 4642.

JULIANO, R. L. 2016. The delivery of therapeutic oligonucleotides. *Nucleic Acids Res,* 44**,** 6518-48.

KACZMAREK, J. C., KOWALSKI, P. S. & ANDERSON, D. G. 2017. Advances in the delivery of RNA therapeutics: from concept to clinical reality. *Genome Med,* 9**,** 60.

KAMALY, N., YAMEEN, B., WU, J. & FAROKHZAD, O. C. 2016. Degradable Controlled-Release Polymers and Polymeric Nanoparticles: Mechanisms of Controlling Drug Release. *Chemical Reviews,* 116**,** 2602-2663.

KAMOUN, E. A., KENAWY, E.-R. S. & CHEN, X. 2017. A review on polymeric hydrogel membranes for wound dressing applications: PVA-based hydrogel dressings. *Journal of Advanced Research,* 8**,** 217-233.

KANG, Y., KIM, J., LEE, Y. M., IM, S., PARK, H. & KIM, W. J. 2015. Nitric oxide-releasing polymer incorporated ointment for cutaneous wound healing. *J Control Release,* 220**,** 624-30.

KHULLAR, M., CHEEMA, B. S. & RAUT, S. K. 2017. Emerging Evidence of Epigenetic Modifications in Vascular Complication of Diabetes. *Frontiers in Endocrinology,* 8.

KIM, H. N., HONG, Y., KIM, M. S., KIM, S. M. & SUH, K.-Y. 2012. Effect of orientation and density of nanotopography in dermal wound healing. *Biomaterials,* 33**,** 8782-8792.

KIM, H. S., SUN, X., LEE, J.-H., KIM, H.-W., FU, X. & LEONG, K. W. 2019. Advanced drug delivery systems and artificial skin grafts for skin wound healing. *Advanced Drug Delivery Reviews,* 146**,** 209-239.

KIM, H. S. & YOO, H. S. 2010. MMPs-responsive release of DNA from electrospun nanofibrous matrix for local gene therapy: In vitro and in vivo evaluation. *Journal of Controlled Release,* 145**,** 264-271.

KIM, J. W., KIM, M. J., KI, C. S., KIM, H. J. & PARK, Y. H. 2017. Fabrication of bi-layer scaffold of keratin nanofiber and gelatin-methacrylate hydrogel: Implications for skin graft. *International Journal of Biological Macromolecules,* 105**,** 541-548.

KIRSNER, R. S., VANSCHEIDT, W., KEAST, D. H., LANTIS II, J. C., DOVE, C. R., CAZZELL, S. M., VARTIVARIAN, M., AUGUSTIN, M., MARSTON, W. A., MCCOY, N. D., CARGILL, D. I., LEE, T. D., DICKERSON JR, J. E., SLADE, H. B. & GROUP, F. T. H.-S. 2016. Phase 3 evaluation of HP802-247 in the treatment of chronic venous leg ulcers. *Wound Repair and Regeneration,* 24**,** 894-903.

KISSENPFENNIG, A., HENRI, S., DUBOIS, B., LAPLACE-BUILHÉ, C., PERRIN, P., ROMANI, N., TRIPP, C. H., DOUILLARD, P., LESERMAN, L., KAISERLIAN, D., SAELAND, S., DAVOUST, J. & MALISSEN, B. 2005. Dynamics and Function of Langerhans Cells In Vivo: Dermal Dendritic Cells Colonize Lymph Node AreasDistinct from Slower Migrating Langerhans Cells. *Immunity,* 22**,** 643-654.

KOH, T. J. & DIPIETRO, L. A. 2011. Inflammation and wound healing: the role of the macrophage. *Expert Rev Mol Med,* 13**,** e23.

KOLLURU, G. K., BIR, S. C. & KEVIL, C. G. 2012. Endothelial dysfunction and diabetes: effects on angiogenesis, vascular remodeling, and wound healing. *Int J Vasc Med,* 2012**,** 918267.

KOMI, D. E. A., KHOMTCHOUK, K. & SANTA MARIA, P. L. 2020. A Review of the Contribution of Mast Cells in Wound Healing: Involved Molecular and Cellular Mechanisms. *Clin Rev Allergy Immunol,* 58**,** 298-312.

KROCK, B. L., SKULI, N. & SIMON, M. C. 2011. Hypoxia-induced angiogenesis: good and evil. *Genes Cancer,* 2**,** 1117-33.

KRZYSZCZYK, P., SCHLOSS, R., PALMER, A. & BERTHIAUME, F. 2018. The Role of Macrophages in Acute and Chronic Wound Healing and Interventions to Promote Pro-wound Healing Phenotypes. *Front Physiol,* 9**,** 419.

KUJATH, P. & MICHELSEN, A. 2008. Wounds - from physiology to wound dressing. *Dtsch Arztebl Int,* 105**,** 239-48.

KURAKULA, M. & RAO, G. 2020. Pharmaceutical assessment of polyvinylpyrrolidone (PVP): As excipient from conventional to controlled delivery systems with a spotlight on COVID-19 inhibition. *J Drug Deliv Sci Technol,* 60**,** 102046.

LALONDE, D., JOUKHADAR, N. & JANIS, J. 2019. Simple Effective Ways to Care for Skin Wounds and Incisions. *Plast Reconstr Surg Glob Open,* 7**,** e2471.

LAN, B., ZHANG, L., YANG, L., WU, J., LI, N., PAN, C., WANG, X., ZENG, L., YAN, L., YANG, C. & REN, M. 2021. Sustained delivery of MMP-9 siRNA via thermosensitive hydrogel accelerates diabetic wound healing. *J Nanobiotechnology,* 19**,** 130.

LANDÉN, N. X., LI, D. & STÅHLE, M. 2016. Transition from inflammation to proliferation: a critical step during wound healing. *Cell Mol Life Sci,* 73**,** 3861-85.

LANDOLINA, N., GANGWAR, R. S. & LEVI-SCHAFFER, F. 2015. Chapter Two - Mast Cells' Integrated Actions with Eosinophils and Fibroblasts in Allergic Inflammation: Implications for Therapy. *In:* ALT, F. W. (ed.) *Advances in Immunology.* Academic Press.

LANGER, V., BHANDARI, P. S., RAJAGOPALAN, S. & MUKHERJEE, M. K. 2015. Negative pressure wound therapy as an adjunct in healing of chronic wounds. *Int Wound J,* 12**,** 436-42.

LEE, K. Y. & MOONEY, D. J. 2012. Alginate: properties and biomedical applications. *Prog Polym Sci,* 37**,** 106-126.

LEE, Y.-H., HONG, Y.-L. & WU, T.-L. 2021. Novel silver and nanoparticle-encapsulated growth factor co-loaded chitosan composite hydrogel with sustained antimicrobility and promoted biological properties for diabetic wound healing. *Materials Science and Engineering: C,* 118**,** 111385.

LI, Q., NIU, Y., DIAO, H., WANG, L., CHEN, X., WANG, Y., DONG, L. & WANG, C. 2017. In situ sequestration of endogenous PDGF-BB with an ECM-mimetic sponge for accelerated wound healing. *Biomaterials,* 148**,** 54-68.

LI, T., LU, X.-M., ZHANG, M.-R., HU, K. & LI, Z. 2022. Peptide-based nanomaterials: Self-assembly, properties and applications. *Bioactive Materials,* 11**,** 268-282.

LI, X., LI, C., ZHANG, W., WANG, Y., QIAN, P. & HUANG, H. 2023. Inflammation and aging: signaling pathways and intervention therapies. *Signal Transduction and Targeted Therapy,* 8**,** 239.

LIN, W. C., HUANG, C. C., LIN, S. J., LI, M. J., CHANG, Y., LIN, Y. J., WAN, W. L., SHIH, P. C. & SUNG, H. W. 2017. In situ depot comprising phase-change materials that can sustainably release a gasotransmitter H(2)S to treat diabetic wounds. *Biomaterials,* 145**,** 1-8.

LINDSEY, S. & LANGHANS, S. A. 2014. Crosstalk of Oncogenic Signaling Pathways during Epithelial-Mesenchymal Transition. *Front Oncol,* 4**,** 358.

LIU, S. Q., VENKATARAMAN, S., ONG, Z. Y., CHAN, J. M. W., YANG, C., HEDRICK, J. L. & YANG, Y. Y. 2014. Overcoming Multidrug Resistance in Microbials Using Nanostructures Self-Assembled from Cationic Bent-Core Oligomers. *Small,* 10**,** 4130-4135.

LIU, Y., PHARR, M. & SALVATORE, G. A. 2017. Lab-on-Skin: A Review of Flexible and Stretchable Electronics for Wearable Health Monitoring. *ACS Nano,* 11**,** 9614-9635.
LIU, Z.-L., CHEN, H.-H., ZHENG, L.-L., SUN, L.-P. & SHI, L. 2023. Angiogenic signaling pathways and anti-angiogenic therapy for cancer. *Signal Transduction and Targeted Therapy,* 8**,** 198.
LOCATELLI, L., COLCIAGO, A., CASTIGLIONI, S. & MAIER, J. A. 2021. Platelets in Wound Healing: What Happens in Space? *Frontiers in Bioengineering and Biotechnology,* 9.
LOMBARDO, D., CALANDRA, P., PASQUA, L. & MAGAZÙ, S. 2020. Self-Assembly of Organic Nanomaterials and Biomaterials: The Bottom-Up Approach for Functional Nanostructures Formation and Advanced Applications. *Materials,* 13**,** 1048.
LONG, W., ZHI, Q. J. T., YEE, Y. W. & WIN, N. M. 2018. Proof-of-concept: 3D bioprinting of pigmented human skin constructs. *Biofabrication,* 10**,** 025005.
LUO, M., ZHAO, F., CHENG, H., SU, M. & WANG, Y. 2024. Macrophage polarization: an important role in inflammatory diseases. *Frontiers in Immunology,* 15.
LUO, S., YANG, G., YE, P., CAO, N., CHI, X., YANG, W.-H. & YAN, X. 2022. Macrophages Are a Double-Edged Sword: Molecular Crosstalk between Tumor-Associated Macrophages and Cancer Stem Cells. *Biomolecules,* 12**,** 850.
LUSHCHAK, V. I., DUSZENKO, M., GOSPODARYOV, D. V. & GARASCHUK, O. 2021. Oxidative Stress and Energy Metabolism in the Brain: Midlife as a Turning Point. *Antioxidants (Basel),* 10.
LV, H., ZHANG, S., WANG, B., CUI, S. & YAN, J. 2006. Toxicity of cationic lipids and cationic polymers in gene delivery. *Journal of controlled release,* 114**,** 100-109.
MAHESWARY, T., NURUL, A. A. & FAUZI, M. B. 2021. The Insights of Microbes' Roles in Wound Healing: A Comprehensive Review. *Pharmaceutics,* 13.
MARDY, S., MIURA, Y., ENDO, F., MATSUDA, I., SZTRIHA, L., FROSSARD, P., MOOSA, A., ISMAIL, E. A. R., MACAYA, A., ANDRIA, G., TOSCANO, E., GIBSON, W., GRAHAM, G. E. & INDO, Y. 1999. Congenital Insensitivity to Pain with Anhidrosis: Novel Mutations in the TRKA (NTRK1) Gene Encoding A High-Affinity Receptor for Nerve Growth Factor. *The American Journal of Human Genetics,* 64**,** 1570-1579.
MARTIN, J. R., NELSON, C. E., GUPTA, M. K., YU, F., SARETT, S. M., HOCKING, K. M., POLLINS, A. C., NANNEY, L. B., DAVIDSON, J. M., GUELCHER, S. A. & DUVALL, C. L. 2016. Local Delivery of PHD2 siRNA from ROS-Degradable Scaffolds to Promote Diabetic Wound Healing. *Advanced Healthcare Materials,* 5**,** 2751-2757.
MARTIN, K. E. & GARCÍA, A. J. 2021. Macrophage phenotypes in tissue repair and the foreign body response: Implications for biomaterial-based regenerative medicine strategies. *Acta Biomater,* 133**,** 4-16.
MARTIN, P. & NUNAN, R. 2015. Cellular and molecular mechanisms of repair in acute and chronic wound healing. *British Journal of Dermatology,* 173**,** 370-378.
MARTINEZ, L. R., HAN, G., CHACKO, M., MIHU, M. R., JACOBSON, M., GIALANELLA, P., FRIEDMAN, A. J., NOSANCHUK, J. D. & FRIEDMAN, J. M. 2009. Antimicrobial and healing efficacy of sustained release nitric oxide nanoparticles against Staphylococcus aureus skin infection. *J Invest Dermatol,* 129**,** 2463-9.
MASENGA, S. K., KABWE, L. S., CHAKULYA, M. & KIRABO, A. 2023. Mechanisms of Oxidative Stress in Metabolic Syndrome. *Int J Mol Sci,* 24.
MASSAGUÉ, J. & SHEPPARD, D. 2023. TGF-β signaling in health and disease. *Cell,* 186**,** 4007-4037.
MATHEW-STEINER, S. S., ROY, S. & SEN, C. K. 2021. Collagen in Wound Healing. *Bioengineering (Basel),* 8.
MCELVAIN, K., KLISTER, J., EBBEN, A., GOPALAKRISHNAN, S. & DABAGH, M. 2022. Impact of Wound Dressing on Mechanotransduction within Tissues of Chronic Wounds. *Biomedicines,* 10.
MCGRATH, J. A. & UITTO, J. 2024. Structure and Function of the Skin. *Rook's Textbook of Dermatology.*
MCINNES, S. J. P., TURNER, C. T., AL-BATAINEH, S. A., AIRAGHI LECCARDI, M. J. I., IRANI, Y., WILLIAMS, K. A., COWIN, A. J. & VOELCKER, N. H. 2015. Surface engineering of porous silicon to optimise therapeutic antibody loading and release. *Journal of Materials Chemistry B,* 3**,** 4123-4133.
MENDES, B. B., CONNIOT, J., AVITAL, A., YAO, D., JIANG, X., ZHOU, X., SHARF-PAUKER, N., XIAO, Y., ADIR, O. & LIANG, H. 2022. Nanodelivery of nucleic acids. *Nature reviews Methods primers,* 2**,** 24.
MOSSER, D. M. & EDWARDS, J. P. 2008. Exploring the full spectrum of macrophage activation. *Nature Reviews Immunology,* 8**,** 958-969.
MUTEEB, G., REHMAN, M. T., SHAHWAN, M. & AATIF, M. 2023. Origin of Antibiotics and Antibiotic Resistance, and Their Impacts on Drug Development: A Narrative Review. *Pharmaceuticals (Basel),* 16.
NAKAMURA, Y., ISHIKAWA, H., KAWAI, K., TABATA, Y. & SUZUKI, S. 2013. Enhanced wound healing by topical administration of mesenchymal stem cells transfected with stromal cell-derived factor-1. *Biomaterials,* 34**,** 9393-9400.

NAKAO, A., IMAMURA, T., SOUCHELNYTSKYI, S., KAWABATA, M., ISHISAKI, A., OEDA, E., TAMAKI, K., HANAI, J. I., HELDIN, C. H., MIYAZONO, K. & TEN DIJKE, P. 1997. TGF-β receptor-mediated signalling through Smad2, Smad3 and Smad4. *The EMBO Journal,* 16**,** 5353-5362.

NATHAN, C. 2006. Neutrophils and immunity: challenges and opportunities. *Nature Reviews Immunology,* 6**,** 173-182.

NAUTA, A., SEIDEL, C., DEVEZA, L., MONTORO, D., GROVA, M., KO, S. H., HYUN, J., GURTNER, G. C., LONGAKER, M. T. & YANG, F. 2013. Adipose-derived Stromal Cells Overexpressing Vascular Endothelial Growth Factor Accelerate Mouse Excisional Wound Healing. *Molecular Therapy,* 21**,** 445-455.

NEGUT, I., DORCIOMAN, G. & GRUMEZESCU, V. 2020. Scaffolds for Wound Healing Applications. *Polymers (Basel),* 12.

NEWSHOLME, P., CRUZAT, V. F., KEANE, K. N., CARLESSI, R. & DE BITTENCOURT, P. I. H., JR 2016. Molecular mechanisms of ROS production and oxidative stress in diabetes. *Biochemical Journal,* 473**,** 4527-4550.

NG, K. W., THAM, W., LIM, T. C. & WERNER HUTMACHER, D. 2005. Assimilating cell sheets and hybrid scaffolds for dermal tissue engineering. *Journal of Biomedical Materials Research Part A,* 75A**,** 425-438.

NICHOLAS, M. N., JESCHKE, M. G. & AMINI-NIK, S. 2016. Cellularized Bilayer Pullulan-Gelatin Hydrogel for Skin Regeneration. *Tissue Engineering Part A,* 22**,** 754-764.

NICKS, B. A., AYELLO, E. A., WOO, K., NITZKI-GEORGE, D. & SIBBALD, R. G. 2010. Acute wound management: revisiting the approach to assessment, irrigation, and closure considerations. *Int J Emerg Med,* 3**,** 399-407.

NIRENJEN, S., NARAYANAN, J., TAMILANBAN, T., SUBRAMANIYAN, V., CHITRA, V., FULORIA, N. K., WONG, L. S., RAMACHAWOLRAN, G., SEKAR, M., GUPTA, G., FULORIA, S., CHINNI, SURESH V. & SELVARAJ, S. 2023. Exploring the contribution of pro-inflammatory cytokines to impaired wound healing in diabetes. *Frontiers in Immunology,* 14.

NORRBY, K. 2002. Mast cells and angiogenesis. *Apmis,* 110**,** 355-71.

NURDEN, A. T., NURDEN, P., SANCHEZ, M., ANDIA, I. & ANITUA, E. 2008. Platelets and wound healing. *Front Biosci,* 13**,** 3532-48.

OHTA, S., IMAIZUMI, Y., OKADA, Y., AKAMATSU, W., KUWAHARA, R., OHYAMA, M., AMAGAI, M., MATSUZAKI, Y., YAMANAKA, S., OKANO, H. & KAWAKAMI, Y. 2011. Generation of human melanocytes from induced pluripotent stem cells. *PLoS One,* 6**,** e16182.

OJOGBO, E., OGUNSONA, E. O. & MEKONNEN, T. H. 2020. Chemical and physical modifications of starch for renewable polymeric materials. *Materials Today Sustainability,* 7-8**,** 100028.

OKONKWO, U. A. & DIPIETRO, L. A. 2017. Diabetes and Wound Angiogenesis. *Int J Mol Sci,* 18.

ONYEKWELU, I., YAKKANTI, R., PROTZER, L., PINKSTON, C. M., TUCKER, C. & SELIGSON, D. 2017. Surgical Wound Classification and Surgical Site Infections in the Orthopaedic Patient. *J Am Acad Orthop Surg Glob Res Rev,* 1**,** e022.

ORTEGA, J. A., BLAS, J. R., OROZCO, M., GRANDAS, A., PEDROSO, E. & ROBLES, J. 2007. Binding affinities of oligonucleotides and PNAs containing phenoxazine and G-clamp cytosine analogues are unusually sequence-dependent. *Org Lett,* 9**,** 4503-6.

PAGE-MCCAW, A., EWALD, A. J. & WERB, Z. 2007. Matrix metalloproteinases and the regulation of tissue remodelling. *Nat Rev Mol Cell Biol,* 8**,** 221-33.

PAN, J. F., LIU, N. H., SUN, H. & XU, F. 2014. Preparation and characterization of electrospun PLCL/Poloxamer nanofibers and dextran/gelatin hydrogels for skin tissue engineering. *PLoS One,* 9**,** e112885.

PASTAR, I., STOJADINOVIC, O., YIN, N. C., RAMIREZ, H., NUSBAUM, A. G., SAWAYA, A., PATEL, S. B., KHALID, L., ISSEROFF, R. R. & TOMIC-CANIC, M. 2014. Epithelialization in Wound Healing: A Comprehensive Review. *Adv Wound Care (New Rochelle),* 3**,** 445-464.

PELLESTOR, F. & PAULASOVA, P. 2004. The peptide nucleic acids (PNAs), powerful tools for molecular genetics and cytogenetics. *European Journal of Human Genetics,* 12**,** 694-700.

PEÑA, O. A. & MARTIN, P. 2024. Cellular and molecular mechanisms of skin wound healing. *Nature Reviews Molecular Cell Biology,* 25**,** 599-616.

PÉREZ, L. A., HERNÁNDEZ, R., ALONSO, J. M., PÉREZ-GONZÁLEZ, R. & SÁEZ-MARTÍNEZ, V. 2021. Hyaluronic Acid Hydrogels Crosslinked in Physiological Conditions: Synthesis and Biomedical Applications. *Biomedicines,* 9.

PETERSEN, M. C. & SHULMAN, G. I. 2018. Mechanisms of Insulin Action and Insulin Resistance. *Physiol Rev,* 98**,** 2133-2223.

PIIPPONEN, M., LI, D. & LANDÉN, N. X. 2020. The Immune Functions of Keratinocytes in Skin Wound Healing. *Int J Mol Sci,* 21.

POUGET, C., DUNYACH-REMY, C., PANTEL, A., SCHULDINER, S., SOTTO, A. & LAVIGNE, J. P. 2020. Biofilms in Diabetic Foot Ulcers: Significance and Clinical Relevance. *Microorganisms,* 8.

PRADHAN, L., NABZDYK, C., ANDERSEN, N. D., LOGERFO, F. W. & VEVES, A. 2009. Inflammation and neuropeptides: the connection in diabetic wound healing. *Expert Rev Mol Med,* 11**,** e2.

PREMAN, N. K., E. S, S. P., PRABHU, A., SHAIKH, S. B., C, V., BARKI, R. R., BHANDARY, Y. P., REKHA, P. D. & JOHNSON, R. P. 2020. Bioresponsive supramolecular hydrogels for hemostasis, infection control and accelerated dermal wound healing. *Journal of Materials Chemistry B,* 8**,** 8585-8598.

PUERTAS-BARTOLOMÉ, M., BENITO-GARZÓN, L., FUNG, S., KOHN, J., VÁZQUEZ-LASA, B. & SAN ROMÁN, J. 2019. Bioadhesive functional hydrogels: Controlled release of catechol species with antioxidant and antiinflammatory behavior. *Materials Science and Engineering: C,* 105**,** 110040.

PUTRA, A., ALIF, I., HAMRA, N., SANTOSA, O., KUSTIYAH, A. R., MUHAR, A. M. & LUKMAN, K. 2020. MSC-released TGF-β regulate α-SMA expression of myofibroblast during wound healing. *J Stem Cells Regen Med,* 16**,** 73-79.

QING, C. 2017. The molecular biology in wound healing & non-healing wound. *Chin J Traumatol,* 20**,** 189-193.

QU, J., ZHAO, X., LIANG, Y., XU, Y., MA, P. X. & GUO, B. 2019. Degradable conductive injectable hydrogels as novel antibacterial, anti-oxidant wound dressings for wound healing. *Chemical Engineering Journal,* 362**,** 548-560.

QUEEN, D., ORSTED, H., SANADA, H. & SUSSMAN, G. 2004. A dressing history. *Int Wound J,* 1**,** 59-77.

ROBY, K. D. & NARDO, A. D. 2013. Innate immunity and the role of the antimicrobial peptide cathelicidin in inflammatory skin disease. *Drug Discov Today Dis Mech,* 10**,** e79-e82.

RODRIGUES, M., KOSARIC, N., BONHAM, C. A. & GURTNER, G. C. 2019. Wound Healing: A Cellular Perspective. *Physiological Reviews,* 99**,** 665-706.

ROSS, E. A., DEVITT, A. & JOHNSON, J. R. 2021. Macrophages: The Good, the Bad, and the Gluttony. *Frontiers in Immunology,* 12.

SANTHAMOORTHY, M., VY PHAN, T. T., RAMKUMAR, V., RAORANE, C. J., THIRUPATHI, K. & KIM, S. C. 2022. Thermo-Sensitive Poly (N-isopropylacrylamide-co-polyacrylamide) Hydrogel for pH-Responsive Therapeutic Delivery. *Polymers (Basel),* 14.

SASAKI, M., ABE, R., FUJITA, Y., ANDO, S., INOKUMA, D. & SHIMIZU, H. 2008. Mesenchymal Stem Cells Are Recruited into Wounded Skin and Contribute to Wound Repair by Transdifferentiation into Multiple Skin Cell Type1. *The Journal of Immunology,* 180**,** 2581-2587.

SCOTT, C. L., T'JONCK, W., MARTENS, L., TODOROV, H., SICHIEN, D., SOEN, B., BONNARDEL, J., DE PRIJCK, S., VANDAMME, N. & CANNOODT, R. 2018. The transcription factor ZEB2 is required to maintain the tissue-specific identities of macrophages. *Immunity,* 49**,** 312-325. e5.

SENNAKESAVAN, G., MOSTAKHDEMIN, M., DKHAR, L. K., SEYFODDIN, A. & FATIHHI, S. J. 2020. Acrylic acid/acrylamide based hydrogels and its properties - A review. *Polymer Degradation and Stability,* 180**,** 109308.

SERHAN, C. N., CHIANG, N. & VAN DYKE, T. E. 2008a. Resolving inflammation: dual anti-inflammatory and pro-resolution lipid mediators. *Nat Rev Immunol,* 8**,** 349-61.

SERHAN, C. N., CHIANG, N. & VAN DYKE, T. E. 2008b. Resolving inflammation: dual anti-inflammatory and pro-resolution lipid mediators. *Nature Reviews Immunology,* 8**,** 349-361.

SHARMA, A., SHARMA, D. & ZHAO, F. 2023a. Updates on Recent Clinical Assessment of Commercial Chronic Wound Care Products. *Adv Healthc Mater,* 12**,** e2300556.

SHARMA, S., MOHLER, J., MAHAJAN, S. D., SCHWARTZ, S. A., BRUGGEMANN, L. & AALINKEEL, R. 2023b. Microbial Biofilm: A Review on Formation, Infection, Antibiotic Resistance, Control Measures, and Innovative Treatment. *Microorganisms,* 11.

SHI, Y., XING, T., ZHANG, H., YIN, R., YANG, S., WEI, J. & ZHANG, W. 2018. Tyrosinase-doped bioink for 3D bioprinting of living skin constructs. *Biomedical Materials,* 13**,** 035008.

SHIEKH, P. A., SINGH, A. & KUMAR, A. 2020. Exosome laden oxygen releasing antioxidant and antibacterial cryogel wound dressing OxOBand alleviate diabetic and infectious wound healing. *Biomaterials,* 249**,** 120020.

SHORT, W. D., WANG, X. & KESWANI, S. G. 2022. The Role of T Lymphocytes in Cutaneous Scarring. *Adv Wound Care (New Rochelle),* 11**,** 121-131.

SILVA, M., DAHERON, L., HURLEY, H., BURE, K., BARKER, R., CARR, ANDREW J., WILLIAMS, D., KIM, H.-W., FRENCH, A., COFFEY, PETE J., COOPER-WHITE, JUSTIN J., REEVE, B., RAO, M., SNYDER, EVAN Y., NG, KELVIN S., MEAD, BENJAMIN E., SMITH, JAMES A., KARP, JEFFREY M., BRINDLEY, DAVID A. & WALL, I. 2015. Generating iPSCs: Translating Cell Reprogramming Science into Scalable and Robust Biomanufacturing Strategies. *Cell Stem Cell,* 16**,** 13-17.

SINGH, S., DATTA, S., NARAYANAN, K. B. & RAJNISH, K. N. 2021. Bacterial exo-polysaccharides in biofilms: role in antimicrobial resistance and treatments. *J Genet Eng Biotechnol,* 19**,** 140.

SINGH, V. P., BALI, A., SINGH, N. & JAGGI, A. S. 2014. Advanced glycation end products and diabetic complications. *Korean J Physiol Pharmacol,* 18**,** 1-14.

SKARDAL, A., MACK, D., KAPETANOVIC, E., ATALA, A., JACKSON, J. D., YOO, J. & SOKER, S. 2012. Bioprinted Amniotic Fluid-Derived Stem Cells Accelerate Healing of Large Skin Wounds. *Stem Cells Translational Medicine,* 1**,** 792-802.

STANCU, B., ILYÉS, T., FARCAS, M., COMAN, H. F., CHIȘ, B. A. & ANDERCOU, O. A. 2022. Diabetic Foot Complications: A Retrospective Cohort Study. *Int J Environ Res Public Health,* 20.

STRECKER-MCGRAW, M. K., JONES, T. R. & BAER, D. G. 2007. Soft Tissue Wounds and Principles of Healing. *Emergency Medicine Clinics of North America,* 25**,** 1-22.

SU, L. J., ZHANG, J. H., GOMEZ, H., MURUGAN, R., HONG, X., XU, D., JIANG, F. & PENG, Z. Y. 2019. Reactive Oxygen Species-Induced Lipid Peroxidation in Apoptosis, Autophagy, and Ferroptosis. *Oxid Med Cell Longev,* 2019**,** 5080843.

SUÁREZ, R., CHAPELA, S. P., ÁLVAREZ-CÓRDOVA, L., BAUTISTA-VALAREZO, E., SARMIENTO-ANDRADE, Y., VERDE, L., FRIAS-TORAL, E. & SARNO, G. 2023. Epigenetics in Obesity and Diabetes Mellitus: New Insights. *Nutrients,* 15.

SUMMERTON, J. & WELLER, D. 1997. Morpholino antisense oligomers: design, preparation, and properties. *Antisense Nucleic Acid Drug Dev,* 7**,** 187-95.

SUN, C., ZENG, X., ZHENG, S., WANG, Y., LI, Z., ZHANG, H., NIE, L., ZHANG, Y., ZHAO, Y. & YANG, X. 2022. Bio-adhesive catechol-modified chitosan wound healing hydrogel dressings through glow discharge plasma technique. *Chemical Engineering Journal,* 427**,** 130843.

SUN, G., ZHANG, X., SHEN, Y. I., SEBASTIAN, R., DICKINSON, L. E., FOX-TALBOT, K., REINBLATT, M., STEENBERGEN, C., HARMON, J. W. & GERECHT, S. 2011. Dextran hydrogel scaffolds enhance angiogenic responses and promote complete skin regeneration during burn wound healing. *Proc Natl Acad Sci U S A,* 108**,** 20976-81.

SUN, H., GAO, N., DONG, K., REN, J. & QU, X. 2014. Graphene Quantum Dots-Band-Aids Used for Wound Disinfection. *ACS Nano,* 8**,** 6202-6210.

SUN, L., XING, J., ZHOU, X., SONG, X. & GAO, S. 2024. Wnt/β-catenin signalling, epithelial-mesenchymal transition and crosslink signalling in colorectal cancer cells. *Biomedicine & Pharmacotherapy,* 175**,** 116685.

TAKAHASHI, K., TANABE, K., OHNUKI, M., NARITA, M., ICHISAKA, T., TOMODA, K. & YAMANAKA, S. 2007. Induction of Pluripotent Stem Cells from Adult Human Fibroblasts by Defined Factors. *Cell,* 131**,** 861-872.

TANZER, M. L. 2006. Current concepts of extracellular matrix. *J Orthop Sci,* 11**,** 326-31.

TARVIRDIPOUR, S., HUANG, X., MIHALI, V., SCHOENENBERGER, C.-A. & PALIVAN, C. G. 2020. Peptide-Based Nanoassemblies in Gene Therapy and Diagnosis: Paving the Way for Clinical Application. *Molecules,* 25**,** 3482.

TEIXEIRA, M. O., MARINHO, E., SILVA, C., ANTUNES, J. C. & FELGUEIRAS, H. P. 2023. Pullulan hydrogels as drug release platforms in biomedicine. *Journal of Drug Delivery Science and Technology,* 89**,** 105066.

THEOCHARIS, A. D., MANOU, D. & KARAMANOS, N. K. 2019. The extracellular matrix as a multitasking player in disease. *The FEBS Journal,* 286**,** 2830-2869.

THIMMAPPA, P. Y., VASISHTA, S., GANESH, K., NAIR, A. S. & JOSHI, M. B. 2023. Neutrophil (dys)function due to altered immuno-metabolic axis in type 2 diabetes: implications in combating infections. *Hum Cell,* 36**,** 1265-1282.

THOMAS, S. 2010. *Surgical dressings and wound management*, Dr Stephen Thomas.

TÓBON-VELASCO, J. C., CUEVAS, E. & TORRES-RAMOS, M. A. 2014. Receptor for AGEs (RAGE) as mediator of NF-kB pathway activation in neuroinflammation and oxidative stress. *CNS Neurol Disord Drug Targets,* 13**,** 1615-26.

TOKATLIAN, T., CAM, C. & SEGURA, T. 2015. Porous Hyaluronic Acid Hydrogels for Localized Nonviral DNA Delivery in a Diabetic Wound Healing Model. *Advanced Healthcare Materials,* 4**,** 1084-1091.

TOTTOLI, E. M., DORATI, R., GENTA, I., CHIESA, E., PISANI, S. & CONTI, B. 2020. Skin Wound Healing Process and New Emerging Technologies for Skin Wound Care and Regeneration. *Pharmaceutics,* 12**,** 735.

TRAUTMANN, A., TOKSOY, A., ENGELHARDT, E., BRÖCKER, E. B. & GILLITZER, R. 2000. Mast cell involvement in normal human skin wound healing: expression of monocyte chemoattractant protein-1 is correlated with recruitment of mast cells which synthesize interleukin-4 in vivo. *J Pathol,* 190**,** 100-6.

TURNER, C. T., MCINNES, S. J., MELVILLE, E., COWIN, A. J. & VOELCKER, N. H. 2017. Delivery of Flightless I Neutralizing Antibody from Porous Silicon Nanoparticles Improves Wound Healing in Diabetic Mice. *Adv Healthc Mater,* 6.

VADEVOO, S. M. P., GURUNG, S., LEE, H.-S., GUNASSEKARAN, G. R., LEE, S.-M., YOON, J.-W., LEE, Y.-K. & LEE, B. 2023. Peptides as multifunctional players in cancer therapy. *Experimental & Molecular Medicine,* 55**,** 1099-1109.

VAN HELDEN, M. J., GOOSSENS, S., DAUSSY, C., MATHIEU, A.-L., FAURE, F., MARCAIS, A., VANDAMME, N., FARLA, N., MAYOL, K. & VIEL, S. 2015. Terminal NK cell maturation is controlled by concerted actions of T-bet and Zeb2 and is essential for melanoma rejection. *Journal of experimental medicine,* 212**,** 2015-2025.

VOWDEN, K., VOWDEN, P. & POSNETT, J. 2009. The resource costs of wound care in Bradford and Airedale primary care trust in the UK. *J Wound Care,* 18**,** 93-4, 96-8, 100 passim.

WALDROP, R., MCLAREN, A., CALARA, F. & MCLEMORE, R. 2014. Biofilm growth has a threshold response to glucose in vitro. *Clin Orthop Relat Res,* 472**,** 3305-10.

WANG, A., LV, G., CHENG, X., MA, X., WANG, W., GUI, J., HU, J., LU, M., CHU, G., CHEN, J., ZHANG, H., JIANG, Y., CHEN, Y., YANG, W., JIANG, L., GENG, H., ZHENG, R., LI, Y., FENG, W., JOHNSON, B., WANG, W., ZHU, D. & HU, Y. 2020. Guidelines on multidisciplinary approaches for the prevention and management of diabetic foot disease (2020 edition). *Burns Trauma,* 8**,** tkaa017.

WANG, C., GUAN, Y. & YANG, J. 2010. Cytokines in the Progression of Pancreatic β-Cell Dysfunction. *Int J Endocrinol,* 2010**,** 515136.

WANG, C., SHIRZAEI SANI, E. & GAO, W. 2022. Wearable Bioelectronics for Chronic Wound Management. *Advanced Functional Materials,* 32**,** 2111022.

WANG, R., LI, J., CHEN, W., XU, T., YUN, S., XU, Z., XU, Z., SATO, T., CHI, B. & XU, H. 2017a. A biomimetic mussel-inspired ε-poly-l-lysine hydrogel with robust tissue-anchor and anti-infection capacity. *Advanced Functional Materials,* 27**,** 1604894.

WANG, Y., MALCOLM, D. W. & BENOIT, D. S. 2017b. Controlled and sustained delivery of siRNA/NPs from hydrogels expedites bone fracture healing. *Biomaterials,* 139**,** 127-138.

WILGUS, T. A., ROY, S. & MCDANIEL, J. C. 2013. Neutrophils and Wound Repair: Positive Actions and Negative Reactions. *Adv Wound Care (New Rochelle),* 2**,** 379-388.

WILKINSON, H. N. & HARDMAN, M. J. 2020. Wound healing: cellular mechanisms and pathological outcomes. *Open Biology,* 10**,** 200223.

WINTER, G. D. 1995. Formation of the scab and the rate of epithelisation of superficial wounds in the skin of the young domestic pig. 1962. *J Wound Care,* 4**,** 366-7; discussion 368-71.

WITJAS, F. M. R., VAN DEN BERG, B. M., VAN DEN BERG, C. W., ENGELSE, M. A. & RABELINK, T. J. 2019. Concise Review: The Endothelial Cell Extracellular Matrix Regulates Tissue Homeostasis and Repair. *Stem Cells Transl Med,* 8**,** 375-382.

WOLF, S. J., MELVIN, W. J. & GALLAGHER, K. 2021. Macrophage-mediated inflammation in diabetic wound repair. *Semin Cell Dev Biol,* 119**,** 111-118.

WU, H., LI, F., WANG, S., LU, J., LI, J., DU, Y., SUN, X., CHEN, X., GAO, J. & LING, D. 2018. Ceria nanocrystals decorated mesoporous silica nanoparticle based ROS-scavenging tissue adhesive for highly efficient regenerative wound healing. *Biomaterials,* 151**,** 66-77.

WU, J., YE, J., ZHU, J., XIAO, Z., HE, C., SHI, H., WANG, Y., LIN, C., ZHANG, H., ZHAO, Y., FU, X., CHEN, H., LI, X., LI, L., ZHENG, J. & XIAO, J. 2016a. Heparin-Based Coacervate of FGF2 Improves Dermal Regeneration by Asserting a Synergistic Role with Cell Proliferation and Endogenous Facilitated VEGF for Cutaneous Wound Healing. *Biomacromolecules,* 17**,** 2168-77.

WU, J., YUK, H., SARRAFIAN, T. L., GUO, C. F., GRIFFITHS, L. G., NABZDYK, C. S. & ZHAO, X. 2022a. An off-the-shelf bioadhesive patch for sutureless repair of gastrointestinal defects. *Science Translational Medicine,* 14**,** eabh2857.

WU, X., BRISEÑO, C. G., GRAJALES-REYES, G. E., HALDAR, M., IWATA, A., KRETZER, N. M., KC, W., TUSSIWAND, R., HIGASHI, Y. & MURPHY, T. L. 2016b. Transcription factor Zeb2 regulates commitment to plasmacytoid dendritic cell and monocyte fate. *Proceedings of the National Academy of Sciences,* 113**,** 14775-14780.

WU, X., HE, W., MU, X., LIU, Y., DENG, J., LIU, Y. & NIE, X. 2022b. Macrophage polarization in diabetic wound healing. *Burns Trauma,* 10**,** tkac051.

XIAO, J., CHEN, S., YI, J., ZHANG, H. & AMEER, G. A. 2017. A Cooperative Copper Metal-Organic Framework-Hydrogel System Improves Wound Healing in Diabetes. *Adv Funct Mater,* 27.

XIE, X. & PERCIPALLE, P. 2018. Elevated transforming growth factor β signaling activation in β-actin-knockout mouse embryonic fibroblasts enhances myofibroblast features. *J Cell Physiol,* 233**,** 8884-8895.

XIONG, Y., ZHANG, X., MA, X., WANG, W., YAN, F., ZHAO, X., CHU, X., XU, W. & SUN, C. 2021. A review of the properties and applications of bioadhesive hydrogels. *Polymer Chemistry,* 12**,** 3721-3739.

XU, H., LV, F., ZHANG, Y., YI, Z., KE, Q., WU, C., LIU, M. & CHANG, J. 2015. Hierarchically micro-patterned nanofibrous scaffolds with a nanosized bio-glass surface for accelerating wound healing. *Nanoscale,* 7**,** 18446-18452.

XU, H. L., CHEN, P. P., ZHUGE, D. L., ZHU, Q. Y., JIN, B. H., SHEN, B. X., XIAO, J. & ZHAO, Y. Z. 2017. Liposomes with Silk Fibroin Hydrogel Core to Stabilize bFGF and Promote the Wound Healing of Mice with Deep Second-Degree Scald. *Adv Healthc Mater,* 6.

XU, J., FANG, H., ZHENG, S., LI, L., JIAO, Z., WANG, H., NIE, Y., LIU, T. & SONG, K. 2021. A biological functional hybrid scaffold based on decellularized extracellular matrix/gelatin/chitosan with high biocompatibility and antibacterial activity for skin tissue engineering. *Int J Biol Macromol,* 187**,** 840-849.

XU, R., WON, J. Y., KIM, C. H., KIM, D. E. & YIM, H. 2019. Roles of the Phosphorylation of Transcriptional Factors in Epithelial-Mesenchymal Transition. *J Oncol,* 2019**,** 5810465.

YADAV, S., SHARMA, A. K. & KUMAR, P. 2020. Nanoscale Self-Assembly for Therapeutic Delivery. *Frontiers in Bioengineering and Biotechnology,* 8.

YAN, L., HAN, K., PANG, B., JIN, H., ZHAO, X., XU, X., JIANG, C., CUI, N., LU, T. & SHI, J. 2021. Surfactin-reinforced gelatin methacrylate hydrogel accelerates diabetic wound healing by regulating the macrophage polarization and promoting angiogenesis. *Chemical Engineering Journal,* 414**,** 128836.

YAO, W., WANG, Z., MA, H., LIN, Y., LIU, X., LI, P. & HE, X. 2024. Epithelial-mesenchymal plasticity (EMP) in wound healing: Exploring EMT mechanisms, regulatory network, and therapeutic opportunities. *Heliyon,* 10**,** e34269.

YIN, M., WAN, S., REN, X. & CHU, C. C. 2021. Development of Inherently Antibacterial, Biodegradable, and Biologically Active Chitosan/Pseudo-Protein Hybrid Hydrogels as Biofunctional Wound Dressings. *ACS Appl Mater Interfaces,* 13**,** 14688-14699.

YOON, D. S., LEE, Y., RYU, H. A., JANG, Y., LEE, K.-M., CHOI, Y., CHOI, W. J., LEE, M., PARK, K. M., PARK, K. D. & LEE, J. W. 2016. Cell recruiting chemokine-loaded sprayable gelatin hydrogel dressings for diabetic wound healing. *Acta Biomaterialia,* 38**,** 59-68.

YUK, H., WU, J. & ZHAO, X. 2022. Hydrogel interfaces for merging humans and machines. *Nature Reviews Materials,* 7**,** 935-952.

ZHANG, J., GUAN, J., NIU, X., HU, G., GUO, S., LI, Q., XIE, Z., ZHANG, C. & WANG, Y. 2015. Exosomes released from human induced pluripotent stem cells-derived MSCs facilitate cutaneous wound healing by promoting collagen synthesis and angiogenesis. *J Transl Med,* 13**,** 49.

ZHAO, L., NIU, L., LIANG, H., TAN, H., LIU, C. & ZHU, F. 2017a. pH and Glucose Dual-Responsive Injectable Hydrogels with Insulin and Fibroblasts as Bioactive Dressings for Diabetic Wound Healing. *ACS Applied Materials & Interfaces,* 9**,** 37563-37574.

ZHAO, X., WU, H., GUO, B., DONG, R., QIU, Y. & MA, P. X. 2017b. Antibacterial anti-oxidant electroactive injectable hydrogel as self-healing wound dressing with hemostasis and adhesiveness for cutaneous wound healing. *Biomaterials,* 122**,** 34-47.

ZHENG, Z., BIAN, S., LI, Z., ZHANG, Z., LIU, Y., ZHAI, X., PAN, H. & ZHAO, X. 2020. Catechol modified quaternized chitosan enhanced wet adhesive and antibacterial properties of injectable thermo-sensitive hydrogel for wound healing. *Carbohydr Polym,* 249**,** 116826.

ZHONG, R., TALEBIAN, S., MENDES, B. B., WALLACE, G., LANGER, R., CONDE, J. & SHI, J. 2023. Hydrogels for RNA delivery. *Nature Materials,* 22**,** 818-831.

ZHOU, C. & YI, Z. 1999. Blood-compatibility of polyurethane/liquid crystal composite membranes. *Biomaterials,* 20**,** 2093-2099.

ZHU, Y., HOSHI, R., CHEN, S., YI, J., DUAN, C., GALIANO, R. D., ZHANG, H. F. & AMEER, G. A. 2016. Sustained release of stromal cell derived factor-1 from an antioxidant thermoresponsive hydrogel enhances dermal wound healing in diabetes. *Journal of Controlled Release,* 238**,** 114-122.

ZOLNIK, B. S., GONZÁLEZ-FERNÁNDEZ, A., SADRIEH, N. & DOBROVOLSKAIA, M. A. 2010. Nanoparticles and the immune system. *Endocrinology,* 151**,** 458-65.

Chapter 3

Role of Zeb2 in macrophage polarization associated with diabetic foot ulcer

3.1. Background

A serious and frequent consequence of chronic diabetes is the development of a diabetic foot ulcer due to microvascular damage caused by high glucose level. Peripheral blood flow is disrupted, which reduces the amount of oxygen and nutrients that can reach the wound (Akkus and Sert, 2022). The immune response is hampered and the healing process is stalled because of this limitation. Immune cells secrete a series of pro-inflammatory cytokines and enzymes to eliminate debris and fight off infections, and these cells play an essential role in damaged tissue management (Chen *et al.*, 2018). High blood sugar levels, on the other hand, make it harder for phagocytes to ingest and kill bacteria, which slows down the healing process and makes the ulcer more vulnerable (Berbudi *et al.*, 2020).

Macrophages play an essential role in wound healing, tissue regeneration, and host defense by establishing a sterile and regulated environment that is necessary for the initiation of repair. When the body heals, macrophages take on an anti-inflammatory role and secrete growth factors that promote angiogenesis, fibroblast proliferation, and tissue regeneration. Their pro- and anti-inflammatory actions are constantly balance out their function in tissue regeneration. Any disruption in the normal activity of macrophage or phenotype might slow down the healing process (Krzyszczyk *et al.*, 2018).

Recent research has exposed the crucial function of epigenetics in insulin resistance, with a specific emphasis on how the acetylation of histone tails regulates both metabolic and mitogenic insulin signaling pathways. Central to this process is the dysregulation of histone acetyltransferases and deacetylases, which greatly contributes to the development of diabetes (Haery *et al.*, 2015). Additionally, the activation of NF-κB is critical for boosting the activity of histone acetyltransferases (HATs), which operate as major transcriptional coactivators (Ashburner *et al.*, 2001). Diabetes, defined by increased protein glycation, leads to the

generation of advanced glycation end products (AGEs) (Goldin *et al.*, 2006), which in turn heightens reactive oxygen species (ROS) production and disturbs enzyme activity (Singh *et al.*, 2001). The build-up of AGEs induces NF-κB activation, boosting the release of inflammatory markers (Tóbon-Velasco *et al.*, 2014). Notably, lowering receptor for advanced glycation end products (RAGE) activity by methylglyoxal induction has been found to reduce NF-κB p65 acetylation and lessen TNF-α production (Uribarri *et al.*, 2011).

3.1.1. Challenges

Hyperglycemia or high blood sugar greatly intensifies the inflammation stage by repressing the activation of genes essential for M2 macrophage polarization and increasing the expression of inflammatory genes. This syndrome creates a milieu of chronic inflammation, indicated by elevated levels of pro-inflammatory cytokines, such as TNF-α, IL-1β, IL-6, and other chemokines. Compounding the problem, the low oxygen environment common to diabetic foot ulcers (DFUs) activates NF-κB signaling pathways, further amplifying pro-inflammatory responses. As cells move from oxidative to glycolytic metabolism, they create increased quantities of ROS (Pérez and Rius-Pérez, 2022). Amidst these processes, the transcription factor ZEB2, also known as SIP1 or ZFXH1B, plays a vital function in the immune system. It orchestrates the maturation of NK cells, the final differentiation of $CD8^+$ effector T cells, and the formation of plasmacytoid and conventional type 2 dendritic cells. Moreover, ZEB2 is crucial in EMT— where epithelial cells turn into mesenchymal cells and strongly impacts the determination of granulocyte-macrophage progenitors (GMPs) (Kim *et al.*, 2022, Scott and Omilusik, 2019a).

3.1.2. Objectives

In this investigation, our aim is –

- To study the expression of Zeb2, a transcription factor in wound macrophages during hyperglycemia.
- To uncover the epigenetic regulation of Zeb2 in influencing macrophage polarity.
- To study the role of acetylation inhibitor in wound healing by downregulating Zeb2.

3.2. Materials and Methods

3.2.1. Materials

All tissue culture materials were procured from Life Technologies/Gibco, and Nunc, Grand Island, NY; and Corning, NY. A comprehensive list of all antibodies, along with their catalog

numbers and the dilutions employed in the experiments, is presented in **Table A (Appendix)**. Vectashield anti-fade mounting medium with DAPI (#H-1500) were purchased from Vector Laboratories, Burlingame, CA.; Lipofectamine^{TM} RNAiMAX Transfection Reagent (#13778-075), and NP40 Cell lysis buffer (#FNN0021) from Invitrogen, Thermo-Scientific, Grand Island, NY; Pierce BCA Protein Assay Kit (#23227), and Halt Protease and Phosphatase Inhibitor Cocktail (#78441) from Thermo Scientific, Waltham, MA, USA; Clarity Western ECL Substrate (#1705060), and iScript Reverse Transcription Supermix (#1708891) from Bio-Rad Laboratories, Hercules, CA; PVDF membranes (cat. no. #548IPVH00010) from Merck, Darmstadt, Germany; PowerUp^{TM} SYBRTM Green Master Mix (#A25742) from Applied Biosystems, Thermo-Scientific, Grand Island, NY; Streptozotocin (#S0130), D-glucose (#G7021), C646 (#SML0002) and silicone sheet (#GBL664581) from Merck, Bangalore, India. 3M Tegaderm 8526IN (#IA410134711) was procured from 3M Science, India. Control siRNA (sc-37007) was procured from Santa Cruz Biotechnology, Inc. Antisense LNA GapmeR (#339517) was procured from Qiagen, Hilden, Germany. Zeb2 siRNA(m) and different gene-specific primers were procured from Integrated DNA Technologies, India, and the sequence details are presented in **Table B (Appendix)**.

3.2.2. Mice models and treatments

Wild-type C57BL/6J male mice, 4-5 weeks old and weighing between 18-22 g, were sourced from the IISER Mohali animal facility. They were acclimated for 5-6 days at the NIPER Mohali animal house under a controlled environment, which included a 12-hour light/dark cycle, a temperature of 23 ± 2 °C, and relative humidity of 55 ± 5%. The mice were provided with a standard pellet diet and water *ad libitum*. For the development of diabetic mice model, C57BL/6J mice were injected Streptozotocin (STZ) intraperitonially following the published protocol (Furman, 2021). After completion of the treatment mice were fed with high fat diet (HFD) pellets (D12492, Research Diet Inc., New Brunswick, NJ) having 60% kcal of fat for 4 weeks for developing diabetes induced complications in mice model. All remaining mice were maintained on SD pellets containing 10% kcal from fat for a duration of 8 weeks. Throughout the experiment, the animals had unrestricted access to sterilized water and food. Blood glucose levels were consistently monitored using an Accu-Chek glucometer (Roche). All mice were subjected to rostral excisional wound following the published protocol (Fischer *et al.*, 2023). One group of STZ-induced HFD mice received intradermal delivery of C646 at the wound edge at various time points. A total of 10 μg C646/ wound was injected by resuspending in PBS in 3 different sites of wound edge. The 70 μL of PBS as vehicle was injected similarly on the 3 different sites on of wound edge of the control STZ-induced HFD group. After certain days

interval, wound images were captured in all groups of mice and the closure area was measured through Image-J analysis. Mice were then sacrificed, wound bed tissues were collected, and processed for further experimental studies. Immediately after collection, tissues were snap frozen in OCT (Leica Biosystems) for cryosectioning. All animal experiments were performed following the guidelines prescribed by and with the approval of the Institutional Animal Ethics Committee (IAEC), NIPER, Mohali, Punjab (Project no.: IAEC/22/37-M).

3.2.3. Human subjects

A total of 17 diabetic and 5 non-diabetic patients have participated in this study. The study population was categorized into two groups based on BMI and blood glucose level. Study subjects having fasting blood glucose level (mmol/L) <5 was considered as non-diabetic group (n = 5) whereas patients with fasting blood glucose level (mmol/L) >7 were considered as diabetic group (n = 17) as presented in the **Table C (Appendix)**. In this study, surgically wound debridement tissue samples were collected from the patients who were admitted to the Dayanand Medical College & Hospital, Ludhiana, Punjab, and underwent surgery. The study protocol for the use of human wound tissue samples was approved by the Institute Ethics Committee (IEC), Dayanand Medical College & Hospital, Ludhiana, Punjab (Protocol no.: DMCH/R&D/2023/172; IEC No.: 2023-831).

3.2.4. Cell culture and treatments

RAW264.7 macrophage was obtained from National Centre for Cell Science (NCCS), Pune, India, and cultured in DMEM (GibcoTM/Life Technologies, #11995073) supplemented with 10% FBS (GibcoTM/Life Technologies, #10082147) and 1% Penicillin-Streptomycin solution (GibcoTM/Life Technologies, #15140122) at 37 °C in a humidified atmosphere with 5% CO_2. Briefly, macrophages (passage no. 5) were with a density of 8 x10^4 cells in 35 mm culture plate until it achieves 90% confluency. The 25 mM D-glucose solution was prepared in PBS for *in vitro* treatment and filtered using 0.4 μm filter before treating the cell. The 20 μM C646 was used for the *in vitro* treatment.

3.2.5. *Zeb2* siRNA transfection

For transfection of Zeb2 siRNA and the corresponding control siRNA, the Lipofectamine RNAiMAX transfection reagent (Invitrogen) was employed in accordance with the manufacturer's instructions. Briefly, RAW264.7 macrophages were seeded at a density of 0.1 x 10^6 cells per well in a 12-well plate containing antibiotic-free complete growth medium and

incubated for 24 hours before transfection. In each well, 100 nM of Zeb2 siRNA or control siRNA was separately mixed with Lipofectamine RNAiMAX reagent in Opti-MEM serum-free medium (Thermo Scientific) and incubated for 5 minutes. The transfection mixture was then added to the cells in the complete growth medium and allowed to incubate for 48 hours. Afterwards, the cells were washed, fresh complete growth medium was added, and the cells were used for subsequent treatments (Patra *et al.*, 2022).

3.2.6. Immunocytochemistry

Cells cultured on sterile glass coverslips overnight were subjected to treatment with or without C646 (20 μM) and Zeb2 siRNA (100 nM) for 24 hours. Post-incubation, cells were rinsed with PBS and fixed using ice-cold methanol for 5 minutes. For intracellular staining, cells were permeabilized with 0.25% Triton X-100 in PBS for 10 minutes at room temperature. Following permeabilization, cells were blocked with 1% BSA in PBS containing 0.1% Tween-20 for 30 minutes at room temperature and then incubated with primary antibodies for 1 hour at room temperature. After three washes with ice-cold PBS (5 minutes each), the cells were exposed to fluorescence-conjugated secondary antibodies for 1 hour in the dark at room temperature. Prior to mounting, cells were washed three additional times with ice-cold PBS (5 minutes each) and then mounted onto glass slides using anti-fade mounting medium with DAPI (Patra *et al.*, 2022). Cellular images were captured using an inverted fluorescence microscope (Leica DMi8, Germany), and subsequent image analysis was performed using LAS X software. Quantification of fluorescence intensity was carried out using ImageJ software (1.48v, NIH, USA).

3.2.7. Immunofluorescence

Wound tissue samples from human and murine sources were immediately rinsed in sterile saline and fixed overnight at 4 °C in 10% neutral buffered formalin. After fixation, the tissues were embedded in OCT (Optimal Cutting Temperature Compound, Sigma) and frozen at temperatures of -80 °C. Cryosectioning was carried out using a Cryotome (Leica CM 1860, Leica Biosystems, Wetzlar, Germany). For immunostaining, 5 μm tissue cryosections were placed on gelatin-coated glass slides, fixed in ice-cold methanol for 5 minutes, and then blocked with 5% BSA in a blocking buffer. The sections were incubated with specific primary antibodies for 1 hour at room temperature. Following washing, the samples were exposed to fluorescence-conjugated secondary antibodies and counter-stained with an anti-fade mounting

medium containing DAPI (Patra *et al.*, 2022). Images were captured using a confocal microscope (Zeiss LSM 880, Germany) and analyzed with Zeiss ZEN lite software.

3.2.8. Hematoxylin & Eosin staining and imaging

Cryosectioning of the tissues was executed as outlined in the manuscript. The tissue sections were mounted on gelatin-coated glass slides and subjected to regressive staining following a meticulous protocol (Patra *et al.*, 2022): initial immersion in 100% ethanol for 20 seconds, repeated twice, succeeded by 90% ethanol for 20 seconds, also repeated twice; the process continued with 80% ethanol for 20 seconds, 70% ethanol for 20 seconds, and 50% ethanol for 20 seconds. The slides were subsequently rinsed with distilled water (dH_2O) for 1 minute. The staining protocol then involved incubation in Harris Hematoxylin for 3 minutes, followed by a 2-minute rinse in water. The slides were further subjected to three brief immersions in an alcohol solution containing 0.3% acetic acid, rinsed in dH_2O, and then dipped in 0.3 % ammonium water to induce bluing, followed by another rinse in water. The procedure continued with passages through 80% ethanol for 20 seconds and staining with 2% Eosin for 30 seconds. Excess stain was removed by washing the sections in 95% ethanol for 20 seconds, repeated twice, and then in 100% ethanol for 20 seconds. Finally, the slides were briefly immersed in xylene before being mounted with DPX mounting medium. The resulting H&E-stained slides were examined using a Leica DMi8 microscope for imaging.

3.2.9. RNA extraction and quantitative PCR

Total RNA was isolated from cells using TRIzol (Invitrogen) (Patra *et al.*, 2022). For tissue samples, including 5 mg of murine and human wound tissue, homogenization was performed with TRIzol using a TissueLyser II (Qiagen, Germany), followed by quantification with a NanoDropTM OneC spectrophotometer (NanoDrop Technologies, Thermo Scientific, Waltham, MA, USA). The extracted RNA (300 ng) was subjected to DNase I treatment and subsequently reverse transcribed with the iScriptTM cDNA Synthesis Kit (Bio-Rad, Hercules, California, USA). Real-time quantitative PCR was carried out using PowerUpTM SYBRTM Green Master Mix (Applied Biosystems) on a QuantStudioTM 5 Real-Time PCR System (Applied Biosystems, Waltham, Massachusetts, USA), employing gene-specific primers. mRNA expression levels were normalized to 18S rRNA using the $^{\Delta\Delta}$CT method. Relative expression or fold change was calculated by the $2^{\Delta\Delta CT}$ formula, with the average fold change derived from these values.

3.2.10. Immunoblotting

Control and treated cells were lysed in NP40 cell lysis buffer (Invitrogen) augmented with Halt protease and phosphatase inhibitor cocktail (Thermo Scientific) and subsequently centrifuged at 13,000 rpm for 10 minutes at 4 °C. Tissue samples from mice and human wounds were homogenized using a TissueLyser II (Qiagen, Germany) in NP40 lysis buffer supplemented with the same inhibitor cocktail. Protein concentrations in the cell lysates were quantified using the BCA Protein Assay Kit (Pierce), following the manufacturer's protocol. For Western blot analysis, 50 µg of protein from each sample were resolved on a 10% SDS–PAGE gel and transferred to PVDF membranes (GE Healthcare Biosciences) using a Turbo Blotting System (Bio-Rad Laboratories). Membranes were blocked with 5% BSA in TBS (Tris-buffered saline) for 1 hour, then incubated overnight with primary antibodies at 4 °C on a rotating shaker. After three washes with TBST (TBS containing 0.1% Tween 20) for 10 minutes each, membranes were probed with peroxidase-conjugated secondary antibodies for 2 hours at room temperature. Following an additional set of three 10-minute washes with TBST, the membranes were treated with Clarity™ Western ECL Substrate (Bio-Rad, Hercules, California, USA) for 5 minutes at room temperature. Protein bands were visualized using a Chemidoc XRS+ System (Bio-Rad Laboratories, Hercules, California, USA) and analyzed with Image Lab Software (Patra *et al.*, 2022).

3.2.11. Enzyme-linked immunosorbent assay (ELISA)

Cytokine levels of IL-1β and TNF-α in the cell culture supernatants from both control and treated cells were assessed using mouse-specific ELISA kits for IL-1β (cat. no. #432604) and TNF-α (cat. no. #430907) (BioLegend, San Diego, CA), in accordance with the manufacturer's instructions. Insulin concentrations in the culture media were determined using mouse ELISA kits (Elabscience), following the prescribed manufacturer's protocols.

3.2.12. Flowcytometry

After various treatments, cells were collected and washed with ice-cold PBS, followed by centrifugation at 1200 rpm for 5 minutes. The resulting cell pellet was incubated with TruStain FcX (anti-mouse CD16/32) antibody for 30 minutes at 4 °C, then washed once with ice-cold PBS. Subsequently, the cells were incubated with antibodies against CD80, CD86, CD163, and iNOS for 1 hour. Following this incubation, the cells were washed with PBS and analyzed using the BD Accuri C6 Plus (BD Accuri, USA).

3.2.13. Statistical analysis

Data analysis was carried out utilizing GraphPad Prism software (version 8.0; GraphPad Software, Inc., La Jolla, CA). Results are expressed as means ± standard deviation (S.D.). Statistical significance was determined through Student's t-test or Multiple t-test, with **P<0.05*, ***P<0.01*, ****P<0.001*, and *#P<0.0001* were considered indicative of significance.

3.3. Results

3.3.1. Hyperglycemia triggers Zeb2 and LDTFs expression that promotes pro-inflammatory responses in wound macrophages

People with chronic diabetes have no such re-epithelialization, as shown histologically by diminished granulation tissue, and extensive inflammatory infiltration (**Fig 3.1A**). The pro-inflammatory macrophages are predominant in diabetes wound samples compared to non-diabetic counterparts together with a notable overexpression of ZEB2 expression in diabetes wound (**Fig. 3.1B, C).** Consistent with other reports, we found that diabetic wounds had higher levels of the pro-inflammatory macrophage markers, *CD80* and *CD86*, and low levels of *CD206*, an anti-inflammatory marker indicating a chronic inflammatory environment at the wound site (**Fig. 3.1D**). On day 7 of post-wounding, STZ-induced high-fat diet (HFD) animals showed significantly higher Zeb2 expression with macrophage infiltration compared to SD fed mice, (**Fig. 3.1E**). Further investigation using RAW 264.7 murine macrophages treated with physiological hyperglycaemic conditions revealed a significant upsurge in Zeb2 protein expression (**Fig. 3.1F, G**) alongside the activation of pNF-κB (**Fig. 3.1H, I**), a pivotal molecule in the inflammatory signalling cascade, culminating in an altered pro-inflammatory macrophage phenotype. Increased production of many inflammatory markers and cytokines (**Fig. 3.1J, K**) and higher levels of iNos compared to Arg1 demonstrated this fact (**Fig. 3.1L, M**). Flow cytometry analysis indicated a considerable elevation of $Cd80^{+}$, $Cd163^{-}$, $Cd86^{+}$, and $iNos^{+}$ populations in HG-treated RAW 264.7 cells relative to controls (**Fig. 3.1N, O**). To understand the unique effects of hyperglycaemia on hematopoietic stem cell (HSC) development, we undertook a gene expression study of major lineage-determining transcription factors (LDTFs). The results revealed that high glucose levels dramatically raised the expression of LDTFs, such as *Oct2*, *Klf6*, and *Pu.1* (**Fig. 3.1.Q**). Additionally, research on human diabetic wounds indicated a considerable rise in *OCT2* and *KLF6* gene expression, underlining the inflammatory cascade inside the wound tissue's complex milieu (**Fig. 3.1R**). The expression patterns of these LDTFs in standard diet (SD) and high-fat diet (HFD) mice

further revealed the inflammatory susceptibility of the wound environment (**Fig. 3.1S**).

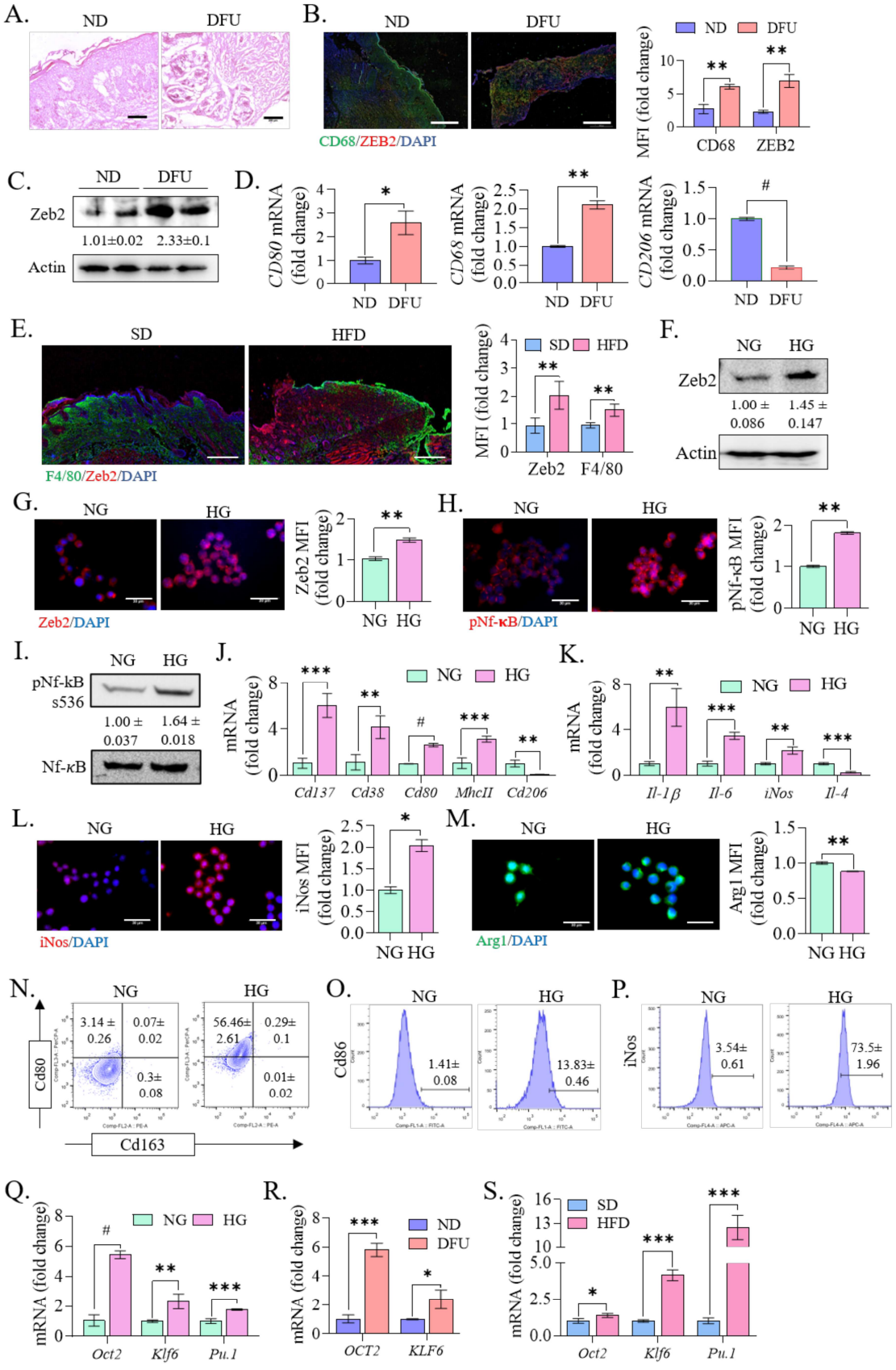

Figure 3.1. *Elevated glucose levels induce the expression of Zeb2 and LDTFs that activate pro-inflammatory pathways within macrophage. (A) H&E staining of non-diabetic and diabetic human wound tissue. (B) Cryosection of non-diabetic (ND) and diabetic patient (DFU) wound tissue stained with ZEB2 (red) and CD68 (green) antibody (objective 10X, scale bar 500 µm), and its quantitative analysis (n=5). (C) Western blot analysis of Zeb2 protein expression in human wound tissue (n=3). (D) mRNA expression of CD80, CD68, and CD206 in human wound tissue (n=3). (E) Cryosection of mice wound tissue stained with Zeb2 (red) and F4/80 (green) antibody (objective 10X, scale bar 1000 µm), and its quantitative analysis (n=3). (F) Western blot analysis of Zeb2 protein expression in HG-induced murine macrophages. (G) Immunofluorescence imaging, and quantitative analysis of Zeb2 expression in (HG)-induced murine macrophages (objective 63X, scale bar 30 µm). (H) Immunofluorescence imaging, and quantitative analysis of pNf-kB in HG-induced murine macrophages (objective 63X, scale bar 30 µm). (I) Western blot analysis of pNf-kB protein expression in HG-induced murine macrophages. (J) mRNA expression of Cd137, Cd38, Cd80, MhcII, and Cd206 in NG and HG murine macrophages. (K) Il-1ß, Il-6, iNod, and Il-4 mRNA expression assessed in NG and HG murine macrophages. Immunofluorescence imaging and quantitative analysis of (L) iNos, and (M) Arg1 in HG murine macrophages (objective 63X, scale bar 30 µm). (N) Flow cytometry analysis of NG and HG murine macrophages against Cd80, and Cd163 cell surface marker. Flow cytometry analysis of NG and HG murine macrophages against (O) Cd86, and (P) iNos. (Q) Oct2, Klf6, and PU.1 mRNA expression assessed by qPCR in NG and HG treated murine macrophages. (R) OCT2, KLF6 mRNA expression in ND and DFU wound sample. (S) Oct2, Klf6, and Pu.1 mRNA expression assessed in SD and HFD mice by qPCR. (T) Oct2, Klf6, and Pu.1 mRNA expression in murine macrophages treated with Zeb2-si transfected macrophages followed by HG induction assessed by qPCR. (U) mRNA expression of MhcII, Cd80, Cd137, and Cd206 in HG, and Zeb2-si+ HG treated murine macrophages. (V) mRNA expression of Il-1ß, Il-6, and Il-4 in HG and Zeb2-si + HG treated murine macrophages. Data are expressed as means ± SD, where *P<0.05, **P<0.01, ***P<0.001, and #P<0.0001 were considered significant difference and ns denotes non-significant difference (Student's or Multiple t-test). All experiments are performed in triplicates.*

In addition, suppressing Zeb2 expression in macrophages by transfecting *Zeb2* siRNA (*Zeb2*-si) worsened the hyperglycaemia-induced expression pattern of LDTFs (**Fig. 3.2A**), and significantly reduced the inflammation (**Fig. 3.2B, C**), suggesting a vital function for Zeb2 in controlling the skewing of pro-inflammatory macrophages at the wound site under hyperglycaemic settings.

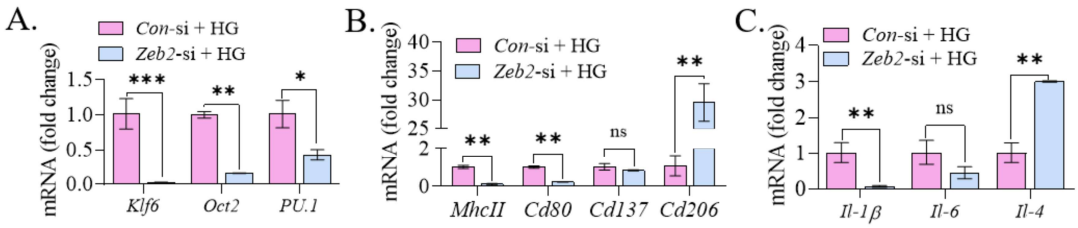

Figure 3.2. *Zeb2 silencing diminish the macrophage polarity in murine macrophages. (A) Oct2, Klf6, and Pu.1 mRNA expression in murine macrophages treated with Zeb2-si transfected macrophages followed by HG induction assessed by qPCR. (B) mRNA expression of MhcII, Cd80, Cd137, and Cd206 in HG, and Zeb2-si+ HG treated murine macrophages. (C) mRNA expression of Il-1ß, Il-6, and Il-4 in*

*HG and Zeb2-si + HG treated murine macrophages. Data are expressed as means ± SD, where *P<0.05, **P<0.01, ***P<0.001, and #P<0.0001 were considered significant difference and ns denotes non-significant difference (Student's or Multiple t-test). All experiments are performed in triplicates.*

3.3.2. Acetylation inhibitor reduces Zeb2 transcriptional expression and prevent hyperglycemia-induced macrophage inflammation

We intended to explore the impact of hyperglycaemia in modifying Zeb2 expression by studying the acetyltransferase profile in diabetic wound macrophages. Our findings demonstrated a substantial overexpression of acetylation enzymes, including *P300*, *Hat1*, and *Moz1*, in hyperglycaemic macrophages compared to normoglycemic controls (**Fig. 3.3A**). This increase was further corroborated by protein expression data, which indicated a substantial elevation of P300 and Hat1 under hyperglycaemic circumstances (**Fig. 3.3B**). Furthermore, the investigation of human diabetic wound tissues indicated a considerable increase in the expression of key acetylation-related enzymes (**Fig. 3.3C**). In STZ-induced HFD animals, a comparable acetylation profile was seen, characterized by a unified increase in P300 enzymes levels (**Fig. 3.3D**). Quantitative acetylome study demonstrated substantial hyperacetylation of many proteins due to high glucose notably at the Lys310 residue on the p65 subunit, hence promoting the pro-inflammatory phenotype in macrophages (Surace and Hedrich, 2019). A histone acetyltransferase P300 inhibitor (Bowers *et al.*, 2010), was used in our study to investigate whether high Zeb2 expression under hyperglycaemic condition is due to acetylation or not. Treatment with C646 resulted decrease in Zeb2 expression in hyperglycemic macrophages, as indicated by immunocytochemistry and immunoblot studies (**Fig. 3.3E, F**). Additionally, C646 administration affected the NF-κB activation profile, demonstrating that reduction of acetyltransferase activity can modulate the post-translational changes of Zeb2, thus, influencing downstream signalling molecules (Huang *et al.*, 2010)(**Fig. 3.3G**). Downregulation of pNF-κB responsible for reduced expression of pro-inflammatory markers, whereas anti-inflammatory remained unaltered (**Fig. 3.3H, I**), which was further confirmed by immunocytochemistry where iNos expression reduced with not much Arg1 alterations in HG treated macrophages following C646 administration (**Fig. 3.3J**) with the downregulation of myeloid lineage-specific transcription factors *Oct2*, *Klf6*, and *Pu.1* (**Fig. 3.3K**). ELISA data further validated these findings, that C646 administration dramatically decreases the expression levels of Il-1β and Tnf-α under hyperglycaemic circumstances (**Fig. 3.3L, M**), indicating the HG induced Zeb2's role in macrophage skewing is driven by acetylation.

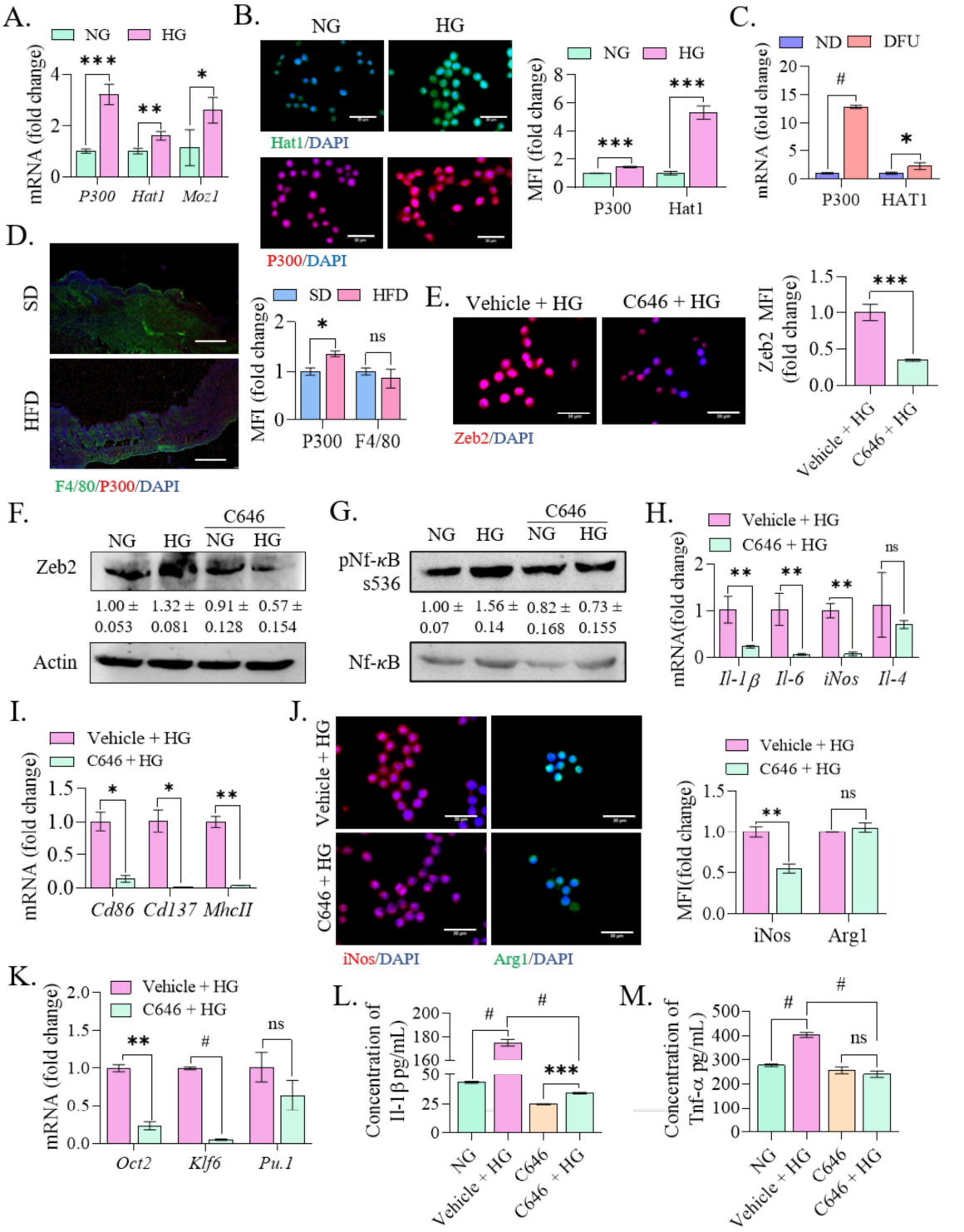

Figure 3.3. *Hyperglycaemia alters the acetylation profile in macrophage population. (A) P300, Hat1, and Moz1 mRNA expression assessed by qPCR in NG and HG treated murine macrophages. (B) Immunofluorescence imaging, and quantitative analysis of Hat1 and P300 (objective 63X, scale bar 30 µm). (C) P300 and HAT1 mRNA expression assessed in ND and DFU. (D) Cryosection of mice wound tissue stained with P300 (red) and F4/80 (green) antibody (objective 10X, scale bar 1000 µm), and its quantitative analysis (n=3). (E) Immunofluorescence imaging, and quantitative analysis of Zeb2 in murine macrophages treated with C646 followed by HG induction (objective 63X, scale bar 30 µm). (F) Western blot analysis of Zeb2 protein expression in murine macrophages treated with C646 followed by HG induction. (G) Western blot analysis of pNf-kB protein expression in murine macrophages treated with C646 followed by HG induction. (H) Il-1ß, Il-6, iNos, and Il-4 mRNA*

*expression measured in murine macrophages treated with C646 followed by HG induction by qPCR. (I) mRNA expression of Cd86, Cd137, and MhcII in murine macrophages treated with C646 followed by HG induction. (J) Immunocytochemistry images and quantitative analysis of iNos and Arg1 in HG and C646 + HG treated murine macrophages. (K) Oct2, Klf6, and Pu.1 mRNA expression in murine macrophages treated with C646 followed by HG induction. Expression of IL-1ß (L), and TNF-α (M) in NG, Vehicle + HG, C646, and C646 + HG treated murine macrophages by ELISA. Data are expressed as means ± SD, where *P<0.05, **P<0.01, ***P<0.001, and #P<0.0001 were considered significant difference and ns denotes non-significant difference (Student's or Multiple t-test or One-way ANOVA). All experiments are performed in triplicates.*

3.3.3. Silencing of Zeb2 protects from HG induced inflammation by halting macrophage polarization skewing

To investigate Zeb2's function in macrophage polarization and inflammation, we silenced Zeb2 by siRNA (*Zeb2*-si) transfection, which resulted in a substantial drop in both Zeb2 mRNA and protein levels (**Fig. 3.4A, B**). This downregulation correspondingly reduced pNF-κB expression (**Fig. 3.4C, D**), thereby, suppressed pro-inflammatory cytokine levels under hyperglycaemic conditions and potentially alleviated the inflammatory macrophage burden, as indicated by the diminished expression of proinflammatory M1 surface markers - *MhcII, Cd80, Cd137*, and upregulated M2 surface marker, *Cd206* (**Fig. 3.4E, F**).

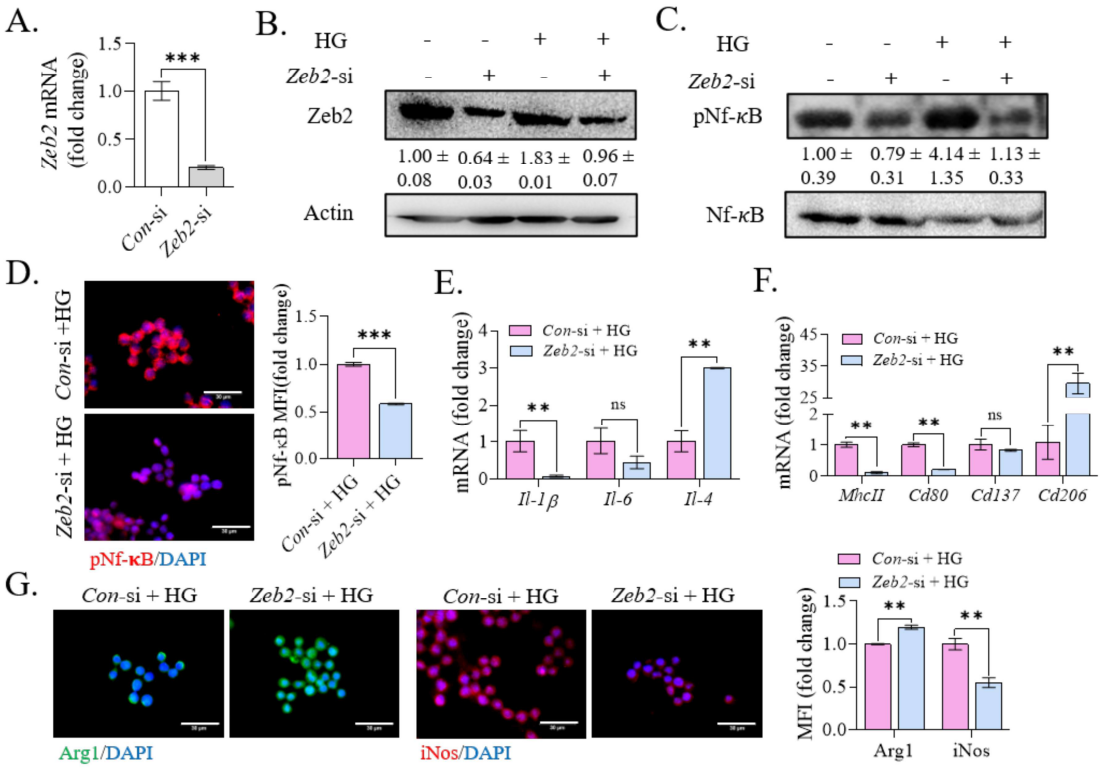

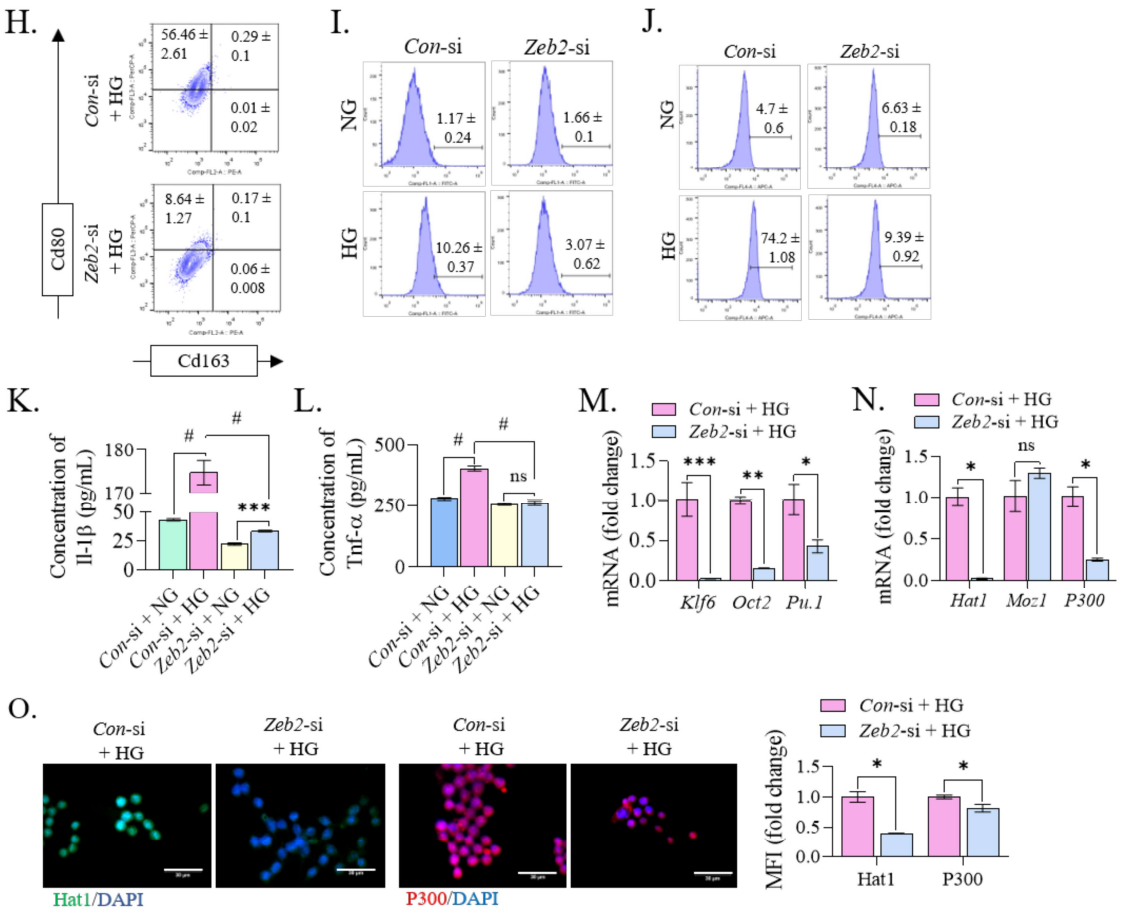

Figure 3.4. *Inhibiting Zeb2 safeguards against hyperglycaemia-induced macrophage inflammation. (A) mRNA expression of Zeb2 in Control siRNA (Con-si) and Zeb2-siRNA (Zeb2-si) transfected murine macrophages. Western blot analysis of Zeb2 (B) and pNf-kB (C) in NG, HG, Zeb2-si, and Zeb2-si + HG treated murine macrophages. (D) Immunofluorescence imaging, and quantitative analysis of pNf-kB in Con-si + HG, and Zeb2-si + HG treated murine macrophages (objective 63X, scale bar 30 µm). (E) mRNA expression of Il-1ß, Il-6, and Il-4 in Con-si + HG and Zeb2-si + HG treated murine macrophages. (F) mRNA expression of MhcII, Cd80, Cd137, and Cd206 in Con-si or Zeb2-si transfected HG treated murine macrophages. (G) Immunofluorescence imaging, and quantitative analysis of Arg1 and iNOS in murine macrophages treated with Con-si or Zeb2-si transfected HG treated murine macrophages (objective 63X, scale bar 30 µm). Flow cytometry analysis of Con-si + HG and Zeb2-si + HG-treated murine macrophages against cell surface marker Cd80 and Cd163 (H); Cd86 (I); and iNos (J). Expression of Tnf-α (K), and Il-1ß (L), in Con-si + NG, Con-si + HG, Zeb2-si + NG, and Zeb2-si + HG-treated murine macrophages by ELISA. (M) Oct2, Klf6, and Pu.1 mRNA expression in murine macrophages treated with C646 followed by HG induction. (N) P300, Hat1, and Moz1 mRNA expression measured in NG and HG-treated murine macrophages. (O) Immunofluorescence imaging, and quantitative analysis of P300 and Hat1 in murine macrophages treated with Con-si and Zeb2-si followed by HG induction (objective 63X, scale bar 30 µm). Data are expressed as means ± SD, where *P<0.05, **P<0.01, ***P<0.001, and #P<0.0001 were considered significant difference and ns denotes non-significant difference (Student's or Multiple t-test or One-way ANOVA). All experiments are performed in triplicates.*

Furthermore, *Zeb2* knockdown led to a decrease in iNos expression, with enhanced Arg1 expression under hyperglycaemic condition (**Fig. 3.4G**). Flow cytometry studies of Cd80,

Cd163 (**Fig. 3.4H**), Cd86 (**Fig. 3.4I**), and iNos (**Fig. 3.4J**), and ELISA data for Tnf-α (**Fig. 3.4K**) and Il-1β (**Fig. 3.4L**), verified the same. The inhibition of Zeb2 expression not only reduces the pro-inflammatory condition by downregulating cytokines and surface indicators but also changes the transcriptional landscape of LDTFs and acetyltransferases, which agrees with the pro-inflammatory profile (**Fig. 3.4M, N**), that were mirrored in the Hat1 and P300 protein expression patterns (**Fig. 3.4O**).

3.3.4. Delivery of acetyltransferase inhibitor ameliorated wound healing in STZ-induced HFD mice model

We have performed wounds on the back of STZ-induced HFD fed diabetic mice and we verified our model through measuring fasting blood glucose levels which was rise markedly over the time in STZ-induced HFD mice compared to SD mice (**Fig. 3.5A**). The detrimental effects of elevated blood glucose become apparent when dermal wounds are inflicted on the diabetic mice, leading to severe wound complications compared with lean mice wound. Intradermal delivery of C646, an acetyltransferase inhibitor, to the wound edge of STZ-induced HFD mice (**Fig. 3.5B**) enhances healing despite the diabetes-induced impediments (**Fig. 3.5C**), with a noticeable reduction in wound size over time. Histological analysis of wound tissue cross-sections through H&E staining reveals a progressive reduction in wound bed depth in treated mice compared to the diabetic model (**Fig. 3.5D**). Inflammatory granulation is observed across all groups by day 3. However, by d7 post-wounding, the C646-treated groups exhibit a thin layer of hyperplastic epidermis, while the diabetic group's wounds remain fully open, devoid of epidermal formation. A pronounced inflammatory accumulation is noted in the diabetic wound group by day 7. C646-treated diabetic wounds showed much lower expression of Zeb2 compared with HFD wound (**Fig. 3.5E**) evidenced by western blot analysis (**Fig. 3.5F**). The healing efficacy in C646 treated cohorts is noticed by the down expression of pro- with high expression of anti-inflammatory markers (**Fig. 3.5G**) long with the diminished Nf-κB activation in d7 post wound tissue (**Fig. 3.5H)**. By day 10 of post-wounding, the C646 treated groups show substantial healing progress, achieving complete epidermal closure and re-epithelialization in contrast to the diabetic group (**Fig. 3.5I)**. These findings underscore the pivotal role of Zeb2 in mitigating chronic inflammatory environments in diabetic wound by modulating acetyltransferase enzyme activity, it is possible to regulate the proinflammatory burden at the wound site and expedite the healing process.

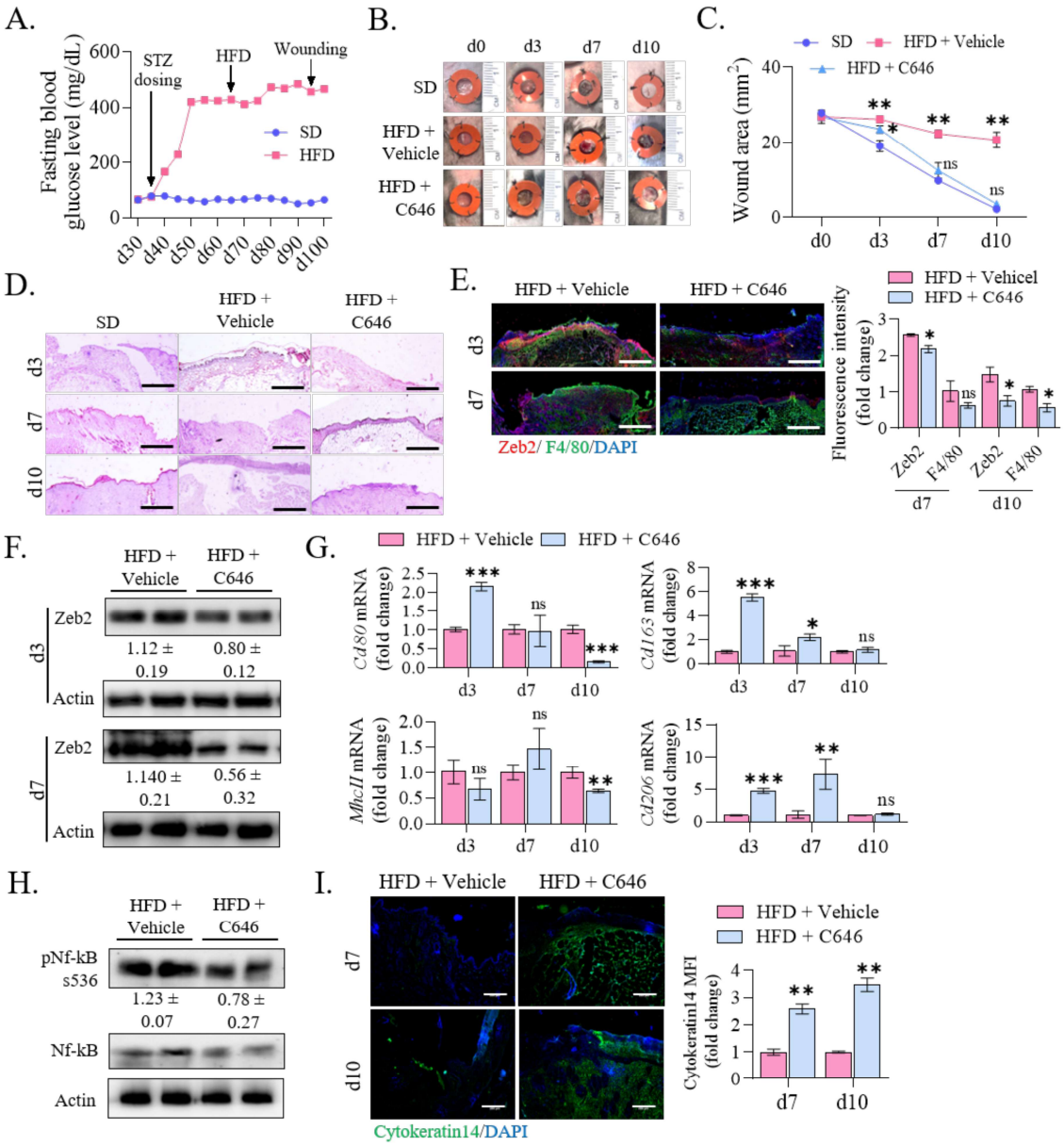

Figure 3.5. *The suppression of acetyltransferase activity ameliorated wound-healing in a high-fat diet mouse model. (A) Fasting blood glucose level of SD and STZ-induced HFD mice. (B) A series of images on the wound area over time of the SD, HFD + Vehicle, and HFD + C646 groups. (C) Wound closure area on the period of healing time in different groups. (D) H & E staining of all murine wound groups (objective 4x, scale bar 1000 µm)(n=3). (E) Immunohistochemistry images and its quantitative analysis by Zeb2 (red) and F4/80 (green) antibody (objective 10X, scale bar 1000 µm) (n=3). (F) Western blot analysis of Zeb2 in d3 and d7 of mice wounds tissue. (G) mRNA analysis of Cd80, MhcII, Cd206, and (H) Western blot analysis of pNf-κB in d7 of mice wound tissue CD163 in HFD + Vehicle, and HFD + C646 groups of mice over a period. (I) Immunohistochemistry images and quantitative analysis of HFD + Vehicle and HFD + C646 group's wound area over time staining by Cytokeratin14 antibody (objective 10X, scale bar 200 µm) (n=3). Data are expressed as means ± SD, where *P<0.05, **P<0.01, ***P<0.001, and #P<0.0001 were considered significant difference and ns denotes non-significant difference (Student's or Multiple t-test). All experiments are performed in triplicates.*

3.4. Discussion

Macrophages serve as central orchestrators in the complex sequence of events during wound healing, seamlessly adapting to the nuanced cues of time and location (Martinez and Gordon, 2014). Numerous studies have unveiled that this highly unregulated, persistent inflammation is primarily orchestrated by inflamed macrophages residing within the wound (Lin *et al.*, 2023, Scott and Omilusik, 2019b). This persistent inflammation stems from dysregulated molecular pathways primarily guided by hyperglycaemia. Our study delves into the effects of glucose induction, which hyperactivates proinflammatory markers (Edgar *et al.*, 2021, Ayala *et al.*, 2019) intricately linked with high Zeb2, a transcription factor (TF), which is widely expressed among hematopoietic lineages (Wu *et al.*, 2016). Zeb2 has a pivotal role in immune cell development, survivability, differentiation (Scott *et al.*, 2016) and maintaining the tissue-specific identities of macrophages (Scott et al., 2018). Previously it was reported that Zeb2 expression was correlated with the reduction of LPS-induced inflammatory burden (Ding *et al.*, 2018), but in contrast, the consistent exposure to TNF-α induced the expression of Zeb2 (Chua et al., 2007). High accumulation of the TNF-α upon hyperglycaemia causes the activation of Zeb2, intensifying proinflammatory responses by binding to cytokine gene promoters' E-box sequences (Kroder *et al.*, 1996).

Furthermore, myeloid lineage-determining transcription factors, like Oct2, Klf6, and Pu.1 sustain the pro-inflammatory state of macrophage lineages, while also promoting Zeb2 activation by binding to its proximal promoter region (Katoh and Katoh, 2009). In hyperglycaemic environments, unregulated acetyltransferase activity, exacerbates Zeb2 activation. P300 and other acetyltransferase family members disrupt SIRT6-FOXA2 interactions with the Zeb2 promoter accumulating by acetylating SIRT6, which activates its transcription (Zhao *et al.*, 2023). Taking into account all these circumstances, our study predominantly delves into the impact of Zeb2, and acetyltransferase activity on proinflammatory signals and explores how inhibiting these factors could potentially reinstate the protective stance of macrophages in chronic diabetic wounds.

Sustain activation of pro-inflammatory cues under hyperglycaemic conditions is associated with hyperactive lysine acetylation by histone and non-histone acetyltransferase-directed unregulated gene expressions (Miao *et al.*, 2004). Activation of P300 (Di Pietrantonio *et al.*, 2023) and other acetyltransferase enzymes leads to a molecular chaos by activating many factors, that ultimately promotes the unregulated chronic inflammation in macrophages under high glucose environment. Many reports revealed that activation of Nf-kB directed inflammatory signals solely depends upon the contribution of chromatin modifying complex

P300/CBP (Mukherjee *et al.*, 2013, Bhatt and Ghosh, 2014, Berghe *et al.*, 1999). Our *in vitro* studies of hyperglycaemic macrophages, *in vivo* studies of diabetic patient wound samples, and STZ-induced HFD mice wound studies also depicted the prophylactic activity of acetyltransferase enzymes. We found that the inhibition of acetyltransferase activity by a P300-specific inhibitor, C646, reduce the inflammatory burden in wound by inhibiting NF-κB activity under hyperglycaemic conditions. C646 also reduced the myeloid-lineage-directed transcription factors level, which also directed the macrophages' prophylactic status.

We also observed the down expressions of Zeb2 over the time in C646-treated wound along with reduced LDTFs, which is known to direct macrophages' persistent inactivation of classical pathways in wound healing- proliferation and remodelling stages (Caputa *et al.*, 2019, Gordon and Martinez, 2010).

Further to examine the exclusive role of hyperglycaemia-induced Zeb2 activation in macrophages-directed inflammatory burden, we have silenced the Zeb2 expression by *Zeb2* siRNA transfection, directed reduction of inflammatory burden even upon high glucose induction in macrophage populations. A notable reduction of LDTFs was noticed in macrophages post *Zeb2*-si transfection, thereby, clarifying the direct participation of Zeb2 on hyperglycaemia-induced molecular chaos.

In summary, our findings demonstrated that hyperglycaemia-induced acetyltransferase activity directed the hyperactivation of Zeb2 expression in wound macrophages, which might restrict the macrophages in M1 polarity in chronic wounds. In contrast, direct administration of acetyltransferase inhibitor, C646, rescued the wound complications in STZ-induced HFD mice by modulating the wound microenvironment inflammation burden by reducing Zeb2 expression, depicting that the reduction of acetylation profile in wound bed ameliorates the Zeb2-induced chronic inflammations. Thus, our study covers how acetylation maintains prolonged inflammatory stage in hyperglycemic condition during wound healing and can be a potential therapeutic way to treat diabetic chronic wound inflammation.

References

AKKUS, G. & SERT, M. 2022. Diabetic foot ulcers: A devastating complication of diabetes mellitus continues non-stop in spite of new medical treatment modalities. *World J Diabetes,* 13**,** 1106-1121.

ASHBURNER, B. P., WESTERHEIDE, S. D. & BALDWIN, A. S., JR. 2001. The p65 (RelA) subunit of NF-kappaB interacts with the histone deacetylase (HDAC) corepressors HDAC1 and HDAC2 to negatively regulate gene expression. *Mol Cell Biol,* 21**,** 7065-77.

AYALA, T. S., TESSARO, F. H. G., JANNUZZI, G. P., BELLA, L. M., FERREIRA, K. S. & MARTINS, J. O. 2019. High Glucose Environments Interfere with Bone Marrow-Derived Macrophage Inflammatory Mediator Release, the TLR4 Pathway and Glucose Metabolism. *Scientific Reports,* 9**,** 11447.

BERBUDI, A., RAHMADIKA, N., TJAHJADI, A. I. & RUSLAMI, R. 2020. Type 2 Diabetes and its Impact on the Immune System. *Curr Diabetes Rev,* 16**,** 442-449.

BERGHE, W. V., DE BOSSCHER, K., BOONE, E., PLAISANCE, S. & HAEGEMAN, G. 1999. The Nuclear Factor-κB Engages CBP/p300 and Histone Acetyltransferase Activity for Transcriptional Activation of the Interleukin-6 Gene Promoter*. *Journal of Biological Chemistry,* 274**,** 32091-32098.

BHATT, D. & GHOSH, S. 2014. Regulation of the NF-κB-Mediated Transcription of Inflammatory Genes. *Frontiers in Immunology,* 5:71.

BOWERS, E. M., YAN, G., MUKHERJEE, C., ORRY, A., WANG, L., HOLBERT, M. A., CRUMP, N. T., HAZZALIN, C. A., LISZCZAK, G., YUAN, H., LAROCCA, C., SALDANHA, S. A., ABAGYAN, R., SUN, Y., MEYERS, D. J., MARMORSTEIN, R., MAHADEVAN, L. C., ALANI, R. M. & COLE, P. A. 2010. Virtual ligand screening of the p300/CBP histone acetyltransferase: identification of a selective small molecule inhibitor. *Chemistry & biology,* 17**,** 471-482.

CAPUTA, G., FLACHSMANN, L. J. & CAMERON, A. M. 2019. Macrophage metabolism: a wound-healing perspective. *Immunology & Cell Biology,* 97**,** 268-278.

CHEN, L., DENG, H., CUI, H., FANG, J., ZUO, Z., DENG, J., LI, Y., WANG, X. & ZHAO, L. 2018. Inflammatory responses and inflammation-associated diseases in organs. *Oncotarget,* 9**,** 7204-7218.

CHUA, H. L., BHAT-NAKSHATRI, P., CLARE, S. E., MORIMIYA, A., BADVE, S. & NAKSHATRI, H. 2007. NF-kappaB represses E-cadherin expression and enhances epithelial to mesenchymal transition of mammary epithelial cells: potential involvement of ZEB-1 and ZEB-2. *Oncogene,* 26**,** 711-24.

DI PIETRANTONIO, N., DI TOMO, P., MANDATORI, D., FORMOSO, G. & PANDOLFI, A. 2023. Diabetes and Its Cardiovascular Complications: Potential Role of the Acetyltransferase p300. *Cells,* 12.

DING, Q., WANG, Y., ZHANG, A. L., XU, T., ZHOU, D. D., LI, X. F., YANG, J. F., ZHANG, L. & WANG, X. 2018. ZEB2 Attenuates LPS-Induced Inflammation by the NF-κB Pathway in HK-2 Cells. *Inflammation,* 41**,** 722-731.

EDGAR, L., AKBAR, N., BRAITHWAITE, A. T., KRAUSGRUBER, T., GALLART-AYALA, H., BAILEY, J., CORBIN, A. L., KHOYRATTY, T. E., CHAI, J. T., ALKHALIL, M., RENDEIRO, A. F., ZIBERNA, K., ARYA, R., CAHILL, T. J., BOCK, C., LAURENCIKIENE, J., CRABTREE, M. J., LEMIEUX, M. E., RIKSEN, N. P., NETEA, M. G., WHEELOCK, C. E., CHANNON, K. M., RYDÉN, M., UDALOVA, I. A., CARNICER, R. & CHOUDHURY, R. P. 2021. Hyperglycemia Induces Trained Immunity in Macrophages and Their Precursors and Promotes Atherosclerosis. *Circulation,* 144**,** 961-982.

FISCHER, K. S., LITMANOVICH, B., SIVARAJ, D., KUSSIE, H. C., HAHN, W. W., HOSTLER, A. C., CHEN, K. & GURTNER, G. C. 2023. Protocol for the Splinted, Human-like Excisional Wound Model in Mice. *Bio Protoc,* 13**,** e4606.

FURMAN, B. L. 2021. Streptozotocin-Induced Diabetic Models in Mice and Rats. *Current Protocols,* 1**,** e78.

GOLDIN, A., BECKMAN, J. A., SCHMIDT, A. M. & CREAGER, M. A. 2006. Advanced Glycation End Products. *Circulation,* 114**,** 597-605.

GORDON, S. & MARTINEZ, F. O. 2010. Alternative Activation of Macrophages: Mechanism and Functions. *Immunity,* 32**,** 593-604.

HAERY, L., THOMPSON, R. C. & GILMORE, T. D. 2015. Histone acetyltransferases and histone deacetylases in B- and T-cell development, physiology and malignancy. *Genes Cancer,* 6**,** 184-213.

HUANG, B., YANG, X. D., LAMB, A. & CHEN, L. F. 2010. Posttranslational modifications of NF-kappaB: another layer of regulation for NF-kappaB signaling pathway. *Cell Signal,* 22**,** 1282-90.

KATOH, M. & KATOH, M. 2009. Integrative genomic analyses of ZEB2: Transcriptional regulation of ZEB2 based on SMADs, ETS1, HIF1alpha, POU/OCT, and NF-kappaB. *Int J Oncol,* 34**,** 1737-42.

KIM, H. R., SEO, C. W., HAN, S. J., LEE, J. H. & KIM, J. 2022. Zinc Finger E-Box Binding Homeobox 2 as a Prognostic Biomarker in Various Cancers and Its Correlation with Infiltrating Immune Cells in Ovarian Cancer. *Curr Issues Mol Biol,* 44**,** 1203-1214.

KRODER, G., BOSSENMAIER, B., KELLERER, M., CAPP, E., STOYANOV, B., MÜHLHÖFER, A., BERTI, L., HORIKOSHI, H., ULLRICH, A. & HÄRING, H. 1996. Tumor necrosis factor-alpha- and

hyperglycemia-induced insulin resistance. Evidence for different mechanisms and different effects on insulin signaling. *The Journal of Clinical Investigation,* 97**,** 1471-1477.

KRZYSZCZYK, P., SCHLOSS, R., PALMER, A. & BERTHIAUME, F. 2018. The Role of Macrophages in Acute and Chronic Wound Healing and Interventions to Promote Pro-wound Healing Phenotypes. *Front Physiol,* 9**,** 419.

LIN, S., WANG, Q., HUANG, X., FENG, J., WANG, Y., SHAO, T., DENG, X., CAO, Y., CHEN, X., ZHOU, M. & ZHAO, C. 2023. Wounds under diabetic milieu: The role of immune cellar components and signaling pathways. *Biomedicine & Pharmacotherapy,* 157**,** 114052.

MARTINEZ, F. O. & GORDON, S. 2014. The M1 and M2 paradigm of macrophage activation: time for reassessment. *F1000Prime Rep,* 6**,** 13.

MIAO, F., GONZALO, I. G., LANTING, L. & NATARAJAN, R. 2004. In Vivo Chromatin Remodeling Events Leading to Inflammatory Gene Transcription under Diabetic Conditions *. *Journal of Biological Chemistry,* 279**,** 18091-18097.

MUKHERJEE, S. P., BEHAR, M., BIRNBAUM, H. A., HOFFMANN, A., WRIGHT, P. E. & GHOSH, G. 2013. Analysis of the RelA:CBP/p300 interaction reveals its involvement in NF-κB-driven transcription. *PLoS Biol,* 11**,** e1001647.

PATRA, D., ROY, S., ARORA, L., KABEER, S. W., SINGH, S., DEY, U., BANERJEE, D., SINHA, A., DASGUPTA, S., TIKOO, K., KUMAR, A. & PAL, D. 2022. miR-210-3p Promotes Obesity-Induced Adipose Tissue Inflammation and Insulin Resistance by Targeting SOCS1-Mediated NF-κB Pathway. *Diabetes,* 72**,** 375-388.

PÉREZ, S. & RIUS-PÉREZ, S. 2022. Macrophage Polarization and Reprogramming in Acute Inflammation: A Redox Perspective. *Antioxidants (Basel),* 11(7):1394.

SCOTT, C. L. & OMILUSIK, K. D. 2019a. ZEBs: Novel Players in Immune Cell Development and Function. *Trends Immunol,* 40**,** 431-446.

SCOTT, C. L. & OMILUSIK, K. D. 2019b. ZEBs: Novel Players in Immune Cell Development and Function. *Trends in Immunology,* 40**,** 431-446.

SCOTT, C. L., SOEN, B., MARTENS, L., SKRYPEK, N., SAELENS, W., TAMINAU, J., BLANCKE, G., VAN ISTERDAEL, G., HUYLEBROECK, D., HAIGH, J., SAEYS, Y., GUILLIAMS, M., LAMBRECHT, B. N. & BERX, G. 2016. The transcription factor Zeb2 regulates development of conventional and plasmacytoid DCs by repressing Id2. *Journal of Experimental Medicine,* 213**,** 897-911.

SCOTT, C. L., T'JONCK, W., MARTENS, L., TODOROV, H., SICHIEN, D., SOEN, B., BONNARDEL, J., DE PRIJCK, S., VANDAMME, N., CANNOODT, R., SAELENS, W., VANNESTE, B., TOUSSAINT, W., DE BLESER, P., TAKAHASHI, N., VANDENABEELE, P., HENRI, S., PRIDANS, C., HUME, D. A., LAMBRECHT, B. N., DE BAETSELIER, P., MILLING, S. W. F., VAN GINDERACHTER, J. A., MALISSEN, B., BERX, G., BESCHIN, A., SAEYS, Y. & GUILLIAMS, M. 2018. The Transcription Factor ZEB2 Is Required to Maintain the Tissue-Specific Identities of Macrophages. *Immunity,* 49**,** 312-325.e5.

SINGH, R., BARDEN, A., MORI, T. & BEILIN, L. 2001. Advanced glycation end-products: a review. *Diabetologia,* 44**,** 129-46.

SURACE, A. E. A. & HEDRICH, C. M. 2019. The Role of Epigenetics in Autoimmune/Inflammatory Disease. *Frontiers in Immunology,* 10:1525.

TÓBON-VELASCO, J. C., CUEVAS, E. & TORRES-RAMOS, M. A. 2014. Receptor for AGEs (RAGE) as mediator of NF-kB pathway activation in neuroinflammation and oxidative stress. *CNS Neurol Disord Drug Targets,* 13**,** 1615-26.

URIBARRI, J., CAI, W., RAMDAS, M., GOODMAN, S., PYZIK, R., CHEN, X., ZHU, L., STRIKER, G. E. & VLASSARA, H. 2011. Restriction of advanced glycation end products improves insulin resistance in human type 2 diabetes: potential role of AGER1 and SIRT1. *Diabetes Care,* 34**,** 1610-6.

WU, X., BRISEÑO, C. G., GRAJALES-REYES, G. E., HALDAR, M., IWATA, A., KRETZER, N. M., KC, W., TUSSIWAND, R., HIGASHI, Y., MURPHY, T. L. & MURPHY, K. M. 2016. Transcription factor Zeb2 regulates commitment to plasmacytoid dendritic cell and monocyte fate. *Proceedings of the National Academy of Sciences,* 113**,** 14775-14780.

ZHAO, K., ZHENG, M., SU, Z., GHOSH, S., ZHANG, C., ZHONG, W., HO, J. W. K., JIN, G. & ZHOU, Z. 2023. MOF-mediated acetylation of SIRT6 disrupts SIRT6-FOXA2 interaction and represses SIRT6 tumor-suppressive function by upregulating ZEB2 in NSCLC. *Cell Rep,* 42**,** 112939.

Chapter 4

Oxidized pullulan exhibits potent antibacterial activity against *Staphylococcus aureus*

4.1. Background

In underdeveloped nations, wound infections account for 70–80% of infection-related deaths and are a major cause of non-healing wound. Diabetic patients are more likely to get their wound infected by bacteria because of the high glucose levels in the wound bed, which provides nutrients for bacteria. The most common bacteria implicated in chronic wound are *Staphylococcus aureus* (79.4%), *Pseudomonas aeruginosa* (40.2%), *Proteus mirabilis* (11.2%), and *Staphylococcus haemolyticus* (4.4%) along with *Klebsiella pneumoniae*, *Enterococcus faecalis*, and *Acinetobacter baumannii*. In the early stages of an infection, *Staphylococcus aureus* is often the most prevalent pathogen, but *Pseudomonas aeruginosa* and other bacteria also play an important role. (Glik *et al.,* 2012). Statistics reveal that 75.3% of wound infections are caused by a solitary bacterial species, while 24.7% are the product of co-infections. The most regularly observed co-infecting bacteria are *S. aureus* and *P. aeruginosa* (23.7%), followed by *E. coli* and *S. aureus* (6.8%), *P. mirabilis* and *P. aeruginosa* (5.1%), as well as *A. baumannii/haemolyticus* and *S. aureus* (5.1%) (Puca *et al.*, 2021). The frequent use of antibiotics has led to the emergence of Multi-medication Resistant Microorganisms (MDRM), culminating in treatment failures and harmful drug effects (Tamma *et al.*, 2017). The bacterial cell envelope, vital for cellular homeostasis and selective permeability, is a key target in drug development due to its role in resistance mechanisms. With the rise of MDRMs and limited effective antibiotics, there is an urgent need for new antibacterial agents targeting the bacterial membrane. Traditional low molecular weight antibiotics often suffer from toxicity and short-lived effects, highlighting the need for innovative antimicrobial polymers with higher selectivity and prolonged action to combat resistant infections (Kenawy *et al.*, 2007).

To the best of our knowledge, previous research on polysaccharide-based scaffolds for chronic wound healing, has continually highlighted the necessity of using chemical crosslinkers

or mixing various polysaccharides to obtain the desired functionality. To confront these challenges, we focused on the fundamental flexibility of the natural polysaccharide pullulan, aiming to harness and expand its capabilities by precise chemical modifications. Specifically, we intended to convert pullulan into a therapeutically active, antibacterial form optimal for chronic wound care. Pullulan, a commercially produced polysaccharide manufactured mainly by the yeast-like fungus *Aureobasidium pullulans*, consists of maltotriose units linked by α-1,4 glycosidic linkages, with further connections via α-1,6 glycosidic bonds (Cheng *et al.*, 2011). This distinctive molecular structure endows pullulan with several advantageous properties, including superior solubility, biocompatibility, and mechanical flexibility. The sticky qualities of pullulan and its derivatives render them intriguing candidates for several biological applications. Pullulan-based materials have been extensively investigated for targeted drug and gene delivery (Singh *et al.*, 2015), tissue engineering scaffolds (Singh *et al.*, 2016), vaccine adjuvants, and capsule coatings (Akiyoshi *et al.*, 1998) owing to their capacity to interact with biological systems safely and effectively.

Polysaccharides, particularly those of natural origin, have gained great attention in wound dressing research due to their biocompatibility, non-immunogenic characteristics, and inherent antioxidant and antibacterial properties (Zhang *et al.*, 2017). Pullulan is known for its high adhesiveness, biocompatibility, anticoagulant activity, anti-thrombotic effects, and anti-inflammatory properties. However, its fundamental lack of bactericidal activity significantly limits its direct effectiveness in fighting bacterial infections. To overcome this issue, we postulated that the judicious insertion of functional groups by chemical modification may provide pullulan with antibacterial properties.

Our goal was to transform pullulan into a multifunctional biomaterial capable of providing excellent infection control while improving tissue compatibility, both of which are required for good wound healing results. In addition to investigating the antibacterial activity of oxidized pullulan, we sought to understand its mechanism of action, focusing on the molecular interactions between the changed polymer and bacterial cells. Such mechanistic insights are critical for improving the material's design and ensuring accuracy and efficacy in specific applications. This study aims to contribute to developing next-generation biopolymer-based scaffolds by addressing the coupled challenges of infection and inflammation in the wound microenvironment, expanding the frontiers of wound care and regenerative medicine.

4.1.1. Challenges

Excessive uncontrolled usage of antibacterial leads to the emerging antibiotic-resistant bacteria, which makes treatment more challenging (Ahmed *et al.*, 2024). Antibiotic resistance

more difficult, often requiring stronger or more expensive medications, and biofilm formation by bacteria further complicate infection control. Therefore, biodegradable and biocompatible biomaterial-based application can address the infection challenges by incorporating antimicrobial agents, disrupting biofilms, and enabling controlled release of antibiotics (Sam *et al.*, 2023). Additionally, they can by incorporating antimicrobial agents, disrupting biofilms, and enabling controlled release of antibiotics.

4.1.2. Objectives

In this investigation, our aim is –

- To synthesize and characterize the oxidized pullulan to increase its therapeutic potential.
- To evaluate the anti-bacterial property of oxidized pullulan against wound microbes.
- To analyse the mechanism of bactericidal action of oxidized pullulan.

4.2. Materials and Methods

4.2.1. Materials

Pullulan was purchased from TCI Chemicals, India; sodium (meta) periodate, DCFDA (2′,7′-dichlorodihydrofluorescein diacetate), $DiSC_3(5)$ (3,3′-dipropylthiadicarbocyanine iodide), crystal violet, ethylene glycol, glutaraldehyde, osmium tetroxide, sulfuric acid, and Müeller-Hinton broth were procured from Sigma-Aldrich, USA; and Luria Bertani broth, Luria Bertani agar, ciprofloxacin, BSA (Bovine Serum Albumin), FBS (Fetal Bovine Serum), and MTT (3-(4,5-dimethylthiazol-2-yl)-2,5- diphenyltetrazolium bromide) reagents were procured from HiMedia, India. LIVE/DEAD BacLight Bacterial Viability Kit, DAPI (4′,6-dia- midino-2-phenylindole), Alexa Fluor 488 Phalloidin, LIVE/DEAD Viability/Cytotoxicity Kit, and Trizol reagent were acquired from Invitrogen, USA. Sodium chloride, sodium bicarbonate, potassium chloride, calcium chloride, ammonium molybdate, DPX (Dibutylphthalate Polystyrene Xylene), malachite green oxalate, sodium citrate, and barium chloride were acquired from SRL, India. DMEM (Dulbecco's Modified Eagle Medium) and RPMI 1640 (Roswell Park Memorial Institute) me- dium was procured from Gibco, USA. Super RT-MuLV kit was utilized from Bio Bharati Life Science Pvt. Ltd., India. HATU (1-[bis(dimethy- lamino) methylene]-1H-1,2,3-triazolo[4,5-b] pyridinium 3-oxide hexa- fluorophosphate), DIEA (N, N-diisopropylethylamine) were acquired from TCI Chemicals, India. Fmoc-Lys (Mtt)-OH, Fmoc-Asn (trt)-OH, Fmoc-Phe-OH, and Fmoc-Gln (trt)-OH were purchased from BLD Pharmaceuticals, India. Different gene-specific primers were acquired from Eurofins Scientific,

India. ASOs (Antisense Oligonucleotides) targeting the B and C-domains of SpA was bought from Integrated DNA Technologies, India. All tissue culture supplies were procured from Tarsons, India and HiMedia, India. Fresh human blood was extracted from healthy human donors, as per the procedure authorized by the institutional biosafety committee (#07/2021-II/IIT/IEC).

4.2.2. Bacterial and mammalian cell culture

In this work, *P. aeruginosa* (strain 10620) and *S. aureus* (strain 7443) were chosen for investigation. These bacterial strains were collected from the Microbial Type Culture Collection (MTCC) at CSIR- IMTECH, Chandigarh, India. Prior to usage, the strains were pre-cultured in Luria Broth (LB) medium at 37 °C for 48 hours. After incubation, the cultures were adjusted to a concentration of 10^8 cells/mL in line with the 0.5 McFarland standard.

Two murine cell lines, normal fibroblasts (L929) (passage no. 2) and macrophages (RAW 264.7) (passage no. 5), were acquired from the NCCS in Pune, India. The L929 cells were cultivated in RPMI-1640, whereas the RAW 264.7 cells were grown in DMEM, both supplemented with 10% FBS and 1% penicillin-streptomycin. The cultures were kept in a humidified incubator set at 37 °C with 5% CO_2 and 95% humidity to guarantee optimum growth conditions.

4.2.3. Oxidation of pullulan

Pullulan was oxidized following a previously published method with slight modifications (Bruneel and Schacht, 1993). In summary, a 4% w/v pullulan solution was reacted with varying concentrations of sodium metaperiodate ($NaIO_4$), with the reaction mixture being continuously stirred at room temperature for 24 hours under dark conditions. To terminate the reaction, an equimolar amount of ethylene glycol was added to the mixture, followed by agitation for an additional 2 hours. The resulting mixture was then purified by dialysis against deionized water for 3 days, with the sink medium being refreshed every 12 hours. Finally, the product was freeze-dried to obtain o-pullulan.

4.2.4. Characterization of o-pullulan

FT-IR spectra of conventional pullulan and derivative o-pullulan were obtained in the ATR (Attenuated Total Reflection) mode employing Bruker Tensor 27 spectrometer from 400 to 4000 cm^{-1} (Haslauer *et al.*, 2019).

The degree of oxidation of pullulan was determined by quantifying the aldehyde content using a hydroxylamine hydrochloride assay (Zhao and Heindel, 1991). o-Pullulan was

dissolved in deionized water, and a 0.72 mol/L hydroxylamine hydrochloride solution was added. The mixture was swirled for 4 hours at 40 °C. Subsequently, the released hydrochloric acid was titrated with 1.0 mol/L NaOH, and the amount of NaOH used was determined. A pullulan solution of comparable concentration served as the blank. The aldehyde content in o-pullulan was then determined using the following equation (triplicate):

$$\text{Mole of CHO present in the polymer} = \frac{V_{NaOH} \times N_{NaOH} \times 10^{-3}\ \text{mol}}{M \times MW}$$

$$\text{CHO (\%)} = \frac{\text{Mole of CHO present in the polymer} \times MW}{M \times \text{Number of functional unit/mol}}$$

Where, V_{NaOH} = Vol (mL) of NaOH consumed in titration
N_{NaOH} = Normality of NaOH
M = Weight of o-pullulan (g)
MW = Molecular weight of o-pullulan
Number of functional unit/mol = 12

The carboxyl content was measured using a modified calcium acetate technique (Kumar and Yang, 2002). Briefly, o-pullulan was suspended in deionized water, and a 0.1 M calcium acetate solution was added. After allowing the combination to react for 1 hour, it was titrated with standardized 0.01 N NaOH, with phenolphthalein acting as the indicator. The carboxyl content was then determined using the following equation (done in triplicate):

$$\text{COOH (\%)} = \frac{(V_{NaOH} - V_b) \times N_{NaOH} \times 45 \times 100}{M}$$

Where, V_{NaOH} = volume (L) of NaOH solution used for the sample titration
V_b = volume (L) of NaOH solution used for control determination
M = weight (g) of the sample
The molecular weight of the carboxyl group is 45.

The presence of iodate (IO_3^-) and iodide (I^-) impurities in o-pullulan was tested using a combination of Energy Dispersive X-ray Spectroscopy (EDX) and a modified halide ion test technique (Willard and Thompson, 1934). Elemental distribution in pullulan and o-pullulan was analyzed using a BrukerSplash 6130 Energy Dispersive X-ray Spectroscopy (EDX) system. To detect iodate (IO_3^-) and iodide (I^-) contamination, a 3.49% (w/v) sodium (meta)-periodate solution was utilized as a positive control. Both pre- and post-dialysis o-pullulan solutions were

tested. To prevent silver salt precipitation, each solution received one or two drops of 5% (v/v) nitric acid, followed by the addition of two drops of 2% (w/v) silver nitrate solution. The appearance of a pale-yellow precipitate of silver iodide indicated the presence of iodide and iodate ions.

The molecular weights of pullulan and o-pullulan (1 mg/mL) were evaluated using an Agilent gel permeation chromatography (GPC) system, which contained an Agilent 1220 refractive index detector and an Agilent GPC/SEC column. Deionized water was utilized as the eluent at a flow rate of 1 mL/min, with measurements done at 25 °C. Calibration of the instrument was accomplished using polyethylene glycol standards of varied molecular weights prior to the analysis.

The X-ray diffraction (XRD) patterns of pullulan and o-pullulan were acquired using a Rigaku Miniflex diffractometer, set at 40 kV and 15 mA. Measurements were done across a 2 θ range of 2 ° to 45 °, using Cu Kα radiation (λ = 0.154 nm). The diffraction angle was scanned at a rate of 2 °/minute.

A 10 mg sample was put in an Al_2O_3 crucible for thermal gravimetric analysis (TGA) using a Mettler Toledo equipment. The temperature was steadily raised from 40 °C to 600 °C at a heating rate of 10 °C/min, and the analysis was done in a nitrogen environment to test the thermal stability of o-pullulan.

Viscometry studies were performed out at 25 ± 0.01 °C by an Anton Parr Rheometer (MCR 101) to evaluate a shift in the viscosity of o-pullulan following modifications.

The surface charge of pullulan and o-pullulan was examined by measuring their zeta potential with a Malvern Zetasizer (Ata Scientific Instruments, Australia). Samples were produced at a concentration of 1 mg/mL in deionized water, and the mean zeta potential was calculated.

4.2.5. Assessment of the Minimal Inhibitory Concentration (MIC) and Minimal Bactericidal Concentration (MBC)

The antibacterial activities of o-pullulan were investigated against *P. aeruginosa* and *S. aureus*. A dose-response study was done to identify both the Minimal Inhibitory Concentration (MIC) and Minimal Bactericidal Concentration (MBC) of o-pullulan for various bacterial species. The MIC was established with a refined broth microdilution method, as described by the National Committee for Clinical Laboratory Standards (NCCLS) (Andrews, 2001).

A bacterial suspension of 5×10^5 CFU/mL was produced in Mueller-Hinton Broth (MHB) and calibrated to a density of 0.5 McFarland standard using a combination of 0.5 mL of 0.048 M $BaCl_2$ and 99.5 mL of 0.18 M H_2SO_4. Serial dilutions of o-pullulan, ranging from 300 μg/mL

to 0.07 ng/mL, were produced in MHB. In a 96-well plate, 100 µL of the adjusted bacterial culture was mixed with the diluted o-pullulan solutions and incubated at 37 °C with shaking at 100 rpm for 24 hours. Ciprofloxacin at 0.5 µg/mL was included as a positive control. Post-incubation, bacterial growth was measured by measuring the absorbance at 600 nm (Wiegand *et al.*, 2008). A time-killing experiment was done using recognized techniques. At predefined intervals, 10^6-fold dilutions of the bacterial inoculum, treated with or without o-pullulan, were plated onto LB agar plates and incubated for the given period. Colony counts were then assessed after 24 hours of incubation at 37 °C.

4.2.6. Susceptibility test

The susceptibility of bacteria to o-pullulan was determined using the disk diffusion assay, following established protocols (Cai *et al.*, 2009). LB agar plates were prepared with 25 mL of agar in 100 mm Petri dishes. Paper discs, each 5 mm in diameter, were dipped in either LB broth (as a blank), pullulan (50 µg/mL), o-pullulan (at its MIC), or ciprofloxacin (0.5 µg/mL) solutions and air-dried for 48 hours. The standardized bacterial suspension was spread evenly across the agar surface, and the discs were placed on the inoculated plates. After incubation at 37 °C for 24 hours, the zones of inhibition surrounding the discs were photographed and analyzed using ImageJ software to measure the effectiveness of the antimicrobial agents.

4.2.7. Viability assay

The viability of *S. aureus* in the presence of o-pullulan was evaluated using the LIVE/DEAD™ BacLight™ Bacterial Viability Kit (Invitrogen), following the manufacturer's guidelines. A standardized bacterial culture was treated with o-pullulan at its MIC, incubated at 37 °C with agitation at 100 rpm for 24 hours. Native pullulan was used as a blank control, while ciprofloxacin served as a positive control. After 24 hours, 50 µL aliquots were withdrawn, stained with the LIVE/DEAD™ reagents, and then placed on glass slides. Cover slips were applied, and the samples were examined under a fluorescence microscope (Leica), using excitation/emission wavelengths of 485/498 nm for SYTO 9 and 535/617 nm for propidium iodide (PI) (Manteca *et al.*, 2005).

4.2.8. HR-TEM (High-Resolution Transmission Electron Microscopy) imaging

Staphylococcus aureus was cultivated to attain the mid-log phase and standardized using McFarland reagent. A control culture was established in LB medium without any polymer, while o-pullulan was introduced to the bacterial inoculum at its MIC. The cultures were then collected and centrifuged at 5500 rpm for 10 minutes at 4 °C, followed by re-suspension in 0.5

mL of phosphate-buffered saline (PBS, pH 7.4). After three washes with PBS, the samples were fixed overnight at 4 °C with 3.5 % (v/v) glutaraldehyde, washed again, and stained with 1% osmium tetroxide for 30 minutes. The samples were dehydrated using an ethanol gradient (30%, 50%, 70%, and 90%), then resuspended in 100% ethanol. Finally, roughly 5 µL of the sample was put on a carbon-coated copper grid (mesh size: 300), air-dried, and analysed using high-resolution transmission electron microscopy (HR-TEM).

4.2.9. Fluorometric measurement of membrane potential

To examine the impact of o-pullulan on the outer membrane of *S. aureus*, we used the voltage-sensitive dye $DiSC_3(5)$ to assess membrane potential alterations. Bacterial cultures were exposed to the MIC of o-pullulan, and 400 µL aliquots of these treated samples were transferred to a 96-well plate pre-loaded with 1 µM $DiSC_3(5)$. The samples were incubated for an additional 5 minutes at 37 °C to promote dye interaction. Fluorescence intensity was then measured using a black polystyrene microtiter plate (Nunc, Thermo Scientific) on an Infinite 200 PRO microplate reader (Tecan, Switzerland), with measurements acquired at excitation and emission wavelengths of 622 nm and 670 nm, respectively (Ma *et al.*, 2017).

4.2.10. Assay of Ca^{2+}-Mg^{2+}-ATPase activity

The activity of Ca^{2+}-Mg^{2+}-dependent ATPase was measured using a modified colorimetric test. *S. aureus* was treated with o-pullulan at its MIC and incubated at different intervals (0, 6, 12, and 24 hours). At each allotted time, samples were taken, centrifuged, and resuspended in cold saline, followed by ultrasonic disruption (Cole-Parmer, USA). A 100 µg aliquot of the enzyme was then combined with the assay solution and incubated for 15 minutes at 37 °C. After incubation, a reagent combination including malachite green oxalate, ammonium molybdate, and sodium citrate was added, and the solution was further incubated for 30 minutes. Absorbance measurements were done at 660 nm using a Multiskan GO spectrophotometer (Thermo, USA), with each sample tested in triplicate (Bouchot *et al.*, 2001).

4.2.11. Biofilm inhibition and degradation assay

The biofilm experiment was done using 48-well polystyrene plates, using standard protocols. Each well was infected with 10 µL of a standardized *S. aureus* culture mixed with 300 µL of Mueller-Hinton Broth. To investigate the antibiofilm activity of o-pullulan, two experimental techniques were used: inhibiting the production of new biofilm and destroying pre-formed biofilm (Segev-Zarko *et al.*, 2015). In the inhibitory investigation, o-pullulan was administered at twice its MIC before biofilm formation and incubated for 24 hours. For biofilm

destruction, o-pullulan was administered after the biofilm had developed and likewise incubated for 24 hours. Controls were incubated at 37 °C for 48 hours without treatment. After incubation, wells were washed three times with 1X PBS to remove unattached bacteria, fixed with 100% methanol for 15 minutes, and then allowed to air dry. The adhering biofilm was dyed with 0.5% crystal violet for 5 minutes at room temperature. Excess stain was rinsed away, and the remaining color was solubilized using 33% acetic acid. The absorbance of the solubilized dye was measured at 590 nm using a microplate reader, with each condition examined in triplicate.

4.2.12. Inoculation of samples in simulated wound fluid (SWF)

The simulated wound fluid (SWF) was prepared according to recognized techniques (Bradford *et al.*, 2009). A 50 mL solution was made, containing 0.2922 g sodium chloride, 0.1684 g sodium bicarbonate, 0.0145 g potassium chloride, 0.01385 g calcium chloride, and 1.65 g bovine albumin, and was kept at 4 °C. Prior to usage, the SWF was equilibrated to room temperature for 1 hour. A standardized *S. aureus* inoculum (OD_{600} = 0.2) was then injected into 10 mL of SWF. To assess the antibacterial effectiveness, o-pullulan was delivered at its MIC to the infected SWF and incubated at 37 °C. Bacterial growth in both untreated control and o-pullulan-treated samples was examined at different time intervals by measuring OD_{600} using a spectrophotometer. The bactericidal action of o-pullulan was further validated by plating 10^6 dilutions of the bacterial inoculum on LB agar plates at comparable time periods.

4.2.13. In silico molecular docking study

This investigation includes developing the PDB (Protein Data Bank) format for o-pullulan using ChemSketch (Hunter, 1997) and SMILES notation, aided by the NCI/CADD Cactus SMILES translator (https://cactus.nci.nih.gov/services/translate/). Protein structures of *Staphylococcal* origin were collected from the Research Collaboratory for Structural Bioinformatics Protein Data Bank (RCSB PDB) (https://www.rcsb.org/pdb) (Berman *et al.*, 2000), DeepMind, and the AlphaFold Protein Structure Database at the European Bioinformatics Institute (EMBL-EBI) (Jumper *et al.*, 2021). These structures were constructed using PyMOL (PyMOL v2.5 - Incentive Product, Schrodinger, LLC). Docking simulations were done using AutoDock (AutoDock 4-Scripps Research, GNU) (Morris *et al.*, 2009), with o-pullulan functioning as the ligand targeting *Staphylococcal* cell wall-anchored (CWA) proteins. The docking findings were examined and modified using LigPlot (LIGPLOT-v2.2, EMBL-EBL) (Wallace *et al.*, 1995), PyMOL, and PLIP (Protein-Ligand Interaction Profiler). Binding interactions were analyzed based on the negative binding energy values and the type

of the ligand interactions to estimate binding affinities.

4.2.14. Synthesis of SpA domain peptides

The synthesis of the peptide sequence (H_2N-Asn-Lys-Phe-Gln-Lys-OH) was accomplished using a revised technique (Halder *et al.*, 2023). Fmoc-protected amino acids (3 equivalents) were linked to a solid-phase resin employing a reagent combination of HATU (2.85 equivalents) and DIEA (5.7 equivalents) in anhydrous DMF during a 4-hour period. Post-coupling, the Fmoc protecting groups were removed by treating the resin with 20% piperidine in DMF for 50 minutes at ambient temperature. The resin was then exposed to three washing cycles with DMF and DCM to eliminate any remaining unreacted chemicals. The final peptide was prepared by deprotecting the side chains and cleaving it from the resin using a cleavage mixture of TFA: TIS/EDT: water (95:2.5:2.5) for 3.5 hours at room temperature. The peptide was precipitated from cold diethyl ether, carefully washed, and then dried under vacuum. The isolated peptide was evaluated using mass spectrometry (XEVO G2-XS QTOF) for characterization.

4.2.15. Electroporation of antisense oligonucleotides (ASO) in *S. aureus*

S. aureus was grown in LB broth to an OD_{600} of around 0.8-0.9 as indicated in the literature (Thompson and Brown, 2021). The culture was collected by centrifugation at 5000 × g for 15 minutes at 4 ºC. The resulting pellet was washed twice with sterile ice-cold water, followed by additional centrifugation. Subsequently, the pellet was treated with ice-cold 10% glycerol, centrifuged at 4 ºC, and then resuspended in 10% glycerol. After a 15-minute incubation at 20 ºC, the pellet was again centrifuged to remove the supernatant. The final pellet was resuspended in ice-cold 10% glycerol, frozen in an isopropanol-dry ice bath, and maintained at -70 ºC for further use. To generate electrocompetent cells, the frozen pellet was thawed, incubated at room temperature for 20 minutes, and resuspended in EC buffer (0.5 M sucrose in 10% glycerol). After centrifugation at 5000 × g for 10 minutes, the cells were resuspended in EC buffer. A 2 µg aliquot of ASO targeting SpA was added, and the mixture was gently agitated before being put to a sterile 1 mm gap cuvette for electroporation utilizing parameters of C = 25 µF, PC = 100 ohm, and V = 2.9 kV (Gene Pulser Xcell). Immediately after electroporation, 1 mL of LB broth at 37 °C was added to the cuvette, mixed gently by pipetting, and transferred to a sterile tube. The cells were incubated at 37 °C for 2 hours, then plated on LB agar plates and treated with o-pullulan.

4.2.16. Fluorescence quenching analysis

The interaction between the SpA short peptide and o-pullulan was examined using a fluorescence quenching test. Phenylalanine fluorescence was evaluated at room temperature by combining o-pullulan with the short peptide at a concentration of 0.05% in a phosphate buffer (pH 7.4). The measurements were made using a Tecan multimode microplate reader. Emission spectra were obtained from 280 to 400 nm, with excitation at 280 nm. Given that o-pullulan displayed low fluorescence at this excitation wavelength, the fluorescence intensities of the SpA short peptide in the presence of o-pullulan were measured at different doses.

4.2.17. RNA extraction from *S. aureus* and gene analysis

RNA extraction from *S. aureus* was carried out using an improved phenol-based technique (Atshan *et al.*, 2012). Cells were originally removed from the culture by centrifugation at 8000 × g for 5 minutes at 4 °C. The pellet was then resuspended in 100 µL of nuclease-free water and subjected to vigorous vortexing for 3 minutes. Following this, 150 µL of a phenol-chloroform mixture (acid phenol) was added, and the solution was vortexed for 1 minute. The mixture was incubated at 70 °C for 30 minutes, with periodic vortexing every 5 minutes. After incubation, the solution was centrifuged at 12000 × g for 15 minutes, and about 100 µL of the upper aqueous phase was transferred to a new tube. To precipitate the RNA, 200 µL of ice-cold isopropanol was added, followed by vigorous vortexing for 3 minutes and centrifugation at 12000 × g for 10 minutes. The supernatant was collected, and the RNA pellet was washed with 200 µL of 70% ethanol before being centrifuged again at 8000 × g for 5 minutes. After allowing the pellet to air-dry for 3 minutes, it was resuspended in 15 µL of nuclease-free water. The RNA concentration was measured using a NanoDrop One/One Micro-volume UV-Vis spectrophotometer (Thermo Fisher Scientific, USA). Subsequently, cDNA synthesis was done on 300 ng of total RNA using the Super RT-MuLV kit, and PCR amplification was completed using a Veriti 96-well thermal cycler (Applied Biosystems).

4.2.18. Cytocompatibility study in eukaryotic cells

To investigate the toxic effects of o-pullulan to eukaryotic cells, the vitality of L929 cells (passage no. 2) was examined using the MTT cell proliferation assay, as previously reported (Bhavya *et al.*, 2022). In this approach, cells (1×10^4 cells/mL) were seeded onto a 96-well plate and left to adhere overnight. The cells were subsequently treated with the MIC amount of o-pullulan for 24 hours. Following the treatment, 10 µL of MTT solution (5 mg/mL) was transferred to each well and the corresponding plates were incubated for 4 hours. After incubation, the supernatants were removed and 100 µL of DMSO was added to each well to

dissolve the formazan crystals. The plates were incubated at 37 °C for 30 minutes, and cell viability was evaluated spectrophotometrically at 570 nm using a Multiskan GO plate reader (Thermo Scientific, USA). The percentage of cell viability was assessed, with the ability to survive of cells exposed just to the media (without treatment) defined as 100% (control).

Calcein AM and propidium iodide (PI) were utilized to distinguish viable from non-viable cells in L929 cultures, adhering to established methodologies (Bhavya *et al.*, 2022). Approximately 3 × 10^4 cells/mL were seeded into 48-well plates and allowed to adhere overnight. Following this, cells were treated with o-pullulan at its MIC concentration for 24 hours. After incubation, the media was carefully removed, cells were thoroughly washed with PBS, and subsequently stained with 1 mL of a dye solution containing 2 µM calcein AM and 4 µM ethidium homodimer-1 for 1 hour at 37 °C. Post-staining, the media was discarded, cells were rinsed with PBS, and fresh media was added. Fluorescence imaging was conducted using a Leica DMi8 microscope, employing fluorescein and rhodamine filters for calcein AM and ethidium homodimer-1, respectively.

For cytoskeletal staining, cells were washed with PBS, fixed with 3.7 % formaldehyde for 10 minutes, and rinsed again with PBS. Permeabilization was carried out using 0.2 % Triton X-100, followed by an additional PBS wash. The cells were then stained with Alexa Fluor 488 Phalloidin for 5-10 minutes at room temperature, and DAPI was used for nuclear staining. Excess stain was removed, cells were mounted on slides with DPX, and allowed to air dry. Microscopic imaging was performed using a Leica DMi8 microscope (Chazotte, 2010).

In this investigation, the intracellular levels of hydroxyl, peroxyl, and other ROS in L929 cells treated with o-pullulan were assessed using the cell-permeable chemical DCFDA (Bhavya *et al.*, 2022). After seeding 3 × 10^4 cells in 48-well plates and allowing for adhesion, the cells were treated to o-pullulan at its MIC concentration and incubated for 24 hours at 37 °C in a 5% CO_2 atmosphere. Hydrogen peroxide (0.01%) served as the positive control. Post incubation, cells were treated with 10 µM DCFDA solution, diluted in serum-free medium, and incubated for 45 minutes at 37 °C in the dark. Fluorescence was later quantified using optical interference filters designed for GFP detection (Ex = 460–495 nm, Em >510 nm) using a Leica DMi8 microscope.

4.2.19. Hemocompatibility test

The hemocompatibility of o-pullulan was investigated using fresh human blood. Red blood cells (RBCs) were extracted using centrifugation at 1500 rpm for 20 minutes, followed by three washes with PBS. The supernatant was discarded, and the RBC pellet was re-suspended in 1 mL of PBS, then further diluted with an additional 9 mL of PBS. An o-pullulan solution at a

concentration of 18.75 µg/mL was added to 1 mL of this diluted RBC sample and incubated at 37 °C for 4 hours. After incubation, the mixture was centrifuged at 10,000 rpm for 10 minutes. To test RBC lysis, 200 µL of the supernatant was collected and its absorbance was measured at 594 nm (Willcox *et al.*, 2008). PBS was employed as a negative control, whereas 1 % Triton-X served as the positive control. The proportion of haemolysis was estimated by comparing the OD_{594} of the sample with that of the positive control.

4.2.20. RNA extraction and gene analysis

The procedure described in section 3.2.9 was used.

4.2.21. Statistical analysis

Data were obtained from at least three separate experiments and values are presented as mean ± SD. The t-test was employed for comparison between two groups, and to compare more than two groups, one-way ANOVA (Analysis of Variance) was employed using GraphPad Prism 8 software. A value of *$P<0.05$*, **$P<0.01$*, ***$P<0.001$*, and *#$P<0.0001$* were considered significant difference and ns indicates non-significant difference.

4.3. Results

4.3.1. Synthesis and characterization of o-pullulan

In this study, we have synthesized oxidized pullulan (o-pullulan) by oxidizing the pullulan utilizing a described technique and also studied its use against wound-related infections. The periodate oxidation changes vicinal diol groups found at the C_2-C_3 region of the polysaccharide chain into di-aldehyde groups (**Fig. 4.1A**). The aldehyde concentration in o-pullulan was evaluated using hydroxylamine hydrochloride titration and presented in **Table D (Appendix)**. A larger concentration of $NaIO_4$ increases the oxidation of polymeric chains, boosting the aldehyde content in o-pullulan. This technique guarantees an adequate degree of post-oxidation while minimizing alkene toxicity (Bruneel and Schacht, 1993). Distinguishing the distinctive aldehyde peak in oxidized polysaccharides gets more challenging as the level of oxidation drops below 50%. For o-pullulan, with just 28% aldehyde content (3.462 mmol/g), any peak at 1728 cm^{-1} is likely to be weak and less conspicuous (**Fig. 4.1B**), making it tough to identify (Li *et al.*, 2011). The carboxyl content in o-pullulan was determined as 0.4% using the calcium acetate technique. When pullulan is oxidized using sodium meta-periodate, it forms iodide and iodate ions, byproducts which are infamous for their toxic effects, adding a layer of complication to

their usage in biomedical applications and known to elicit allergic responses and may injure host cells (Vermeulen *et al.*, 2010).

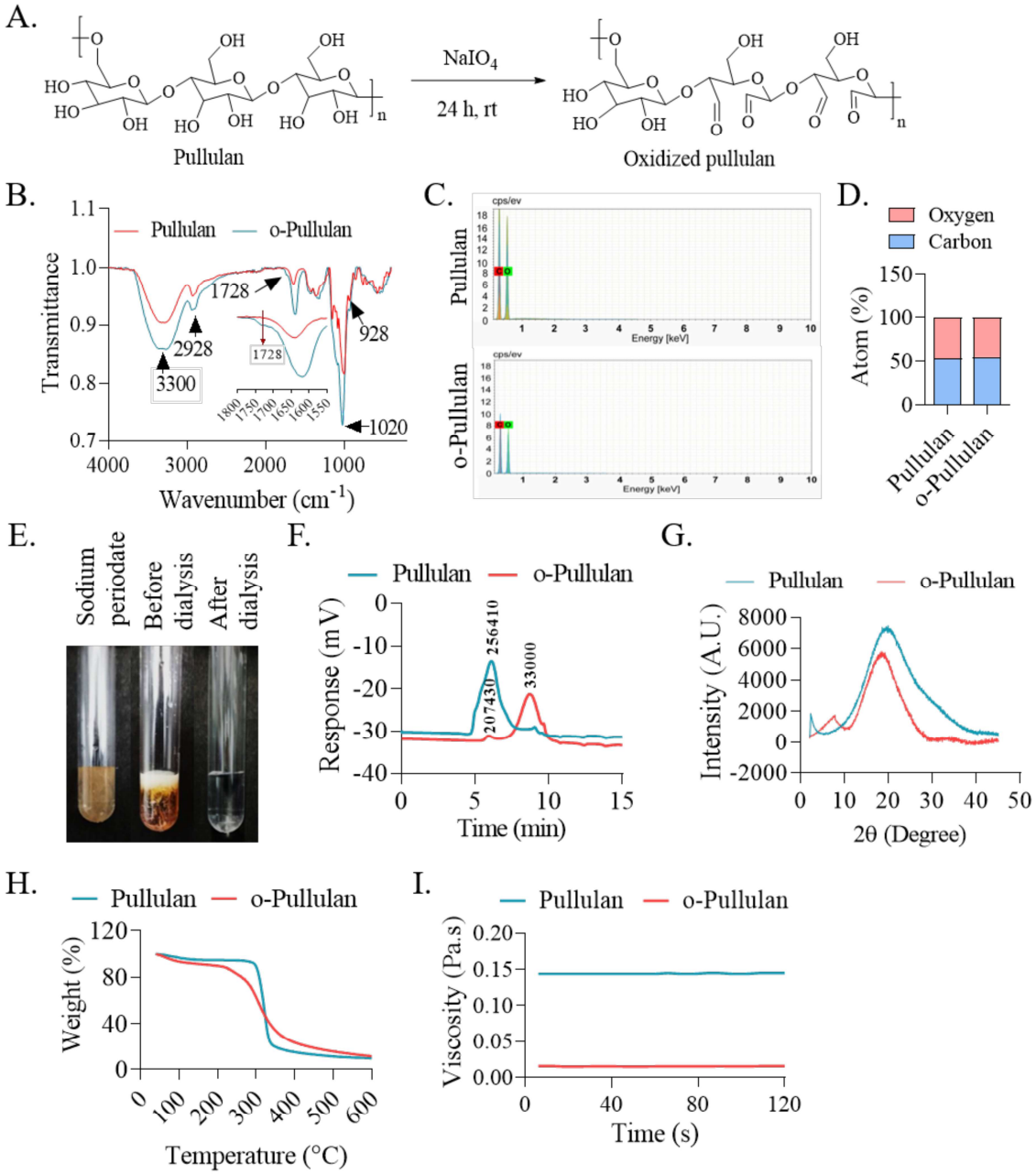

Figure 4.1. *Synthesis and characterization of oxidized pullulan (o-pullulan). (A) Oxidation of pullulan by sodium (meta)-periodate to form o-pullulan. (B) FT-IR spectra of pullulan and o- pullulan. (C) Energy dispersive X-ray (EDX) spectra of pullulan, and o-pullulan. (D) Elemental analysis by EDX. (E) Pictorial images of iodate ions containing solutions. Physical characterization of pullulan and o-pullulan by (F) GPC; (G) PXRD; (H) TGA; and (I) Viscosity analysis.*

To explore the occurrence of iodine byproducts, we employed EDX and halide ion assays. The EDX analysis established the atomic percentages of carbon and oxygen in the maltotriose

units of pullulan (C: 53.12%; O: 46.87%) and o-pullulan (C: 55.07%; O: 44.93%), therefore verifying the distinctive elemental makeup of polysaccharides and absence of iodine byproducts (**Fig. 4.1C, D**). During the halide ion test, the formation of a light brown precipitate in the sodium (meta)-periodate and o-pullulan solution prior to dialysis showed the existence of iodine byproducts. Conversely, the clear solution found after dialysis verified the successful elimination of these byproducts, suggesting the purification of the polymer solution (**Fig. 4.1E**).

Maltotriose units in pullulan, coupled by α-1, 6 linkages, provide it flexibility and a distinctive amorphous XRD characteristic. Periodate oxidation introduces aldehyde groups at C_2 and C_3, cleaving the glucopyranose ring and increasing flexibility, which compromises crystallinity. This oxidation changes the diffraction angle from 19.8 ° (pullulan) to 18.4 ° and 7.7 ° (o-pullulan), with the crystalline peak lowering from 59.29 ° to 33.94 ° (**Fig. 4.1G**). The increased peak at 7.7° implies shorter, more mobile chains owing to the changed structure (Kwaambwa *et al.*, 2007). Thermo-gravimetric analysis delivers information on changes in the mass of materials induced by temperature or time in a controlled way, and this analysis is important for analyzing the breakdown and oxidation process. **Fig. 4.1H** demonstrates the decline in the thermal stability of o-pullulan.

The thermal stability of o-pullulan, with an onset temperature (T_{onset}) of 216 °C, is drastically lowered compared to pullulan's 295 °C. This drop is related to the incorporation of reactive aldehyde groups into the polymer backbone. Additionally, o-pullulan demonstrates a substantial drop in viscosity to 0.01 Pa.s, in contrast to 0.14 Pa.s for pullulan (**Fig. 4.1I**). This decline is likely due to the oxidative cleavage of the glucopyranose ring and/or partial breakdown of glycosidic linkages (Rinaudo, 2010).

4.3.2. Evaluation of antibacterial activity of o-pullulan

The antibacterial activity of o-pullulan was evaluated against Gram-positive *S. aureus* and Gram-negative *P. aeruginosa*, demonstrating a unique pattern of action (**Fig. 4.2A**). Against *S. aureus*, o-pullulan displayed a clear dose-dependent bactericidal effect, but its impact on *P. aeruginosa* was more limited, demonstrating bacteriostatic activity with resistance at lower levels (**Table E, Appendix**). To explore further into its efficacy, the MIC and MBC were computed for both bacteria, presenting a fuller picture of o-pullulan's antibacterial capabilities (Andrews, 2001). The MIC and MBC values were found to be 18.75 µg/mL and 40.68 µg/mL against *S. aureus*, and 37.5 µg/mL and 300 µg/mL against *P. aeruginosa*, respectively. This highlights the bactericidal activity against *S. aureus* and bacteriostatic nature against *P. aeruginosa* of o-pullulan, with represents MBC/MIC ratios greater than 4 (Mogana *et al.*,

2020), which is likely due to the protective lipopolysaccharides in the outer membrane of Gram-negative bacteria.

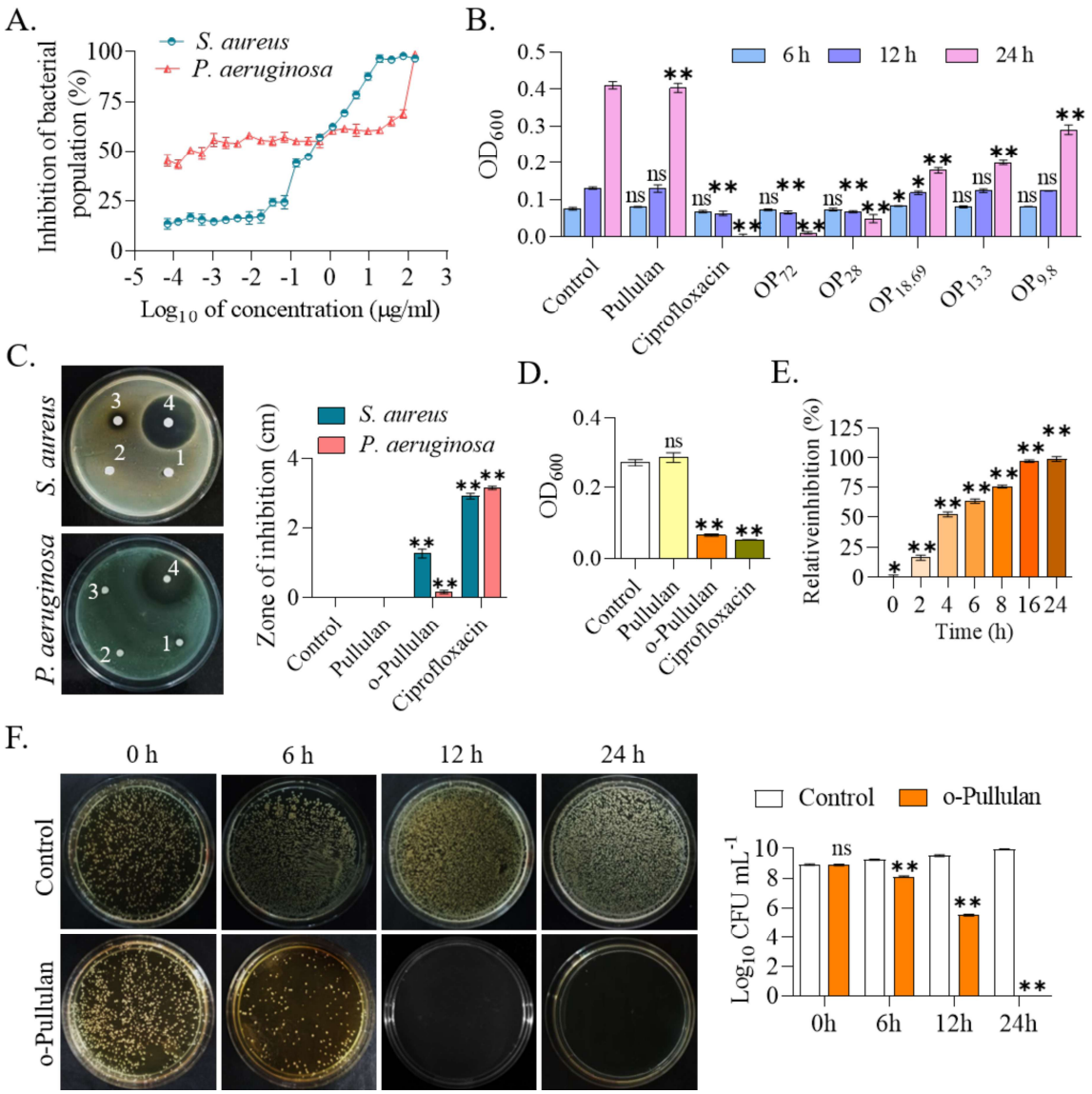

Figure 4.2. *Antibacterial property of o-pullulan. (A) Dose-dependent study of o-pullulan against S. aureus and P. aeruginosa to evaluate MIC and MBC. (B) Antibacterial activity of o-pullulan containing different degrees of aldehyde groups at different time points. (C) Disk diffusion study to check the susceptibility against S. aureus and P. aeruginosa: (1) Control, (2) Pullulan, (3) o-Pullulan, and (4) ciprofloxacin; and quantitative analysis. (D) Effect of pullulan, o-pullulan, and ciprofloxacin on*

To further investigate, *S. aureus* was exposed to o-pullulan with varying aldehyde content at the same MIC dose. As seen in **Fig. 4.2B**, altering the degree of $NaIO_4$-mediated oxidation influenced its antibacterial efficacy against *S. aureus*. Lower doses of $NaIO_4$ (174.5, 87.25, and 43.62 mg) mediated oxidation showed minimal antibacterial activity, and excessive aldehyde content can result in alkene toxicity within eukaryotic systems. Therefore, 349 mg of NaIO4

was optimized for pullulan oxidation to achieve the highest bactericidal efficiency with minimal alkene toxicity (LoPachin and Gavin, 2014).

S. aureus demonstrated extraordinary sensitivity to o-pullulan, with a clear 1.2 cm diameter inhibitory zone, suggesting significant bactericidal action. In contrast, pullulan revealed no similar impact in disk diffusion experiments (**Fig. 4.2C**). Additionally, bacterial growth measurements at 600 nm confirmed that o-pullulan exerted potent bactericidal effects, effectively eradicating the *S. aureus* population, similar to the antibiotic ciprofloxacin (**Fig. 4.2D**).

The time-dependent bactericidal activity of o-pullulan was strikingly evident. At its MIC dose, o-pullulan swiftly eradicated 50% of the *S. aureus* population within just 4 hours, with bacterial inhibition increasing steadily over time (**Fig. 4.2E**). After 24 hours of treatment, no visible *S. aureus* growth was observed in the culture media, a result further confirmed by plating the inoculum on LB agar plates. Remarkably, o-pullulan achieved a 70% reduction in the number of *S. aureus* colony-forming units (CFUs) within 6 hours, ultimately leading to complete inhibition after 24 hours (**Fig. 4.2F**).

4.3.3. Mechanisms of bactericidal activity

To delve into the bactericidal mechanism of o-pullulan, a fluorescence-based live/dead staining experiment was conducted. The membrane-compromising effects of o-pullulan were unmistakable, as evidenced by the heightened levels of propidium iodide (PI) staining in bacterial cells treated with o-pullulan, compared to those treated with pullulan after 12 hours of incubation (**Fig. 4.3A**). Further confirmation of o-pullulan's membrane-disrupting action against *S. aureus* came from HR-TEM analysis, which unveiled significant morphological alterations in the bacterial membrane. In the control group, untreated *S. aureus* exhibited intact membranes with smooth surfaces and no signs of distortion (**Fig. 4.3B**). However, upon treatment with o-pullulan, the bacterial outer layer appeared disrupted and the cells displayed noticeable morphological changes. These observations suggest that o-pullulan can breach the bacterial membrane, likely due to the presence of di-aldehyde groups, which are absent in pullulan, leading to its bactericidal effects.

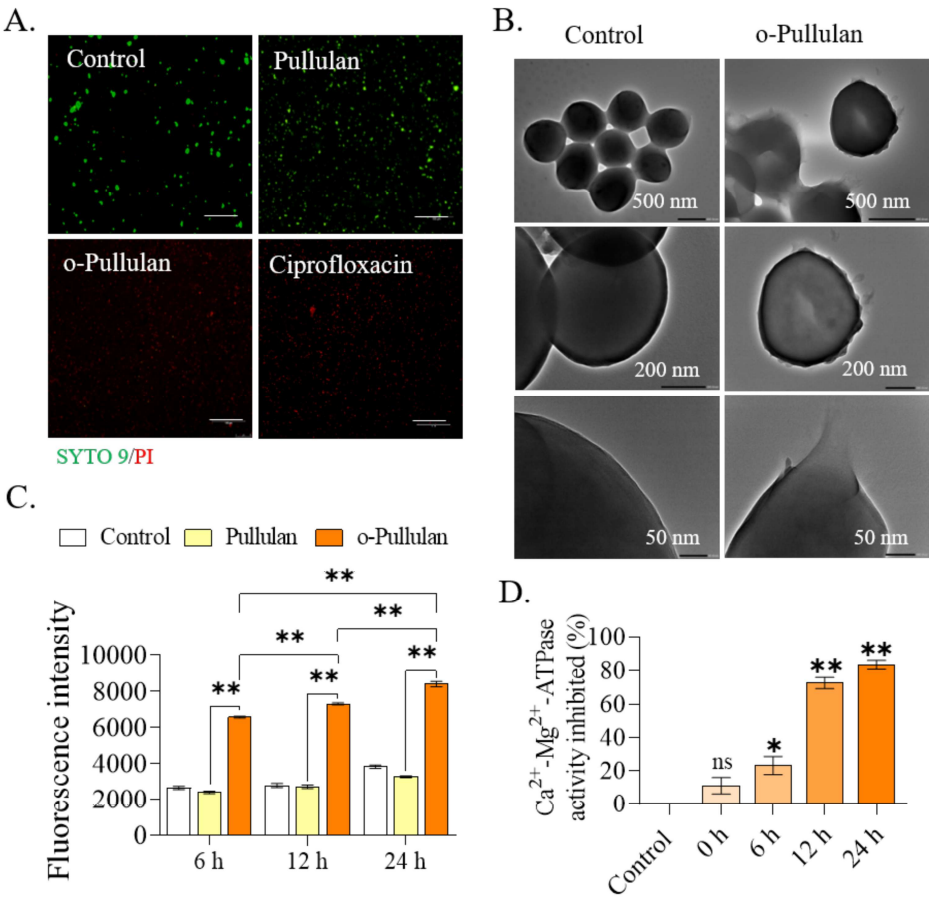

Figure 4.3. *The bactericidal activity of o-pullulan against S. aureus. (A) Live/dead staining of S. aureus in control (untreated) and treated (pullulan/ o-pullulan/ ciprofloxacin) samples. (Objective 10X, scale bar 100 µm) (n = 3). (B) HR-TEM images of S. aureus in untreated (control) and o-pullulan treated samples. (n = 3). (C) Measurement of membrane depolarization at different time points after o-pullulan treatment. (D) Percentage of Ca^{2+}-Mg^{2+}-ATPase activity inhibition in a time-dependent manner after o-pullulan treatment. Data are expressed as mean ± SD of three independent experiments, *p < 0.05; and **p < 0.01 were considered as significant difference (Student's t-test).*

Changes in membrane potential drive shifts in cellular shape and viability via modifying morphogenic proteins linked with the bacterial envelope. The membrane potential of *S. aureus* was evaluated using the lipophilic fluorescent dye $DiSC_3(5)$. Incubation with o-pullulan dramatically depolarized the lipid bilayer of *S. aureus*, resulting in a roughly three-fold increase in relative fluorescence intensity after 6 hours of treatment compared to both control and pullulan-treated samples (**Fig. 4.3C**). The hypothesized binding of o-pullulan to bacterial surface macromolecules could promote fast membrane depolarization, facilitating charge transfer and efficiently deconstructing the electrochemical barrier across the microbial cell surface. This disturbance is known to impact the location of multiple conserved proteins that govern cell division. Thus, the dissipation of membrane potential in *S. aureus* presumably

represents the mechanism by which o-pullulan exerts its deadly effects (Strahl and Hamoen, 2010).

Upon treatment with o-pullulan, Ca^{2+}-Mg^{2+}-ATPase activity was decreased by 23.26% at 6 hours, 72.68% at 12 hours, and 83.44% at 24 hours (**Fig. 4.3D**). This reduction inhibits the outward migration of stored intracellular calcium, leading to an osmotic imbalance, enhanced ROS generation, and consequent cell death. The Ca^{2+}-Mg^{2+}-ATPase, a crucial membrane-bound enzyme, is vital for regulating calcium transport and maintaining ionic homeostasis across the cell membrane. Depolarization of the membrane causes a fast input of calcium, further undermining cellular homeostasis (Carraro and Bernardi, 2016).

4.3.4. Molecular docking study of o-pullulan with bacterial membrane proteins

To explain the antibacterial action of o-pullulan, we undertook an in-silico molecular docking investigation targeting a range of bacterial cell-wall attached (CWA) proteins. These CWA proteins are important to the survival and pathogenicity of *S. aureus*. Therefore, effective targeting of these proteins could boost the antibacterial activity against *S. aureus*. Our study intended to provide thorough insights into how o-pullulan interacts with various CWA proteins of *S. aureus*, improving its potential as a therapeutic drug (Bubeck Wardenburg *et al.*, 2007). The proteins listed in **Tables F** and **G, (Appendix)** are extracted from PDB and AlphaFold protein structure database, respectively. Among the proteins analyzed, the Staphylococcal Protein A exceeding 100 °, supporting the presence of hydrogen bonds between o-pullulan and SpA (**Fig. 4.4A, B**).

A peptide matching to the B and C domains of the SpA protein— showing interactions with o-pullulan in the molecular docking study was produced and then examined by mass spectrometry for characterisation (**Fig. 4.4C**). The peptide was incubated with o-pullulan, and its interaction profile was assessed by fluorescence quenching tests. Initially, the SpA peptide sequence (0.01%) exhibited an emission peak at 320 nm. However, the addition of o-pullulan (0.05%) led to a large decline in emission intensity, hinting to a robust interaction between the peptide and o-pullulan (**Fig. 4.4D**). Furthermore, a concentration-dependent variation in emission intensity was found when the SpA peptide interacted with various quantities of o-pullulan. This experiment suggests a dose-dependent interaction between o-pullulan and the SpA peptide (**Fig. 4.4E**).

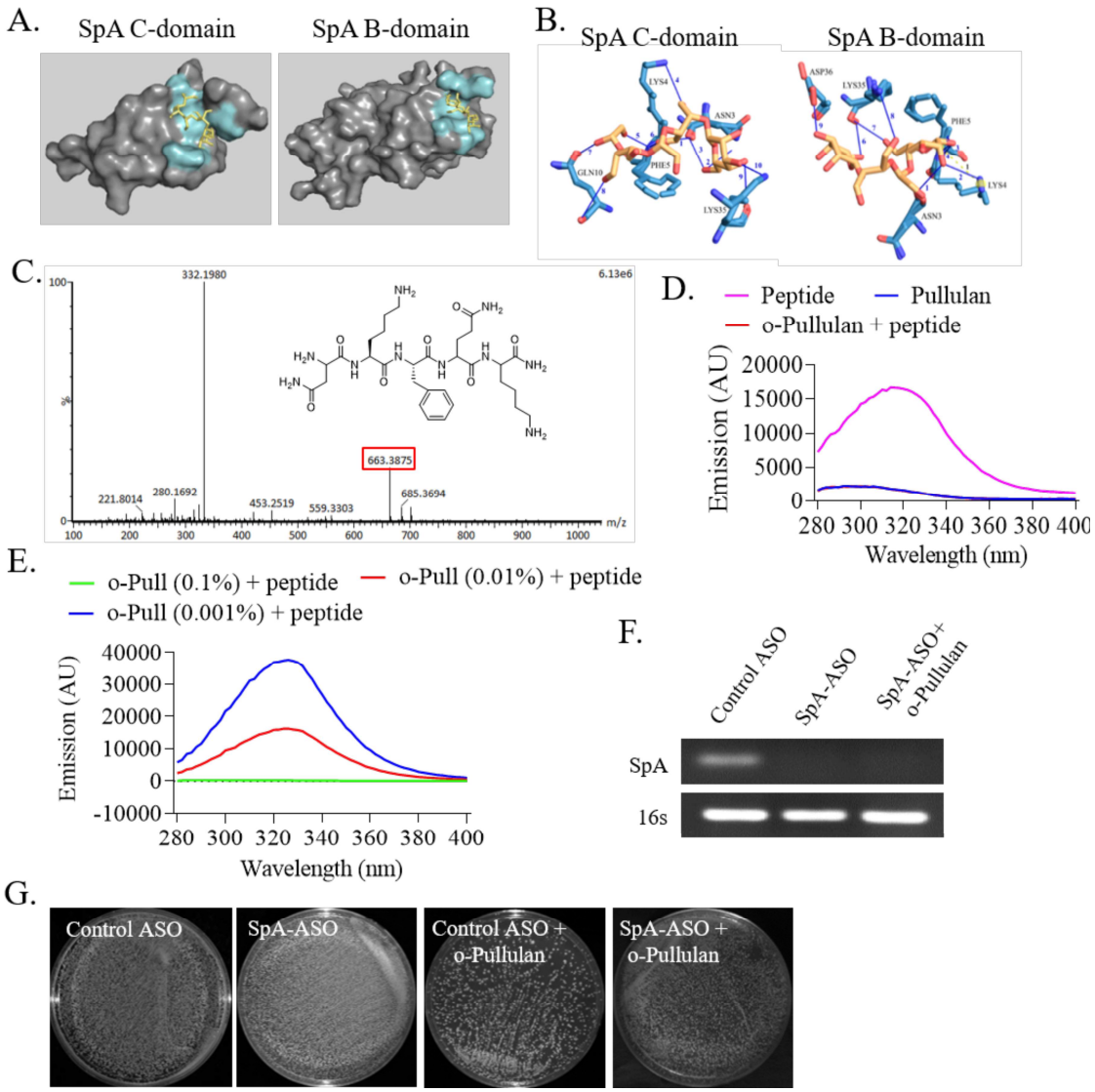

Figure 4.4. *Molecular docking of o-pullulan with Staphylococcal protein A. (A) Surface model of B-domain and C-domain of S. aureus protein-A (SpA) with o-pullulan. (B) Images representing the binding interaction of B-domain and C-domain of SpA with o-pullulan. (C) Mass spectrum of H_2N-Asn-Lys-Phe-Gln-Lys-OH. (D) Fluorescence quenching activity upon binding of SpA with o-pullulan. (E) A concentration-dependent alteration of emission intensity; (F) Gene expression profile of SpA upon silencing. (G) Alteration in o-pullulan binding affinity upon SpA silencing (SpA-ASO).*

To confirm the effect of o-pullulan upon SpA binding, firstly *S. aureus* was electroporated with antisense oligonucleotides (ASO) targeting the SpA gene, and the efficiency of knockdown was validated by PCR analysis (**Fig. 4.4F**). Following a 2-hour incubation with o-pullulan, the transformed *S. aureus* culture was plated on LB agar. Although SpA silencing (SpA-ASO) did not affect the transformed *S. aureus* survivability after 2 hours, the bactericidal activity of o- pullulan was substantially hindered in transformed *S. aureus* (**Fig. 4.4G**). These data reveal that o-pullulan exerts its antibacterial activity by targeting the SpA protein, leading

to collapse of the cell wall-associated membrane and resultant bacterial cell death. Further investigation is essential to properly define the mechanism by which o-pullulan interacts with SpA and induces the death of *S. aureus*.

4.3.5. O-pullulan have potent inhibition of biofilm formation

Bacterial biofilm generates a complex environment, where various bacterial cell colonies form permanent clusters that are particularly resistant to antibiotics and chemical treatments. This resistance sustains persistent infections that have major health, pharmacological, and industrial repercussions. Notably, tissue-associated biofilm infections are more likely among patients with chronic illnesses that disrupt the skin barrier (Sivaranjani et al., 2018). Destabilization of the membrane integrity is known to generate a detrimental influence on the bacterial population and hinder biofilm growth. Syto 9/PI staining reveals that o-pullulan greatly inhibited the formation of biofilm (**Fig. 4.5A**). Prior to biofilm formation, treating *S. aureus* with o-pullulan at twice its MIC for 24 hours resulted in a 60% decrease in biofilm formation capabilities (**Fig. 4.5B**). In contrast, adding o-pullulan to pre-established *S. aureus* biofilms had only a limited effect, suppressing the biofilm by only 18% (**Fig. 4.5C**). These data imply that o-pullulan is beneficial in reducing the development of *S. aureus* biofilms, possibly boosting its overall antibacterial activity against this pathogen.

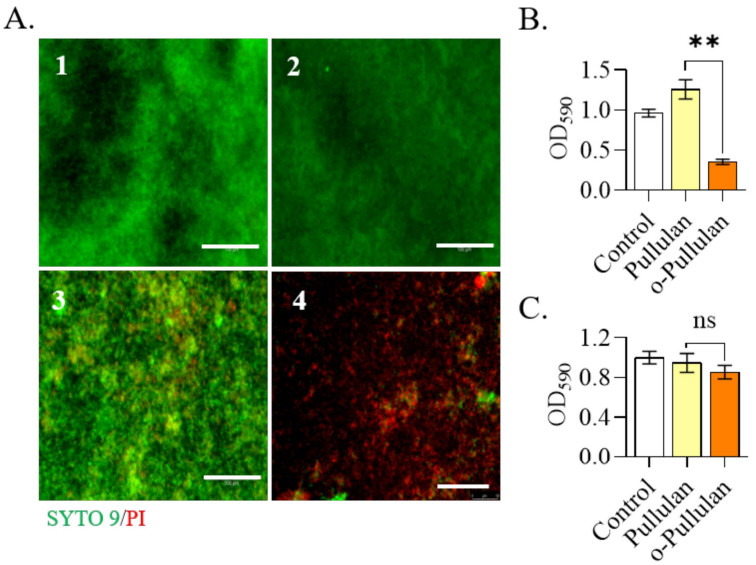

Figure 4.5. *Antibiofilm activity of o-pullulan against S. aureus. (A) Live/dead images of biofilm after SYTO9/PI staining in different conditions: (1) Untreated, (2) Pullulan-treated, (3) Established biofilm treated with o-pullulan, and (4) o-Pullulan-treated. (Objective 10X, scale bar 100 µm) (n = 3). (B) Inhibition of biofilm formation; and (C) Degradation of established biofilm. Data are expressed as mean ± SD from three independent experiments, #p<0.05; *p<0.01; and **p<0.001 were considered significant difference.*

4.3.6. Antimicrobial activity in simulated wound fluid (SWF)

The bactericidal activity of o-pullulan against *S. aureus* in SWF at several time periods were investigated, and findings suggested a considerable suppression of this bacterial growth following treatment with o-pullulan. It was confirmed by plating the treated inoculum in the LB agar plate at different time points after the treatment and counting the CFU/mL (**Fig. 4.6A** and **B**), which revealed about 50% CFU growth reduction at 6 h, while no viable change in growth curve was observed after incubation for 12 h and 24 h (**Fig. 4.6C**). These data imply that o-pullulan can prolong its bactericidal action in SWF for a longer duration.

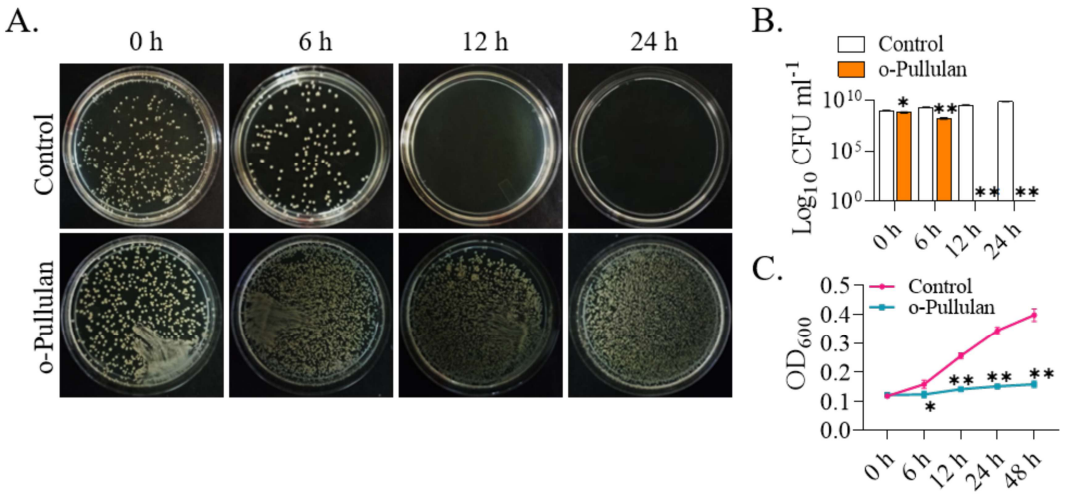

Figure 4.6. *Bactericidal activity of o-pullulan in simulated wound fluid (SWF) at different time points. (A) Images of S. aureus colony after treatment with o-pullulan in SWF, and (B) bacterial density expressed as log CFU ml^{-1} of S. aureus after 24 h of incubation with o-pullulan (lower panel); and (C) Effect of o-pullulan on S. aureus inoculated SWF. Data are presented as mean ± SD from three independent experiments, *p< 0.05; and **p< 0.01 were considered significant difference.*

4.3.7. Cytocompatibility assessments

To evaluate the cytotoxicity of o-pullulan on mammalian cells, an MTT assay was conducted using mouse fibroblasts (L929). The findings demonstrated that the MIC of o-pullulan did not induce significant cytotoxic effects (**Fig. 4.7A**), suggesting that o-pullulan is unlikely to adversely impact mammalian cells within the wound bed. To further establish the non-toxic nature of o-pullulan, L929 cells were treated with the MIC dosage of o-pullulan and stained with Calcein AM and PI. No substantial variation in cellular health was found in o-pullulan-treated cells as compared to the control (**Fig. 4.7B**). In addition to the metabolic activity and cell survival tests, we also examined the influence of o-pullulan on intracellular ROS formation. For this, control and o-pullulan treated L929 cells were stained with DCFDA,

however, no significant variation in intracellular ROS generation was identified in o-pullulan-treated cells as compared to the control one (**Fig. 4.7C**). To assess the cellular F-actin organization in response to o-pullulan treatment, L929 cells were stained with the phalloidin-FITC, a specific stain for F-actin. Fluorescence pictures of control and o-pullulan-treated L929 cells exhibited typical adhesion, natural form, and integrity of F-actin without any substantial modification of cytoskeleton structure (**Fig. 4.7D**). Nonetheless, a recent work (Zheng *et al.*, 2022) indicated that o-pullulan (OP@0.5) contained 3.73 ± 0.13 mmol/g aldehyde which shown high biocompatibility in mouse models without any major harm. In our investigation, we also observed that o-pullulan contains a smaller level of aldehyde (28% ~ 3.462 mmol/g). These studies suggest that the moderate aldehyde concentration in o-pullulan likely hinders its interaction with protein amino groups, thereby contributing to its little tissue toxicity. It is also plausible that the aldehyde groups in o-pullulan are either not sufficiently reactive to create lasting covalent adducts with proteins or that any such adducts are swiftly metabolized or eliminated from the body.

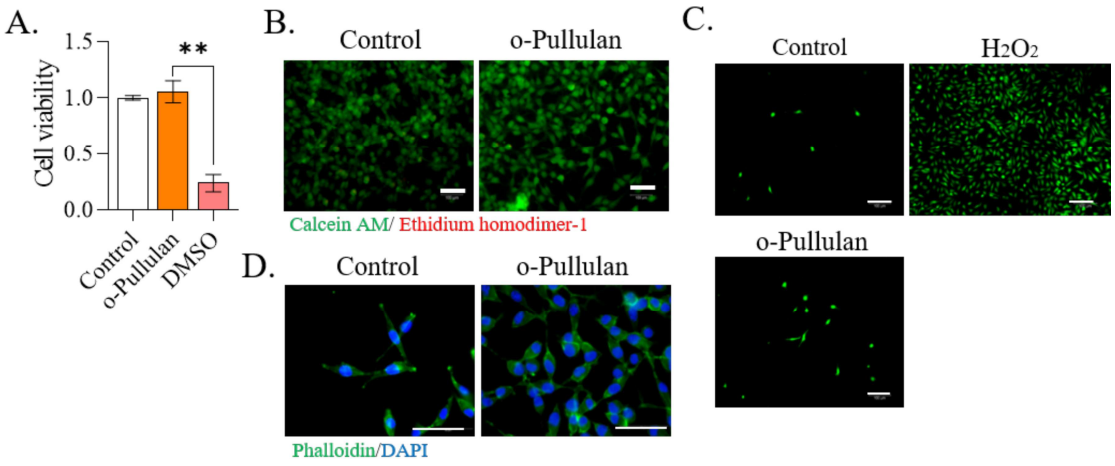

Figure 4.7. *Cytocompatibility of o-pullulan. (A) MTT assay using L929 cells. (B) Live/dead staining of L929 cells. (Objective 10X, scale bar 100 µm) (n = 3). (C) Images showing the intracellular ROS activity in L929 cell line treated with o-pullulan. H_2O_2 was used as a positive control for intracellular ROS production. (Objective 10X, scale bar 100 µm) (n = 3). (D) Cytoskeleton staining of untreated (control) and o-pullulan treated L929 cells. (Objective 63X, scale bar 50 µm) (n = 3). Data are presented as mean ± SD from three independent experiments, **p< 0.01 were considered significant difference.*

4.3.8. Immunotoxicity and Hemocompatibility assessment

Immunotoxicity examination of prospective medicinal compounds is an important part of understanding the inflammatory responses of immune cells against the test chemicals that could impede the safety and effectiveness profiles. Previous research established the immunotoxic

nature of certain substances that enhance cellular inflammation by upregulating the production of specific pro-inflammatory cytokines (Dobrovolskaia, 2015). To investigate the immunotoxicity of o-pullulan, RAW 264.7 murine macrophages were treated with o-pullulan (18.75 µg/mL) for 6 hours. Subsequently, RT-qPCR study was done to analyze the expression of numerous inflammatory marker genes. Treatment with o-pullulan did not substantially affect the expression of pro-inflammatory markers (*Tnf-α*, *Csf-1*, *Mcp-1*, *Tlr2*, *Ccl5*, *MhcII*, *Ifn-γ*, and *NF-κB*) or anti-inflammatory markers (*Arg-1*, and *Il-4*) compared to untreated macrophages, except for *Il-1β*, *Il-6*, and *iNos* (**Fig. 4.8A**). This shows that o-pullulan is likely non-immunotoxic.

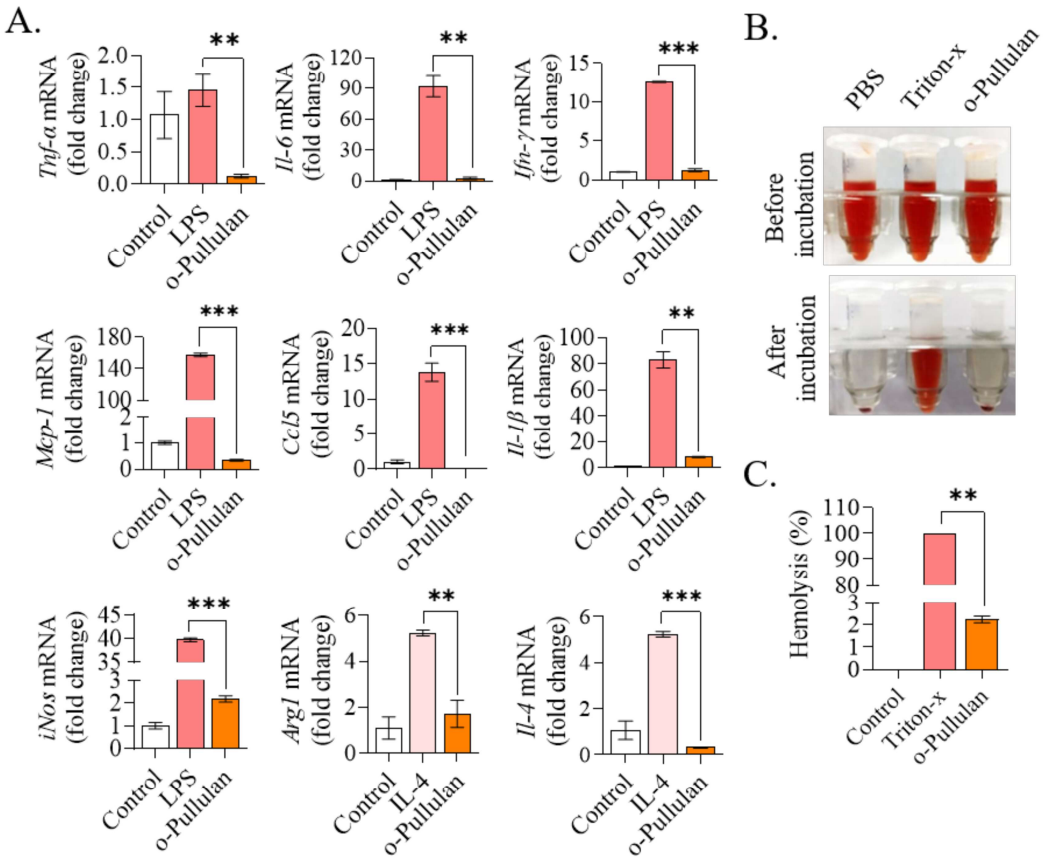

Figure 4.8. *Immunotoxicity and hemotoxicity of o-pullulan. (A) Expression profile of inflammatory markers in macrophages; (B) Images of haemolytic activity in different groups; and (C) Percentage haemolytic activity of o-pullulan. Data are presented as mean ± SD from three independent experiments, **p < 0.01; and ***p < 0.001 were considered as significant difference.*

We also performed the haemolysis experiment to evaluate the hemocompatibility of o-pullulan, as the red blood cells (RBCs) are known to supply information on the overall body reaction to biopolymers (Oostingh *et al.*, 2011). Incubation with o-pullulan did not cause any

modification in RBCs as compared to the control, although the treatment of RBCs with triton-X (positive control) created a brilliant crimson solution due to the whole RBC rupture (**Fig. 4.8B**, **C**). Thus, o-pullulan is hemocompatible and ideal for targeted site applications. The three key requirements for biomaterials are biocompatibility, biomechanics, and bioactivity. The inclusion of aldehyde groups in the polymer backbone of o-pullulan promotes cell adherence by generating Schiff base interactions with free amines in the glycoprotein network.

4.4. Discussion

In this study, we have fully examined and reported on the antibacterial properties of o-pullulan, especially against the wound-infecting pathogens *Staphylococcus aureus* and *Pseudomonas aeruginosa*. These properties were achieved via an oxidative change of the pullulan polymer chain, converting it into o-pullulan by a one-step oxidation method. This unique modification constitutes a huge success, as we have proved for the first time that o-pullulan not only affects the integrity of bacterial membranes but also hampers the functional activity of the SpA protein, which is anchored in the bacterial cell wall. These observations significantly validate our hypothesis that altering the molecular composition of pullulan into its oxidative form dramatically improves its antibacterial and anti-biofilm activity.

Further mechanistic studies revealed that the di-aldehyde groups present in oxidized pullulan (o-pullulan) play a pivotal role in establishing covalent linkages with unprotonated amines found on cell wall-associated proteins of bacteria. This binding interaction disrupts the functionality of membrane transport proteins and interferes with membrane-associated enzymatic systems, thereby impairing essential bacterial processes and exerting a strong antibacterial effect. These interactions not only hinder bacterial growth but also compromise the bacteria's ability to maintain structural integrity and function effectively, making o-pullulan a promising antimicrobial agent. Importantly, the biocompatibility profile of o-pullulan was extensively studied, demonstrating that it is cytocompatible, haemocompatible, and non-immunotoxic. These properties underscore its potential for safe and effective use in treating non-healing diabetic wound, particularly for preventing infections in open wounds and minimizing bacterial burden in chronic wounds.

Given its possible antibacterial characteristics and compatibility with biological systems, o-pullulan emerges as a strong prospect for application in wound care. It may be effectively blended with many types of dressing materials, such as gauze, gels, or creams, for medicine delivery and wound healing purposes. The ability of o-pullulan to not only prevent infection but also promote the wound healing process makes it a crucial addition to the field of advanced wound care.

References

AHMED, S. K., HUSSEIN, S., QURBANI, K., IBRAHIM, R. H., FAREEQ, A., MAHMOOD, K. A. & MOHAMED, M. G. 2024. Antimicrobial resistance: Impacts, challenges, and future prospects. *Journal of Medicine, Surgery, and Public Health,* 2**,** 100081.

AKIYOSHI, K., KOBAYASHI, S., SHICHIBE, S., MIX, D., BAUDYS, M., WAN KIM, S. & SUNAMOTO, J. 1998. Self-assembled hydrogel nanoparticle of cholesterol-bearing pullulan as a carrier of protein drugs: Complexation and stabilization of insulin. *Journal of Controlled Release,* 54**,** 313-320.

ANDREWS, J. M. 2001. Determination of minimum inhibitory concentrations. *Journal of Antimicrobial Chemotherapy,* 48**,** 5-16.

ATSHAN, S. S., SHAMSUDIN, M. N., LUNG, L. T., LING, K. H., SEKAWI, Z., PEI, C. P. & GHAZNAVI-RAD, E. 2012. Improved method for the isolation of RNA from bacteria refractory to disruption, including S. aureus producing biofilm. *Gene,* 494**,** 219-24.

BERMAN, H. M., WESTBROOK, J., FENG, Z., GILLILAND, G., BHAT, T. N., WEISSIG, H., SHINDYALOV, I. N. & BOURNE, P. E. 2000. The Protein Data Bank. *Nucleic Acids Res,* 28**,** 235-42.

BHAVYA, K., MANTIPALLY, M., ROY, S., ARORA, L., BADAVATH, V. N., GANGIREDDY, M., DASGUPTA, S., GUNDLA, R. & PAL, D. 2022. Novel imidazo[1,2-a]pyridine derivatives induce apoptosis and cell cycle arrest in non-small cell lung cancer by activating NADPH oxidase mediated oxidative stress. *Life Sciences,* 294**,** 120334.

BOUCHOT, A., JAILLET, J. D., BONHOMME, A., ALESSANDRO, N. P., LAQUERRIERE, P., KILIAN, L., BURLET, H., GOMEZ-MARIN, J. E., PLUOT, M., BONHOMME, P. & PINON, J. M. 2001. Detection and localization of a Ca2+-ATPase activity in Toxoplasma gondii. *Cell Struct Funct,* 26**,** 49-60.

BRADFORD, C., FREEMAN, R. & PERCIVAL, S. L. 2009. In vitro study of sustained antimicrobial activity of a new silver alginate dressing. *J Am Col Certif Wound Spec,* 1**,** 117-20.

BRUNEEL, D. & SCHACHT, E. 1993. Chemical modification of pullulan: 1. Periodate oxidation. *Polymer,* 34**,** 2628-2632.

BUBECK WARDENBURG, J., PATEL, R. J. & SCHNEEWIND, O. 2007. Surface proteins and exotoxins are required for the pathogenesis of Staphylococcus aureus pneumonia. *Infect Immun,* 75**,** 1040-4.

CAI, Z., VALLIS, K. A. & REILLY, R. M. 2009. Computational analysis of the number, area and density of gamma-H2AX foci in breast cancer cells exposed to (111)In-DTPA-hEGF or gamma-rays using Image-J software. *Int J Radiat Biol,* 85**,** 262-71.

CARRARO, M. & BERNARDI, P. 2016. Calcium and reactive oxygen species in regulation of the mitochondrial permeability transition and of programmed cell death in yeast. *Cell Calcium,* 60**,** 102-7.

CHAZOTTE, B. 2010. Labeling cytoskeletal F-actin with rhodamine phalloidin or fluorescein phalloidin for imaging. *Cold Spring Harb Protoc,* 2010**,** pdb.prot4947.

CHENG, K.-C., DEMIRCI, A. & CATCHMARK, J. M. 2011. Pullulan: biosynthesis, production, and applications. *Applied Microbiology and Biotechnology,* 92**,** 29-44.

DOBROVOLSKAIA, M. A. 2015. Pre-clinical immunotoxicity studies of nanotechnology-formulated drugs: Challenges, considerations and strategy. *J Control Release,* 220**,** 571-83.

GLIK, J., KAWECKI, M., GAŹDZIK, T. & NOWAK, M. 2012. The impact of the types of microorganisms isolated from blood and wounds on the results of treatment in burn patients with sepsis. *Pol Przegl Chir,* 84**,** 6-16.

HALDER, M., NARULA, M. & SINGH, Y. 2023. Supramolecular, Nanostructured Assembly of Antioxidant and Antibacterial Peptides Conjugated to Naproxen and Indomethacin for the Selective Inhibition of COX-2, Biofilm, and Inflammation in Chronic Wounds. *Bioconjug Chem*.

HASLAUER, K. E., HEMMLER, D., SCHMITT-KOPPLIN, P. & HEINZMANN, S. S. 2019. Guidelines for the Use of Deuterium Oxide (D(2)O) in (1)H NMR Metabolomics. *Anal Chem,* 91**,** 11063-11069.

HUNTER, A. D. 1997. ACD/ChemSketch 1.0 (freeware); ACD/ChemSketch 2.0 and its Tautomers, Dictionary, and 3D Plug-ins; ACD/HNMR 2.0; ACD/CNMR 2.0. *Journal of Chemical Education,* 74**,** 905.

JUMPER, J., EVANS, R., PRITZEL, A., GREEN, T., FIGURNOV, M., RONNEBERGER, O., TUNYASUVUNAKOOL, K., BATES, R., ŽÍDEK, A., POTAPENKO, A., BRIDGLAND, A., MEYER, C., KOHL, S. A. A., BALLARD, A. J., COWIE, A., ROMERA-PAREDES, B., NIKOLOV, S., JAIN, R., ADLER, J., BACK, T., PETERSEN, S., REIMAN, D., CLANCY, E., ZIELINSKI, M., STEINEGGER, M., PACHOLSKA, M., BERGHAMMER, T., BODENSTEIN, S., SILVER, D., VINYALS, O., SENIOR, A. W., KAVUKCUOGLU, K., KOHLI, P. & HASSABIS, D. 2021. Highly accurate protein structure prediction with AlphaFold. *Nature,* 596**,** 583-589.

KENAWY, E.-R., WORLEY, S. D. & BROUGHTON, R. 2007. The Chemistry and Applications of Antimicrobial Polymers: A State-of-the-Art Review. *Biomacromolecules,* 8**,** 1359-1384.

KUMAR, V. & YANG, T. 2002. HNO3/H3PO4–NANO2 mediated oxidation of cellulose — preparation and characterization of bioabsorbable oxidized celluloses in high yields and with different levels of oxidation. *Carbohydrate Polymers,* 48**,** 403-412.

KWAAMBWA, H. M., GOODWIN, J. W., HUGHES, R. W. & REYNOLDS, P. A. 2007. Viscosity, molecular weight and concentration relationships at 298K of low molecular weight cis-polyisoprene in a good solvent. *Colloids and Surfaces A: Physicochemical and Engineering Aspects,* 294**,** 14-19.

LI, H., WU, B., MU, C. & LIN, W. 2011. Concomitant degradation in periodate oxidation of carboxymethyl cellulose. *Carbohydrate Polymers,* 84**,** 881-886.

LOPACHIN, R. M. & GAVIN, T. 2014. Molecular Mechanisms of Aldehyde Toxicity: A Chemical Perspective. *Chemical Research in Toxicology,* 27**,** 1081-1091.

MA, W., ZHANG, D., LI, G., LIU, J., HE, G., ZHANG, P., YANG, L., ZHU, H., XU, N. & LIANG, S. 2017. Antibacterial mechanism of daptomycin antibiotic against Staphylococcus aureus based on a quantitative bacterial proteome analysis. *Journal of Proteomics,* 150**,** 242-251.

MANTECA, Á., FERNÁNDEZ, M. & SÁNCHEZ, J. 2005. A death round affecting a young compartmentalized mycelium precedes aerial mycelium dismantling in confluent surface cultures of Streptomyces antibioticus. *Microbiology (Reading),* 151**,** 3689-3697.

MOGANA, R., ADHIKARI, A., TZAR, M. N., RAMLIZA, R. & WIART, C. 2020. Antibacterial activities of the extracts, fractions and isolated compounds from Canarium patentinervium Miq. against bacterial clinical isolates. *BMC Complementary Medicine and Therapies,* 20**,** 55.

MORRIS, G. M., HUEY, R., LINDSTROM, W., SANNER, M. F., BELEW, R. K., GOODSELL, D. S. & OLSON, A. J. 2009. AutoDock4 and AutoDockTools4: Automated docking with selective receptor flexibility. *J Comput Chem,* 30**,** 2785-91.

OOSTINGH, G. J., CASALS, E., ITALIANI, P., COLOGNATO, R., STRITZINGER, R., PONTI, J., PFALLER, T., KOHL, Y., OOMS, D., FAVILLI, F., LEPPENS, H., LUCCHESI, D., ROSSI, F., NELISSEN, I., THIELECKE, H., PUNTES, V. F., DUSCHL, A. & BORASCHI, D. 2011. Problems and challenges in the development and validation of human cell-based assays to determine nanoparticle-induced immunomodulatory effects. *Part Fibre Toxicol,* 8**,** 8.

PUCA, V., MARULLI, R. Z., GRANDE, R., VITALE, I., NIRO, A., MOLINARO, G., PREZIOSO, S., MURARO, R. & DI GIOVANNI, P. 2021. Microbial Species Isolated from Infected Wounds and Antimicrobial Resistance Analysis: Data Emerging from a Three-Years Retrospective Study. *Antibiotics (Basel),* 10.

RINAUDO, M. 2010. Periodate Oxidation of Methylcellulose: Characterization and Properties of Oxidized Derivatives. *Polymers,* 2**,** 505-521.

SAM, S., JOSEPH, B. & THOMAS, S. 2023. Exploring the antimicrobial features of biomaterials for biomedical applications. *Results in Engineering,* 17**,** 100979.

SEGEV-ZARKO, L., SAAR-DOVER, R., BRUMFELD, V., MANGONI, M. L. & SHAI, Y. 2015. Mechanisms of biofilm inhibition and degradation by antimicrobial peptides. *Biochem J,* 468**,** 259-70.

SINGH, R. S., KAUR, N. & KENNEDY, J. F. 2015. Pullulan and pullulan derivatives as promising biomolecules for drug and gene targeting. *Carbohydrate Polymers,* 123**,** 190-207.

SINGH, R. S., KAUR, N., RANA, V. & KENNEDY, J. F. 2016. Recent insights on applications of pullulan in tissue engineering. *Carbohydrate Polymers,* 153**,** 455-462.

SIVARANJANI, M., SRINIVASAN, R., ARAVINDRAJA, C., KARUTHA PANDIAN, S. & VEERA RAVI, A. 2018. Inhibitory effect of α-mangostin on Acinetobacter baumannii biofilms - an in vitro study. *Biofouling,* 34**,** 579-593.

STRAHL, H. & HAMOEN, L. W. 2010. Membrane potential is important for bacterial cell division. *Proceedings of the National Academy of Sciences,* 107**,** 12281-12286.

TAMMA, P. D., AVDIC, E., LI, D. X., DZINTARS, K. & COSGROVE, S. E. 2017. Association of Adverse Events With Antibiotic Use in Hospitalized Patients. *JAMA Intern Med,* 177**,** 1308-1315.

THOMPSON, T. A. & BROWN, P. D. 2021. Small interfering RNAs targeting agrA and sarA attenuate pathogenesis of Staphylococcus aureus in Caenorhabditis elegans. *J Infect Dev Ctries,* 15**,** 1868-1875.

VERMEULEN, H., WESTERBOS, S. J. & UBBINK, D. T. 2010. Benefit and harm of iodine in wound care: a systematic review. *Journal of Hospital Infection,* 76**,** 191-199.

WALLACE, A. C., LASKOWSKI, R. A. & THORNTON, J. M. 1995. LIGPLOT: a program to generate schematic diagrams of protein-ligand interactions. *Protein Eng,* 8**,** 127-34.

WIEGAND, I., HILPERT, K. & HANCOCK, R. E. W. 2008. Agar and broth dilution methods to determine the minimal inhibitory concentration (MIC) of antimicrobial substances. *Nature Protocols,* 3**,** 163-175.

WILLARD, H. H. & THOMPSON, J. J. 1934. Qualitative Tests for Periodate and Iodate in the Presence of Each Other1. *Journal of the American Chemical Society,* 56**,** 1827-1828.

WILLCOX, M. D., HUME, E. B., ALIWARGA, Y., KUMAR, N. & COLE, N. 2008. A novel cationic-peptide coating for the prevention of microbial colonization on contact lenses. *J Appl Microbiol,* 105**,** 1817-25.

ZHANG, W., ZHANG, X., ZOU, K., XIE, J., ZHAO, S., LIU, J., LIU, H., WANG, J. & WANG, Y. 2017. Seabuckthorn berry polysaccharide protects against carbon tetrachloride-induced hepatotoxicity in mice via anti-oxidative and anti-inflammatory activities. *Food & Function,* 8**,** 3130-3138.

ZHAO, H. & HEINDEL, N. D. 1991. Determination of degree of substitution of formyl groups in polyaldehyde dextran by the hydroxylamine hydrochloride method. *Pharm Res,* 8**,** 400-2.

ZHENG, W., ZHANG, Z., LI, Y., WANG, L., FU, F., DIAO, H. & LIU, X. 2022. A novel pullulan oxidation approach to preparing a shape memory sponge with rapid reaction capability for massive hemorrhage. *Chemical Engineering Journal,* 447**,** 137482.

Chapter 5

Development of cost-effective hydrogel to deliver *Zeb2* ASO efficiently to treat the chronic diabetic wound

5.1. Background

Wound healing, from a physiological perspective, is a finely tuned series of interconnected biological events. However, this harmony is disrupted in chronic non-healing wounds due to activation of various complex cellular interactions governed by regulatory pathways and signalling networks (Sun et al., 2014, Wong et al., 2015). Both patients' and society's quality of life are profoundly affected by the therapeutic care of chronic wounds (Haagsma et al., 2016). Bacterial infections may impede the healing process of cutaneous wounds because the skin's protective barrier is damaged. In the setting of diabetic wounds, this vulnerability is worsened by prolonged hyperglycemia, which encourages bacterial invasion and disrupts the intracellular redox balance, leading to ongoing inflammation at the wound site (Liu et al., 2020). In diabetes situations, the high blood sugar environment skews macrophages towards the M1 type, increasing inflammation and leading to tissue damage and overall organ malfunction (Tsalamandris et al., 2019).

Although antibiotics and anti-inflammatory medicines are often used in the treatment of diabetic wounds, there is a growing challenge over the drug resistance and the occurrence of side effects (Selva Olid et al., 2015). In this context, hydrogels provide a flexible and adaptable alternative. These substances not only reduce bacterial and inflammatory problems, but also allow for the accurate and slow and sustained release of drug, promoting improved tissue healing and regrowth (Olteanu et al., 2024). The three-dimensional geometry and high-water content of hydrogels make them a perfect vehicle for the controlled release of antibiotics (Li et al., 2018), antioxidants (Zhao et al., 2020), and cytokines (Chen et al., 2018), all to promote skin regeneration. Polysaccharides such as chitosan, hyaluronic acid, pullulan, and alginate are emerging as top contenders for hydrogel wound dressings, due to their remarkable biocompatibility, natural degradability, and specialized biological properties (Sun et al., 2022).

The use of chitosan and its byproducts is on the rise in the fields of tissue engineering and regenerative medicine due to its potent anti-bacterial activity, ability to improve functional recovery via axonal regeneration, and inflammation reduction (Wang et al., 2018). Being non-toxic, non-immunogenic, non-carcinogenic, pullulan and its derivatives are widely used as molecular chaperones, drug delivery agents, and vaccinations (Singh et al., 2017). Additionally, the anti-oxidant property of pullulan enhances the effectiveness of biomedical applications including infectious biology infectious biology (Silva et al., 2018).

Extensive research and clinical findings demonstrated that polysaccharide-based composite hydrogel dressings offer superior protection and foster more rapid and effective tissue regeneration by accelerating wound healing, reducing scarring, and alleviating pain, thus, making them a safe and highly effective treatment option (Sun et al., 2022). Traditional wound dressing does not provide enough moisture for wound healing and protection against bacterial contamination (Blacklow et al., 2019). Furthermore, freshly repaired tissues are often injured during their removal. There remains significant untapped potential in advancing wound care by targeting "micro" factors, including cellular behavior, protein signaling, and peptide regulation— dimensions that are frequently overshadowed by the predominant focus on "macro" aspects like moisture retention and pressure control in existing commercial treatments. Therefore, gene silencing techniques offer significant potential for overcoming chronic wound healing issues, particularly using locked nucleic acid (LNA) and modified ASOs (Wahlestedt et al., 2000). These ASOs, with their DNA core and modified nucleotides, inhibit protein synthesis by either RNAse H1-mediated mRNA degradation or blocking the translational machinery (Dias and Stein, 2002). Enhanced by LNAs and phosphorothioate backbones, they exhibit increased stability and resistance to degradation, while their reduced size facilitates cellular uptake through “gymnosis” (Stein et al., 2010, Hagedorn et al., 2018, Crooke et al., 2017).

5.1.1. Challenges

Numerous fundamental problems prevent hydrogel-based gene delivery from being widely used for chronic diabetic wounds. In diabetic wounds, decreased cellular activity and altered membrane dynamics restrict gene transfection, but inflammation and oxidative stress degrade therapeutic genes, vectors, and hydrogels. High wound exudates, protease activity, and off-target effects, all limit extended and concentrated administration. Compatibility between hydrogels and vectors complicates matters, necessitating vector protection while maintaining controlled release. Biocompatibility remains an issue, as hydrogels and vectors can cause

immunological reactions or harm, particularly in immune-sensitive people. Mechanical and physiological issues, such as maintaining structural integrity, reacting to fluctuating glucose levels, and insufficient vascularization, further restrict deployment. The stability of therapeutic payloads within hydrogels is critical to minimizing deterioration, and designing scalable, cost-effective systems of consistent quality is challenging.

To address these challenges, we proposed the design of a multifunctional hydrogel system composed of oxidized pullulan and quaternized chitosan, endowed with intrinsic antioxidant and antibacterial properties. This system will be further enhanced by the incorporation of Zeb2 ASO, encapsulated using invivofectamine, to assess its therapeutic efficacy in promoting wound healing in a chronic diabetic wound model.

5.1.2. Objectives

In this investigation, our aim is –

- To prepare and characterize a multifunctional hydrogel system to incorporate *Zeb2* ASO, encapsulated using invivofectamine for sustain release.
- To study the efficacy of *Zeb2* ASO incorporated hydrogel in restricting macrophage inflammation.
- To assess the therapeutic potential of *Zeb2* ASO incorporated hydrogel in diabetic wound healing.

5.2. Materials and Methods

5.2.1. Materials

Pullulan was purchased from TCI Chemicals, India; GTMAC (glycidyltrimethylammonium chloride) (#50053), sodium (meta) periodate (#S1878), DCFDA (2′,7′-ichlorodihydrofluorescein diacetate) (#287810), tween-20 (#P2287), ethylene glycol (#1265515), CTAB (cetyltrimethylammonium bromide) (#H6269), PVP (polyvinylpyrrolidone) (#P5288), chloroform, isoamyl alcohol (#C0549) were procured from Sigma-Aldrich, USA; Tris base (#TC072), chitosan (#TC242), Luria Bertani broth (#G557), Luria Bertani agar (#SM557D), ciprofloxacin (#SD060A), doxorubicin hydrochloride (#TC4200), BSA (Bovine Serum Albumin) (#TC545), and MTT (3-(4,5-dimethylthiazol-2-yl)-2,5- diphenyltetrazolium bromide) (#MB186) reagents were procured from HiMedia, India. Glycine (#1610718), Immun-Blot® PVDF Membrane (#1620177), Precision Plus Protein Dual Color Standards (#1610374EDU), Clarity Western ECL Substrate (#1705061), and iScript™

cDNA Synthesis Kit (#1708890) were purchased from Bio-Rad Laboratories (Hercules, CA, USA). LIVE/DEAD Viability/ Cytotoxicity Kit (#L3224), Invivofectamine™ 3.0 Reagent (#IVF3001), Pierce BCA Protein Assay Kit (#A65453) and Halt Protease and Phosphatase Inhibitor Cocktail (#78442) and Trizol reagent (#15596026) were acquired from Invitrogen, USA. Sodium chloride (#41721), sodium bicarbonate (#45437), potassium chloride (#38630), calcium chloride (#97080) was acquired from SRL, India. PowerUp SYBR Green Master Mix (#A25742) was procured from Applied Biosystems, Thermo Fisher Scientific. VECTASHIELD Antifade Mounting Medium with DAPI (#H-1200-10) was procured from Vector Laboratories (Burlingame, CA). All tissue culture materials were procured from Life Technologies/Gibco, and Nunc, Grand Island, NY; and Corning, NY. Description of all the antibodies including catalog numbers, and the dilutions used in different experiments were given in **Table A (Appendix).** Different gene-specific primers, *Control* ASO and *Zeb2* ASO were designed and bought from Integrated DNA Technologies, India presented in **Table B (Appendix)**.

5.2.2. Synthesis and characterization of oxidized pullulan and quaternized chitosan

Pullulan was oxidized and characterized following a previously published method (Roy et al., 2023) and characterized by the FT-IR. The degree of oxidization was determined by hydroxylamine hydrochloride titration method.

Chitosan was subjected to quaternization through a reaction with GTMAC, following a previously established protocol with slight modifications (Rwei et al., 2014). The initial step involved dissolving 0.138 g of chitosan in 10 mL of deionized water that contained 0.5% acetic acid. The chitosan solution was then meticulously mixed with 0.34 mL of GTMAC in a nitrogen environment and heated to 50 °C for 18 hours. After the reaction was complete, the product was precipitated by pouring the mixture into cold acetone. After removing any unreacted GTMAC from the resultant solid by washing it with methanol, the product was dried in a vacuum oven for 6 hours. The end product, quaternized-chitosan, is a white powder that was characterized using Fourier transform infrared spectroscopy. Using a trinitrobenzenesulfonic acid titration experiment, the level of quaternization was determined.

5.2.3. Development and physical characterization of o-Pullulan-q-Chitosan hydrogels

The o-pullulan-q-chitosan (OP@QC) hydrogel was seamlessly crafted by blending oxidized pullulan and quaternized chitosan in aqueous solution at various mass ratios. Gelation occurred swiftly within 15 minutes at 37 °C with gentle vortexing. Rheological properties were

characterized using an Anton Paar Rheometer (MCR 101), with hydrogel samples placed between parallel plates separated by a 0.5 mm gap. Measurements of the elasticity modulus (G') and viscosity modulus (G") were performed through a frequency sweep from 0.01 to 100 rad/s at 1% strain, and amplitude sweep from 0.1% to 1000% strain at 37 °C to determine the linear viscoelastic range (LVE) for hydrogels.

To assess the hydrogel's degradation profile, a swelling and degradation study was conducted. Post-fabrication, the hydrogel's initial weight was recorded. The hydrogel was then immersed in PBS and incubated at 37 °C with stirring at 120 rpm for various time intervals. At each specified time, the buffer was discarded, and the hydrogel was weighed again. Weight gain indicated swelling, while weight loss indicated degradation. The results were expressed as a percentage of swelling, calculated using the following equation:

$$\text{Swelling ratio (\%)} = ((W_s - W_0)/ W_0)100$$

W_s is the weight of swollen hydrogel at time t and W_0 is the initial weight.

5.2.4. Doxorubicin release profile

Doxorubicin (1 mg/mL) was incorporated into the oxidized pullulan before hydrogel formation. The hydrogels were incubated for 30 minutes to facilitate complete crosslinking, then placed in a vial with PBS and maintained at 37 °C with stirring at 120 rpm. At specified intervals, aliquots were withdrawn and replaced with an equal volume of fresh PBS. The release of doxorubicin from the hydrogel was quantified using fluorescence spectroscopy, measuring absorbance at 560 nm.

5.2.5. Bacterial and mammalian cell culture

In this work, *P. aeruginosa* (strain 10620) and *S. aureus* (strain 7443) were chosen for investigation. These bacterial strains were collected from the Microbial Type Culture Collection (MTCC) at CSIR- IMTECH, Chandigarh, India. Prior to usage, the strains were pre-cultured in Luria Broth (LB) medium at 37 °C for 48 hours. After incubation, the cultures were adjusted to a concentration of 10^8 cells/mL in line with the 0.5 McFarland standard.

Two murine cell lines, normal fibroblasts (L929) and macrophages (RAW 264.7), were acquired from the NCCS in Pune, India. The L929 cells were cultivated in RPMI-1640, whereas the RAW 264.7 cells were grown in DMEM, both supplemented with 10% FBS and 1% penicillin-streptomycin. The cultures were kept in a humidified incubator set at 37 °C with 5% CO_2 and 95 % humidity to guarantee optimum growth conditions.

5.2.6. *In vitro* antibacterial activity

The antimicrobial activity of the hydrogel was evaluated against *S. aureus* and *P. aeruginosa* (Roy et al., 2023). Bacteria were cultured at 37 °C for 24 hours and standardized using the McFarland method. Subsequently, the bacterial suspensions were exposed to 100 µL of oxidized pullulan and quaternized chitosan-based hydrogel (OP@QC) at 37 °C with continuous shaking at 120 rpm. At various time points, aliquots of the bacterial solution (diluted 10^6 times) were plated onto LB agar to assess the antibacterial activity by counting colony-forming units after 24 hours. Additionally, bacterial growth was monitored by measuring the optical density at 600 nm after 24 hours of incubation with the hydrogel.

Syto9/ PI staining was implemented by LIVE/DEAD™ BacLight™ Bacterial Viability Kit (Invitrogen), to determine the ability of OP@QC hydrogel to destroy the membranes of these bacteria. The detailed procedure described earlier in section 4.2.7.

Anti-biofilm activity was assessed by culturing *S. aureus* and *P. aeruginosa* bacteria with the OP@QC hydrogel followed by incubation in static condition at 37 °C for 48 hours. The detailed procedure described earlier in section 4.2.11.

5.2.7. Cytocompatibility evaluation of hydrogel

Cytotoxicity of hydrogel was evaluated on the murine L929 cells by MTT, live/dead assay, and ROS activity assessment (Roy et al., 2023). Cells were seeded in 96-well plates at a density of approximately 1×10^4 cells/ well and cultured in 200 µL of DMEM supplemented with 10% (v/v) fetal bovine serum (FBS) at 37 °C for 24 hours under a humidified atmosphere with 5% CO_2. The detailed procedure described earlier in section 4.4.18. After the OP@QC hydrogel was fabricated in a 96-well plate, 5×10^3 cells per well were seeded onto the hydrogel and cultured in 150 µL of DMEM supplemented with 10% (v/v) fetal bovine serum (FBS) at 37 °C under a humidified atmosphere of 5% CO_2 for 24 hours. Following the incubation period, the medium was removed, and the cells were stained with calcein-AM (2 µM) and propidium iodide (4.5 µM). After 1 hour of incubation, images were captured from different areas using a Zeiss Axioscope, which allowed the visualization of cell viability and morphology.

Macrophage polarization upon incubation with OP@QC hydrogel was evaluated using RAW264.7 cells by assessing the expression of inflammatory genes. Cells were seeded on the hydrogel at a density of 0.1×10^6 cells and cultured for 24 hours. A separate set of cells was treated with 1 µg/mL of LPS as a positive control to compare the inflammatory response and

potential macrophage polarization. Following incubation, the cells were collected and processed for gene expression profile.

5.2.8. ASO encapsulation in OP@QC

Control ASO (*Con* ASO) and *Zeb2* ASO were used to incorporate into the OP@QC hydrogel after encapsulating by invivofectamine. Total 5 μM of ASO was properly mixed with the invivofectamine following the manufacturer's protocol. Then the solution was mixed with 50 μL of 10% OP solution and incubate for 5 minutes at room temperature in 2 mL of micro-centrifuge tube. After that 50 μL of 1% QC solution was added to the ASO mixed OP solution and briefly vortexed. The mixture was incubated for 15 minutes at room temperature for the perfect gelation.

5.2.9. *In vitro* ASO releasing profile from OP@QC

To check the releasing activity of ASO from the hydrogel system, *Con* ASO and *Zeb2* ASO encapsulated OP@QC was fabricated in the 48 well plate at the volume of 100 μL. After the gel formation 0.1 $\times 10^6$ RAW264.7 cells were seeded on the ASO encapsulated hydrogel system upon addition of 1 ml of culture medium and incubate for different time period. Following incubation, the cells were harvested following the published methodology (Garcia et al., 2019). Briefly the procedure carried out by at 37 °C for 20 min using 0.25% (w/v) trypsin, followed by filtration through 0.22 μm filters to remove hydrogel debris. After that cells were washed with PBS and cultured for 48 hours. After that cells were collected and processed for gene expression analysis.

5.2.10. Mice models and treatments

The animal facility at IISER Mohali was contacted to get male mice of the wild-type C57BL/6J strain. The mice were four to five weeks old and weighed 18-22 g. The NIPER Mohali animal housing facility provided a regulated environment for the subjects. A 12-hour/night cycle was part of it, as was a temperature range of 23–26 °C and a relative humidity of 55% and fed with normal pellet diet (standard diet, SD) and water *ad libitum*. SD mice were randomly divided into two groups (n = 5 in each group) and subjected to 6.00 mm of rostral excisional wound following the published protocol (Fischer et al., 2023). One group of mice received OP@QC hydrogel to check the any alterations in wound healing phenomena after hydrogel application. After certain days interval wound images were capture in all groups of mice. Mice were then sacrificed, wound bed tissues were collected, and processed for further

experimental studies. Immediately after collection, tissues were snap frozen in OCT (Leica Biosystems) for cryo-sectioning. All animal experiments were performed following the guidelines prescribed by and with the approval of the Institutional Animal Ethics Committee (IAEC), NIPER, Mohali, Punjab (Project no.: IAEC/22/37-M).

To evaluate the *Zeb2* ASO efficacy, STZ induced HFD diabetic mice wound model was developed by full-thickness skin wounds with a diameter of 6 mm which were created on the backs of these STZ-HFD mice with biopsy punch needle (Rowland et al., 2023). Detailed procedure described earlier in section 3.4.2. One group of STZ-induced HFD mice received with *Con* ASO and another group with *Zeb2* ASO incorporated OP@QC at the total volume of 100 µL hydrogel/ wound for 3 days. At different time interval, wound images were capture in all groups of mice and the closure area was measured through Image-J analysis. Mice were then sacrificed on day 3, day 7 and day 10, wound bed tissues were collected, and processed for further experimental studies. Immediately after collection, tissues were snap frozen in OCT (Leica Biosystems) for cryo-sectioning. For RNA and protein-based analysis, tissues were preserved in -80 °C.

5.2.11. RNA extraction and quantitative PCR for hydrogel incubated cells

Upon incubation of cells with OP@QC hydrogel cells were harvested and RNA was extracted using CTAB extraction buffer (Wang and Stegemann, 2010) to assess the inflammatory gene expression profile. Briefly, collected cells were mixed with pre-warmed CTAB extraction buffer (2.0% CTAB (Sigma), 2.0% polyvinylpyrrolidone (PVP 40; Sigma), 1.4 M sodium chloride (NaCl, Sigma), 100 mM Tris-HCl (pH 8.0; Sigma), 20 mM ethylenediaminetetraacetic acid (EDTA; Sigma), and 1.0% beta-mercaptoethanol (Sigma) in RNase-free water) and vortexed for 8 minutes at room temperature. Then, equal volume of chloroform-isoamyl alcohol (24:1) was added to the mixture and centrifuged for 15,000 ×g at room temperature. The transparent upper phase was again extracted with an equal volume of chloroform-isoamyl alcohol and separated upper phase was mixed with equal amount of isopropanol (IPA) and centrifuged for 15 min at 15,000 ×g at room temperature. The supernatant was discarded and pellet was washed with 75% of ethanol at 10000 ×g. The washed pellets were dissolved in RNase-free water and quantified using a Nano Dro spectra-photometer (Nanodrop2000, Thermo Fisher Scientific, USA). The cDNA synthesization and real-time PCR was carried out by following procedure described earlier in section 3.2.9.

Total RNA from the murine wound tissue was isolated using TRIzol (Invitrogen) (Patra et al., 2022). The detailed procedure of RNA extraction and real-time PCR are described earlier in section 3.2.9.

5.2.12. Immunofluorescence

The procedure described in section 3.2.6 was used.

5.2.13. Hematoxylin & Eosin staining and imaging

The procedure described in section 3.2.8 was used.

5.2.14. RNA extraction and Quantitative PCR

The procedure described in section 3.2.9 was used.

5.2.15. Immunoblotting

The procedure described in section 3.2.10 was used.

5.2.16. Statistical analysis

Data analysis was carried out utilizing GraphPad Prism software (version 8.0; GraphPad Software, Inc., La Jolla, CA). Results are expressed as means ± standard deviation (S.D.). Statistical significance was determined by Student's t-test or Multiple t-test, $*P<0.05$, $**P<0.01$, $***P<0.001$, $\#P<0.0001$ were considered significant difference and ns indicates non-significant difference.

5.3. Results

5.3.1. Preparation and characterization of oxidized-pullulan and quaternized-chitosan based hydrogel

To expedite wound healing, a polymer-based hydrogel was meticulously engineered by chemically modifying pullulan and chitosan (**Fig. 5.1**). Pullulan was oxidized using sodium periodate, resulting in the production of numerous aldehyde and hemiacetal groups throughout the backbone, which may then react with amines of chitosan molecule to produce biodegradable imine bonds. The oxidized product was named oxidized pullulan (OP), whose synthesis was described in the previous *Chapter-4*.

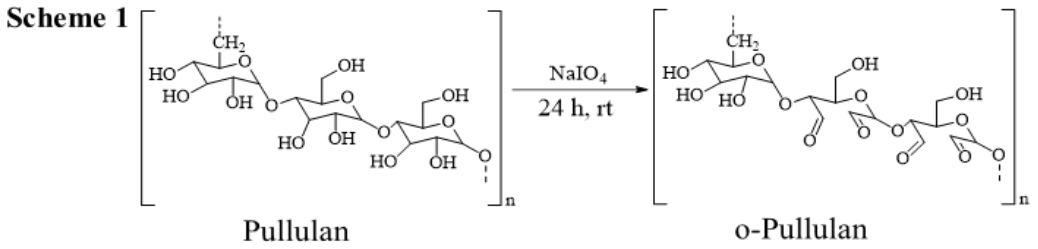

Figure 5.1. *Sodium-(meta) periodate-mediated oxidation of pullulan polymer.*

Then quaternized chitosan (QC) was produced by treating chitosan with glycidyltrimethylammonium chloride (GTMAC) (**Fig. 5.2A**). The FT-IR indicated a distinctive stretching vibration peak for the methyl in the quaternary ammonium groups at 1484 cm^{-1}. Absence of -NH_2 deformation vibration peak at 1580 cm^{-1} in QC compared to the chitosan, indicated the incorporation of quaternized group to the primary amine (**Fig. 5.2B**). The degree of quaternization was assessed by trinitrobenzenesulfonic acid titration and was found approximately 15% ± 5.

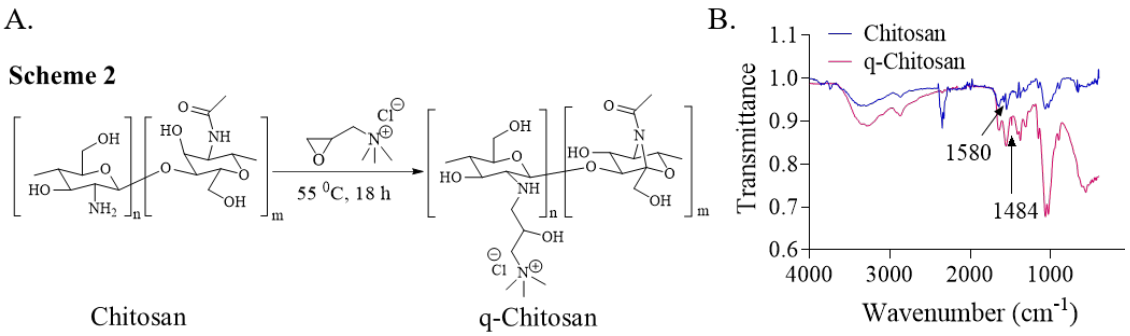

Figure 5.2. *Quaternization of chitosan molecule. (A) Chitosan quaternization by GTMAC. (B) FT-IR spectrum of chitosan and quaternized chitosan.*

To study the development of the OP@QC hybrid hydrogel, aqueous solutions of the biopolymers were combined in mass ratios of 10:2, 10:1, 1:5, and 2:5 for OP to QC. As illustrated in **Fig. 5.3A**, a semi-solid, transparent hydrogel was created at a 10:1 mass ratio, owing to the covalent cross-linking among the polysaccharides, predominantly driven by imine bonds. In contrast, the other mass ratios failed to form a semi-solid hydrogel system due to an inadequately crosslinked network. The mechanical characteristics of the composite hydrogel were then examined using dynamic rheology analysis under various mechanical testing settings (**Fig. 5.3B-D**). The G′ (storage modulus) values were continuously above the G″ (loss modulus) for the OP@QC hydrogel during the amplitude sweep from 0.01% to 1000% strain, showing that it maintained a gel-like condition (**Fig. 5.3B**). As the strain reached roughly 400%, G″

surpassed G′, marking a change from gel to sol and the rupture of the hydrogel's crosslinked network around 630%. The OP@QC hydrogel maintained its gel state throughout an angular frequency range of 0.1 to 100 rad/s at 1% strain (**Fig. 5.3C**), exhibiting stability. The self-healing capability of the hybrid hydrogel was subsequently evaluated. **Fig. 5.3D** indicates that G′ modulus considerably dropped when exposed to a high strain of 100% with angular frequency 10 rad/s, suggesting a transition to a sol phase. As the strain dropped to 1% with angular frequency 10 rad/s, the sol reformed into a gel, validating the self-healing characteristics of the OP@QC hydrogel. Under physiological circumstances involving repeated stretching and compression, the self-healing property of the hydrogel is critical for preserving its structural integrity. The swelling degradation study (**Fig. 5.3E**) of the hydrogel indicated highest swelling of 25% at 8 hours at pH 9.0, resulting in hydrophilicity and consequently degradation. We investigated the water retention characteristics of the hydrogel by subjecting it to a controlled environment at 37 °C within a humidified chamber over different time intervals. The results demonstrated that at 37 °C, the hydrogel was capable of preserving up to 60% of its initial water content after an 18-hour period (**Fig. 5.3F**). This water preservation capability of OP@QC hydrogel might enhance wound healing by facilitating cellular migration, mitigating pain, reducing infection risk, and improving scar formation, thereby creating an ideal environment for accelerated and effective recovery.

Given our attention on drug release applications in diabetic chronic wound, we explored the controlled release of the doxorubicin in a PBS at pH 7.4 (**Fig. 5.3G**). A cumulative release of doxorubicin was plotted over time. The hydrogel gradually released the drug over a 24 hours period, demonstrating sustained and controlled release. Upon degradation at 8 hours the releasing profile extended up to approximately 70% at 24 hours, which exhibited the highest regression fit within the Korsemeyer-Peppas exponential model and revealing a Fickian diffusion mechanism. The 24-hour releasates from the doxorubicin-loaded OP@QC hydrogel, after incubation with L929 cells, were analysed to assess the cellular uptake of the released doxorubicin. Subsequent to incubation, a pronounced signal at 595 nm was detected in the cells, indicating effective uptake of the released doxorubicin. To investigate the direct uptake of doxorubicin from the hydrogel by the cells, murine fibroblast L929 cells were cultured on the doxorubicin-loaded hydrogel. Following a 24-hour incubation, microscopic analysis of the cells revealed a green fluorescence signal at 595 nm, indicating successful internalization of the doxorubicin (**Fig 5.3H**). The data confirmed that doxorubicin or any drug molecule, upon being released from the hydrogel system, is effectively internalized by the cells when it comes into contact with them. This indicates that the hydrogel may facilitates the direct delivery of

doxorubicin or any drug to the cells, allowing for its efficient uptake and subsequent cellular incorporation.

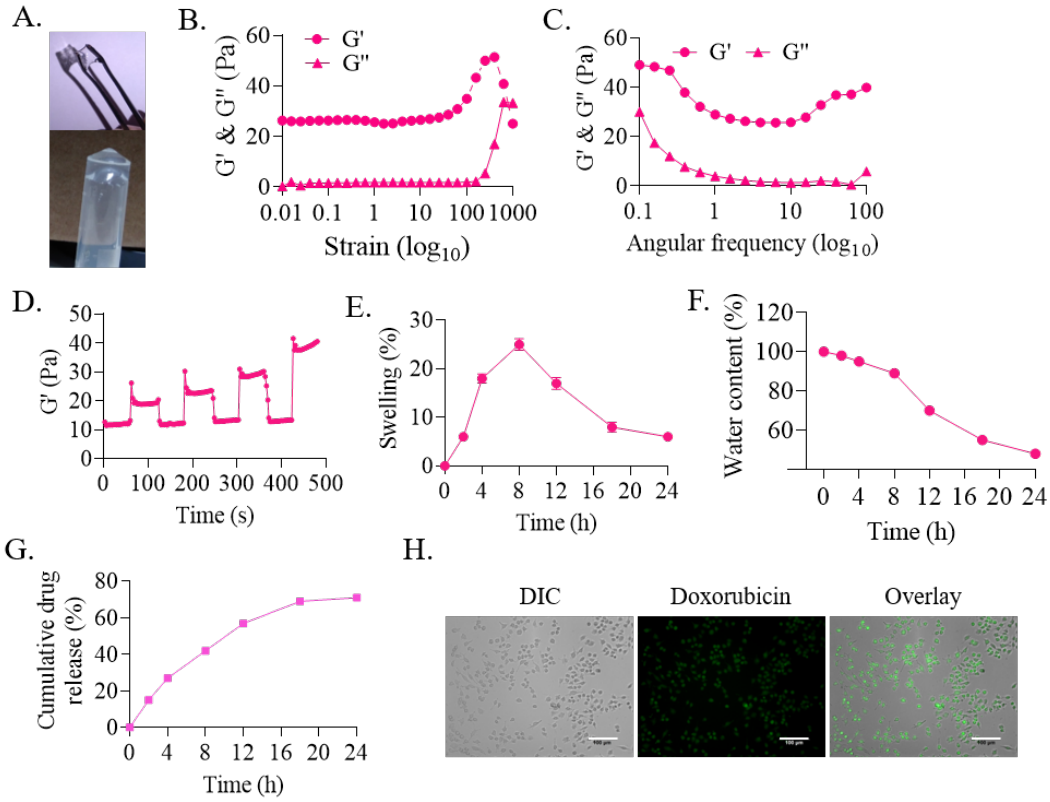

Figure 5.3. *Fabrication and physical characterization of oxidized pullulan (OP) and quaternized chitosan (QC)-based hydrogel system (OP@QC). (A) Pictorial image of OP@QC after hydrogel formation. The hydrogel was characterized by: (B) amplitude sweep, and (C) frequency sweep to evaluate the linear-viscoelastic (LVE) region. (D) The self-healing capability of the hydrogel. (E) The swelling degradation capability of the OP@QC. (F) Water retention capability of hydrogel. (G) Releasing profile of doxorubicin from the hydrogel system at pH 7.4. (H) Direct incorporation of released doxorubicin into the L929 cells, seeded on the doxorubicin-loaded hydrogel.*

5.3.2. *In vitro* antibacterial activity of OP@QC hydrogel

Infections caused by drug-resistant bacteria pose a significant challenge to the wound healing process. The antimicrobial potential of the OP@QC hydrogel was evaluated against both Gram-negative *(Pseudomonas aeruginosa)* and positive *(Staphylococcus aureus)* bacteria, which are predominant in diabetic wound. Bacterial suspensions (~10^6 CFU/mL) were incubated with the OP@QC hydrogel for a period of 24 hours. **Fig. 5.4A** displays a marked reduction in *S. aureus population* in contrast to *P. aeruginosa* that exhibited significantly less growth inhibition compared to control. The OP@QC hydrogel demonstrated a bacterial eradication efficiency of approximately 71.2 ± 5.67% against *S. aureus* and 30.4 ± 9.49%

against *P. aeruginosa*. This differential response highlights the hydrogel's potent bactericidal efficacy against Gram-positive *S. aureus*, with modest impact on Gram-negative *P. aeruginosa*.

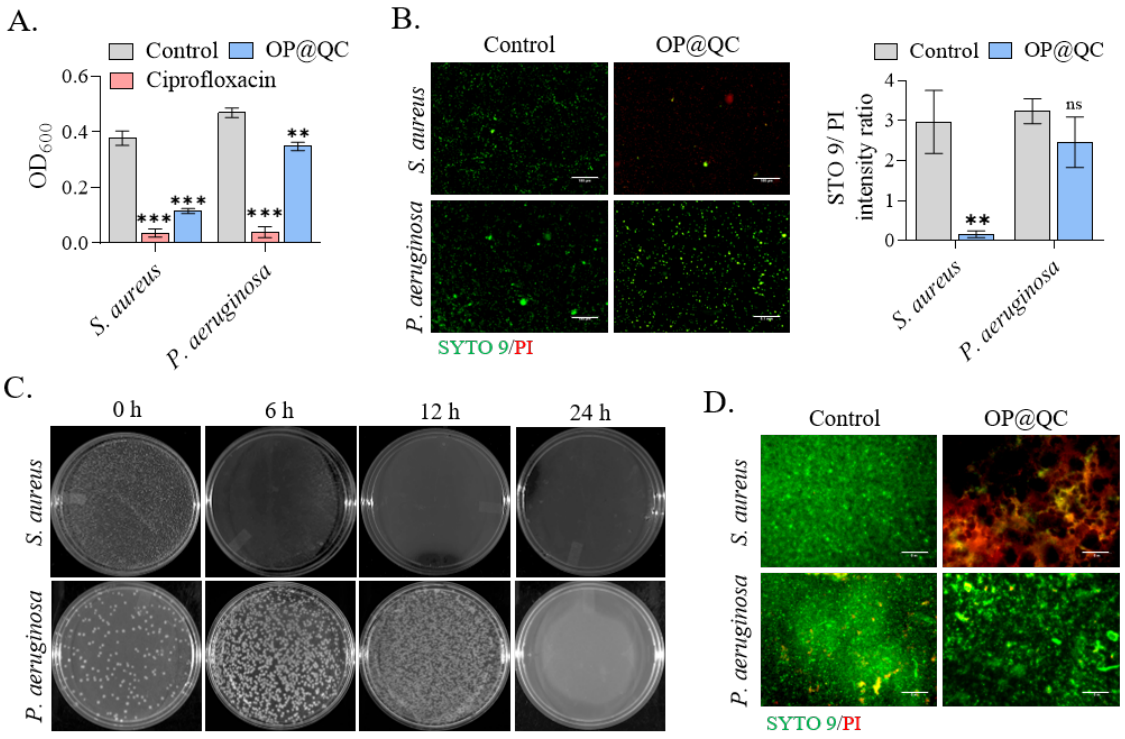

Figure 5.4. *Antibacterial activity of OP@QC hydrogel. (A) Bacterial growth inhibition activity of OP@QC against S. aureus and P. aeruginosa. (B) Live/dead staining of S. aureus and P. aeruginosa in control (untreated) and treated (OP@QC) samples. (objective 20X, scale bar 100 µm) (n = 3). (C) Colony images of S. aureus and P. aeruginosa at different time points. (D) Inhibition of biofilm formation activity of o-pullulan against S. aureus and P. aeruginosa. (objective 20X, scale bar 100 µm) (n = 3). Data are expressed as means ± SD; **P<0.01 ***P<0.001 were considered significant difference (Student's t-test).*

For further evidence of killing action of hydrogel, we evaluated bacterial membrane permeability, through the LIVE/DEAD™ BacLight™ Bacterial Viability Kit. The use of propidium iodide (PI), which penetrates compromised bacterial membranes and emits red fluorescence under excitation, provided clear evidence of membrane disruption. The **Fig. 5.4B** illustrates intense red fluorescence within *S. aureus* treated with OP@QC hydrogel after 24 hours, signifying considerable disruption of the cell membranes of bacteria. In contrast, *P. aeruginosa* showed less amount of death after incubation with hydrogel for 24 hours. Time-dependent assessments of bacterial growth inhibition demonstrated a notable decrease in *S. aureus* colonies as early as 6 hours of hydrogel exposure (**Fig. 5.4C**). In contrast, *P. aeruginosa* colonies showed a significant reduction only after an extended incubation period of 24 hours.

Biofilm formation is a frequent issue in wound infections. To assess the efficacy of OP@QC hydrogel in disrupting bacterial biofilms, a plate culture assay was conducted. After plating bacteria on OP@QC hydrogel for 24 hours, robust and intense red fluorescence signals were detected in *S. aureus* biofilms, indicating substantial biofilm disruption. In comparison, *P. aeruginosa* biofilms exhibited less pronounced fluorescence (**Fig. 5.4D**). No significant red fluorescence was observed in the untreated biofilms, confirming the hydrogel's effectiveness in targeting biofilm-associated bacteria.

5.3.3. Bio-compatibility of OP@QC hydrogel

As a preliminary step in determining the hydrogel's biological activity, we treated it with L929 fibroblasts cells to assess its cytotoxicity. There was extensive green fluorescence in the live/dead experiment, proving that the cells were alive and evenly distributed throughout the hydrogel surface (**Fig. 5.5A**). As shown in **Fig. 5.5B**, quantitative examination of cell viability using the MTT test showed that after 24 hours of culture, the hydrogel group had viability similar to the control group. The mitochondrial health is also evaluated in L929 cells due to its significance in energy production, regulation of apoptosis, and maintenance of cellular homeostasis. Mitochondrial dysfunction is often an early sign of cellular damage. Unlike the cells treated with CCCP, which showed significant damage to the mitochondria (**Fig. 5.5C**), the OP@QC hydrogel maintained the integrity of the mitochondria, as evidenced by the prominent red JC aggregates. These results imply that the OP@QC hydrogel is safe for mammalian cells.

In context of immune response, macrophages undergo polarization into distinct phenotypes- pro-inflammatory M1 or reparative M2, depending upon the environmental cues, including the molecular properties of biomaterials they interact with. This polarization dramatically influences the wound healing process, influencing inflammation resolution and tissue regeneration. Thus, we are interested to study the polarization of RAW264.7 macrophages upon incubation with OP@QC hydrogel. Lipopolysaccharide (LPS) is used as a positive control for stimulating M1 polarization. After 24 hours of incubation with the OP@QC hydrogel, RAW264.7 macrophages produced less expressions of proinflammatory cytokines as compared with control, indicated in **Fig. 5.5D** suggests non-immunotoxic nature of our hydrogel system.

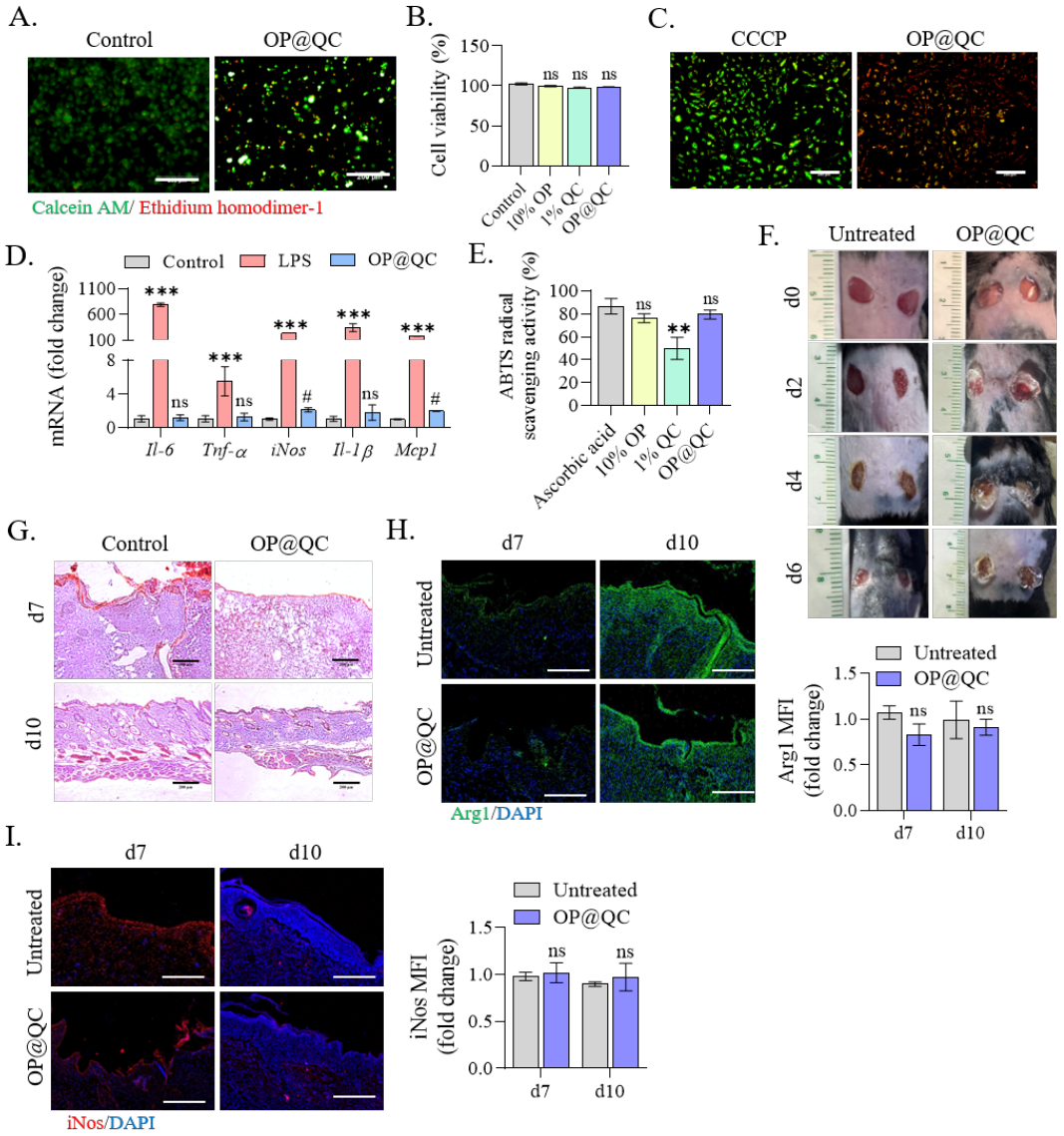

Figure 5.5. *Cytocompatibility of OP@QC hydrogel. (A) Live/dead imaging of L929 cells as a control and after seeding upon OP@QC (objective 10X, scale bar 200 µm). (B) MTT assay OP@QC and its components using L929 cells where control is untreated cells. (C) Evaluation of mitochondrial health in OP@QC treated L929 cells by using JC-1. (D) Expression profile of pro-inflammatory markers in OP@QC treated murine macrophages. (E) Antioxidant activity of ascorbic acid as appositive control, PO@QC and its components using ABTS scavenging assay. (F) Pictorial images of control (untreated) and OP@QC-treated murine wound at different time points. (G) Hematoxylin and eosin staining of untreated and OP@QC treated day 7 and 10 murine wound tissue. (H) Immunohistochemistry images and quantitative analysis of untreated and OP@QC-treated group's wound area over time staining by Arg1 antibody (objective 10X, scale bar 300 µm)(n=3). (I) Immunohistochemistry images and quantitative analysis of untreated and OP@QC- treated group's wound area over time staining by iNos antibody (objective 10X, scale bar 300 µm) (n=3). Data are presented as mean ± SD from three independent experiments., and ***P<0.001 and #P<0.0001 whereas ns indicates non-significant difference were considered as significant difference (Student's t-test).*

The ROS scavenging activity of OP@QC hydrogel system was evaluated using the ABTS cation assay (**Fig. 5.5E**), which indicated 85% of ROS activity reduction upon hydrogel

treatment. Whereas 10% OP and 1% QC also showing ROS scavenging activity of 80% and 50% respectively. The scavenging of the ROS will result in the reduction of the extracellular ROS activity in the wound site. The ascorbic acid exhibited inhibitory activity against the ABTS cation of 85% at concentration of 1 μg/mL.

We next examined the *in vivo* biocompatibility of the hydrogel (**Fig 5.5F**). The OP@QC hydrogel displayed 100% disintegration within 24 hours of application, showing its applicability for short-term therapeutic settings. We then conducted a detailed histological investigation employing Haematoxylin and Eosin (H & E) staining on subcutaneous tissue samples obtained from the application areas at days 7 and 10. This study revealed no notable histopathological abnormalities, both control and OP@QC-treated wounds displayed hair follicle growth, confirming the hydrogel's participation in helping tissue regeneration and does not generate any local tissue damage (**Fig. 5.5G**). Upon healing, reduction of pro-inflammatory iNos expression and upregulation of anti-inflammatory Arg1 expression indicates no local inflammatory response upon OP@QC application in the murine wound site (**Fig. 5.5H-K**).

5.3.4. Assessing the efficacy of *Zeb2* ASO encapsulated OP@QC hydrogel

In our *in vitro* experiment analysis, Zeb2 emerged as a crucial transcription factor with a fundamental role in macrophage polarization. By regulating genes important for inflammation and tissue repair, Zeb2 influences macrophage activity and the overall inflammatory environment. In the arena of chronic inflammation, Zeb2's modulation of macrophage polarization may crucially drive disease progression. Notably, inhibiting Zeb2 in hyperglycaemic macrophages drastically decreases inflammatory signals while establishing an anti-inflammatory environment (**Fig. 3.5**). Thus, we have designed *Zeb2* ASO and transfected in murine macrophages RAW264.7 to check its efficacy and found almost 80% gene silencing (**Fig. 5.6A**). Then we co-cultured murine macrophages with hydrogel for 24 hours containing either *Zeb2* ASO or *Control* ASO (*con* ASO) and analysed *Zeb2* expression patterns. The data revealed that *Zeb2* ASO was successfully released from hydrogel and absorbed into the macrophages as it significantly reduced *Zeb2* expression profile over the time compared with control (**Fig. 5.6B**).

5.3.5. *Zeb2* ASO loaded OP@QC hydrogel accelerated the diabetic wound healing

The efficacy of *Zeb2* ASO-loaded OP@QC hydrogel in diabetic wound healing was comprehensively evaluated in diabetic mice which were subjected to streptozotocin (STZ)

injections and a high-fat diet (HFD), characterized by fasting blood glucose levels reaching 400 mg/dL. Two random groups were established: one group received the *Con* ASO hydrogel, while the other was treated with the *Zeb2* ASO-incorporated hydrogel. We also keep standard diet fed mice in our experiment as reference control.

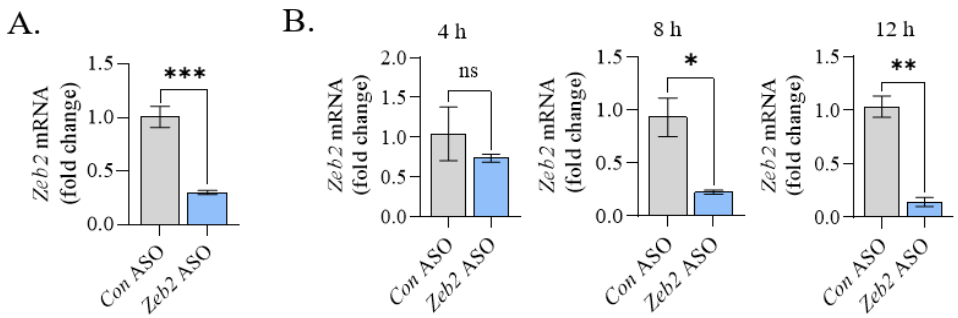

Figure 5.6. *Validation of Zeb 2 ASO (A) mRNA expression of Zeb2 in Con ASO and Zeb2 ASO transfected murine RAW264.7 macrophages. (B) Zeb2 expression in murine macrophages incubated with Zeb2 ASO or Con ASO incorporated OP@QC hydrogel, at different time points. Data are presented as mean ± SD from three independent experiments, and *P<0.05, **P<0.01, and ***P<0.001 were considered as significant difference, whereas ns indicates non-significant difference (Student's t-test).*

By the seventh day of post-wounding, the group treated with *Zeb2* ASO hydrogel exhibited notable improvement in wound healing, with the wound tissue exhibiting significant closure (**Fig. 5.7A**). Wound area quantitative analysis indicated that wounds treated with *Zeb2* ASO hydrogel had a ~70% improvement in wound closure compared to the control group (**Fig. 5.7B**). Histopathological examination using hematoxylin and eosin (H & E) staining further depicted significant tissue regeneration in treated group. The OP@QC hydrogel-treated wounds displayed a substantially intact epidermis and dermis with a well-organized fibrous collagen structure, closely mimicking the histological appearance of normal skin (**Fig. 5.7C**). Furthermore, the presence of developing hair follicles suggested successful healing of the dermal layer. The *Con* ASO-treated wounds displayed significant inflammatory cell infiltration, whereas wounds treated with *Zeb2* ASO hydrogel showed a notable reduction in inflammatory cell accumulation over the healing period (**Fig. 5.7D**). This was indicative of decreased inflammatory response and improved repair. Western blot analysis provides greater insight into the molecular processes driving the purported therapeutic effects. It indicated that *Zeb2* ASO treatment effectively downregulated *Zeb2* expression within the wounded tissue throughout the healing process (**Fig. 5.7E**). This downregulation of Zeb2, a transcription factor involved in macrophage polarization, correlated with decreased inflammation by reducing phosphorylated NF-κB expression at day 7 of post wounding (**Fig. 5.7F**) and thus improved

wound healing. Interestingly, myeloid lineage-derived transcription factors (MLDTFs) were observed to be downregulated in the *Zeb2* ASO-treated group, further indicating that the chronic inflammatory load was decreased in this group (**Fig. 5.7G**). In conclusion the *Zeb2* ASO encapsulated OP@QC hydrogel treatment in diabetic wound models gives an extraordinary promise for accelerating wound closure and improving tissue regeneration, thus offering an advanced approach to treat diabetic chronic non-healing wounds.

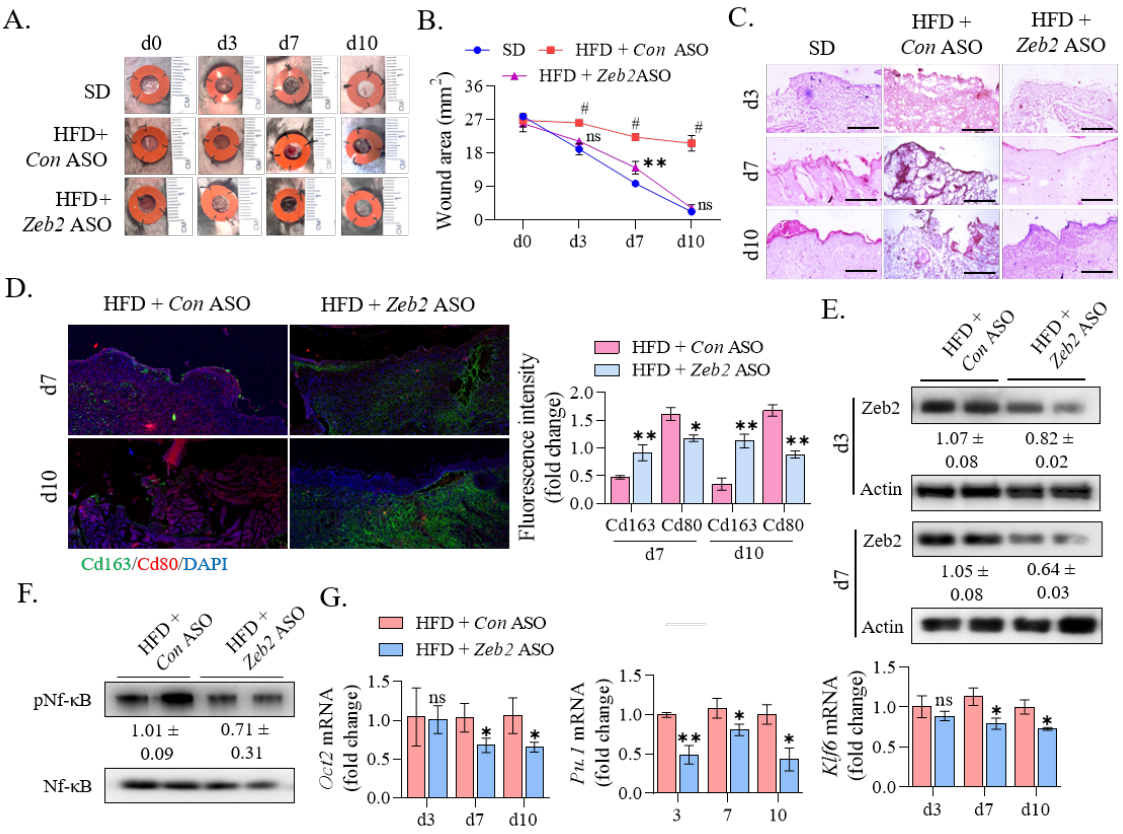

Figure 5.7. *The suppression of Zeb2 ameliorated wound-healing complications in STZ induced high-fat diet mouse model. (A) A series of images on the wound area over time of the SD, HFD + Con ASO and HFD + Zeb2 ASO (n = 3). (B) Wound closure area of SD, HFD + Con ASO and HFD + Zeb2 ASO groups of mice. (C) H&E staining of all murine wound groups (objective 10X, scale bar 300 µm). (D) Immunohistochemistry images and quantitative analysis of wound area staining by macrophages' markers; Cd163 (green), Cd80 (red) in Con ASO and Zeb2 ASO treated diabetic groups (objective 10X, scale bar 300 µm) (n = 3). (E) Western blot analysis of Zeb2 in HFD + Con ASO and HFD + Zeb2 ASO groups of murine wound tissue at day 3 and day 7. (F) Western blot analysis of pNf- kB in HFD + Con ASO and HFD + Zeb2 ASO groups of day 7 murine wound tissue. (G) mRNA expression profile of different myeloid lineage derived transcription factors in mice wound tissue after the treatment of Con ASO and Zeb2 ASO at different time points. Data are presented as mean ± SD, and *P<0.05, **P<0.01, and #P<0.0001 were considered as significant difference (Student's t-test), whereas ns indicates non-significant difference. SD, standard diet; HFD, high fat diet.*

5.3.6. *Zeb2* ASO treatment reduced the inflammatory burden in diabetic wound healing

Moreover, we observed *Zeb2* ASO treatment led to a declination of other pro-inflammatory markers like Il-1β, iNos, Il-6, Tnf-α (**Fig. 5.8A**) and a notable elevation in anti-inflammatory cytokines, especially Il-4 and Il-10, compared to the control HFD wounds (**Fig. 5.8B**). These findings reveal that whilst the control diabetic wounds retained a high degree of inflammation, the *Zeb2* ASO treatment effectively decreased the local inflammatory response. By enhancing the polarization of macrophages towards the M2 phenotype and promoting the release of anti-inflammatory cytokines. *Zeb2* ASO treatment permitted a change from an inflammatory to a reparative tissue milieu. This change is crucial for enhancing the overall healing process and decreasing chronic inflammation associated with diabetic wounds. Treatment with *Zeb2* ASO in diabetic murine wounds resulted in a substantial decrease in the pro-inflammatory load as the healing process advanced over the time. Cd80 and Cd86, surface markers of M1 macrophages, were remarkably lowered (**Fig. 5.8D**), while Cd206 and Cd163 (**Fig. 5.8E**), markers for M2 macrophages, were elevated following *Zeb2* ASO treatment. This modification in macrophage phenotype reflects a trend towards a more reparative and less inflammatory environment. Immunohistochemical staining revealed fresh insights into the cytokine expression within the wounds. *Zeb2* ASO treatment led to an overexpression of Arg1, an anti-inflammatory cytokine (**Fig. 5.8F**) and a concurrent downregulation of iNos, the pro-inflammatory cytokine (**Fig. 5.8G**).

5.3.7. *Zeb2* ASO treatment accelerated angiogenesis by reducing inflammatory burden in diabetic wound

M2 macrophages cultivate an environment that encourages the creation of new blood vessels, thereby, helping tissue regeneration and speeding the repair of wounded tissues. In this context, the study of pro-angiogenic markers revealed fascinating insights into the role of Zeb2 inhibition in encouraging wound healing of chronic diabetes. Notably, *Zeb2* ASO directed suppression of chronic inflammation led to a rise in the mRNA expression of key angiogenic factors, such as Tgf-β, Cd31, and VE-cadherin, which were identified on day 7 and day 10 of post-wound (**Fig. 5.9A**), suggesting a positive sign of neovascularization. Immuno-histochemical staining of day 7 post wound tissue indicated a considerable increase of Cd31 expression in the *Zeb2* ASO-treated mice, compared to the *Con* ASO (**Fig. 5.9B).** Similarly, the expression of α-Sma in day 10 wound tissue of *Zeb2* ASO-treated group (**Fig. 5.9C**). In contrast, the *Con* ASO treated mice showed considerable wound tissue disintegration in the day 10,

indicative of poor tissue remodeling, probably driven by chronic inflammation and limited vascular supply. Further, on day 10, the expression of cytokeratin14 was much higher in the *Zeb2* ASO-treated mice, corresponding with a more robust and well-formed epithelial layer (**Fig. 5.9D**) compared with the *Con* ASO group, which displayed thinner and less developed epithelial tissue, indicating a delay in wound healing.

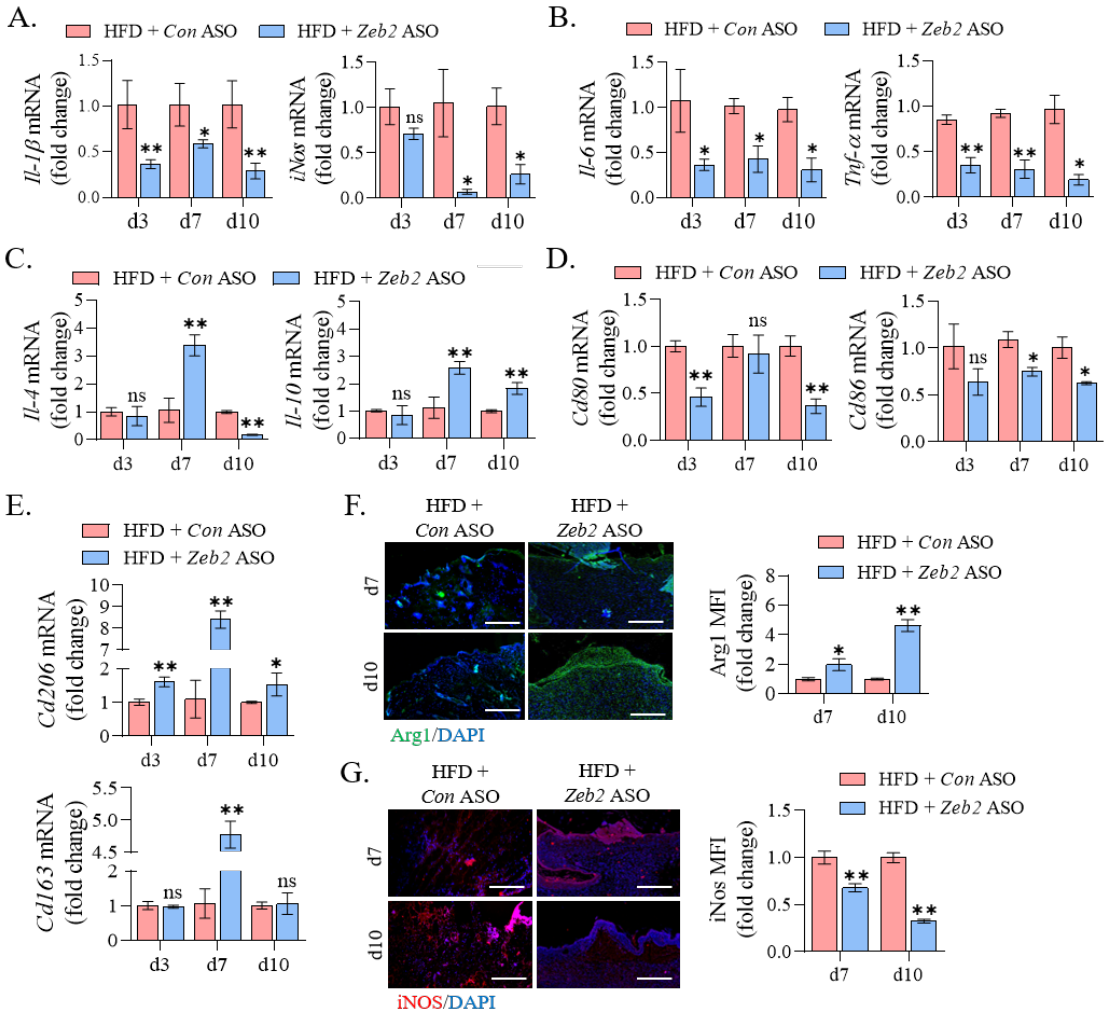

Figure 5.8. *Inhibiting Zeb2 safeguards against diabetes-induced macrophage inflammation. (A, B) mRNA expression profile of pro-inflammatory cytokines in diabetic wound tissue after treatment of control ASO and Zeb2 ASO in diabetic mice. (C) mRNA expression profile of anti-inflammatory cytokines in control ASO and Zeb2 ASO-treated murine wound tissue at different time points. mRNA expression profile of pro-inflammatory (D) and anti-inflammatory (E) macrophage markers in in mice wound tissue after the treatment of Con ASO and Zeb2 ASO at different time points. (F) Immunohistochemistry images and quantitative analysis of control ASO and Zeb2 ASO incorporated hydrogel-treated diabetic group's wound area over time staining by anti-inflammatory cytokine Arg1 antibody (objective 10X, scale bar 300 μm) (n = 3). (G) Immunohistochemistry images and quantitative analysis of control ASO and Zeb2 ASO incorporated hydrogel-treated diabetic group's wound area over time staining by pro-inflammatory cytokine iNos antibody (objective 10X, scale bar 300 μm) (n = 3). Data are presented as mean ± SD, and ***P<0.001 and #P<0.0001 were considered as significant difference (Student's t-test), whereas ns indicates non-significant difference.*

Collectively, our findings imply that the inclusion of *Zeb2* ASO into the OP@QC hydrogel provides enhance diabetic wound healing by promoting facilitating faster recovery and more complete tissue regeneration.

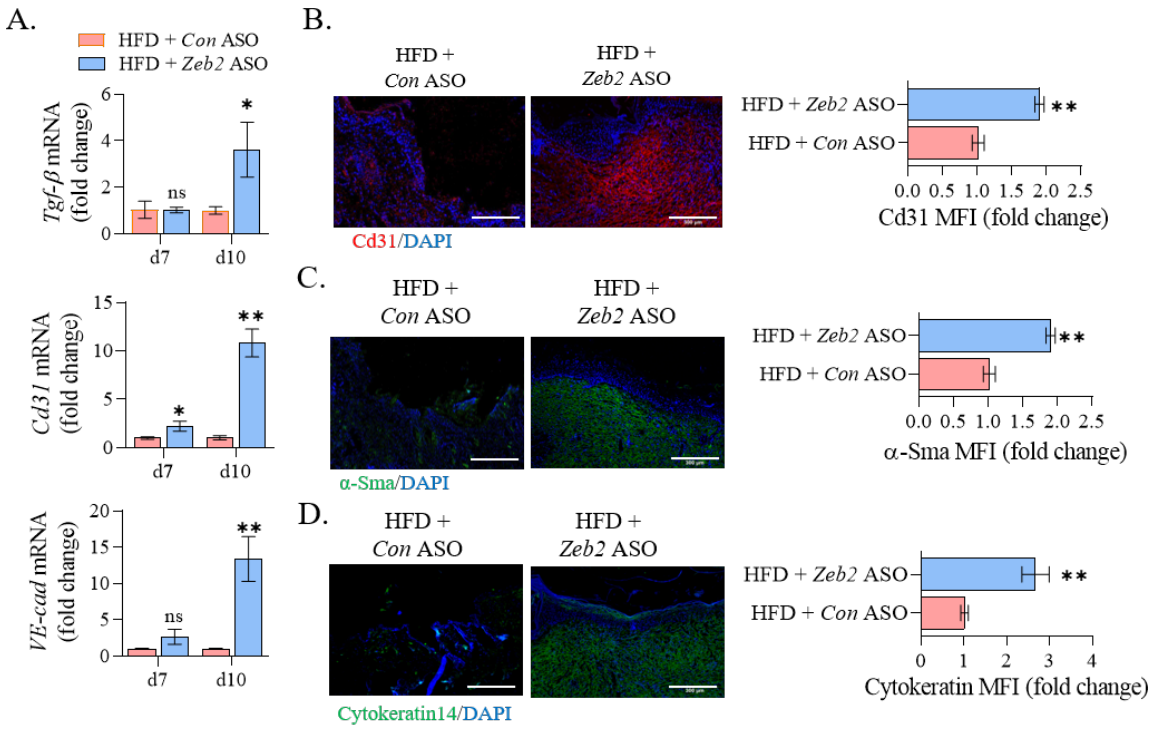

Figure 5.9. *Zeb2 ASO incorporated OP@QC hydrogel promoted angiogenesis during the wound healing by reducing chronic inflammation in diabetic wound. (A) mRNA expression of pro-angiogenic markers in diabetic murine wound after treating with Zeb2 ASO incorporated OP@QC hydrogel. (B) Immunohistochemistry images and quantitative analysis of control ASO and Zeb2 ASO-treated day 7 diabetic wound tissue staining by Cd31 antibody (objective 10X, scale bar 300 μm)(n=3). (C) Immunohistochemistry images and quantitative analysis of control ASO and Zeb2 ASO-treated day 10 diabetic wound tissue staining by α-Sma antibody (objective 10X, scale bar 300 μm)(n=3). (D) Immunohistochemistry images and quantitative analysis of control ASO and Zeb2 ASO treated day 7 diabetic wound tissue staining Cytokeratin14 antibody (objective 10X, scale bar 300 μm)(n=3). Data are presented as mean ± SD from three independent experiments, and ***P<0.001 and #P<0.0001 were considered as significant difference (Student's t-test), whereas ns indicates non-significant difference.*

5.4. Discussion

The preparation and characterization of oxidized pullulan (OP) and quaternized chitosan (QC) based hydrogels and its efficacy have marked a significant advancement in wound care technology. The oxidative modification of pullulan has been extensively studied for its potential in developing hydrogels with improved mechanical and swelling characteristics (Elangwe et al., 2023), which forms a semi-solid, transparent hydrogel, resulting from effective crosslinking through imine bonds. The aldehyde groups present in OP facilitate crosslinking with the amine

groups of chitosan, resulting in a novel OP@QC hydrogel formulation with enhanced properties including robust mechanical properties, as evidenced by dynamic rheology analysis. The storage modulus (G′) was consistently higher than the loss modulus (G″), indicating that the hydrogel maintained a gel-like behavior. It was reported that hydrogels with higher G′ values exhibit better mechanical stability, crucial for wound healing applications (Gounden and Singh, 2024). Moreover, the hydrogel exhibited notable self-healing properties, with the G′ modulus dropping under high strain and reforming when the strain was reduced. Self-healing behavior is a critical feature for wound dressings, as it allows the hydrogel to recover and maintain its functionality even after physical damage (Abd-ElSalam et al., 2024). The swelling behavior of the hydrogel showed a 25 % increase in volume at pH 9.0, indicating high hydrophilicity. This property is beneficial for wound care, as it facilitates the retention of moisture, a key factor in promoting wound healing. Water retention studies revealed that the hydrogel could maintain 60% of its initial water content at 37 °C for up to 18 hours. This finding makes it advantageous over others, where maintaining a moist environment is essential for effective wound healing (Junker et al., 2013). Controlled drug release from hydrogels is an important component in therapeutic applications, , where delayed and targeted administration is needed to decrease systemic toxicity and maximize effectiveness (Li et al., 2023). In our study we found that OP@QC hydrogel effectively released doxorubicin which was absorbed by murine fibroblast L929 cells, evidenced by green fluorescent signals. The efficacy of released ASO demonstrated a release profile up to 8 hours, coinciding with the onset of hydrogel disintegration, resulting in Zeb2 downregulation in treated macrophages lasting up to 12 hours before 100% degradation of the hydrogel. Therefore, it needed multiple application at the wound sites. Collectively, these characteristics underscore the potential of OP@QC hydrogels as advanced materials for wound care applications, offering improved mechanical stability, self-healing capability, moisture retention, and localized release which are critical for effective wound management.

The antibacterial efficiency of OP@QC hydrogel was examined against both Gram-positive and Gram-negative bacteria. The component of the hydrogel OP has shown binding affinity to the cell wall protein SpA of *S. aureus*, which direct cellular lysis and provide a potent bactericidal activity (**Fig. 4.3** & **4.4**). Along with the QC, the synergistic antibacterial effect impart a robust bactericidal effect, enhancing their therapeutic potential; which reveals a strong impact against *Staphylococcus aureus* and moderate activity against *Pseudomonas aeruginosa*, which is especially helpful in wound healing applications where infections typically delay the healing processes (Ahmadian et al., 2022). Since o-pullulan moiety binds with the cell wall protein SpA, which is absent in the wall of *P. aeruginosa* and this is the reason that OP@QC

hydrogel is not showing bactericidal effect against *P. aeruginosa* but showing bacteriostatic effect. Not only that this hydrogel also has capability to destruct existing wound biofilms. Biofilm production is a serious barrier in chronic wound treatment, and hydrogels capable of destroying biofilms are increasingly recognized for their therapeutic potential. However, cytocompatibility assay and assessing mitochondrial health in L929 fibroblast cells exhibited no substantial toxicity against mammalian cells, supporting the safety profile of the OP@QC hydrogel for prospective biomedical applications. Moreover, the hydrogel demonstrated potential immunomodulatory effects by lowering the expression of pro-inflammatory markers when compared to LPS-treated positive controls, which are commonly employed as a model for producing an inflammatory response, encouraging OP@QC hydrogel to boost wound healing process, thus, making it a better option for treating chronic wounds and other inflammation-related disorders.

Earlier findings demonstrated the relevance of macrophage polarization in wound healing, particularly in diabetes situations where inflammation persists, leading to delayed healing (Wolf et al., 2021). *In vivo* investigations using diabetic mice models indicated the therapeutic effectiveness of the *Zeb2* antisense oligonucleotide (ASO)-loaded OP@QC hydrogel in decreasing inflammation, promoting angiogenesis leads to rapid wound healing. This hydrogel, altered M1 to M2 ratio by switching M1 macrophage to M2, which is important for resolving chronic inflammation and encouraging tissue repair. Histological examination of the treated wounds demonstrated quicker closure, decreased inflammatory cell infiltration, and improved angiogenesis, evidenced by the presence of essential angiogenic markers, such as Cd31 and α-Sma.

Therefore, our OP@QC hydrogel proves as a multimodal approach to boost wound healing process at diabetic scenario. In this study, the *Zeb2* ASO-loaded hydrogel not only tackles the inflammatory problems associated with diabetic wounds but also creates an environment favorable to tissue repair and regeneration.

References

ABD-ELSALAM, H.-A. H., REFAEEY, O. A., WAKED, K. G., ELSHERBINY, K. A., ALEAM, A. M., IBRAHIM, M. Q., FARAG, M. H., NASEF, A. M. & ELMESHAD, A. N. 2024. A Review Exploring the Wound-Healing Activity of Self-Healing Hydrogels: Fabrication, Characterization, Mechanism, and Biomedical Applications. *Journal of Cluster Science,* 35**,** 2019-2037.

AHMADIAN, Z., GHEYBI, H. & ADELI, M. 2022. Efficient wound healing by antibacterial property: Advances and trends of hydrogels, hydrogel-metal NP composites and photothermal therapy platforms. *Journal of Drug Delivery Science and Technology,* 73**,** 103458.

BLACKLOW, S. O., LI, J., FREEDMAN, B. R., ZEIDI, M., CHEN, C. & MOONEY, D. J. 2019. Bioinspired mechanically active adhesive dressings to accelerate wound closure. *Sci Adv,* 5**,** eaaw3963.

CHEN, C., LIU, Y., WANG, H., CHEN, G., WU, X., REN, J., ZHANG, H. & ZHAO, Y. 2018. Multifunctional Chitosan Inverse Opal Particles for Wound Healing. *ACS Nano,* 12**,** 10493-10500.

CROOKE, S. T., WANG, S., VICKERS, T. A., SHEN, W. & LIANG, X.-H. 2017. Cellular uptake and trafficking of antisense oligonucleotides. *Nature biotechnology,* 35**,** 230-237.

DIAS, N. & STEIN, C. 2002. Antisense oligonucleotides: basic concepts and mechanisms. *Molecular cancer therapeutics,* 1**,** 347-355.

ELANGWE, C. N., MOROZKINA, S. N., OLEKHNOVICH, R. O., POLYAKOVA, V. O., KRASICHKOV, A., YABLONSKIY, P. K. & USPENSKAYA, M. V. 2023. Pullulan-Based Hydrogels in Wound Healing and Skin Tissue Engineering Applications: A Review. *Int J Mol Sci,* 24.

FISCHER, K. S., LITMANOVICH, B., SIVARAJ, D., KUSSIE, H. C., HAHN, W. W., HOSTLER, A. C., CHEN, K. & GURTNER, G. C. 2023. Protocol for the Splinted, Human-like Excisional Wound Model in Mice. *Bio Protoc,* 13**,** e4606.

GARCIA, J. P., STEIN, J., CAI, Y., RIEMERS, F., WEXSELBLATT, E., WENGEL, J., TRYFONIDOU, M., YAYON, A., HOWARD, K. A. & CREEMERS, L. B. 2019. Fibrin-hyaluronic acid hydrogel-based delivery of antisense oligonucleotides for ADAMTS5 inhibition in co-delivered and resident joint cells in osteoarthritis. *Journal of Controlled Release,* 294**,** 247-258.

GOUNDEN, V. & SINGH, M. 2024. Hydrogels and Wound Healing: Current and Future Prospects. *Gels,* 10.

HAAGSMA, J. A., GRAETZ, N., BOLLIGER, I., NAGHAVI, M., HIGASHI, H., MULLANY, E. C., ABERA, S. F., ABRAHAM, J. P., ADOFO, K., ALSHARIF, U., AMEH, E. A., AMMAR, W., ANTONIO, C. A., BARRERO, L. H., BEKELE, T., BOSE, D., BRAZINOVA, A., CATALÁ-LÓPEZ, F., DANDONA, L., DANDONA, R., DARGAN, P. I., DE LEO, D., DEGENHARDT, L., DERRETT, S., DHARMARATNE, S. D., DRISCOLL, T. R., DUAN, L., PETROVICH ERMAKOV, S., FARZADFAR, F., FEIGIN, V. L., FRANKLIN, R. C., GABBE, B., GOSSELIN, R. A., HAFEZI-NEJAD, N., HAMADEH, R. R., HIJAR, M., HU, G., JAYARAMAN, S. P., JIANG, G., KHADER, Y. S., KHAN, E. A., KRISHNASWAMI, S., KULKARNI, C., LECKY, F. E., LEUNG, R., LUNEVICIUS, R., LYONS, R. A., MAJDAN, M., MASON-JONES, A. J., MATZOPOULOS, R., MEANEY, P. A., MEKONNEN, W., MILLER, T. R., MOCK, C. N., NORMAN, R. E., OROZCO, R., POLINDER, S., POURMALEK, F., RAHIMI-MOVAGHAR, V., REFAAT, A., ROJAS-RUEDA, D., ROY, N., SCHWEBEL, D. C., SHAHEEN, A., SHAHRAZ, S., SKIRBEKK, V., SØREIDE, K., SOSHNIKOV, S., STEIN, D. J., SYKES, B. L., TABB, K. M., TEMESGEN, A. M., TENKORANG, E. Y., THEADOM, A. M., TRAN, B. X., VASANKARI, T. J., VAVILALA, M. S., VLASSOV, V. V., WOLDEYOHANNES, S. M., YIP, P., YONEMOTO, N., YOUNIS, M. Z., YU, C., MURRAY, C. J. & VOS, T. 2016. The global burden of injury: incidence, mortality, disability-adjusted life years and time trends from the Global Burden of Disease study 2013. *Inj Prev,* 22**,** 3-18.

HAGEDORN, P. H., PERSSON, R., FUNDER, E. D., ALBÆK, N., DIEMER, S. L., HANSEN, D. J., MØLLER, M. R., PAPARGYRI, N., CHRISTIANSEN, H. & HANSEN, B. R. 2018. Locked nucleic acid: modality, diversity, and drug discovery. *Drug Discovery Today,* 23**,** 101-114.

JUNKER, J. P., KAMEL, R. A., CATERSON, E. J. & ERIKSSON, E. 2013. Clinical Impact Upon Wound Healing and Inflammation in Moist, Wet, and Dry Environments. *Adv Wound Care (New Rochelle),* 2**,** 348-356.

LI, S., DONG, S., XU, W., TU, S., YAN, L., ZHAO, C., DING, J. & CHEN, X. 2018. Antibacterial Hydrogels. *Advanced Science,* 5**,** 1700527.

LI, X., XU, X., XU, M., GENG, Z., JI, P. & LIU, Y. 2023. Hydrogel systems for targeted cancer therapy. *Front Bioeng Biotechnol,* 11**,** 1140436.

LIU, W., OU-YANG, W., ZHANG, C., WANG, Q., PAN, X., HUANG, P., ZHANG, C., LI, Y., KONG, D. & WANG, W. 2020. Synthetic Polymeric Antibacterial Hydrogel for Methicillin-Resistant Staphylococcus aureus-Infected Wound Healing: Nanoantimicrobial Self-Assembly, Drug- and Cytokine-Free Strategy. *ACS Nano,* 14**,** 12905-12917.

OLTEANU, G., NEACȘU, S. M., JOIȚA, F. A., MUSUC, A. M., LUPU, E. C., IONIȚĂ-MÎNDRICAN, C. B., LUPULIASA, D. & MITITELU, M. 2024. Advancements in Regenerative Hydrogels in Skin Wound Treatment: A Comprehensive Review. *Int J Mol Sci,* 25.

PATRA, D., ROY, S., ARORA, L., KABEER, S. W., SINGH, S., DEY, U., BANERJEE, D., SINHA, A., DASGUPTA, S., TIKOO, K., KUMAR, A. & PAL, D. 2022. miR-210-3p Promotes Obesity-Induced Adipose Tissue Inflammation and Insulin Resistance by Targeting SOCS1-Mediated NF-κB Pathway. *Diabetes,* 72**,** 375-388.

ROWLAND, M. B., MOORE, P. E., BUI, C. & CORRELL, R. N. 2023. Assessing wound closure in mice using skin-punch biopsy. *STAR Protocols,* 4**,** 101989.

ROY, S., HALDER, M., RAMPRASAD, P., DASGUPTA, S., SINGH, Y. & PAL, D. 2023. Oxidized pullulan exhibits potent antibacterial activity against S. aureus by disrupting its membrane integrity. *Int J Biol Macromol,* 249**,** 126049.

RWEI, S.-P., CHEN, Y.-M., LIN, W.-Y. & CHIANG, W.-Y. 2014. Synthesis and Rheological Characterization of Water-Soluble Glycidyltrimethylammonium-Chitosan. *Marine Drugs,* 12**,** 5547-5562.

SELVA OLID, A., SOLÀ, I., BARAJAS-NAVA, L. A., GIANNEO, O. D., BONFILL COSP, X. & LIPSKY, B. A. 2015. Systemic antibiotics for treating diabetic foot infections. *Cochrane Database Syst Rev,* 2015**,** Cd009061.

SILVA, N. H. C. S., VILELA, C., ALMEIDA, A., MARRUCHO, I. M. & FREIRE, C. S. R. 2018. Pullulan-based nanocomposite films for functional food packaging: Exploiting lysozyme nanofibers as antibacterial and antioxidant reinforcing additives. *Food Hydrocolloids,* 77**,** 921-930.

SINGH, R. S., KAUR, N., RANA, V. & KENNEDY, J. F. 2017. Pullulan: A novel molecule for biomedical applications. *Carbohydrate Polymers,* 171**,** 102-121.

STEIN, C., HANSEN, J. B., LAI, J., WU, S., VOSKRESENSKIY, A., H∅ G, A., WORM, J., HEDTJÄRN, M., SOULEIMANIAN, N. & MILLER, P. 2010. Efficient gene silencing by delivery of locked nucleic acid antisense oligonucleotides, unassisted by transfection reagents. *Nucleic acids research,* 38**,** e3-e3.

SUN, B. K., SIPRASHVILI, Z. & KHAVARI, P. A. 2014. Advances in skin grafting and treatment of cutaneous wounds. *Science,* 346**,** 941-945.

SUN, Y., LI, D., YU, Y. & ZHENG, Y. 2022. Insights into the Role of Natural Polysaccharide-Based Hydrogel Wound Dressings in Biomedical Applications. *Gels,* 8**,** 646.

TSALAMANDRIS, S., ANTONOPOULOS, A. S., OIKONOMOU, E., PAPAMIKROULIS, G. A., VOGIATZI, G., PAPAIOANNOU, S., DEFTEREOS, S. & TOUSOULIS, D. 2019. The Role of Inflammation in Diabetes: Current Concepts and Future Perspectives. *Eur Cardiol,* 14**,** 50-59.

WAHLESTEDT, C., SALMI, P., GOOD, L., KELA, J., JOHNSSON, T., HÖKFELT, T., BROBERGER, C., PORRECA, F., LAI, J. & REN, K. 2000. Potent and nontoxic antisense oligonucleotides containing locked nucleic acids. *Proceedings of the National Academy of Sciences,* 97**,** 5633-5638.

WANG, L. & STEGEMANN, J. P. 2010. Extraction of high quality RNA from polysaccharide matrices using cetyltrimethylammonium bromide. *Biomaterials,* 31**,** 1612-8.

WANG, Y., TAN, H. & HUI, X. 2018. Biomaterial scaffolds in regenerative therapy of the central nervous system. *BioMed research international,* 2018**,** 7848901.

WOLF, S. J., MELVIN, W. J. & GALLAGHER, K. 2021. Macrophage-mediated inflammation in diabetic wound repair. *Semin Cell Dev Biol,* 119**,** 111-118.

WONG, S. L., DEMERS, M., MARTINOD, K., GALLANT, M., WANG, Y., GOLDFINE, A. B., KAHN, C. R. & WAGNER, D. D. 2015. Diabetes primes neutrophils to undergo NETosis, which impairs wound healing. *Nat Med,* 21**,** 815-9.

ZHAO, X., LIANG, Y., HUANG, Y., HE, J., HAN, Y. & GUO, B. 2020. Physical Double-Network Hydrogel Adhesives with Rapid Shape Adaptability, Fast Self-Healing, Antioxidant and NIR/pH Stimulus-Responsiveness for Multidrug-Resistant Bacterial Infection and Removable Wound Dressing. *Advanced Functional Materials,* 30**,** 1910748.

Chapter 6 |

Summary

6.1. Highlights

This thesis highlights the critical influence of Zeb2 in driving macrophage-mediated chronic inflammation under the hyperglycemic conditions, which is typical factor causing diabetic foot ulcers. It also showcases a novel one-step chemical modification of pullulan that significantly inhibits *Staphylococcus aureus* growth, providing the foundation for the oxidized pullulan-quaternized chitosan hydrogel (OP@QC). This advanced hydrogel serves as a delivery platform for *Zeb2 ASO*, which aids in macrophages skewing with the outcome of marked reduction in chronic inflammation, enhanced neovascularization, and a dramatic acceleration of wound healing. This study has brought to light the following significant insights:

1. Macrophages are the conductors in the symphony of wound healing, seamlessly adapting to time and location cues to drive tissue repair. However, in the chronic diabetic microenvironment, these cells become trapped in a relentless cycle of chronic inflammation. The root of this dysfunction is a constant barrage of hyperglycemia, that overwhelms the natural healing process.
2. This study finds out the intricate dynamics of Zeb2 in diabetic wound, a crucial transcription factor results in the locking of macrophages in a proinflammatory state that perpetuates chronic inflammation by exacerbating the inflammatory cascade.
3. Amid the complex molecular choreography of diabetes-driven inflammation, acetyltransferases, such as P300, take on a pivotal yet disruptive role. It is overexpressed in hyperglycemic environments, which leads to destabilization of gene regulation by modifying chromatin architecture and amplifying inflammatory signaling pathways, thus, fueling unchecked inflammatory responses.
4. Inhibiting P300 with the selective inhibitor C646 successfully interrupts the inflammatory cascade by downregulating *Zeb2* expression, resulting in a substantial decrease in

inflammatory markers in diabetic mice, which emphasizes the possibility of targeting acetyltransferase activity to quieten chronic inflammation.

5. In the investigation of hydrogel-based oligonucleotide delivery, a one-step oxidation process of pullulan to o-pullulan inculcates the ability to attack bacterial membranes and impede the functional activity of the SpA protein. It has a great biocompatibility profile-cytocompatibility, hemocompatibility, and non-immunotoxicity.
6. Furthermore, upon fabrication of oxidized pullulan (OP) and quaternized chitosan (QC)-based hydrogel (OP@QC), its mechanical properties are enhanced and it exhibits remarkable ability to self-heal, ensuring the integrity of the wound dressing even after physical damage. The hydrogel's water retention abilities provide a consistent, healing-friendly environment, which is crucial for wound recovery over extended periods.
7. Beyond its structural advantages, the OP@QC hydrogel also demonstrates controlled drug delivery capabilities, and exhibits potent antibacterial activity, which positions them as formidable tools in the fight against wound infections.
8. In the purpose of silencing Zeb2 in wound, Zeb2 ASO incorporated OP@QC hydrogel effectively altering macrophage polarization from a pro-inflammatory (M1) to an anti-inflammatory (M2) state and also accelerates wound healing by reducing prolonged inflammation.
9. *Zeb2* ASO integrated OP@QC also produces a healing-friendly milieu, by increasing neovascularization, evidenced by the presence of markers, like CD31 and α-SMA, demonstrates improved tissue regeneration and wound angiogenesis.

6.2. Conclusions

This study reveals the pivotal role of macrophage regulation in wound healing, spotlighting the transcription factor, *Zeb2,* as a key player in managing inflammation, particularly in chronic diabetic wounds. Our research uncovers the relentless inflammatory environment, driven by acetyltransferase activity particularly P300, Hat1 leads to elevated Zeb2 levels. This persistent high Zeb2 perpetuates macrophage inflammation, which obstructs natural healing processes. Through both *in vitro* macrophage studies and *in vivo* diabetic wound models, we demonstrated that inhibiting acetyltransferase activity with P300-specific inhibitors, such as C646, significantly curbed the Zeb2-mediated inflammation. C646 treatment notably reduces pro-inflammatory markers and myeloid-lineage transcription factors. In diabetic mice, intradermal C646 administration alleviates inflammation, shifts macrophage polarization from the M1 to the M2 phenotype, and promotes wound healing.

Furthermore, this study presents a novel approach involving a simple chemical modification of the pullulan backbone, which significantly enhances its antibacterial activity against *Staphylococcus aureus* by disrupting its membrane integrity. The di-aldehyde groups in oxidized pullulan (o-pullulan) play a critical role in targeting cell wall proteins, leading to impaired bacterial function. The demonstrated biocompatibility of o-pullulan, including its cytocompatibility and non-immunotoxicity, which supports its potential for medical use. With its strong antibacterial properties and compatibility with wound care materials, o-pullulan emerges as a promising candidate for advanced wound dressings, and offering dual benefits of infection control and enhanced wound healing.

We also explored the innovative use of oxidized pullulan (OP) and quaternized chitosan (QC)-based hydrogels as a therapeutic platform for diabetic wound care. The OP@QC hydrogel's dual functionality— combining antimicrobial activity with controlled drug delivery highlights its potential for advanced wound care. By incorporating *Zeb2* antisense oligonucleotides (ASO) into the hydrogel, we created a localized, sustained-release system that modulates the inflammatory microenvironment at the wound site. In diabetic wound models, the *Zeb2* ASO-loaded hydrogel significantly improved wound closure, by reducing inflammation, and promoted new blood vessel formation, as evidenced by angiogenic markers, like CD31 and α-SMA.

These findings open new avenues for targeted macrophage modulation in chronic wound management and establishes Zeb2 inhibition and acetyltransferase regulation as promising therapeutic targets. The successful integration of advanced biomaterials, such as OP@QC hydrogels, into wound care therapies offers a great promise for revolutionizing the treatment of diabetic wounds and other inflammation-related conditions.

6.3. Contributions to existing knowledge

This research focuses on understanding how high blood sugar levels affect wound healing, specifically by looking at the inflammation process. The goal is to identify key factors that keep macrophages, in an inflamed state in diabetic wounds. The study also explore the material potential for wound dressings that can reduce harmful effects, like oxidative stress and low-grade infections, in chronic wounds. Additionally, it can control the release of oligonucleotides in diabetic wound and regulate the immune cells polarity and promote better healing.

Hyperglycemia in diabetes impairs wound healing by accumulating advanced glycation end-products (AGEs), which restricts therapeutic molecules to perform function. Chronic inflammation, driven by elevated pro-inflammatory cytokines, further hinders tissue repair. In

this study, we found that elevated glucose levels increase inflammation and macrophage polarization by upregulating Zeb2 and acetyltransferase activity. Overactivation of P300, Hat1 boosts pro-inflammatory markers and Zeb2 expression, while inhibiting acetylation with C646 reduced inflammation and Zeb2 levels in hyperglycemic macrophages and significantly enhanced wound healing. Also, Zeb2 suppression shifts macrophages toward an anti-inflammatory phenotype, potentially resolving hyperglycemia-induced chronic wound complications.

In chronic wounds, bacterial biofilms form a resilient barrier, protecting pathogens from antibiotics and immune responses. These biofilms exhibit dynamic adaptability, contributing to resistance against even the most advanced therapeutic interventions. The challenge of drug resistance is further compounded by the overuse of antibiotics, which fosters the emergence of more robust, difficult-to-treat bacterial strains. To address this challenge, we functionalized the biopolymer pullulan to enhance its therapeutic efficacy. Oxidized pullulan demonstrated potent antibacterial activity against *Staphylococcus aureus*, a common pathogen in chronic wounds. Molecular docking studies revealed that oxidized pullulan interacts with the bacterial membrane protein SpA, inhibiting Ca^{2+}-Mg^{2+}-ATPase activity and inducing membrane depolarization, which leads to the lysis of *S. aureus* cells and reduces biofilm formation. Due to its compatibility with mammalian cells, blood cells and lack of immunotoxicity, oxidized pullulan presents a viable option for use in medical devices and implants to prevent infections in open wounds and combat bacterial contamination in chronic wounds.

Administering therapeutic agents to diabetic wounds presents significant challenges due to various physiological and biochemical barriers. Factors such as impaired blood circulation, elevated reactive oxygen species (ROS) activity, high protease activity, and low-grade bacterial infections—especially in peripheral areas like the feet—substantially impede the effective delivery of medications to the wound site. Despite these obstacles, advanced drug delivery systems, including hydrogels, nanoparticles, and smart bandages, offer promising approaches to enhance treatment efficacy and address these challenges effectively. We fabricated a hydrogel composed of 10% oxidized pullulan (o-pullulan) and 1% quaternized chitosan (q-chitosan), utilizing their potent antibacterial and antioxidant properties to deliver *Zeb2* ASO. In STZ-induced HFD mice, the hydrogel treatment demonstrated significant wound healing efficacy, marked by a reduction in pro-inflammatory markers and an increase in anti-inflammatory markers and angiogenesis markers. The percentage of wound area closure was also significantly improved with *Zeb2* ASO treatment. Targeting Zeb2 inhibition in wound-resident macrophages would be a promising approach to counteract hyperglycemia-induced

macrophage polarization and expedite wound healing.

6.3. Future perspectives

Zeb2's involvement in chronic inflammation is a noteworthy advancement in the field of diabetic chronic wound healing, thus, establishing a strong basis for future investigations and practical implementations. The work highlights the significant consequences of these discoveries and outlines important avenues for further investigation:

1. Our study lays the groundwork for deciphering Zeb2's influence on macrophage polarization and chronic inflammation. Further investigation with Zeb2 knock out mice study might explore the mechanisms by which Zeb2 influences the behavior of macrophages in the presence of high blood sugar levels, perhaps revealing its associations with other regulatory proteins and cellular communication networks. By broadening the scope of our work to include the impact on other kinds of immune cells, we may uncover more insights into the function of Zeb2 in immune control.
2. The triumph of *Zeb2* ASO-loaded hydrogels in accelerating wound healing in diabetic mice highlights the promise of targeted gene therapies for chronic wound care. Future research could create smart hydrogels that adapt specific wound conditions that could revolutionize therapeutic efficacy.
3. The exhibited antibacterial and biocompatibility characteristics of o-pullulan-based hydrogels present new prospects for combining these materials into enhanced wound care treatments. Future investigation can focus on optimizing the formulation of hydrogels for particular types of wounds, notably those with severe or multi-drug-resistant infections. Additionally, studying combinations of o-pullulan with other biocompatible polymers or drugs can further increase the efficacy of wound dressings.
4. While our work indicates the biocompatibility of OP@QC hydrogels, long-term investigations are required to determine their safety and effectiveness in clinical settings. Evaluating possible interactions with various kinds of tissues, monitoring for any delayed detrimental effects, and ensuring that the hydrogels operate effectively over long durations will be critical for their successful translation into clinical application.

In summary, the positive findings from our study establish the framework for future research and development in wound care and therapeutic applications. Continued investigation and innovation in these areas have the potential to profoundly improve DFU patient outcomes.

Table A. List of antibodies used.

Antibody	**Dilution**	**Company**	**Catalog No.**
Phospho-NF-κBp65 (S-536)	1:1000 for ICC 1:2000 for WB	Abcam	#ab86299
NF-κB	1:1000 for WB	Invitrogen	#PA1-186
iNOS	1:400 for ICC 1:400 for IHC 1:1500 for FC	Cell Signaling Technology	#13120
Arginase 1	1:50 for ICC 1:400 for IHC	Cell Signaling Technology	#93668
F4/80	1:50 for IHC	Santa Cruz Biotechnology	#sc-377009
CD68	1 μg/mL for IHC	Abcam	#ab125212
β-actin	1:1000 for WB	Invitrogen	#AM4302
Zeb2	1:100 for IHC	Santa Cruz Biotechnology	#sc-271984
CD80	1 μg/mL for IHC	Abcam	#ab254579
CD163	1 μg/mL for IHC	Abcam	#ab182422
Oct2	1:200 for ICC	Cloud clone	#PAB554Hu01
HAT1	1:200 for ICC	Cloud clone	#PAB952Mu01
P300	1:200 for ICC	Abclonal	#A13016
Anti-Mouse IgG (Alexa Fluor 488 conjugated)	1:1000 for ICC 1:1000 for IHC	Cell Signaling Technology	#4408
Anti-Rabbit IgG (Alexa Fluor 488 conjugated)	5 μg/mL for ICC 1:500 for IHC	Invitrogen	#A-11034
HRP conjugated Anti-Mouse IgG antibody	1:20000 for WB	Sigma-Aldrich	#A9044
HRP conjugated Anti-Rabbit	1:20000 for WB	Sigma-Aldrich	#A9169

IgG antibody			
TruStainFcXTM (anti-mouse CD16/32)	0.1 µg/million cells for FC	BioLegend	#101319
PE/Cy5 anti-mouse CD80	5 µL/ million cells	BioLegend	#104712
FITC anti-mouse CD86	2 µL/ million cells	BioLegend	#105006
APC anti-human CD163	5 µL/million cells for FC	BioLegend	#326510

Table B. Primer sequences used.

Mouse primers		
Gene	**Forward (5'-3')**	**Reverse (5'-3')**
CD163	TGCTCAGGAAACCAATCCCA	ACCTCCACTCTTCCAGCG
CD206	TTCAGCTATTGGACGCGAGG	GAATCTGACACCCAGCGGAA
CD86	CTGTAGGCAGCACGGACTTG	CATGGTGCATCTGGGGTCCAT
MHC-II	GAAGACGACATTGAGGCCGA	GGAACACAGTCGCTTGAGGA
IL-4	GCATGGCCCAGAAATCAAGG	GAGAAATCGATGACAGCGCC
iNOS	CTTGGTGAAGGGACTGAGCTG	CGTTCTCCGTTCTCTTGCAGT
B-Actin	GTACTCTGTGTGGATCGGTGG	AGGGTGTAAAACGCAGCTCAG
IL-6	GGGACTGATGCTGGTGACAA	ACAGGTCTGTTGGGAGTGGT
HAT 1	TTTCGGTTACAAGGGCCTGA	CAACATCATCTGCCTCCACAC
MOZ1	CTGTCCAACCAGCCGCCAA	GCTTCCAGACTCGGGTATCTCC
PU.1	GCAGGGGATCTGACCAACCT	AGTCATCCGATGGAGGGGC
Zeb2	CCAGAGGAAACAAGGATTTCAG	AGGCCTGACATGTAGTCTTGTG
Oct2	AATGGACCCGACATTAACCA	AAATGGTCGTTTGGCTGAAG
KLF	AGCCTATCTTGCCGTCCTTT	CGCCTCGGGTTCATTTC
Human primers		
Gene	**Forward (5'-3')**	**Reverse (5'-3')**
P300	GGCTGTATCAGAGCGTATTGTC	CCTCGAAATAAGGCAATTCC
ZEB2	CCAGAGGAAACAAGGATTTCAG	AGGCCTGACATGTAGTCTTGTG
CD80	CTCTTGGTGCTGGCTGGTCTTT	GCCAGTAGATGCGAGTTTGTGC
CD68	TACATGGCGGTGGAGTACAA	AGGTGGACAGCTGGTGAAAG
OCT2	GCACCACCCACCAAATGTTC	GCCTTCCCTTGAACTCTCCC
CD163	GTAGCGGGAGAGTGGAAGTG	TCCAAATGCGTCCAGAACCT
MOZ1	CTCATCTCCTGTGCCGACTG	TTTGGCATACGGGTGAGTGG
HAT 1	TCGGAAATGGCGGGATTTGG	CGGAACATTGTTGACAGGCT
KLF	AGGATCGAGGCTTGTGATGC	GTAGCCCAAAAATGCCCACC
B-ACTIN	ACAGAGCCTCGCCTTTGCC	TCCCAGTTGGTGACGATGC
Staphylococcal primers		

Gene	**Forward (5'-3')**	**Reverse (5'-3')**
SpA	CGGAGTACATGTCGTTAAACCT	GGTTTGCTGGTTGCTTCTTATC
FmtA1	GGTGAACAAGAAACCGGCAT	CGCTTTCATTTGTGCCCTCT
FmtA2	TGTCATTGCAGTCGTAACGC	TGCTTGCGTATCATCTTGAGGT
16s	ATGCAAGTCGAGCGAAC	TGTCTCAGTTCCAGTGTGGC
siRNA and ASO		
Zeb2 siRNA (m)	5'-T*A*A* TACCT*TTG*GGTTCT*C*T*C -3'	
Con ASO (non-targeting)	5′- +T*+A*+G*C*C*T*G*T*C*A*C*T*T*+C*+T*+C -3′	
Zeb2 ASO (m)	5'-+T*+A*+A* T*A*C*C*T*T*T*T*G*G*G*T*T*C*T*+C*+T*+C -3'	
SpA ASO	5'- +A*+T*+C*AAACCTG*GTCAAG*A*A*+C+T+T -3′	

Table C. Patient demographic details.

Pathological features	
Non-diabetic patients:	
Number of patients	5
Age (median range)	53 ± 6.4
Gender	Male (n = 4), Female (n = 1)
BMI (median range)	22.16 ± 1.91
Fasting serum glucose (mmol/L)	4.0547 ± 1.21
Diabetic patients	
Number of patients	17
Age (median range)	56.75 ± 5.53
Gender	Male (n = 13), Female (n = 4)
BMI (median range)	28.725 ± 5.71
Fasting serum glucose (mmol/L)	11.68624 ± 5.61

Table D. Percent aldehyde content of o-pullulan oxidized using different amounts of sodium meta-periodate.

Sample	**Amount of $NaIO_4$ (mg)**	**% of -CHO**
OP_{72}	698	72
OP_{28}	349	28
$OP_{18.69}$	174.5	18.69
$OP_{13.3}$	87.25	13.3
$OP_{9.8}$	43.62	9.8

Table E. Bactericidal activity of o-pullulan against *S. aureus* and *P. aeruginosa.*

Concentration of o-pullulan	**% Inhibition**			
	S. aureus		***P. aeruginosa***	
300 µg/mL	98.84315	±1.0219	99.06	±0.7794
150 µg/mL	98.65726	±0.556096	98.67136	±1.238823
75 µg/mL	97.8152	±0.988644	68.76395	±2.168676
37.5 µg/mL	96.05744	±0.973735	65.11086	±2.306946
18.75 µg/mL	96.52742	±1.859158	60.69636	±0.99322
9.38 µg/mL	87.58997	±1.849696	60.22951	±1.163157
4.68 µg/mL	78.34765	±1.796991	60.63647	±3.037512
2.34 µg/mL	69.23925	±0.439846	61.47007	±0.827282
1.17 µg/mL	62.33254	±1.230876	60.45231	±1.377983
0.55 µg/mL	57.0294	±1.431569	55.21594	±3.367482
0.28 µg/mL	47.2165	±1.203504	55.15701	±1.910917
137.5 ng/mL	43.86568	±1.921462	55.12267	±0.287682
68.75 ng/ml	24.25101	±3.304962	57.13172	±2.516933
34.38 ng/mL	24.27892	±1.972895	55.09753	±2.228573
17.19 ng/mL	17.11395	±3.16588	55.43888	±1.465982
8.59 ng/mL	16.40811	±3.155737	57.92106	±1.719107
4.3 ng/mL	16.35996	±1.687099	53.90964	±0.910771
2.15 ng/mL	15.51875	±1.16204	54.3361	±2.771552
1.07 ng/mL	14.58246	±1.616115	55.64054	±3.247385
0.53 ng/mL	15.56711	±2.663283	48.8417	±3.164066
0.27 ng/mL	16.66932	±2.034773	50.49992	±1.475262
0.13 ng/mL	14.6479	±1.787503	43.17832	±2.199831
0.07 ng/ml	13.46583	±2.604514	45.15129	±2.967494

Table F. List of cell wall-anchored proteins of *S. aureus* extracted from PDB.

Name of Protein	**PDB ID**	**Binding Energy (ΔG)**
C domain of protein A	4NPE	-6.05
B domain of protein A	4NPF	-2.88
D domain of protein A	1DEE	1.52
FemX	6SNR	4.25
Surface protein-sdrc	6LXH	3.48
SdrD	4JDZ	4.15
lanRFPdam	4JEO	3.8
SdrE	5IHW	4.6
Collagen adhesin (CNA)	2F68	5.56
IsdB-N2	3RTL	4.5
IsdA NEAT	2ITE	3.25
NEAT domain of IsdH	2H3K	2.2
SasG E1-G52	5DBL	3.7
SasG E-G52 module	3TIP	4.7
C-terminal fragment of SraP	4M03	3.18
Middle fragment of SraP	4M02	1.98
Lipoprotein, HtsA	3EIW	0.56
Extracellular Solute-binding Protein	4HW8	-1.73
FtsA	3WQU	1.87
Ebh	4KJM	3.33

Table G. List of cell wall anchored proteins of *S. aureus* extracted from AlphaFold Protein Structure Database.

Name of Protein	UniPort ID	Binding Energy (ΔG)
Divalent metal cation transporter	Q2G2G3	0.53
EBPS	Q53630	1.18
IcaB	A0A830ZQF5	0.15
IcaC	Q9K380	-1.06
Na/H antiporter A1	Q2FZV1	4.02
Na/H antiporter B1	Q2FZV2	0.96
Osmoprotectant transporter	Q2FW63	2.73
Magnesium transporter	Q2FZQ5	2.95

Table H. Interaction of o-pullulan with SPA B-domain.

Hydrogen bond									
Index	**Residue**	**Amino acid**	**Distance H-A**	**Distance D-A**	**Donor Angle**	**Protein donor**	**Side chain**	**Donor atom**	**Acceptor atom**
1	3	ASN	2.32	3.16	165.12	Y	Y	49 [N]	951 [O]
2	5	PHE	2.15	2.79	149.17	Y	N	84 [N]	927 [O]
3	10	GLN	3.32	3.93	122.55	Y	N	206 [O]	935 [O]
4	35	LYS	1.7	2.59	170.83	Y	Y	625 [N]	955 [O]
Salt bridge									
Index	**Residue**	**Amino acid**	**Distance**	**Protein positive**		**Ligand group**		**Ligand atoms**	
1	4	LYS	5.18	Y		Carbonyl		1968, 1973	

Table I. Interaction of o-pullulan with SPA C-domain.

Hydrogen bond									
Index	**Residue**	**Amino acid**	**Distance H-A**	**Distance D-A**	**Donor angle**	**Protein donor**	**Side chain**	**Donor atom**	**Acceptor atom**
1	3	ASN	2.32	3.16	165.12	Y	Y	49 [N]	951 [O]
2	4	LYS	3.27	3.97	138	Y	Y	74 [N]	960 [O]
3	5	PHE	2.15	2.79	149.17	Y	N	84 [N]	927 [O]
4	10	GLN	3.32	3.93	122.55	Y	N	206 [O]	935 [O]
5	35	LYS	1.7	2.59	170.83	Y	Y	625 [N]	955 [O]